A CONTRIBUTION TO THE VIBRATIONAL ANALYSIS OF METAL COMPLEXES WITH PYRIDINE AND RELATED LIGANDS

A thesis submitted to the

UNIVERSITY OF CAPE TOWN

in fulfilment of the requirements for the degree of

Doctor of Philosophy

by

PAUL FELIX MARIA VERHOEVEN

Licentiaat in de wetenschappen groep scheikunde

(UNIVERSITEIT ANTWERPEN)

Department of Inorganic Chemistry
University of Cape Town
Rondebosch 7700
Republic of South Africa

September 1984

"Da dacht ich oft: Schwatzt noch so hoch gelehrt,
Man weiss doch nichts als was man selbst erfährt;"

aus Oberon, der zweite Gesang,

von C.M. WIELAND (1733-1813)

ACKNOWLEDGEMENTS

My sincere thanks and appreciation are due to Professor D.A. Thornton for his supervision and understanding during this work, my colleagues of the department of Inorganic Chemistry and members of the School of Chemical Sciences for their interest and help, Professor B.J. van der Veken of the University of Antwerp for his computer programmes, and my colleague and friend, Mr. H. Hofmans of the same University for his invaluable assistance in the thermal analyses data.

In particular, I am grateful to Professor H. O. Desseyn, University of Antwerp, to Professor W.J. Orville-Thomas, University of Salford, and to Professor R.D. Gillard, University College in Cardiff, for their stimulating and helpful discussions.

Financial assistance from the University of Cape Town, Research Grants Committee and the South African Council for Scientific and Industrial Research is gratefully acknowledged.

Finally, I would like to thank Miss H.M. Dreyer for the typing of this thesis, Dr. S.C. Yorke for proof-reading and last, but not least, Miss E.B. Lutsch for her valued friendship and moral support.

SUMMARY

A series of forty-seven pyridine complexes of cobalt(II) halides of the type CoL_2X_2 have been synthesized and characterized by microanalysis, thermal analysis and infrared spectroscopy. The computational methods and spectroscopic techniques that have been applied in the structural analysis of the complexes, are summarized in chapter 1.

In chapter 2, an account is given of the two possible stereochemistries of the complexes of type CoL_2X_2, where L are variously substituted pyridines. The cobalt can be tetrahedrally coordinated or the compounds exist as a polymeric chain where the cobalt atoms are joined by bridging halide groups leading to an octahedral environment for the metal. On the basis of intermolecular steric interaction due to the substituent on the pyridine ring, we can explain the stability and hence, the more favourable occurrence of one form rather than the other. The far-infrared spectra are reported and the metal-ligand stretching frequencies are assigned. The relative contribution of π-bonding between the cobalt and the nitrogen ring atom is strongly dependent on the nature of the substituent in the pyridine ring. Electron withdrawing substituents shift νCo-N to higher frequencies consistent with Co$\rightarrow$N π-bonding.

The theory behind the analysis of the normal modes of vibration for polyatomic molecules is discussed briefly in chapter 3. Two approximation methods for the calculation of force constants, the eigenvector method of BECHER and MATTES and the matrix polynomial expansion method of ALIX are described and discussed with regard to their limitations and practical usefulness. The purpose of a normal coordinate analysis is twofold: firstly, to give more accurate description of the fundamental vibrations in terms of their potential energy distribution, and secondly, to calculate force constants which allow us to examine chemical bonds on a quantitative basis.

Examples of normal coordinate treatments are found in chapter 4. Theoretical vibrational analyses of (1) the infrared-active vibrations of square-planar *cis*-$[PtL_2X_2]$, where L is aniline, pyrazine and imidazole and X is chloride and nitrate; and (2) the skeletal vibrations of the tetrahedral CoL_2X_2 complexes are given. The results of such an analysis were supported by isotopic spectroscopic data.

The pyridine complexes of cobalt(II) halides were investigated by thermogravimetric analysis and differential scanning calorimetry and the results are presented in chapter 5. A possible structure of the thermal decomposition products $CoLX_2$ and $CoL_{2/3}X_2$ was deduced from infrared spectroscopic measurements. The nature and the strength of the metal-ligand bond is discussed in terms of some reported heats of decomposition and other spectroscopic properties of the cobalt(II) complexes.

TABLE OF CONTENTS

CHAPTER 1

PHYSICAL METHODS AND COMPUTATION

1.1 INFRARED SPECTRA

The mid-infrared spectra were recorded on Perkin-Elmer models 180 and 983 spectrophotometers using both the evacuable pellet die technique and Nujol mulls between potassium bromide plates. The far-infrared spectra were determined as Nujol mulls between polyethylene plates on a Digilab FTS-16 B/D interferometer.

The quoted wavenumber accuracy of the spectrophotometers is $\pm$ 2 cm^{-1} for the 4000-2000 cm^{-1} region and $\pm$ 1 cm^{-1} for the 2000-180 cm^{-1} region, their reproducibility is better than 0.1 cm^{-1}. A resolution of 0.5 cm^{-1} can be obtained using the highest scan mode. The model 983 is based on a double-beam, ratio-recording with pre-sample chopping principle and has integral data handling as well as digital displaying facilities. The optics involved are a purgable F4.2 monochromator with 4 gratings and 9 filters[1]. The FTS-16 B/D is an automatic ratio recording, far infrared vacuum interferometer with a resolution to 0.5 cm^{-1} throughout the spectral range of 500 to 10 cm^{-1}. The instrument consists of a model 296A Michelson interferometer, four interchangeable Mylar beamsplitters, a high pressure mercury arc source, stored ratio optics and a remotely controlled sample carriage, a triglycine sulfate detector, an analog-to-digital converter, a data system with 8K of core memory, a 1.2 million word moving head disk, a digitally controlled plotter and related soft- and hardware[2].

1.2 RAMAN SPECTRA

The Raman spectra were recorded on a Coberg PHO instrument using a Spectra Physics Model 164 Ar^{+}-laser for excitation and the 488.0 nm line with interference filters to remove plasma lines. Laser powers

were kept around 150 mW at the sample. The complexes are coloured and amorphous in nature, creating problems for Raman spectroscopy. The powdered compounds reflect large amounts of the incident radiation in all directions, causing weak Raman scattering, stray light and ghost lines to appear. Because of absorption of laser excitation radiation (due to the breadth of the absorption bands), the complex will decompose in a couple of minutes, so that no spectra could be obtained. Also the less critical resonance Raman effect can occur, altering the relative intensities of certain bands. The major difficulty of burning could be overcome by using a spinning cell, in which the sample is being continuously rotated in the laser beam, in combination with vertical translation along its rotation axis, thus spreading out the laser intensity over a larger cylindric surface of the compound. In view of the poor quality and the low signal-to-noise ratio, even when recorded at low temperature (-160^{o}C), no spectra are reported. Finally, it should be pointed out that in Raman, the relative intensities of combination and overtone bands are much weaker than in infrared. Consequently all the vibrational bands observed are due to fundamental transitions, unless they are part of Fermi-resonance systems.

1.3 ELECTRONIC SPECTRA

The electronic spectra were run on a Varian Superscan 3 ultra-violet and visible spectrophotometer in the absorbance mode using spectroscopic solvents in 10 mm cells.

1.4 THERMAL ANALYSIS

The thermal curves were obtained by Mr. H. Hofmans at the University of Antwerp (R.U.C.A.), Belgium on a Du Pont R90 thermal analyzer. The thermogravimetric analyses were performed on the thermobalance model 951

which has built-in derivative facility and can detect a rate of weight change as small as 5 μg/min. The differential scanning calorimetry measurements were done on the cell base model 910, operating to a maximum temperature of 600°C. Scanning on the 990 recorder, can be taken at two different sensitivities simultaneously.

1.5 MICROANALYSIS

Microanalyses were performed by Mr. W.R.T. Hemsted, Organic Chemistry Department, University of Cape Town on a Heraeus universal combustion analyser model CHN-MICRO.

1.6 COMPUTATION

All computations were carried out at the computer centre of the University of Cape Town on a Sperry-Univac series 1100 computer. The programmes were originally written by Dr. B. Van der Veken, labo anorganische chemie, University of Antwerp (R.U.C.A.), Belgium, and were updated to the level 10R1 in FORTRAN(ASCII). The programme package consists of the following routines and I.B.M.-EPL subroutines.

name of routine	purpose
CART	calculation of molecular geometry from internal coordinates[3]
GMATRIX	calculation of the kinetic energy coefficients
BECMAT	calculation of a force field from a set of vibrational frequencies by the eigenvector method of Becher and Mattes
POLEXP	calculation of a force field from a set of vibrational frequencies by the matrix polynomial expansion method of Alix
GFMATRIX	calculation of vibrational frequencies from G and F matrices

name of subroutine	purpose
SORB	list interatomic distances
MATIN	read control card and matrix data elements from a logical unit number MY
MXOUT	produce an output listing of any sized array on logical unit number MX
LOC	compute a vector subscript for an element in a matrix of specified storage mode
MINV	invert a matrix by the Gauss-Jordan method (ref. 4, Chapter 9)
EIGEN	compute eigenvalues and eigenvectors of a real symmetric matrix by the Jacobi method (ref. 4, Chapter 9 and ref. 5)
NROOT	compute eigenvalues and eigenvectors of a real non-symmetric matrix of the form $B^{-1}.A$ (ref. 4, Chapter 9)

The last subroutine is also used in performing a canonical correlation analysis as documented in ref. 6.

REFERENCES

1. "Model 983 Infrared Spectrophotometer Operator's Manual", Perkin-Elmer Ltd., England, 1981.

2. "Spectrometer Technical Manual M091-0033", Digilab Inc., U.S.A. (Mass.).

3. H.B. THOMPSON, *J. Chem. Phys.*, 47(1967)3407.

4. W.W. COOLEY, P.R. LOHNES, "Multivariate Procedures for the Behavioural Sciences", John Wiley, New York, 1962.

5. J. GREENSTADT, in "Mathematical Methods for Digital Computers", Chapter 7, (A. RALSTON and H.S. WILF eds.), John Wiley, New York, 1960.

6. W.W. COOLEY, P.R. LOHNES, "Multivariate Data Analysis". Chapter 6, John Wiley, New York, 1971

CHAPTER 2

THE STRUCTURE AND VIBRATIONAL SPECTRA OF $[CoL_2X_2]$ COMPLEXES, WHERE X = Cl AND Br AND L = VARIOUSLY SUBSTITUTED PYRIDINES

2.1 GENERAL INTRODUCTION

Historically, the application of cobalt compounds to colouring glass and glazes goes back to very ancient times. The discovery of a necklace which consists of blue glass beads amongst semi-precious stones, dating back to 2250 B.C., suggests that cobalt was introduced intentionally into the glass. Egyptian statuettes dating from the 5th Dynasty (2680-2530 B.C.) have been decorated with cobalt colours and cobalt-coloured blue glass was found in the ruins of Troy (1200 B.C.) and of Pompeii, destroyed in 79 A.D. It is spectrophotometrically proven that cobalt is the major colouring agent of the "Portland Vase" (between 100 B.C.-100 A.D.) which is considered as the finest example of late Greek glass-blowing technique[1].

The origin of the term cobalt is controversial. According to ref.2 the earliest recorded use of the term appeared in Agricola's "Bermannus" in 1530, under the name 'kobelt' referring to a substance found in the silver mines of Saxony (Erzgebirge). The 'kobelt' is now believed to have been arsenical-cobalt, a mineral frequently encountered in these mines. Or it could have originated from the German word 'Kobold', meaning mischievous spirit, a term given by injured miners who associated their sufferings with imaginary beings. More variations of the word appeared later. These later terms referred generally to impure or unknown, hard-to-refine earths or materials which do not necessarily contain the element cobalt.

As major applications, the cobalt compounds are used for colouring glass and ceramics, the cobalt oxides for coatings, and various cobalt alloys which are corrosion and high-temperature resistant are used as

metal-working materials. The strong catalytic properties of cobalt metal for the synthesis of liquid hydrocarbons were developed by FISCHER and TROPSCH[3] in 1925. The importance of the element in the soil for cattle nutrition, as trace-element in human nutrition and in vitamin B_{12} is now well-realized. Since World War II, radioactive ^{60}Co, has found numerous applications as an emitter of gamma rays, e.g., in radiation therapy for cancer treatment[4].

Cobalt occurs in nature with arsenic (Cobaltite; CoAsS) and with nickel (Skutterudite; $(Co,Ni,Fe)As_3$). The four types of cobalt minerals are : cobalt arsenides, cobalt sulphides, cobalt sulpharsenides and various oxidised cobalt minerals. The major cobalt deposits are in Zaïre, Zimbabwe, Morocco, Canada, the U.S.A., the U.S.S.R. and Cuba. It is recovered commercially as a co- or by-product with metals such as copper, nickel and silver by smelting, by hydrometallurgy, by electrowinning or by a combination of the latter two extractive processes[4].

The two most common oxidation states of cobalt are 2+ and 3+. Trivalent cobalt forms an immense number of complexes, of which the majority contain nitrogen donor atoms. Most of these complexes are quite stable, covalent coordination bonds (d^2sp^3) being formed. According to hybridization theory, the six 3d electrons of the cobaltic ion become paired, leaving two vacant orbitals in the 3d shell capable of accepting donor electron pairs. With only a few exceptions, the Co(III) complexes of ammonia and ammines invariably have octahedral geometry, while divalent cobalt exhibits mainly a coordination number of either six or four. Co(II) forms tetrahedral complexes more readily than any other transition-metal ion. From ref.5, we read : "This is in accord with the fact that for a d^7 ion, ligand field stabilization energies disfavor the tetrahedral configuration relative to the octahedral one to a smaller extent than for any other d^n ($1 \leq n \leq 9$) configuration". Because of the small difference in stability

between octahedral and tetrahedral forms, there are several cases in which Co(II) complexes of the same ligands exists in both forms and which also may be in equilibrium with one another. Examples are; (1) some $Co(H_2O)_4^{2+}$ is shown to be in equilibrium with $Co(H_2O)_6^{2+}$ [6], and (2) two isomers of dibromo-*N*-bis(pyridinecarboxaldehyde)cobalt(II)[7] and of dichlorobis(4-vinylpyridine)cobalt(II)[8,9] have been isolated. Octahedral compounds of type CoL_2X_2 consisting of halogen-bridging groups, can completely dissociate to the tetrahedral species in various dilute solutions. Thermodynamic data for the tetrahedral-octahedral configurational equilibrium :

$$CoL_2X_2 + 2L \rightleftharpoons CoL_4X_2 \qquad (1)$$

have been reported previously by NELSON and collaborators[10].

The two stereochemistries about the cobalt can be determined on the basis of their colours and magnetic properties. Octahedral complexes are typically pale red or mauve, whereas the tetrahedral ones vary from sky blue to intense blue. The visible spectra of tetrahedral complexes show molar absorbances of about 10^2 times greater than those of octahedral complexes. This is due to the absence of a centre of symmetry in tetrahedral complexes, which removes the parity-selection rule[11]. The effective magnetic moments of tetrahedrally coordinated cobalt(II) fall within the range 3.8-4.7 BM if measured near room temperature. The lower limit is the spin-only moment calculated for the three unpaired electrons corresponding to the $(e)^4(t_2)^3$-configuration. In octahedral complexes, where a considerably larger orbital contribution is expected, the observed moments lie in the range 4.8-5.2 BM.

The primary aim of this chapter is to present a far-infrared study

of an extensive series of coordination compounds containing cobalt, substituted pyridines and halogens. In many cases, far-infrared spectroscopy is the only tool available for their study, since most of the complexes are amorphous and polymeric in nature. Hence, solubility problems are encountered. Attention is particularly given to the location of the metal-ligand vibrations which was the only subject for investigation in the early sixties. The development of commercial far-infrared instrumentation with a low-frequency limit of at least 200 cm^{-1} was responsible for this. Today, better resolution and reproducibility of the spectra can be obtained and, in combination with the application of new spectroscopic techniques (like matrix-isolation or high-pressure methods) more reliable and detailed spectroscopic work can be performed. Two excellent books, dealing with metal-ligand bonds and their related vibrations have been written by D.M. ADAMS[12] and by J.R. FERRARO[13] who have summarised all previous work up to 1966 and 1969, respectively.

The infrared data on metal-halide vibrations is extensive and the assignment of the metal-halide stretching vibrations is well established. This is due to the facts that (1) the M-X bands which have high intensity, normally appear within the range of detection; and (2) an easy method of assignment based on substitution of one halide by others can be applied. However, for complexes containing bridging halogens the assignment is much more complicated since these bands are located around and below 200 cm^{-1}. In this region, the bridging M-X stretching vibrations (ν_bM-X) are usually overlapped with the bending vibrations and others. The metal-nitrogen vibrations, generally weak to medium in nature, have received less attention. In most papers prior to 1970, only tentative assignments are published, probably because good Raman spectra were and still are difficult to obtain due to the absorption of exciting radiation by the

coloured complexes.

The stereochemistry of the cobalt-substituted pyridine complexes are explained in terms of steric effects which can be related principally to that of the substituent. The existence of π-bonding between cobalt and the ring nitrogen is much debated. In the last Section, account is given for the relative importance of a π-contribution to the cobalt-pyridine bond.

2.2 PREPARATION AND ANALYSIS OF COMPLEXES

The complexes were prepared by methods described in the literature[10,14,15]. The cobalt(II) halides (order of 10^{-1} mole) were dissolved in absolute ethanol (30ml) and warmed. The complexes, CoL_2X_2, were prepared by adding the stoichiometric amount of ligand (2×10^{-1} mole) to the warm solution with stirring. Precipitation of the crystalline product either occurred immediately or after cooling the solution. Where possible, the compounds were recrystallized from ethanol, washed with 'dry' ether and allowed to dry overnight over silica gel under reduced pressure. The complexes were left stored in a desiccator, since on standing in air, some compounds take up water from the atmosphere[16]. In most cases yields were nearly quantitative (> 70%) and the composition and purity of all compounds were determined by elemental analysis (C, H, N) of which the analytical data are given in Tables 2.1, 2.2, 2.3.

TABLE 2.1

Elemental analyses on the complexes $[CoL_2X_2]$, X = Cl and Br.

complex	calculated (found)		
	%C	%H	%N
$Co(py)_2Cl_2$	41.7	3.5	9.7
	(41.6)	(3.5)	(9.8)
$Co(py)_2Br_2$	31.9	2.7	7.4
	(31.8)	(2.7)	(7.4)
$Co(py\text{-}d_5)_2Cl_2$	40.3	3.4	9.4
	(40.1)	(3.4)	(9.3)
$Co(py\text{-}d_5)_2Br_2$	31.0	2.6	7.2
	(31.0)	(2.7)	(7.2)

TABLE 2.2

Elemental analyses on the complexes $[Co(R\text{-}py)_2Cl_2]$.

R	calculated (found)		
	%C	%H	%N
3-Br	26.9	1.8	6.3
	(27.0)	(1.8)	(6.3)
3-Cl	33.6	2.3	7.8
	(33.6)	(2.3)	(7.9)
$3\text{-}CH_3$	45.6	4.5	8.9
	(45.6)	(4.5)	(8.9)
3-CN	42.6	2.4	16.6
	(42.5)	(2.4)	(16.6)

TABLE 2.2 continued/

Elemental analyses on the complexes $[Co(R\text{-}py)_2Cl_2]$.

R	calculated (found)		
	%C	%H	%N
3-COC_6H_5	58.1	3.7	5.6
	(58.0)	(3.7)	(5.6)
3-$COCH_3$	45.2	3.8	7.5
	(45.2)	(3.9)	(7.5)
3-$CONH_2$	38.5	3.2	15.0
	(38.4)	(3.2)	(14.9)
3-$COOCH_3$	41.6	3.5	6.9
	(41.6)	(3.5)	(7.0)
3-COOH	38.3	2.7	7.4
	(38.4)	(2.9)	(7.4)
3,4-di-CH_3	48.9	5.3	8.1
	(48.9)	(5.2)	(8.1)
3,5-di-CH_3	48.9	5.3	8.1
	(48.2)	(5.2)	(8.3)
4-$C(CH_3)_3$	54.0	6.6	7.0
	(53.9)	(6.5)	(7.0)
4-C_6H_5	60.0	4.1	6.4
	(59.9)	(4.2)	(6.5)
4-C_2H_5	48.9	5.3	8.1
	(48.4)	(5.4)	(8.1)
4-CH_3	45.6	4.5	8.9
	(45.6)	(4.6)	(8.8)
4-CN	42.6	2.4	16.6
	(42.5)	(2.5)	(16.7)

TABLE 2.2 continued/

Elemental analyses on the complexes $[Co(R\text{-}py)_2Cl_2]$.

R	calculated (found)		
	%C	%H	%N
4-COC_6H_5	58.1	3.7	5.6
	(58.3)	(3.7)	(5.5)
4-$COCH_3$	45.2	3.8	7.5
	(45.0)	(3.8)	(7.5)
4-$CONH_2$	38.5	3.2	15.0
	(38.6)	(3.3)	(15.0)
4-$COOCH_3$	41.6	3.5	6.9
	(41.8)	(3.6)	(6.9)
4-COOH	38.3	2.7	7.4
	(38.4)	(2.8)	(7.5)
4-$N(CH_3)_2$	44.9	5.4	15.0
	(43.9	(5.4)	(14.7)
4-NH_2	37.8	3.8	17.6
	(37.6)	(3.8)	(17.5)
4-OH	37.5	3.2	8.8
	(37.5)	(3.2)	(8.7)

TABLE 2.3

Elemental analyses on the complexes $[Co(R\text{-}py)_2Br_2]$.

R	calculated (found)		
	%C	%H	%N
3-Br	22.4	1.5	5.2
	(22.5)	(1.5)	(5.2)

TABLE 2.3 continued/

Elemental analyses on the complexes $[Co(R\text{-}py)_2Br_2]$.

R	calculated (found)		
	%C	%H	%N
3-Cl	26.9	1.8	6.3
	(26.9)	(1.8)	(6.3)
3-CH_3	35.6	3.5	6.9
	(35.6)	(3.5)	(6.9)
3-COC_6H_5	49.3	3.1	4.8
	(49.3)	(3.1)	(4.8)
3-$COCH_3$	36.5	3.1	6.1
	(36.6)	(3.1)	(6.1)
3-$CONH_2$	31.1	2.6	12.1
	(31.1)	(2.6)	(12.1)
3-$COOCH_3$	34.1	2.9	5.7
	(34.2)	(2.9)	(5.7)
3-COOH	31.0	2.2	6.0
	(31.6)	(2.3)	(6.0)
3,4-di-CH_3	38.8	4.1	6.5
	(38.9)	(4.1)	(6.5)
3,5-di-CH_3	38.8	4.1	6.5
	(38.8)	(4.2)	(6.6)
4-C_6H_5	49.9	3.4	5.3
	(50.0)	(3.4)	(5.3)
4-C_2H_5	38.8	4.1	6.5
	(38.9)	(4.1)	(6.5)
4-CH_3	35.6	3.5	6.9
	(35.5)	(3.4)	(6.9)

TABLE 2.3 continued/

Elemental analyses on the complexes $[Co(R\text{-}py)_2Br_2]$.

R	calculated (found)		
	%C	%H	%N
4-CN	33.8	1.9	13.1
	(33.8)	(1.8)	(13.2)
$4\text{-}COC_6H_5$	49.3	3.1	4.8
	(49.5)	(3.1)	(4.7)
$4\text{-}COCH_3$	36.5	3.1	6.1
	(36.8)	(3.1)	(6.1)
$4\text{-}CONH_2$	31.1	2.6	12.1
	(31.5)	(2.7)	(12.1)
$4\text{-}COOCH_3$	34.1	2.9	5.7
	(34.0)	(2.9)	(5.7)
$4\text{-}N(CH_3)_2$	36.3	4.4	12.1
	(36.3)	(4.4)	(12.0)

2.3 STRUCTURE OF THE COMPLEXES

The first study on the structure of $M(py)_2X_2$ type complexes, where X = halogens, using various physical methods was made by GILL *et al.*[16]. $[Co(py)_2Cl_2]$ exists in two modifications : a stable violet form and an unstable blue form. The high density violet form (D = 1.75) involves octahedrally coordinated cobalt atoms which are linked together by halide bridges, resulting in a polymeric structure. The blue isomer is tetrahedral, has a lower density (D = 1.50) and is monomeric. Recently, the existence of a second polymorph of the violet form, at low temperature,

has been demonstrated[17] and crystallographically determined by CLARKE and MILLEDGE[18]. A reversible solid-state phase transformation occurring between these two forms at about 150 K was observed and discussed[18].

The range of stable cobalt(II) complexes with substituted pyridines is given in Table 2.4. To our knowledge the crystal structures of only dichlorobis(pyridine)cobalt(II) and dichlorobis(4-methylpyridine)-cobalt(II)[23] have been reported. However, much data[24,25,26] is available on tetrahedrally and octahedrally coordinated Co from related structural species; the normal bond lengths for Co-N is 2.03 Å or 2.15 Å, respectively. The structures seem to be dependent upon which halogen and which substituent is present. The general factors which determine the stereochemistry of transition-metal halide complexes have been discussed by NYHOLM[27,28], who showed that other factors besides the purely electrostatic model in ligand field theory have to be taken in consideration. Various suggestions as to which is the most important and significant one in pyridine complexes have been developed.

Firstly, GILL *et al.*[16] assumed that the coordination number (CN) of the Co(II) ion depends on the polarizability of the ligands. In accordance with Pauling's electroneutrality principle, the authors state that the number of ligands which will be taken up by the metal is such as to reduce its charge to nearly zero. If the ligand is easily polarized, the charge transfer in each coordination bond is relatively large and the smaller of two possible CN's can be expected. Hence, the existence of the hexa-coordinated water ion and the tetra-coordinated chloride ion of cobalt(II) is understood.

Secondly, NELSON *et al.*[10] reported from the results of a thermodynamic investigation of the configurational equilibrium (1) in chloroform, that the nature of ligand X has a striking effect on the position

of the equilibrium. It is important to note that NELSON[10] evaluated the roles of the charge distribution in the metal-ligand bond in solution, i.e. in a situation where lattice forces are non-existent. The large variations in the equilibrium constants are explained in terms of entropy effects and correlations are made with the solid-state configurations, thereby confirming the interpretations of GILL. He suggested that the mechanism by which the electroneutrality principle operates, is not a simple inductive one but may well involve important mesomeric interactions between the central metal ion and the atoms attached to it. The effect of increasing charge transfer from X to M is to enhance the release of non-bonding metal *d*-electrons to anti-bonding pyridine π-orbitals. The extent of the $d\pi$-$p\pi$ overlap is strongly influenced by the nature of the halide in the order: I > Br > Cl.

Thirdly, Nelson's work is criticized by GRADDON *et al.*[19] who doubted the accuracy of the entropy data, since some dissociation of $[Co(py)_2X_2]$ into species of unknown constitution takes place. They were unable to find any evidence supporting the Co-N double bond or any difference in the bonding of the pyridine molecules in the octahedral and tetrahedral complexes from their ir spectra. To explain the relative stabilities of their complexes, the authors assumed a steric interaction between the non-bonding electron pairs on the ligands and the metal d-orbitals on the one hand and the non-bonding electron pairs of neighbouring ligands on the other. The CN of a metal atom is controlled by the number and distribution of the non-bonding electron pairs on the donor atoms; a restriction of CN can be expected when the number of electron pairs is large, and particularly if the electron clouds are also diffuse. Hence, establishing that the preference for octahedral stereochemistry increased in the order I << Br < Cl. A much smaller effect of the heterocyclic base, but in order of decreasing basicity, was observed in cobalt(II) halide complexes

with 4-substituted pyridines[29].

Some of the most important factors which will decide whether the complexes, listed in Table 2.4, adopt a monomeric tetrahedral or a polymeric octahedral form are summarized below. We believe that a delicate balance of these effects exists and a small change in the contribution of any one will govern the observed configuration.

(1) As stressed earlier[28], crystal field effects have a great influence. Some notable examples are found in Table 2.5. The greater driving force for NiL_2X_2 to form octahedral complexes corresponds to the higher stabilization by the d-orbital splitting energies in an octahedral field for the d^8 ion than for the d^7 ion. For Zn^{2+}, where of course no crystal field stabilization is possible, the tetrahedral structure is determined by ligand properties such as size, shape, polarizability and π-acceptor capacities.

(2) Within a series of complexes with the same metal, the stereochemistry is halogen-dependent. The complexes with pyridine, 4-bromopyridine and 4-phenylpyridine exist as the octahedral form in the chloro-isomer, but transform to a tetrahedral coordination if chloride is replaced by bromide.

(3) The dependence on the substituent is demonstrated in terms of intermolecular steric interaction between the pyridine molecules as a result of the substituent. In this case crystal packing is the deciding factor. Let us assume, as basis, the polymeric chain of $CoCl_2$ groups which is not expected to change much from the given parameters listed in Fig. 2.1. The pyridine rings lie in planes parallel to each other and perpendicular to the $CoCl_2$-plane. Any further deviations from this structure, as for instance, due to electronic effects of the substituent are neglected. By introducing substituents in the 4-positions of the ring, i.e. the marked point 'x' in Fig. 2.1, one can visualize that these groups have to

fit within 3.66 Å from each other in order not to be affected by strong repulsive forces. Thus, the size (2 X r_{vdw}) of the substituent-group must be smaller than the pyridine-pyridine separation, DS. The steric model allows us to explain the existence of the dimethyl- and the 4-methyl-pyridine complexes as tetrahedral, while, e.g., the phenylpyridine and the chloropyridine complexes can adopt the octahedral, polymeric form(+). In addition, the more obvious intramolecular steric effects do occur in such cases as the 2-methylpyridine or the 2-halogenopyridine compounds.

(+) values of van der Waals radii are taken from HUHEEY[30] and references cited therein.

group	r_{vdw}(Å)
CH_3	2.00
C_6H_5	1.70

TABLE 2.4

Stereochemistry of stable complexes of cobalt halides (chloro and bromo) with various substituted pyridines.

tetrahedral		octahedral	
$Co(py)_2Br_2$		$Co(py)_2Cl_2$	
$Co(\alpha\text{-pic})_2Cl_2$	(a)	$Co(2\text{-cyanopy})_2Cl_2$	(b)
$Co(\alpha\text{-pic})_2Br_2$	(a)	$Co(2\text{-cyanopy})_2Br_2$	(b)
$Co(\beta\text{-pic})_2Cl_2$		$Co(3\text{-cyanopy})_2Cl_2$	
$Co(\beta\text{-pic})_2Br_2$		$Co(3\text{-cyanopy})_2Br_2$	
$Co(\gamma\text{-pic})_2Cl_2$		$Co(4\text{-cyanopy})_2Cl_2$	
$Co(\gamma\text{-pic})_2Br_2$		$Co(4\text{-cyanopy})_2Br_2$	

TABLE 2.4 continued/

Stereochemistry of stable complexes of cobalt halides (chloro and bromo) with various substituted pyridines.

tetrahedral	octahedral
$Co(3,4\text{-lut})_2Cl_2$	$Co(nic)_2Cl_2$
$Co(3,4\text{-lut})_3Br_2$	$Co(nic)_2Br_2$
$Co(3,5\text{-lut})_2Cl_2$	$Co(isonic)_2Cl_2$
$Co(3,5\text{-lut})_2Br_2$	$Co(3\text{-Clpy})_2Cl_2$
$Co(2\text{-Clpy})_2Cl_2$ (c)	$Co(3\text{-Clpy})_2Br_2$
$Co(2\text{-Clpy})_2Br_2$ (c)	$Co(3\text{-Brpy})_2Cl_2$
$Co(2\text{-Brpy})_2Cl_2$ (c)	$Co(3\text{-Brpy})_2Br_2$
$Co(2\text{-Brpy})_2Br_2$ (c)	$Co(4\text{-Brpy})_2Cl_2$ (c)
$Co(4\text{-Brpy})_2Br_2$ (c)	$Co(3\text{-benzoylpy})_2Cl_2$
$Co(4\text{-Clpy})_2Cl_2$ (c)	$Co(3\text{-benzoylpy})_2Br_2$
$Co(4\text{-Clpy})_2Br_2$ (c)	$Co(4\text{-phenylpy})_2Cl_2$
$Co(4\text{-benzoylpy})_2Cl_2$	$Co(methnic)_2Cl_2$
$Co(4\text{-benzoylpy})_2Br_2$	$Co(methnic)_2Br_2$
$Co(4\text{-phenylpy})_2Br_2$	$Co(methisonic)_2Cl_2$
$Co(3\text{-ethylpy})_2Cl_2$ (d)	$Co(methisonic)_2Br_2$
$Co(3\text{-ethylpy})_2Br_2$ (d)	$Co(nicotinamide)_2Cl_2$
$Co(4\text{-ethylpy})_2Cl_2$	$Co(nicotinamide)_2Br_2$
$Co(4\text{-ethylpy})_2Br_2$	$Co(isonicotinamide)_2Cl_2$
$Co(4\text{-aminopy})_2Cl_2$	$Co(isonicotinamide)_2Br_2$
$Co(4\text{-dimethylaminopy})_2Cl_2$	$Co(3\text{-acetylpy})_2Cl_2$
$Co(4\text{-dimethylaminopy})_2Br_2$	$Co(3\text{-acetylpy})_2Br_2$
$Co(4\text{-hydroxypy})_2Cl_2$	$Co(4\text{-acetylpy})_2Cl_2$
$Co(4\text{-}tert\text{-butylpy})_2Cl_2$	$Co(4\text{-acetylpy})_2Br_2$

TABLE 2.4 continued/

Stereochemistry of stable complexes of cobalt halides (chloro and bromo) with various substituted pyridines.

tetrahedral	octahedral
$Co(4\text{-vinylpy})_2Cl_2$ (e)	$Co(4\text{-formylpy})_2Br_2$ (f)

α-pic = 2-methylpyridine, β-pic = 3-methylpyridine,
γ-pic = 4-methylpyridine, 3,4-lut = 3,4-dimethylpyridine,
3,5-lut = 3,5-dimethylpyridine, nic = 3-pyridinecarboxylic acid,
isonic = 4-pyridinecarboxylic acid, methnic = methyl-3-pyridinecarboxylate,
methisonic = methyl-4-pyridinecarboxylate,
(a) ref.19, (b) ref.20, (c) ref.21, (d) ref.22, (e) ref.8,
(f) ref.7.

TABLE 2.5

Stable structures of $M(py)_2X_2$ complexes.

M \ X	Cl	Br	I
$Co(d^7)$	o.p.	t.m.	t.m.
$Ni(d^8)$	o.p.	o.p.	t.m.
$Zn(d^{10})$	t.m.	t.m.	t.m.

o.p. = octahedral polymeric

t.m. = tetrahedral monomeric

Dist.	Co-Co	3.66
(Å)	Co-Cl	2.49
	Co-N	2.15
Angle	Co-Co-N	90°

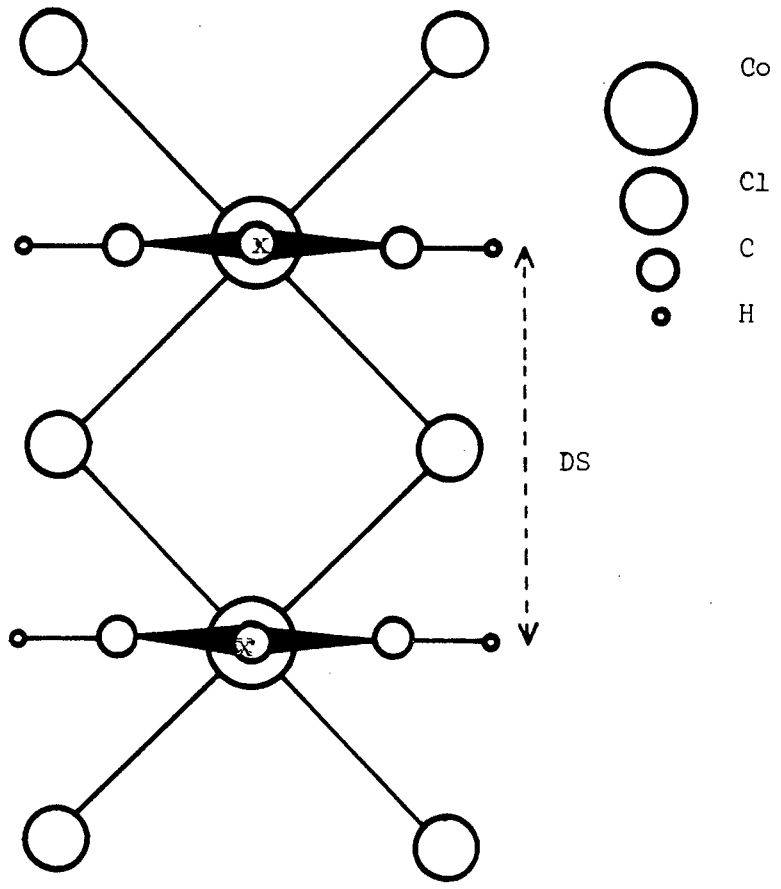

Fig. 2.1 : Structural parameters and a projection in the $CoCl_2$ - plane of the polymeric form $[Co(py)_2Cl_2]$.

The polymeric compounds have negligible solubility in most solvents. In suitable solvents which do not displace pyridine ligands from them, the octahedral complexes become four-coordinate as indicated by the blue colour of the solution. A summary of some relevant data on the highest energy transition, $^4A_2(F) \longrightarrow {}^4T_1(P)^*$ for tetrahedral systems[31] is given in Table 2.6. The visible spectra are given in Figs. 2.2 to 2.5. The absorption bands are complex envelopes because a number of transitions to doublet excited states are possible[32], and these acquire some intensity by means of spin-orbit coupling[33,34].

However, considering the relatively large and similar separations between the absorption maxima, an alternative explanation for the fine structure of the absorption band is the appearance of vibronically allowed transitions[+]. Although molecules exhibiting small vibrational frequencies would be expected to have the highest occupation of levels above the vibrational ground state[35], Fig. 2.6 shows that the population of the first excited state at room temperature becomes unimportant for energy separations greater than 400 cm^{-1}. Furthermore, the populations of successively higher levels decrease exponentially. Thus, hot bands originating from excited vibrational states of the electronic ground state are not expected to contribute in the absorption envelope. The distribution of the total absorption intensity over the transitions from the lowest vibrational level of the electronic ground state to higher vibrational levels in the excited state, is in accordance with the Franck-Condon principle. By promotion of an electron from a bonding or non-bonding orbital to an anti-bonding orbital, the bond of the molecule is considerably weakened and the equilibrium bond distance in the

---

* Symmetry consideration (C_{2v}) of the complexes of type CoL_2X_2 should split the visible band into three symmetry-allowed transitions, $^4A_2 \rightarrow {}^4A_2$, $^4A_2 \rightarrow {}^4B_1$ and $^4A_2 \rightarrow {}^4B_2$, as reported by J. FERGUSON, *J.Chem.Phys.*, 32(1960)528.

\+ A vibronic transition is a one-photon process which involves one quantum of vibrational energy, as compared to no quanto in a pure electronic transition[35].

TABLE 2.6

High-energy electronic (*d-d*) absorptions[a] of four-coordinated $[CoL_2X_2]$ complexes with substituted pyridines (in nm).

Ligand, L	X = Cl				X = Br			solvent
py	575[b]	608	634	660	594	630	644	chloroform
3-CH_3OCOpy	575	608	638	660	595	633	650	chloroform
4-CH_3OCOpy	574	605	638	663	595	631	648	chloroform
3-H_2NCOpy	590	655			620	650	680	acetonitrile
3-Clpy	590	630	662		618	672		acetonitrile
4-C_6H_5COpy	574	605	636	665	593	630	645	chloroform
4-H_2Npy	580	610	628					acetonitrile
4-$(CH_3)_2N$py	578	610	628					acetonitrile

[a] absorption maxima are underlined, other wavelengths correspond to shoulders

[b] estimated errors on maxima and shoulders are 2 and 5 nm, respectively

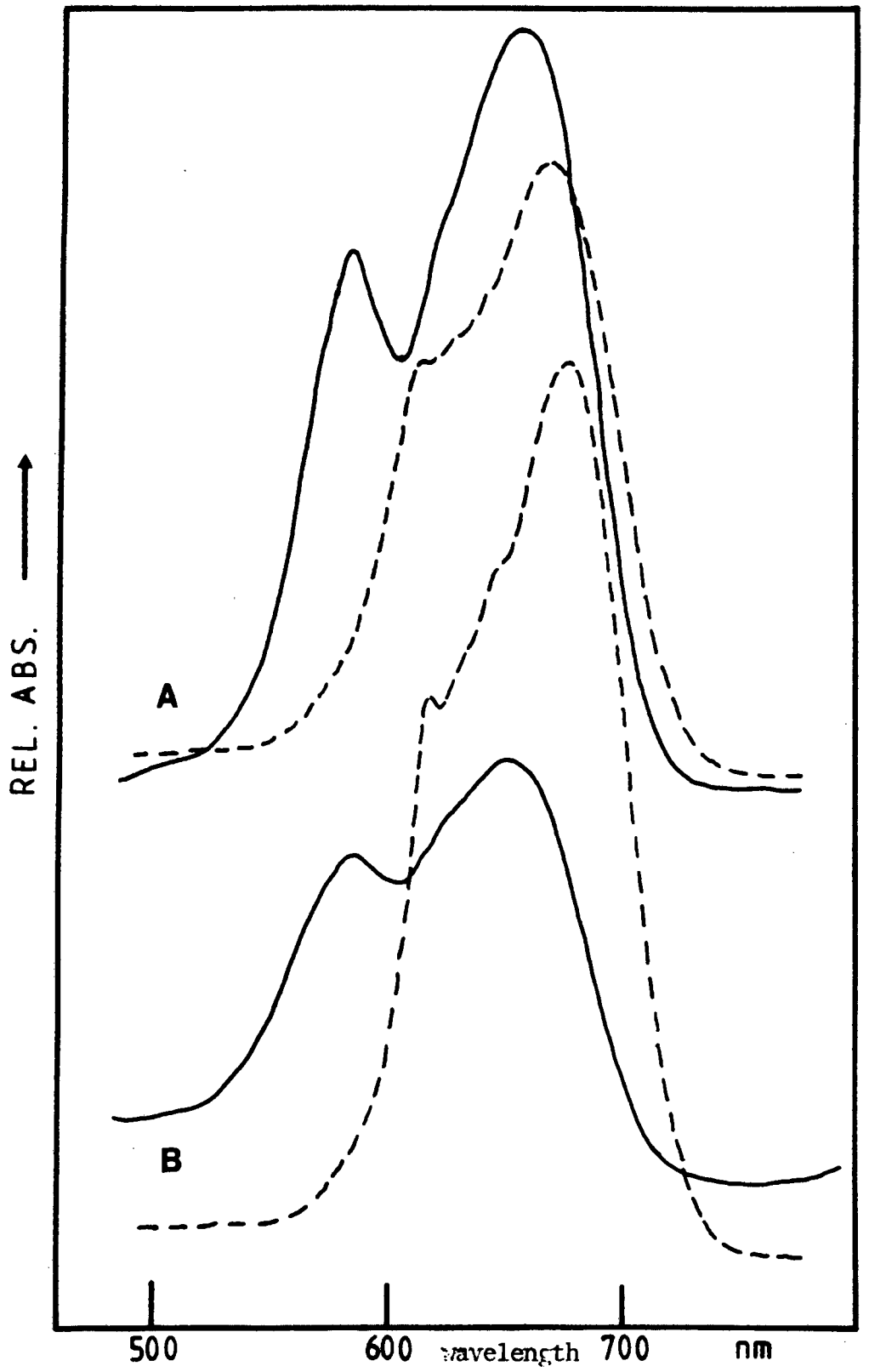

Fig. 2.2 : The visible spectra of A, $Co(3\text{-}Clpy)_2X_2$ and B, $Co(3\text{-}H_4NCOpy)_2X_2$, where X = Cl (——) or Br (– – –).

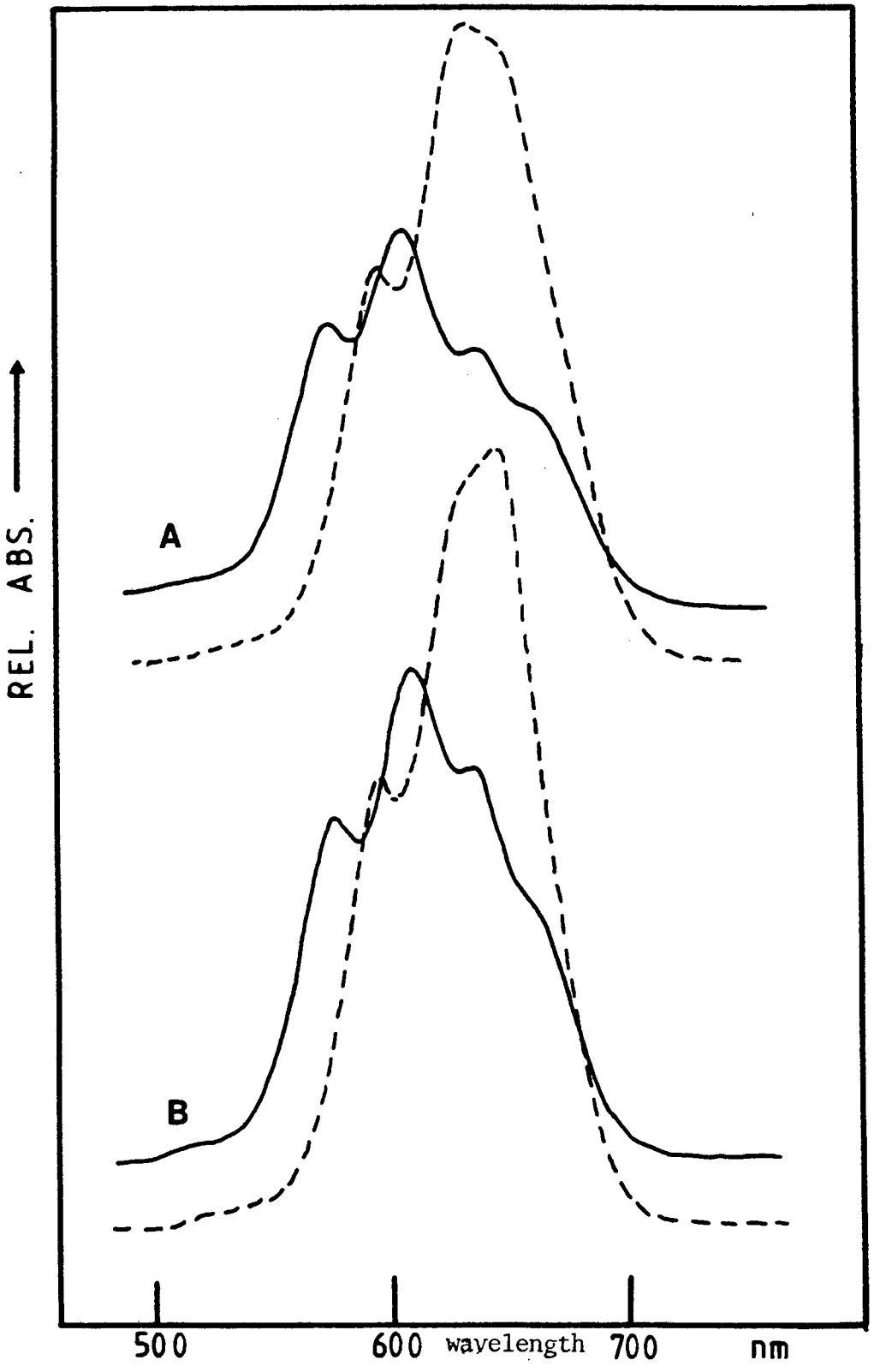

Fig. 2.3 : The visible spectra of A, $Co(4\text{-}C_6H_5COpy)_2X_2$ and B, $Co(py)_2X_2$, where X = Cl (———) or B (– – –).

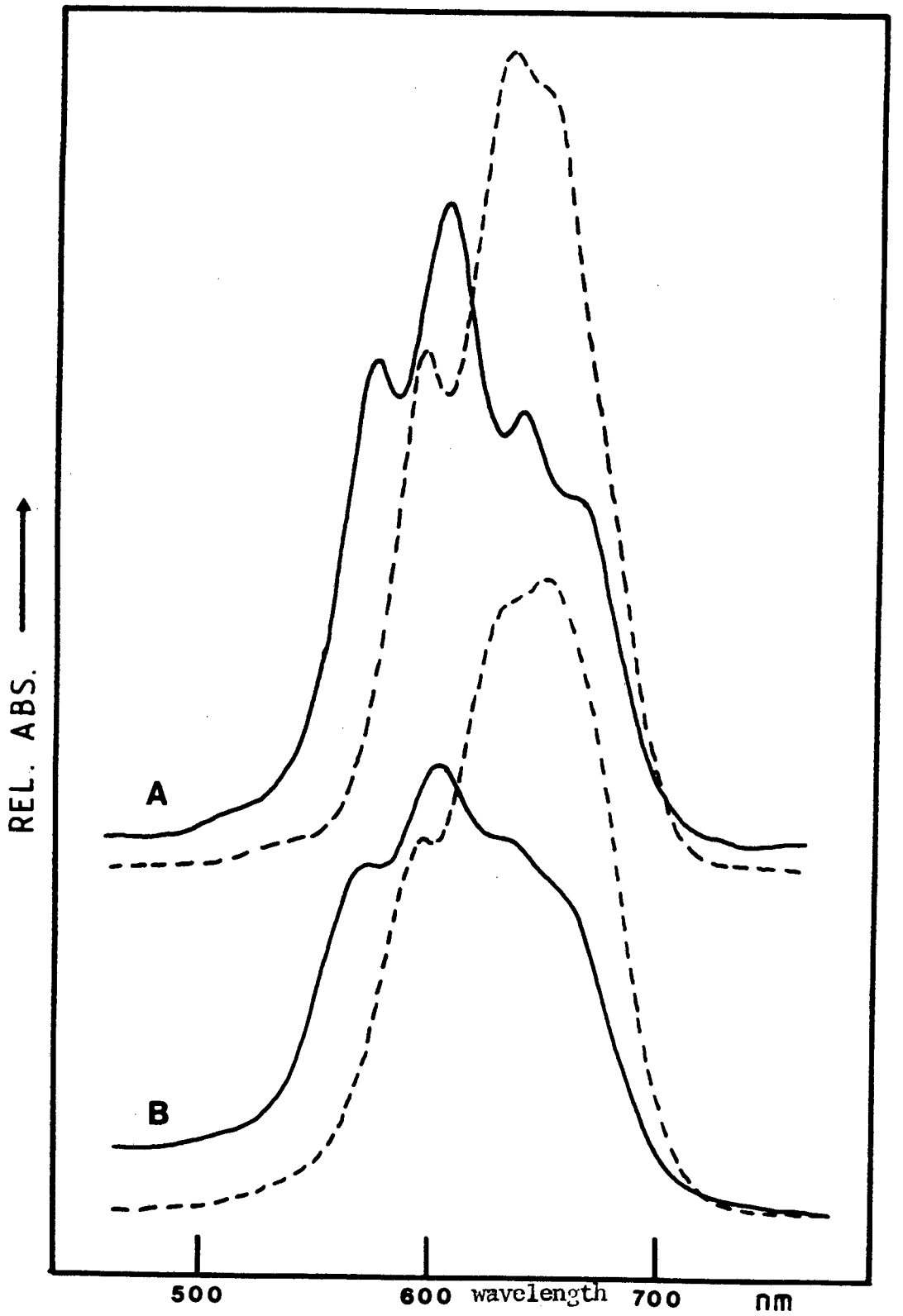

Fig. 2.4 : The visible spectra of A, $Co(4\text{-}CH_3OCOpy)_2X_2$ and B, $Co(3\text{-}CH_3OCOpy)_2X_2$, where X = Cl (——) or Br (— — —).

Fig. 2.5 : The visible spectra of

A, $Co(py)_2Cl_2$;

B, $Co(4\text{-}(CH_3)_2Npy)_2Cl_2$

and C, $Co(4\text{-}H_2Npy)_2Cl_2$.

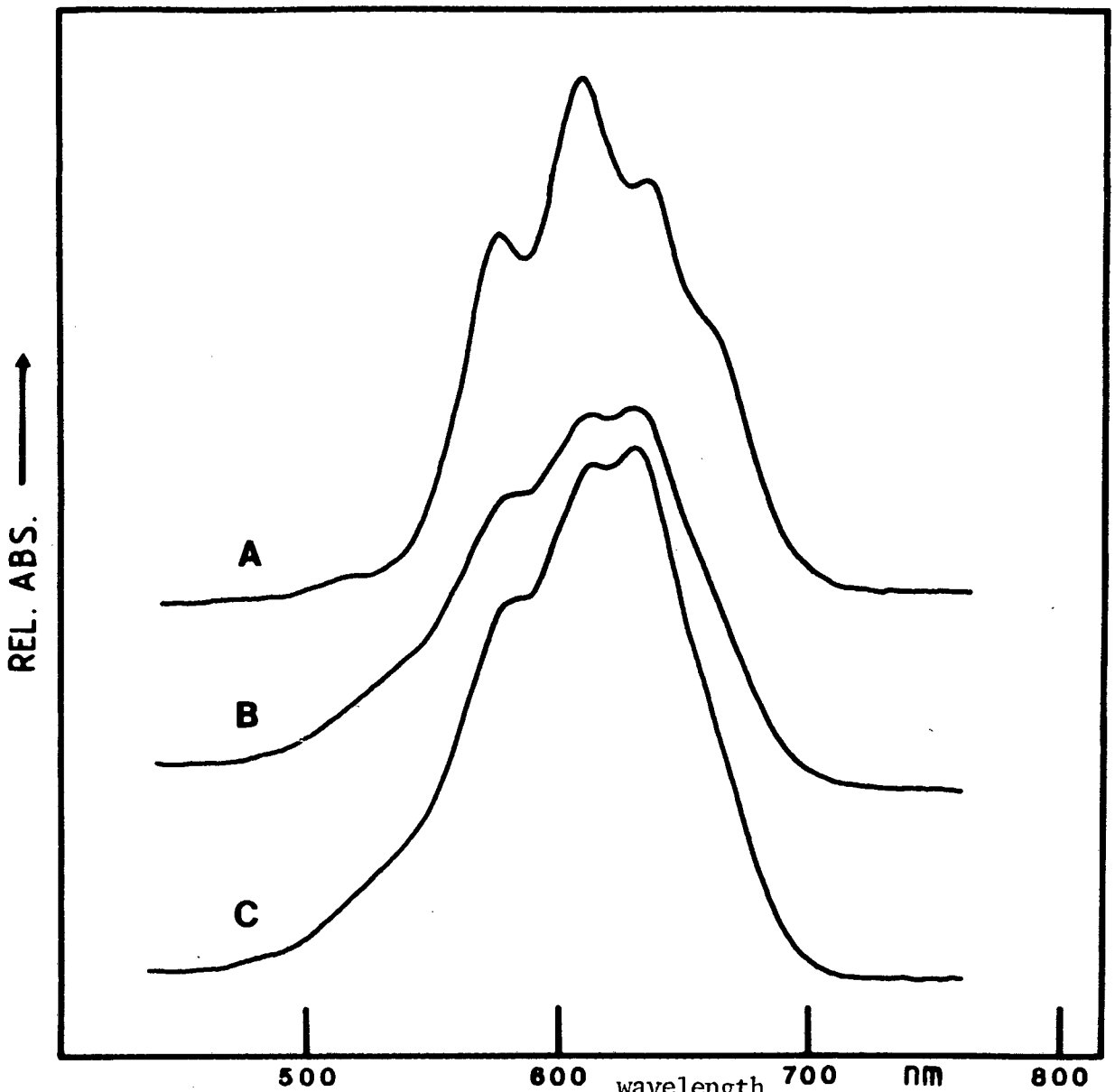

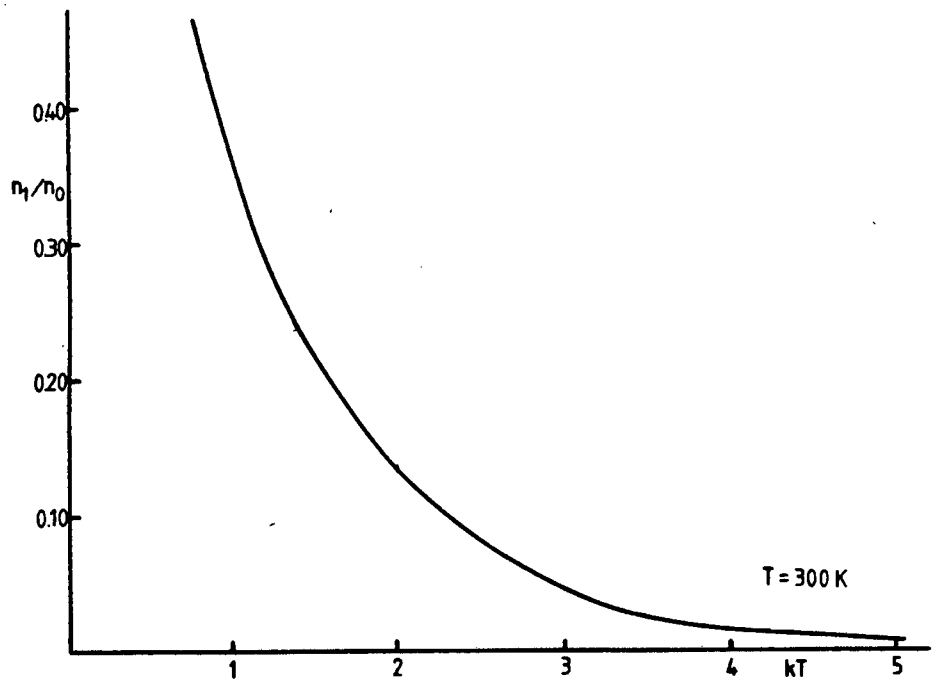

Fig. 2.6 : Relative thermal population of the lowest vibrationally excited state as a function of the energy level separation, expressed in terms of kT units. [1kT = 209 cm^{-1} at 300 K]

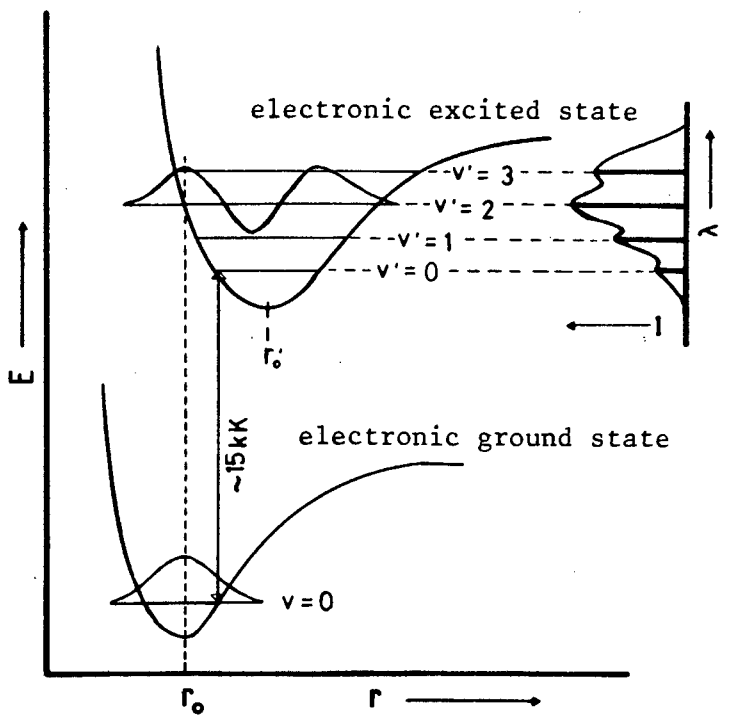

Fig. 2.7 : Illustration of the Franck-Condon principle, the vibronic transitions (0-1, 0-2, 0-3) and the relative intensities of the absorption bands.

excited state is greater than the corresponding distance in the ground state[36]. Fig. 2.7 illustrates the possible electronic transitions. The potential curves are drawn to give maximum overlap between v = 0 and v' = 2 vibrational wave functions. We see that the spacing between the vibronic transitions reveal some information on the vibrational frequencies of the molecule in its excited electronic state.

The methylpyridine complexes are more soluble. The electronic spectra of cobalt(II) complexes of all possible isomers of mono- and di-methylpyridines as well as two of the isomeric trimethylpyridines have recently been reported by VALLARINO and DARBY[37].

2.4 FAR-INFRARED VIBRATIONAL SPECTRA OF THE COMPLEXES

2.4.1 Methods of assigning metal-to-ligand vibrations

The normal modes of vibration give rise to observable infrared bands when, during the course of vibration, a change occurs in the dipole moment of the molecule. In order for a molecular vibration to be Raman active there must be a change in the induced dipole moment resulting from a change in the polarizability of the molecule. The most important spectral region for coordination compounds is the low-frequency region since direct information concerning the structure of the complex and the nature of the metal-ligand bonds can be obtained. However, the locations of the metal-ligand bands are often complicated by lattice (external) modes, intra- or inter-molecular interaction, lowering of symmetry and vibrational coupling.

Usually, reliable vibrational assignment of the metal-ligand frequencies are made by one or a combination of the methods, briefly described below.

1. A comparison of the spectra between the free ligand and its metal complex will show new bands in the low-frequency region (i.e. below about 600 cm^{-1}), attributable to the metal-ligand vibrations. However, care must be taken, since some ligand vibrations may be activated in this region by complex formation. The metal-ligand stretching bands will appear in the same spectral region for a series of metal complexes with similar substituted ligands. A comparison of the spectra of complexes in which the coordinated metal ion is changed through, e.g. the first transition series, will reveal shifts in metal-ligand stretching frequencies in sympathy with the contribution of the crystal field stabilization energy (CFSE)[38]. Typical double-humped curves are obtained in plotting νM-L versus 3d-orbital population of the metals. It is essential that such a series consist of structurally related complexes, i.e. identical coordination numbers.

2. Theoretical calculations of the metal-ligand frequencies can be undertaken, if a good estimation of the internal force constants and the molecular geometry are known. The parameters may be borrowed from parent model compounds.

3. A relatively simple method which leads in many cases to a clear-cut assignment, involves substitution of the metal and/or the ligand atoms directly bonded to the metal by stable isotopes[39].

3a. The metal isotope technique.

NAKAMOTO[40,41], firstly reported and utilized heavy metal isotopes in assigning metal-ligand vibrations of coordination compounds. Assuming that the force constants are unaltered by isotopic substitution, the metal-sensitive bands are shifted by the mass effect only. The magnitude of these shifts are relatively small but well outside the range of experimental error if a proper choice of the isotope is made. For the

pairs $^{64}Zn/^{68}Zn$ and $^{58}Ni/^{62}Ni$ having relatively larger mass differences, the observed shifts range from 5 to 2 cm^{-1} and from 10 to 3 cm^{-1} for the M-L stretching modes, respectively.

3b. The multiple isotopic labelling method.

This technique which involves mainly labelling the ligand atoms, is extensively used in this laboratory and experimentally proven to be by far the most reliable method[42]. Many cases are reported[43,44,45] where previous assignments based on the metal-isotope effect and/or a normal coordinate analysis, required substantial revision to account for the effects of multiple isotopic substitution. The largest shifts (up to about 900 cm^{-1}) can be expected by replacing hydrogen by deuterium atoms. It should be noted that metal-ligand vibrations as well as ligand vibrations involving the motion of the labelled atom, are shifted. The major limitation appears to be the cost and availability of stable isotopes and the unability of the isotopic substitution method in general, to distinguish clearly the M-L bending modes, since the bending modes are frequently shifted by less than 2 cm^{-1}. Insensitivity or reduced sensitivity of the metal-ligand bands to isotopic substitution will also result in complexes where strong vibrational coupling exists.

2.4.2 Discussion of the assignments of free pyridine

Numerous investigations of the Raman and infrared spectra of pyridine have been reported in the literature. We will summarise here only those contributions which we think are important and lead to the basis for a more accurate and secure vibrational assignment of free pyridine. The first extensive work was presented in a paper by KLINE and TURKEVICH[46] in which they have analysed the vibrational spectrum of pyridine by comparison with that of benzene. The assignment of the vibrational modes of

benzene has been made by WILSON[47] on a group-theoretical basis and extended by LANGSETH and LORD[48] to derivatives lacking degenerate vibrations. The remarkable similarity between the normal modes of the two molecules can be understood in the following way. Although the symmetry is changed from D_{6h} to C_{2v}, no drastic effects on force constants or large mass effects are introduced by replacing CH groups by the isoelectronic and nearly isobaric nitrogen atoms. By taking the normal modes of pyridine as those of benzene KLINE and TURKEVICH[64] were able to locate all the pyridine ring vibrations, but showed that the hydrogen vibrations could only be assigned tentatively. On passing from a monosubstituted benzene to pyridine three modes (numbers 7a, 9b and 17b) corresponding to one hydrogen stretch, one planar hydrogen bend and one out-of-plane bend, were omitted. The assignment as found by them together with the vibrational frequencies which they reported as averages from earlier, i.e., pre-1944, independent Raman and infrared studies, are given in column 2 of Table 2.7.

More reliable is the study by CORRSIN *et al.*[49] which involved additional spectroscopic data obtained from the spectra of pyridine-d_5 and the deuterated benzenes. The results appear in column 3 of Table 2.7. WILMSHURST *et al.*[50] have reported the infrared spectrum of pyridine and some deuterated derivatives in the vapour state. The band contours supported in most part the assignment of Corrsin but it was found necessary to reassign the b_2 frequencies to give agreement between calculated and observed thermodynamic functions within experimental error. The distribution of the fundamental frequencies according to Wilmshurst is given in column 4 of Table 2.7. The first normal coordinate treatment of pyridine was carried out by LONG and THOMAS[51]. Their approach to the force field in which valence force constants were transferred from benzene with due allowance for the change of symmetry, is based on the above stated similarity of the two molecules. The authors reported an average error

of 3.1% and concluded that the calculated frequencies are in agreement with the assignments of Wilmshurst; also the amendments introduced by the latter workers to the type b_2 modes are generally supported by the calculations.

Recently, DILELLA and STIDHAM[52,53] have provided excellent spectroscopic work. The liquid phase Raman and the liquid and vapour phase ir spectra of eight deuterium substituted pyridines were completely analysed, imposing sum and product rule constraints on the vibrational assignments. They suggested the appearance of a very weak Raman band at 1007 cm^{-1} as the highest b_2 fundamental, i.e., much higher than ever reported by most earlier investigators. Selection of this band was based on the explanation of the polarized Raman band at 1412 cm^{-1} as an a_1 combination band of b_2 fundamentals at 406 cm^{-1} and 1007 cm^{-1}. Further, they altered the two fundamentals in the region 700-750 cm^{-1}, locating the 703 cm^{-1} mode to an out-of-plane ring deformation (ν_{25}). Confirmation of their assignment was found by comparison of the calculated thermodynamic properties of pyridine with published experimental values. The fundamental frequencies reported by DILELLA[52] are shown in column 5 of Table 2.7.

Approximate force field calculations were performed by DRAEGER[54] on pyridine, its deuterated analogues and 19 methyl derivatives using the experimental frequencies of DILELLA. A modified valence force field was determined which reproduces the 777 observed frequencies within an average error of 0.98%. DRAEGER's reported vibrational fundamentals are given in column 6 or Table 2.7. Note that the choice of 1293 cm^{-1} as a fundamental is preferred above the usual 1345-1375 cm^{-1} band. The author stated that this band and the 1227 cm^{-1} in the same symmetry block, are mixed to a large extent. Both bands were calculated to be mainly C-C-H in-plane bends, and because the 1293 cm^{-1} mode has slightly

TABLE 2.7

The literature fundamental frequencies and assignments of pyridine

species	I	II (a)	II (b)	III	IV	V	VI	assignment[c]
a_1	ν_1	2	3054	3054	3054	3057	3079	
	ν_2	13	3054	3054	3054	3057	3057	ν(CH)
	ν_3	20a	3075	3036	3036	3057	3034	
	ν_4	8a	1580	1580	1583	1581	1581	
	ν_5	19a	1485	1482	1482	1483	1483	νring
	ν_6	9a	1139	1218	1218	1217	1217	
	ν_7	18a	884	1068	1068	1069	1067	δ(CH)
	ν_8	12	1028	1029	1030	1030	1030	
	ν_9	1	990	992	992	991	991	νring
	ν_{10}	6a	604	605	605	603	603	δring
b_1(R,IR)	ν_{11}	20b	3075	3083	3083	3079	3079	
	ν_{12}	7b	3054	3054	3036	3034	3034	ν(CH)
	ν_{13}	8b	1570	1572	1572	1574	1574	
	ν_{14}	19b	1440	1439	1439	1437	1437	
	ν_{15}	14	1723	1375	1375	1355	1293[d]	νring
	ν_{16}	3	1210	1217	1218	1227	1227	
	ν_{17}	15	1139	1148	1148	1146	1146	
	ν_{18}	18b	1037	1068	1085	1069	1069	δ(CH)

TABLE 2.7 continued/

The literature fundamental frequencies and assignments of pyridine

	I	II (a)	II (b)	III	IV	V	VI	assignment[c]
b_1(R,IR)	ν_{19}	6b	604	652	652	654	654	δring
a_2(R,-)	ν_{20}	17a	1061	981	981	980	980	γ(CH)
	ν_{21}	10a	747	886	886	884	884	
	ν_{22}	16a	404	374	374	380	380	γring
b_2(R,IR)	ν_{23}	5	941	942	942	1007[d]	941	γ(CH)
	ν_{24}	10b	710	749	886	941	884	
	ν_{25}	4	652	675	749	703	747	γring
	ν_{26}	11	669	703	700	747	703	γ(CH)
	ν_{27}	16b	374	405	405	406	406	γring

(a) Wilson's band numbering

(b) values from column 11 of Table 1 in paper of KLINE and TURKEVICH[46]

(c) description of mode based on AKYÜZ *et al.*[55] and references cited therein

(d) see text page 36

more C-C and C-N stretching character, it is assigned as the number 14 mode in benzene.

We can conclude that although the vibrational spectrum of pyridine has been studied many times, there remains some doubt regarding a number of vibrational modes of free pyridine, especially the controversial assignment of the b_2 fundamentals as demonstrated above.

2.4.3 Discussion of the assignments of complexed pyridine

(i) ligand vibrations

It is well established by various spectroscopists that most of the pyridine vibrations show definite increases in frequency on co-ordination. These shifts can be as much as 20 or 30 cm^{-1} for first-row transition metal complexes and are found to be metal-dependent[55]. Other modes of pyridine remain virtually unchanged in frequency, while the out-of-plane in-phase C-H bending mode (the "umbrella" mode, ν_{26} or number 11 in Wilson's notation) is the only band which exhibits a significant bathochromic shift. This remarkable fact will be discussed in Section 2.6 as a possible indication for the existence of π back-bonding in pyridine complexes. Competing explanations for the origin of these shifts are put forward by some workers. Firstly, FILIMONOV and BYSTROV[56] concluded that the elevation of the vibrational frequencies is associated with the donor-acceptor interaction mechanism. The strengthening of the bonds within the pyridine ring is explained by the change in hybridization which increases the s-character of the orbitals participating in each of the nitrogen σ-bonds on intermolecular interaction. The authors found confirmation from X-ray structural data, showing the enlargement of the C-N-C angle which takes place along with it. Secondly,

TAKAHASHI *et al.*[57] reported the frequency shifts of pyridine in several hydrogen donor solvents and were able to distinguish the hydrogen bonded from the non-hydrogen bonded bands for the in-plane ring vibrations, numbers 1, 6a, 8a and 19b, undergoing the largest shifts. They concluded that: "considerable changes of electron distribution which strengthen the chemical bonds within the ring" occurs, thus suggesting a change in the force field of the base on complexation. Thirdly, different interpretations involving mechanical interactions of the ligand vibrations with the stretching and bending vibrations generated by the hydrogen bond or the metal-to-ligand bond formations, are presented by CUMMINGS and WOOD[58] for the former and, by AKYÜZ *et al.*[55] for the latter bond type. In their paper on the intermolecular force field of the hydrogen bond, CUMMINGS and WOOD[58] examined several hydrogen bonded phenol-pyridine complexes. The notable outcome of their calculations is that most of the shifts are accounted for by the presence of the intermolecular force field alone, together with changes in the phenol C-O-H bending force constant, but without any significant changes in the internal force constants of pyridine. Finally, we mention the simplified normal coordinate analysis on a coordinated model of pyridine, as performed by AKYÜZ *et al.*[55], which shows that kinetic coupling of the a_1 modes with the metal-ligand stretching mode is responsible for the upward shifts in frequency. Contrary to TAKAHASHI *et al.*[57] these authors stated that the force fields of free and coordinated pyridine will be very similar, since with any definite changes in the force field of the ring, it is expected that all such ring vibrations should be affected, which is clearly not the case. Hence, the electron density over the aromatic ring must remain approximately constant upon coordination. It is suggested, also by GILL *et al.*[59], that back-bonding from the metal plays a part in maintaining a constant electron density.

In the survey on metal-ligand and related vibrations by ADAMS[12], we read that : "Although the spectrum of complexed pyridine is little changed from that of the free base, the minor shifts or splittings are related to the stereochemistry of the complexes". In other words, the positions of the pyridine bands can be used to determine the stereochemistry, since the ring vibrations are sensitive to the structural arrangement of the pyridine molecules. CLARK and WILLIAMS[60] initially indicated that the magnitude of the shift of the 604 cm^{-1} band (number 6a) upon co-ordination to a given metal is distinctive for complexes with tetrahedral and octahedral stereochemistry. We observe that the lowest ligand band (number 16b) occurs at 425 cm^{-1} for the tetrahedral form and at 432 cm^{-1} for the octahedral form of $[Co(py)_2Cl_2]$. In the spectra of the monomer (Fig. 2.60 D) this band shows additional splitting : a shoulder on the low-frequency side at about 420 cm^{-1}. The magnitudes of such shifts appear to be independent of the halogen. However, disagreement exists wherever ir data are used as the only criterion in assessing the stereochemistry of complexes where pyridine is being replaced by its derivatives. GILL and KINGDON[21] reported that too small differences between the spectra of tetrahedral and polymeric octahedral complexes with methyl and halogen-substituted pyridine exist, to make such a clear distinction. This is in contrast with a statement by GRADDON and WATTON[19]. We conclude that, while major shifts can be related to the overall configuration of the complex, the splittings are probably due to (1) the interaction of the pyridine molecules in the primitive cell, (2) lattice symmetry splitting, or (3) small rotations of pyridine around the metal-ligand bond, allowing small distortions to relieve steric strain in some complexes (cf. Sec.2.3).

The assignments of the ligand vibrations in the spectrum of $Co(py)_2X_2$ are straightforwardly made in accordance with previous work[61,62].

The vibrational analyses for the pyridine and the pyridine-d_5 complexes are given in Tables 2.8 and 2.9. The ratio between the corresponding bands (deuterated:undeuterated) falls into the range 0.94 ± 0.04 for the ring vibrations (numbers 8a, 8b, 19a, 14, 12, 1, 6a, 16b) and in the range 0.79 ± 0.06 for the vibrations involving the C-H modes (numbers 3, 9a, 15, 18a, 18b, 17a, 10a, 10b, 5, 11). A single exception is noted for the band (number 16a) near 380 cm^{-1} which yields an anomalously low ratio of 0.86, being essentially a ring vibration.

The application of the ratio, ν^D/ν^H, has been proven by THORNTON and co-workers to be distinctive for the C-H stretching or bending modes and the ring stretching or bending modes of quinoline, aniline, pyridine[63], pyrazine[64] and imidazole[65,66] in metal complexes. Distinction between these coordinated ligand modes and the metal-ligand modes may also be achieved since the latter generally yield ν^D/ν^H ratios very close to unity.

(ii) metal-ligand vibrations

In the earliest far-infrared studies on the metal halide complexes containing nitrogen-donor ligands, the metal-halogen stretching modes could be unambiguously assigned to the most intense bands, supported by the effects of halogen substitution. Aroung 1965, only tentative locations of the metal-nitrogen stretching frequencies were reported by CLARK and WILLIAMS[60], ALLAN *et al.*[68], McWHINNIE[69], FRANK and ROGERS[70] and GILL and KINGDON[21], because these bands occur near the limits of detection for the spectrometers used at that time. Data on metal-ligand vibrations and their assignments became more reliable when they were based on the effects of isotopic substitution and variable temperature experiments, as reported by LEVER *et al.*[71]. In the absence of isotopic data, the identification of

TABLE 2.8 Infrared frequency data (cm^{-1}) and assignments for $[Co(py)_2X_2]$, where X = Cl and Br.

chloro-		bromo-		Assignment	
solid	mull	solid	mull		
3105w	3110w			20b	ν(C-H)
3063w	3070w			2	
3040w	3045w			13	
300w	3005vw			20a,7b	
1645vw	1645w		1657vw	1 + 6a	
1607vs	1606vs	1607vs 1598sh	1607vs 1595sh	8a	ν(ring)
1577w	1578w	1571vw	1571w	8b	
1493vs	1493vs	1488s 1485.5s	1485s	19a	
1450vvs	1450vs	1447vvs	1446.5vs	19b	
1400vw	1405vvw				
1365w	1366w	1357vwbr		14	
1240w	1241m	1240vwbr	1240w	3	δ(C-H)
1222m	1222s	1217.5sh 1215m	1217sh 1215s	9a	
1151mw	1152m	1160w 1154sh	1160m	15	
1085ms	1084vs			18b	
1062vw	1061w	1067s	1066s		
1043ms	1043vs	1045.5s	1044.5s	12	ν(ring)
1015ms	1014vs	1014.5m 1009sh	1014s 1009sh	1	
954vw	952vw		940vw		

TABLE 2.8 continued/

chloro-		bromo-		Assignment	
solid	mull	solid	mull		
878vw	878vw	880vvw	883w	10b	
760vs	759vs	759s	759s	4	
757sh					
750m		750s	750s		
692vvs	692vvs	695.5vs	694vs	11	γ(C-H)
		689vs	686vs		
		676m	675msh		
636s	635s	643s	642.5s	6a	δ(ring)
432s	432s	425m	424.5s	16b	γ(ring)
		418w	417.5sh		

TABLE 2.9 Raman frequency data (cm^{-1}) and assignments for pyridine, $[Co(py)_2Cl_2]$ and its d_5-labelled analogue.

pyridine[a]			$[Co(py)_2Cl_2]$			Assignment[b]	
unlabelled	d_5	ratio	unlabelled	d_5	ratio		
A	B	B/A	C	D	D/C		
1582	1551	0.98	1610	1558	0.97	ν_4	
1574	1537	0.98	1577	1533	0.97	ν_{13}	
1483	1339	0.90	1493			ν_5	ν(ring)
1438	1301	0.90				ν_{14}	
1355	1230	0.91				ν_{15}	
1227	1041	0.85	1247	1010		ν_{16}	
1217	887	0.73	1232	977		ν_5	δ(C-H)
1147	867	0.76	1157	897	0.78	ν_{17}	
1069	838 824	0.78 0.77	1080			$\nu_7+\nu_{18}$	
1031	1009	0.98				ν_8	ν(ring)
1007	824	0.82	1020	837	0.82	ν_{23}	γ(C-H)
991	963	0.97				ν_9	ν(ring)
980	815	0.83				ν_{20}	
942	769	0.82	950			ν_{24}	
884	690	0.78		690		ν_{21}	γ(C-H)
750	633	0.84	737			ν_{25}	
709	535	0.75				ν_{26}	
653	625	0.96	651	623	0.96	ν_{19}	δ(ring)
604	582	0.96	632 527	607	0.96	ν_{10}	
407	370	0.91				ν_{27}	γ(ring)
380	328	0.86	352			ν_{22}	
			213	210	0.99		ν(Co-N)
			158	150	0.95		δ(Co-N)

(a) experimental data from DILELLA and STIDHAM[52].

(b) the band numbering system is identical to that of LONG and THOMAS[67]; for a relation to Wilson's band numbering, see Table 2.7.

these internal vibrational modes is accomplished with great difficulty since coupling with ligand modes of the same symmetry will generally occur. In recent work, more systematic investigations such as the effects of varying the metal atom[14], ligand base strentsh, ligand electronic and steric factors have been carried out. LEVER *et al.*[72], BURGESS[73], GOLDSTEIN*et al.*[74], VALLARINO *et al.*[37] showed that the metal-ligand vibrational frequencies are markedly influenced by the mass and the electronic and steric effects of the substituents in the pyridine ring. Although the pyridine-metal halide complexes were among the first compounds to be studied by far-infrared spectroscopy, there remains some controversy about the location of the metal-ligand modes, particularly the bending vibrations. This is partly a result of the occurrence of these bands at very low energies, usually below 160 cm^{-1}, where they are expected to couple with lattice (external) vibrations.

An illustration of the assignment problem of $[Zn(py)_2Cl_2]$ is summarized in Table 2.10, which shows the markedly different frequencies proposed by various investigators. NAKAMOTO *et al.*[76] based their results on substitution effects arising from the ^{64}Zn and ^{68}Zn isotopes and deuterated pyridine (py-d_5). Both Raman and ir spectra were reported. From pressure and temperature dependence studies of the Raman-active frequencies, WONG[77,78] calculated strong coupling between the internal vibrational modes. Furthermore, coupling of these fundamentals with the lattice vibrations in the crystal became apparent. More recently, THORNTON *et al.*[79] supported the assignment made by Nakamoto. Nevertheless, the Zn(II) complex is the one which is the most widely studied and assignments concerning the stretching modes exhibit the greatest measure of agreement among the various investigators.

The structural characterization of metal complexes by means of their far-infrared band patterns below 400 cm^{-1} is now well established

TABLE 2.10

Differences in the low-frequency assignments of $[Zn(py)_2Cl_2]$.

fundamental mode at (cm^{-1})	reported assignments of POSTMUS *et al.* 1967[75]	NAKAMOTO *et al.*[76] 1972 THORNTON *et al.*[79] 1978	WONG[77,78] 1974-75
326	ν_{as} Zn-Cl	ν_{as} Zn-Cl	ν_{as} Zn-Cl
296	ν_{s} Zn-Cl	ν_{s} Zn-Cl	ν_{s} Zn-Cl + δCl-Zn-Cl
220	ν Zn-N	ν_{as} Zn-N	ν_{as} Zn-N + δCl-Zn-N
202	δZn-Cl	ν_{s} Zn-N	δCl-Zn-Cl + ν_{s} Zn-Cl
153	δ Zn-N	δN-Zn-N	lattice vibration
141	lattice	δCl-Zn-N	ν_{s} Zn-N + δCl-Zn-Cl
106	vibrations	δCl-Zn-Cl	δCl-Zn-N + ν_{as} Zn-N

and applied. Symmetry considerations require two νM-N and two νM-X ir-active modes for tetrahedral complexes of formula ML_2X_2 with C_{2v} symmetry. We adopt the band numbering : ν_1 and ν_2 for νM-X and ν_3 and ν_4 for νM-N. Similarly, for polymeric octahedral complexes $[ML_2X_2]$ of C_i summetry one νM-N and two νM-X ir-active modes are expected. An alternative way of treating the vibrations of chain polymers will be referred to later in this Section. Previous work in this department involved the assignment of the νM-N and νM-X bands of metal chloride complexes of pyridine[80] on the basis of the band shifts induced by deuteration of the pyridine ring and by varying the coordinated metal ion. Since the spectra were recorded down to 150 cm^{-1} only one deformation mode, ν_5 (for δN-M-N), could be located. In this work, we have extended the lower spectral region to 50 cm^{-1}, in order to obtain information on the other deformation modes e.g. ν_6 and ν_7 which are δN-M-X and δX-M-X, respectively.

It is well known that the Zn(II) and blue Co(II) halide complexes or pyridine are isostructural[81], both exhibiting tetrahedral coordination. Because of the very close similarity: a band-for-band correspondence of the spectra of both complexes is observed (see Fig. 2.8), assignment of the parent $[Co(py)_2X_2]$ complexes may be made with confidence. Table 2.11 shows our assignment and frequency data for all halide-analogues of Zn(II) and Co(II). The results agree very well with those reported in the literature. The assignment of the spectra, taking into account the coupling between the metal-ligand modes in the bromo- and iodo-analogues[76], is further supported, firstly by the shifts to lower frequencies of the metal-ligand modes involving the halogen atom, X, when X is progressively changed from Cl to Br to I, and secondly, by the work of BARANOVSKII and MAZO[82]. These authors reported

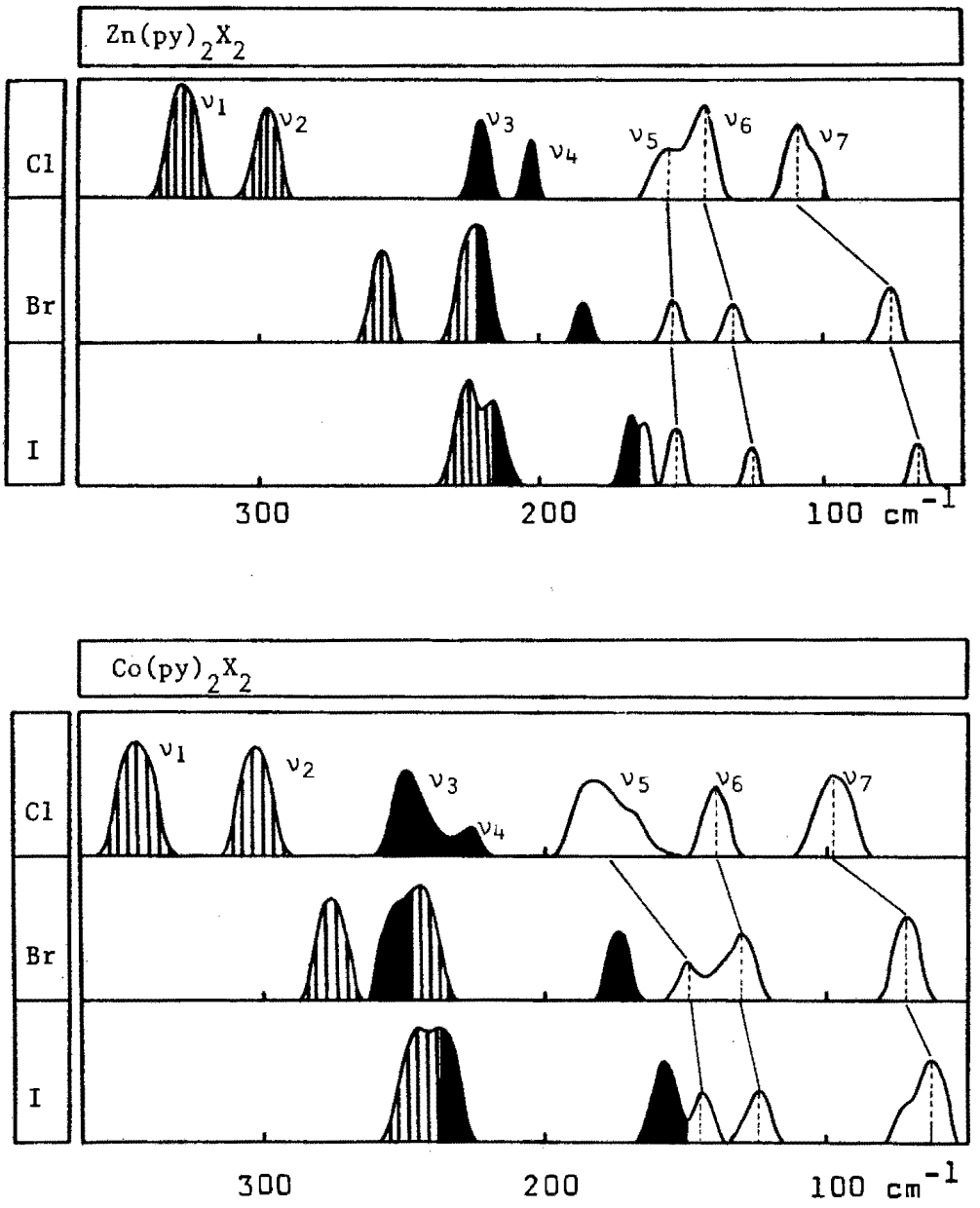

Fig. 2.8 : The far-infrared spectra of tetrahedral $M(py)_2X_2$ complexes. Bands with vertical bars: νM-L ; solid bands: νM-X ; ν_5, ν_6 and ν_7 are the deformation modes.

TABLE 2.11 Frequencies (cm^{-1}) and assignments of infrared bands in the spectra of tetrahedral $M(py)_2X_2$ complexes.

compounds	νM-X	νM-N	δN-M-N	δN-M-X	δX-M-X	other bands	ref.
$Zn(py)_2Cl_2$	327vs 295s	219s 201m	154sh	140s	102s		
$Zn(py)_2Br_2$	255s 221vs[a]	221vs[a] 182w	153w	130m	77m		
$Zn(py)_2I_2$	224vs 215sh	215sh[a] 166m	150sh	123m	64wbr	159sh	
$Co(py)_2Cl_2$	347vs 304vs	251s 226m	168m	138s	98mbr	185m	
	347(346)[b] 306(305)	253(243)		142(140)	101(104) 94(92)		82
$Co(py)_2Br_2$	277vs 244vs	253sh 175m	150w	131m	72s		
	277(280) 252sh	246(244)			74(66)	181 176(176) 151 LM 132 LM	82
$Co(py)_2I_2$	246vs 238vs[a]	238vs[a] 159s	145m	125m	76sh 64s		
	240(235)	247			68(56)	265sh 161(158) 145(146) 125 LM	82

[a] overlapped by other band ; LM represents lattice mode

[b] values in brackets were obtained by the authors in $CHCl_3$ solution

solution spectra of $[Co(py)_2X_2]$, enabling them to assign some bands to lattice vibrations. Because of the low signal-to-noise ratio of the published solution spectra and, the fact that not all of the observed bands were assigned, some doubts may rise on the information obtained. Nevertheless, we may conclude that the lattice vibrations are relatively weak and unimportant above 100 cm^{-1}. This is not surprising, since the coordination compounds in question comprise mainly covalently bonded molecules. A comparison of the stretching frequencies in Table 2.11, shows that those of the Co(II) complex are between 32 and 7 cm^{-1} higher than those of the Zn(II) complex. This is mainly attributed to the crystal field stabilization for the d^7 ion. The effect of the greater ionic mass of Zn is unimportant.

Ideally, one should record solution measurements to be certain that lattice vibrations and other solid-state effects will be eliminated and not be responsible for any complications in the ir spectra. However, most of the monomeric $[Co(R\text{-}py)_2X_2]$ complexes have limited solubility in solvents which are suitable for the spectral region being investigated and which will not themselves displace any ligands; also, background absorption arising from the solution will obscure any information below about 250 cm^{-1}. As already mentioned, the polymeric complexes are virtually insoluble in all solvents. Hence, only solid state (pellets or mulls) spectra are reproduced in this work. We may refer to the results of CLARK and WILLIAMS[60]: "the frequency of a given band in solution is only slightly higher than in the solid state, and the band shapes are unchanged". The far-infrared spectra of tetrahedral and octahedral $[Co(R\text{-}py)_2X_2]$, where X = Cl, Br or I, are depicted in Figs. 2.9 to 2.56, where bands observed in the ligand spectra are marked by 'L'.

The assignment of the metal-ligand modes of tetrahedral $[Co(R\text{-}py)_2X_2]$ complexes are shown in Tables 2.12 and 2.13. The observed stretching

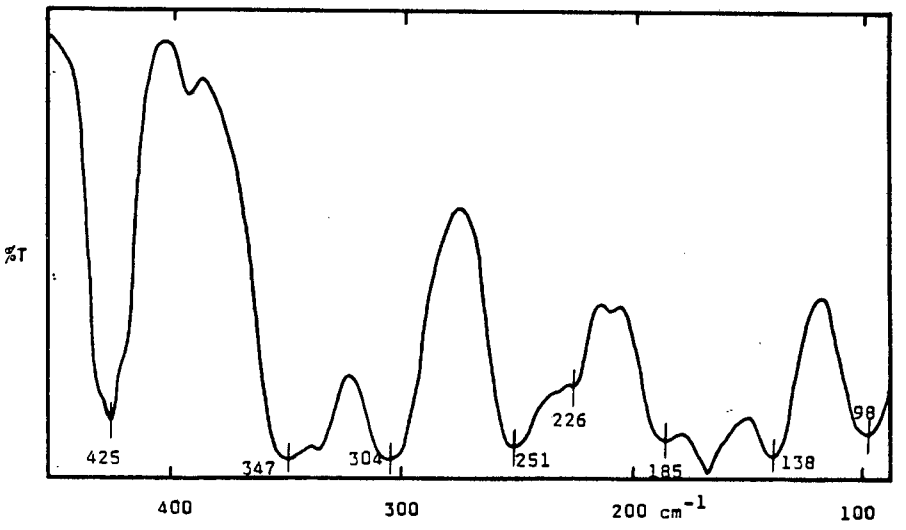

Fig. 2.9 : The far-infrared spectrum of $Co(py)_2Cl_2$.

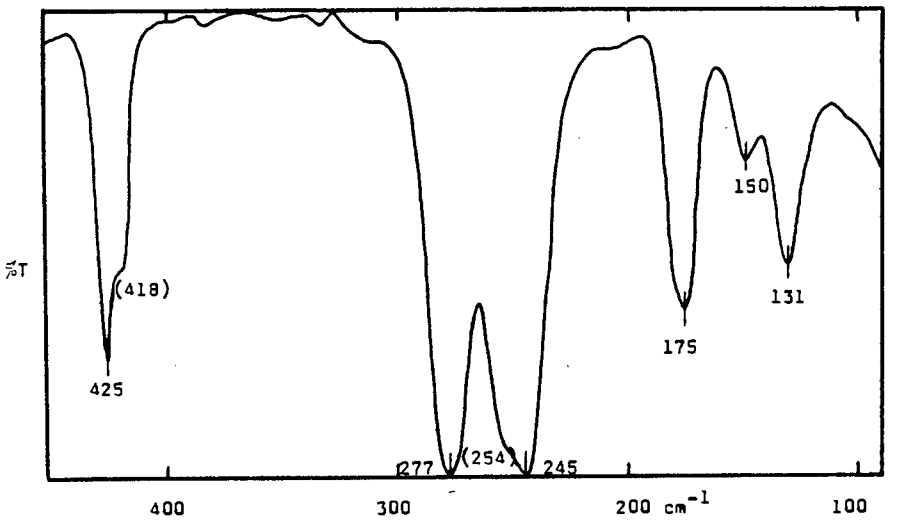

Fig. 2.10 : The far-infrared spectrum of $Co(py)_2Br_2$.

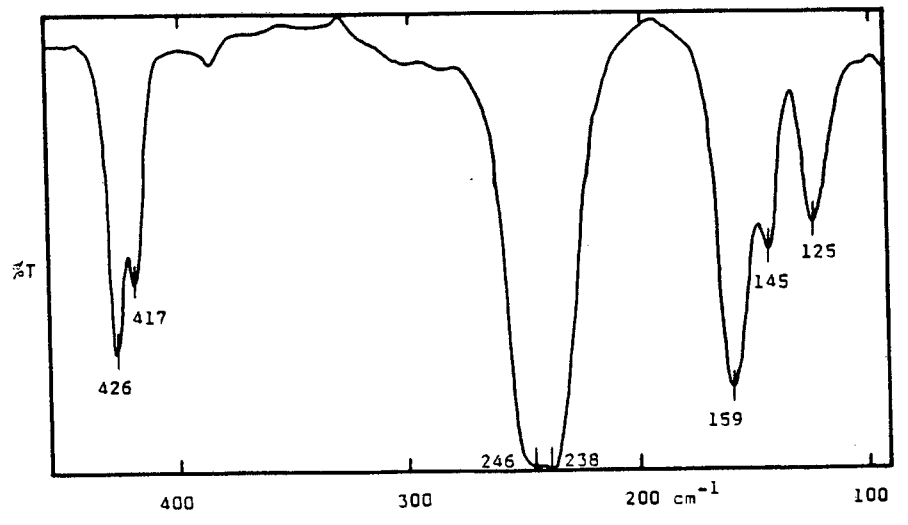

Fig. 2.11 : The far-infrared spectrum of $Co(py)_2I_2$.

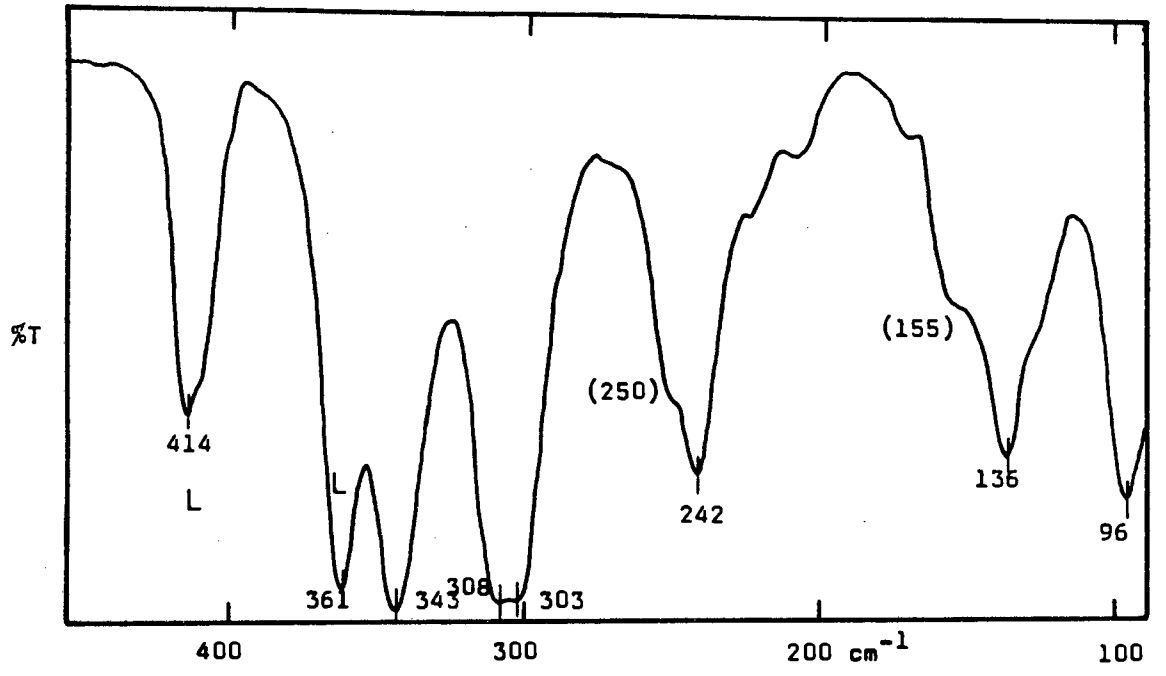

Fig. 2.12 : The far-infrared spectrum of $Co(3\text{-}CH_3py)_2Cl_2$.

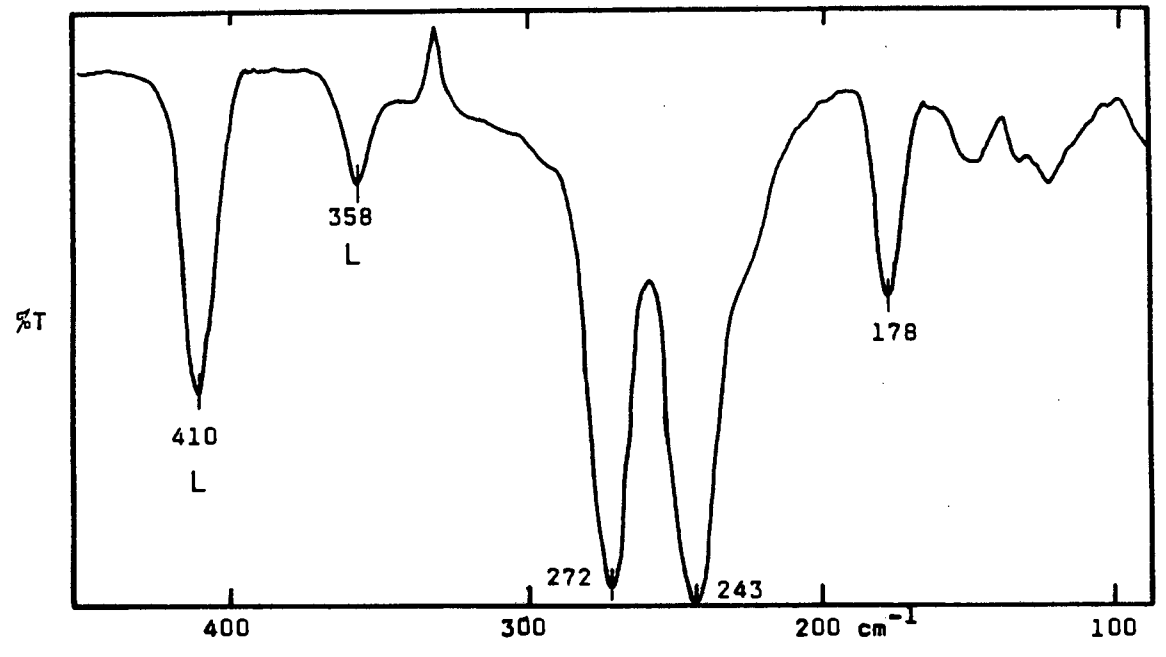

Fig. 2.13 : The far-infrared spectrum of $Co(3\text{-}CH_3py)_2Br_2$.

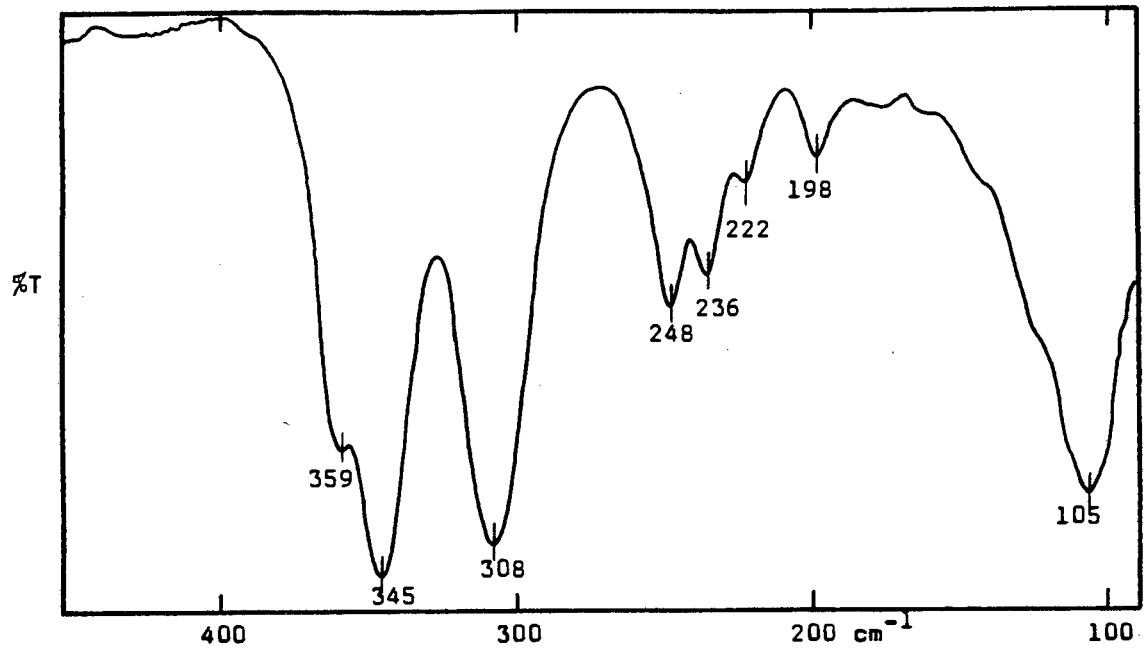

Fig. 2.14 : The far-infrared spectrum of $Co(4\text{-}CH_3py)_2Cl_2$.

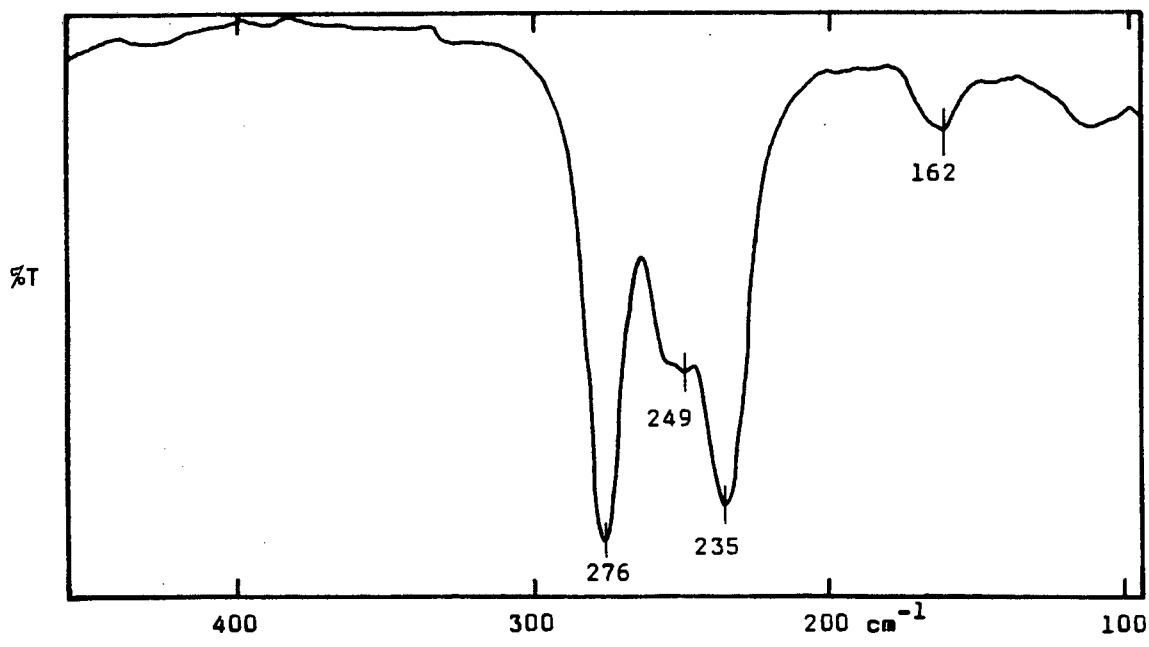

Fig. 2.15 : The far-infrared spectrum of $Co(4\text{-}CH_3py)_2Br_2$.

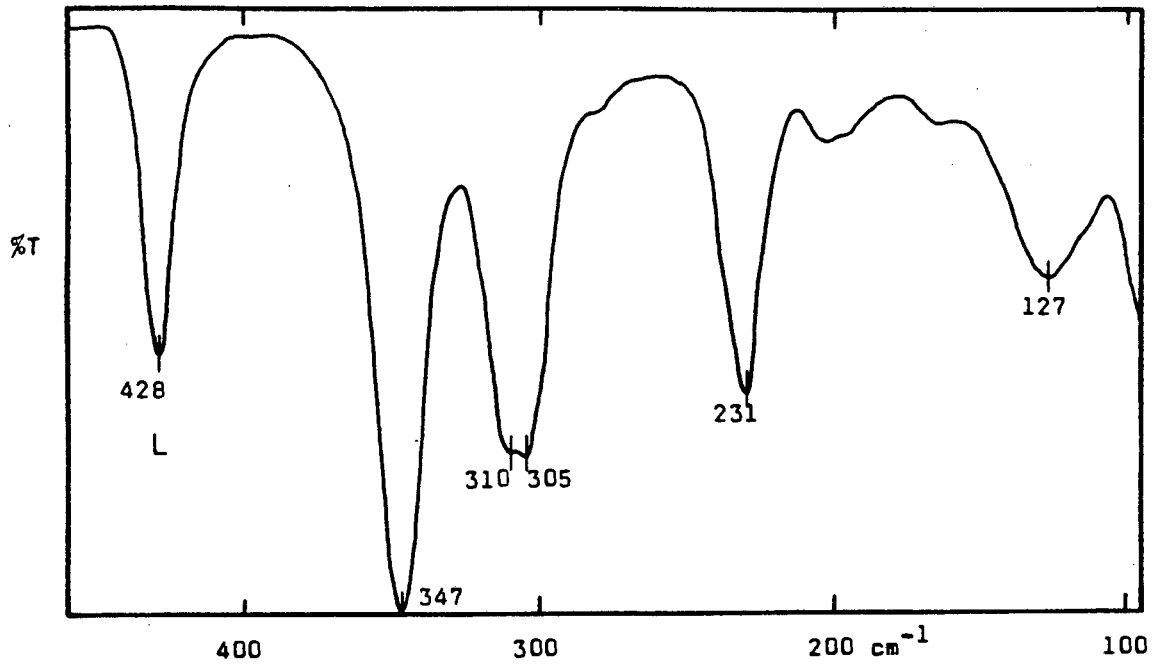

Fig. 2.16 : The far-infrared spectrum of $Co(3,4\text{-di-}CH_3py)_2Cl_2$.

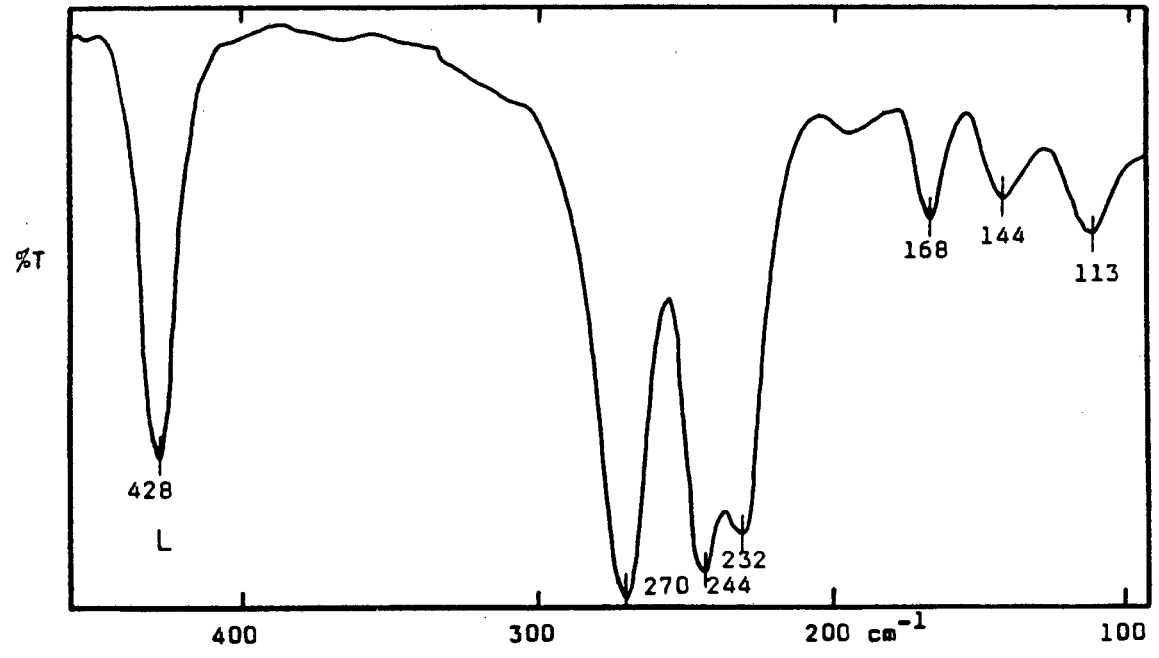

Fig. 2.17 : The far-infrared spectrum of $Co(3,4\text{-di-}CH_3py)_2Br_2$.

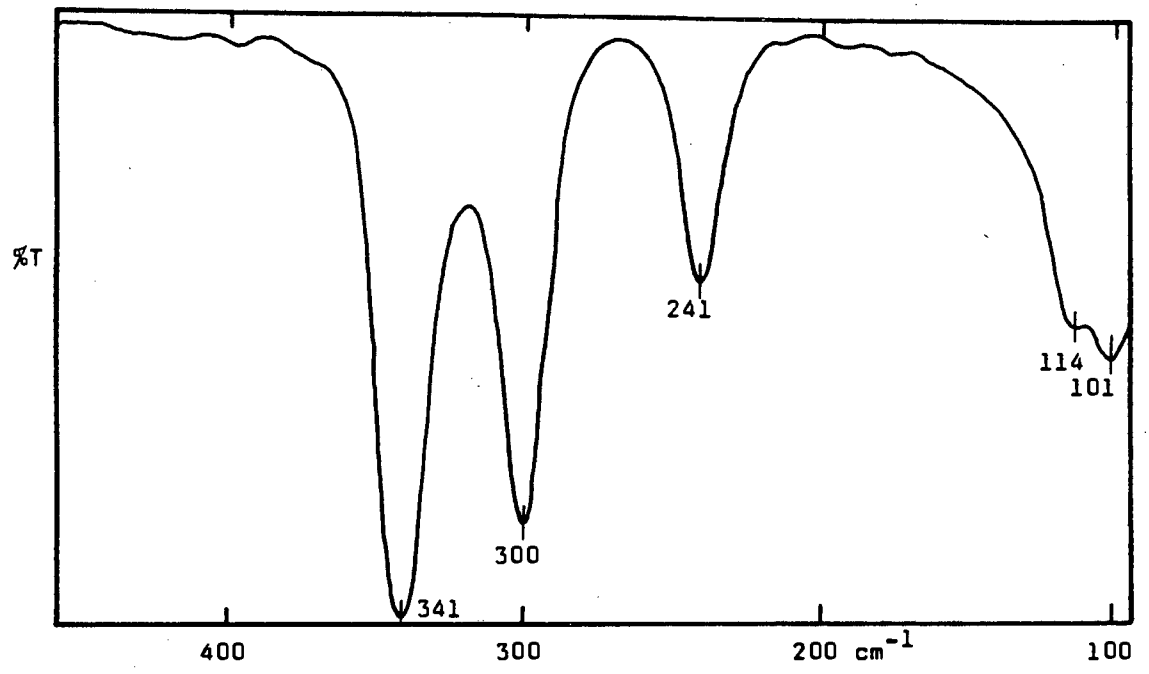

Fig. 2.20 : The far-infrared spectrum of $Co(4\text{-}C_2H_5py)_2Cl_2$.

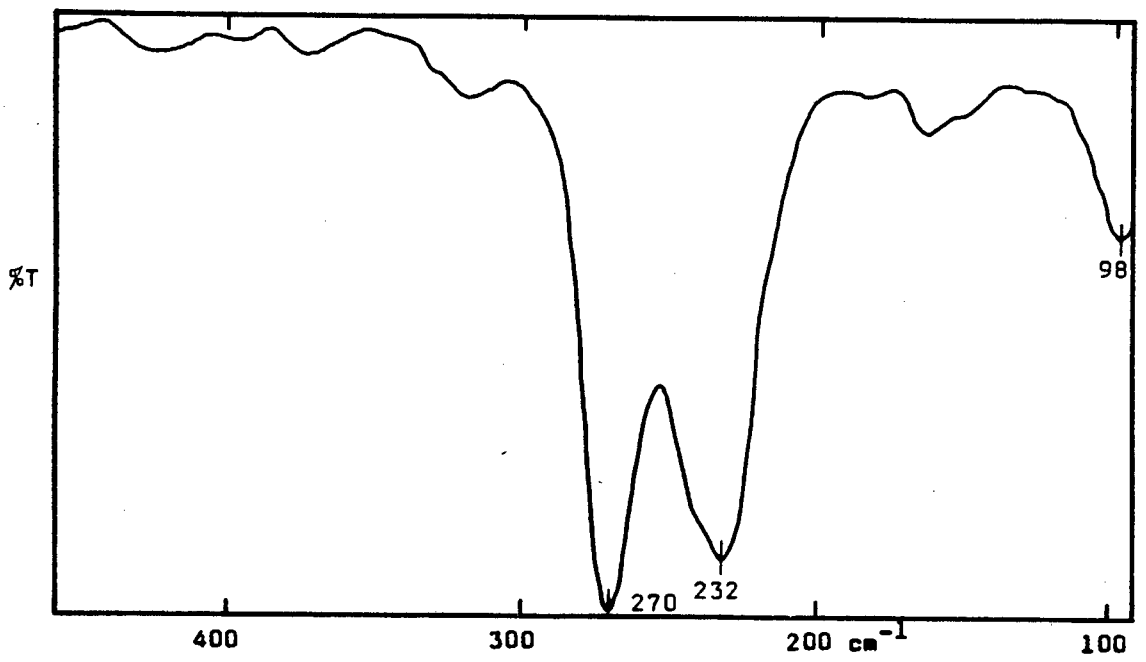

Fig. 2.21 : The far-infrared spectrum of $Co(4\text{-}C_2H_5py)_2Br_2$.

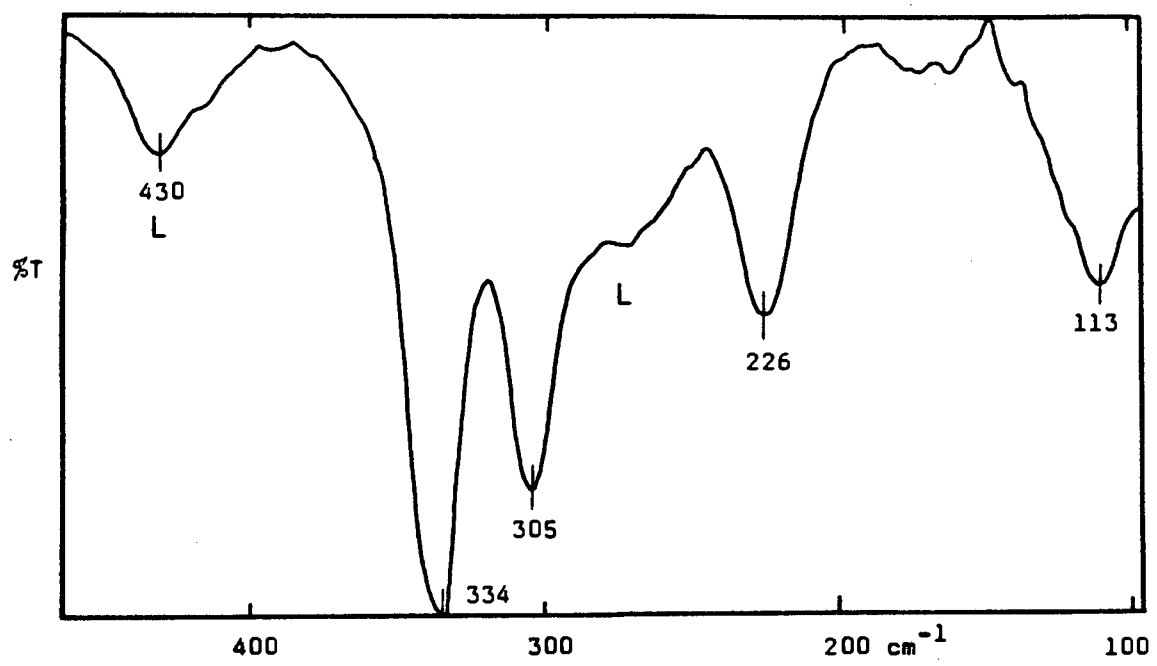

Fig. 2.22 : The far-infrared spectrum of $Co(4\text{-}(CH_3)_2Npy)_2Cl_2$.

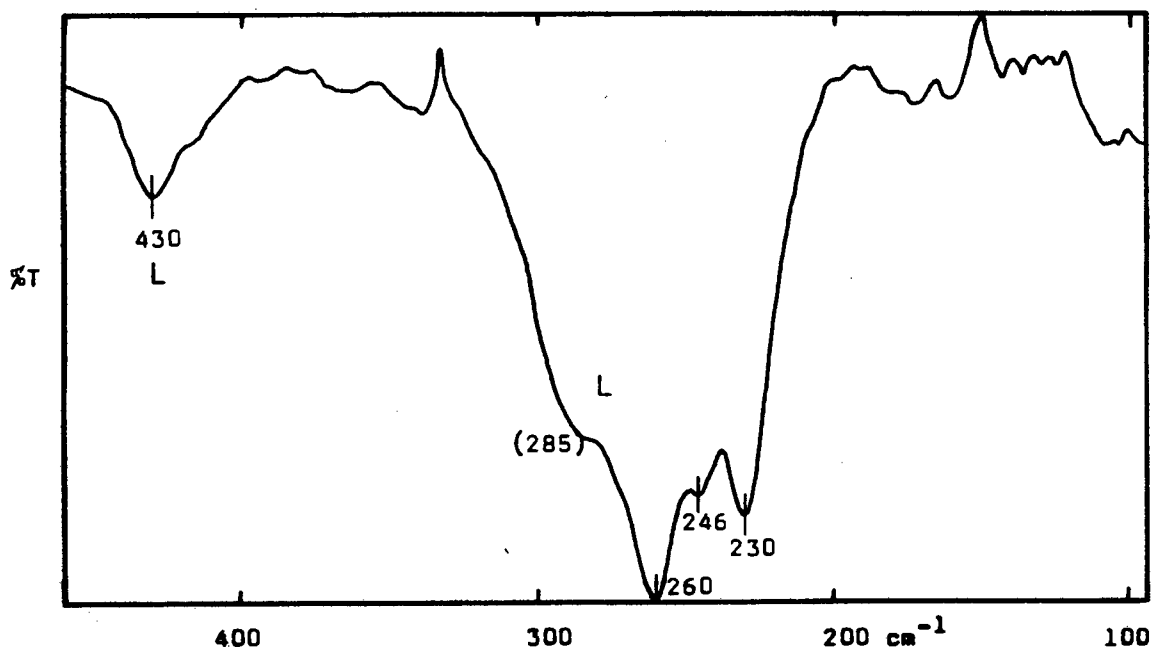

Fig. 2.23 : The far-infrared spectrum of $Co(4\text{-}(CH_3)_2Npy)_2Br_2$.

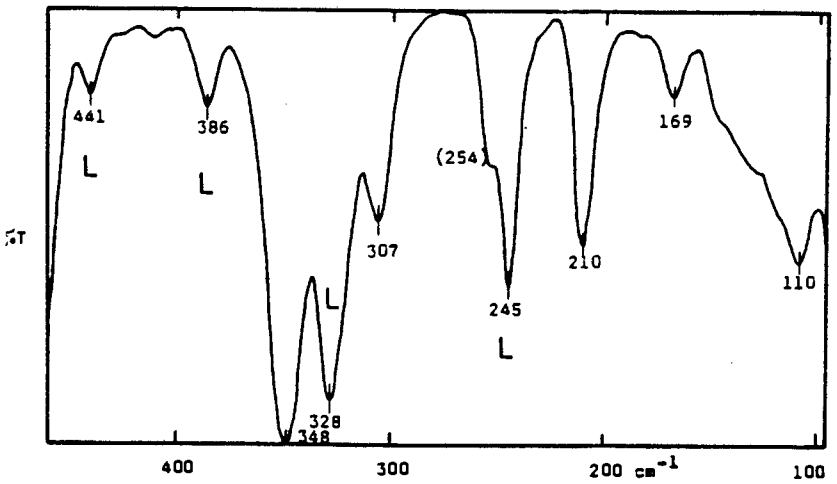

Fig. 2.24 : The far-infrared spectrum of $Co(4\text{-}C_6H_5COpy)_2Cl_2$.

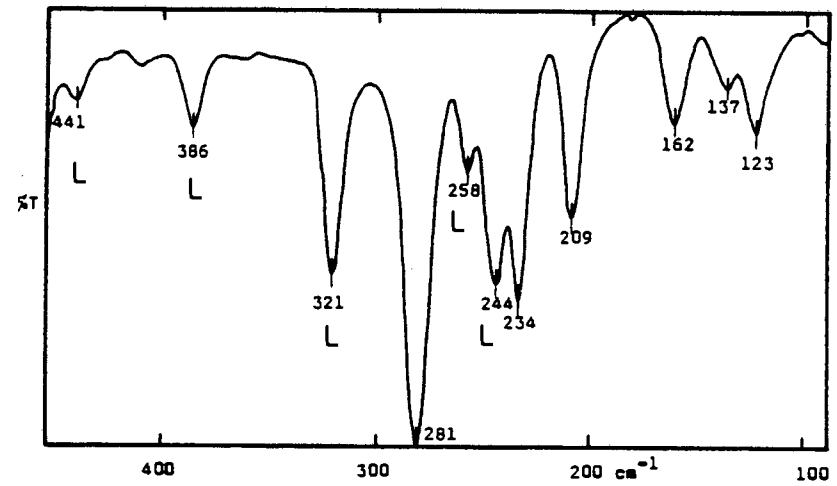

Fig. 2.25 : The far-infrared spectrum of $Co(4\text{-}C_6H_5COpy)_2Br_2$.

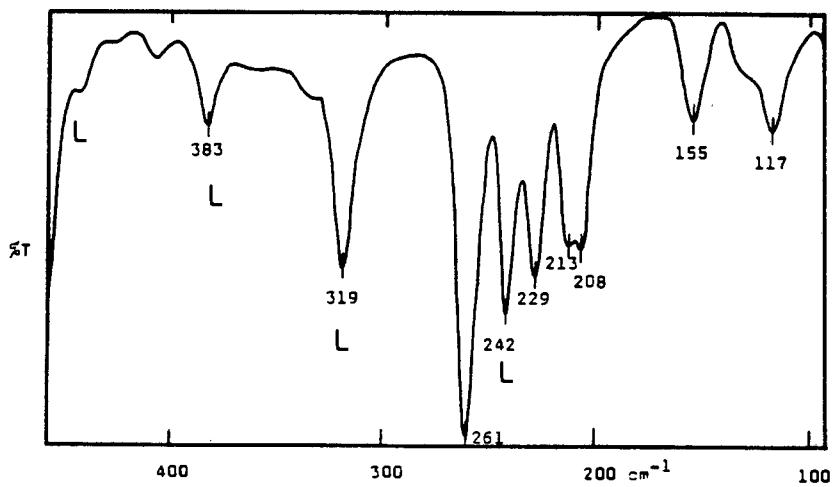

Fig. 2.26 : The far-infrared spectrum of $Co(4\text{-}C_6H_5COpy)_2I_2$.

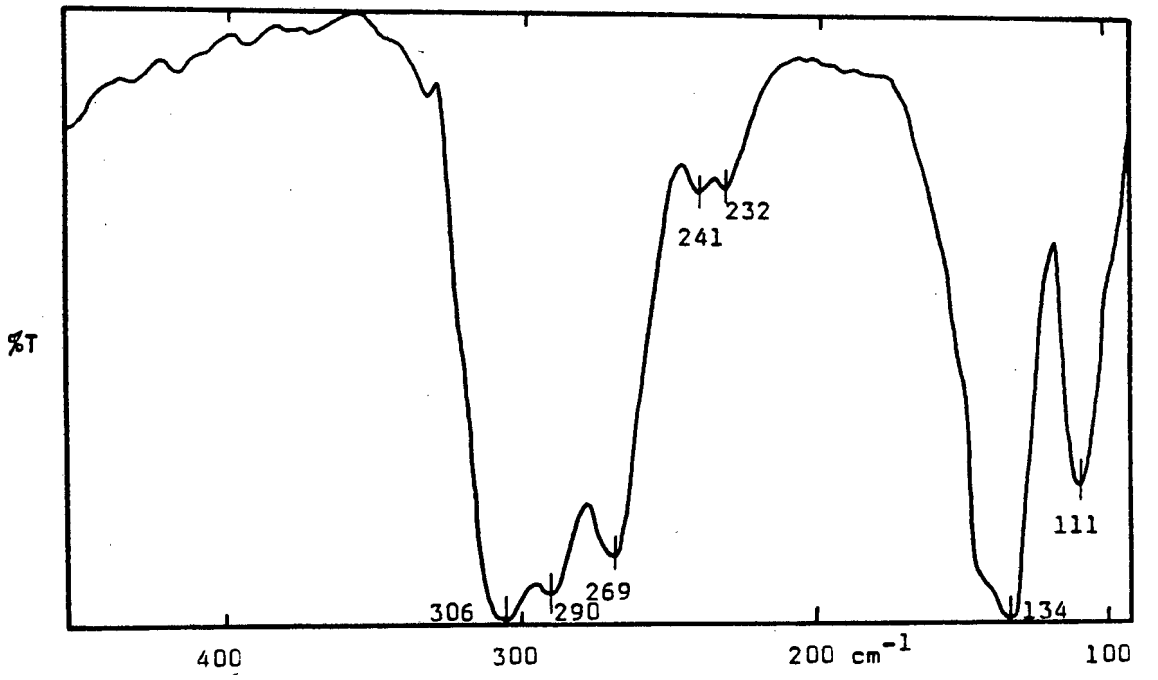

Fig. 2.27 : The far-infrared spectrum of $Co(4\text{-}HOpy)_2Cl_2$.

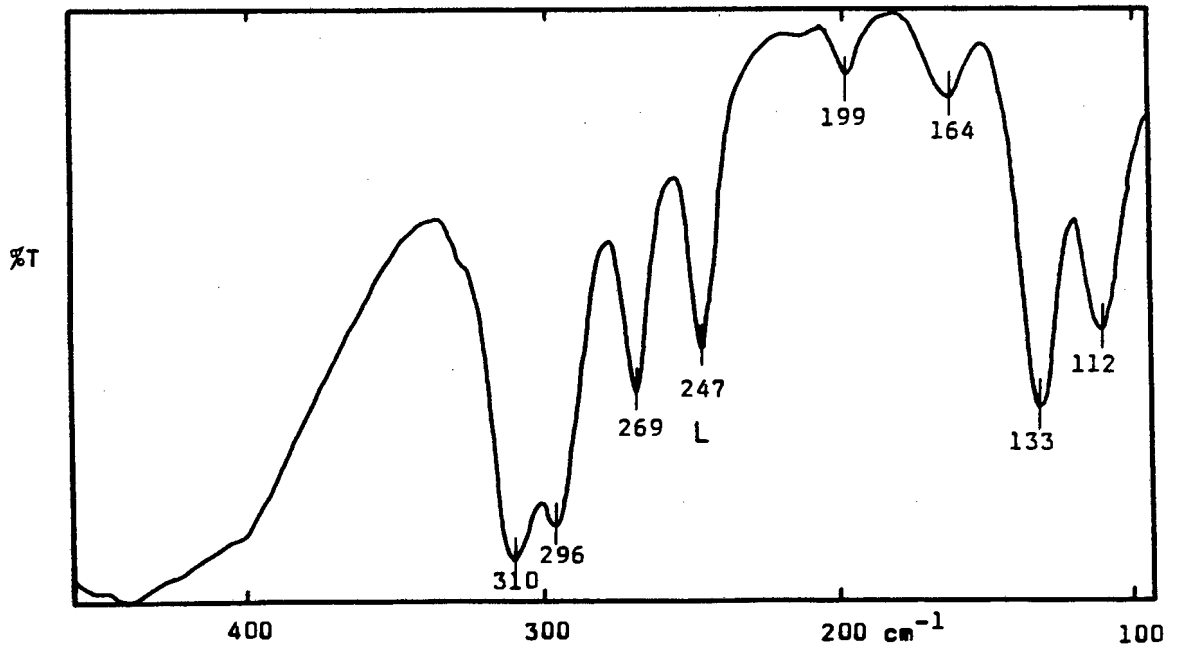

Fig. 2.28 : The far-infrared spectrum of $Co(4\text{-}H_2Npy)_2Cl_2$.

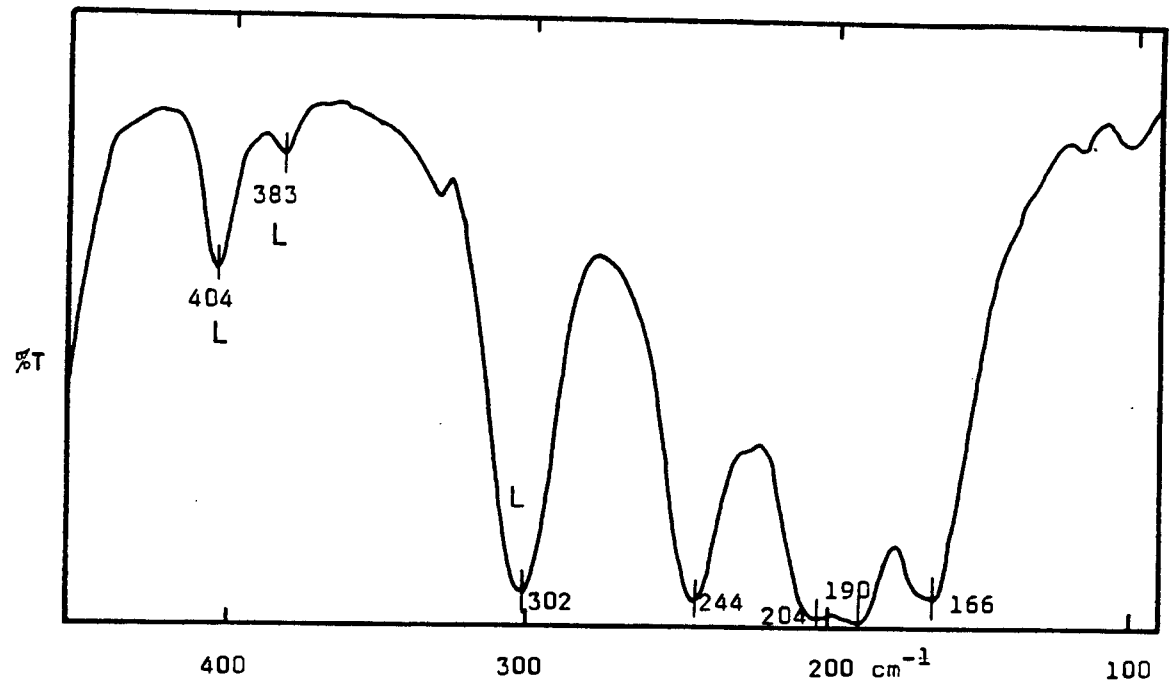

Fig. 2.29 : The far-infrared spectrum of $Co(4\text{-}HOOCpy)_2Cl_2$.

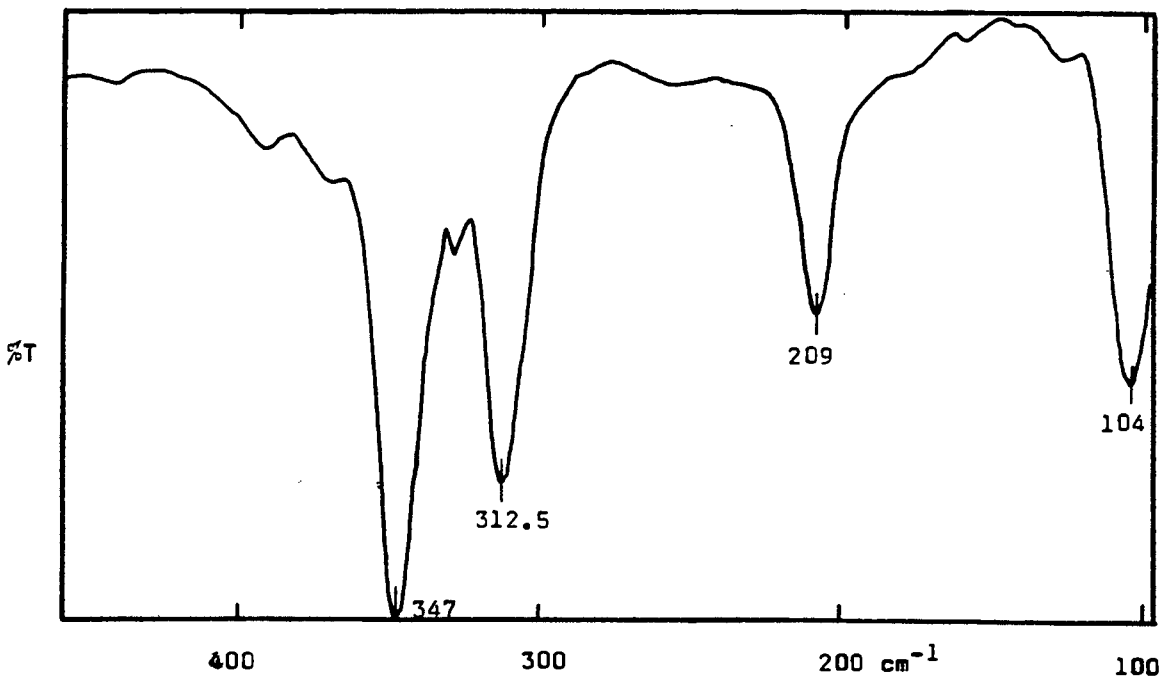

Fig. 2.30 : The far-infrared spectrum of $Co(4\text{-}(CH_3)_3Cpy)_2Cl_2$.

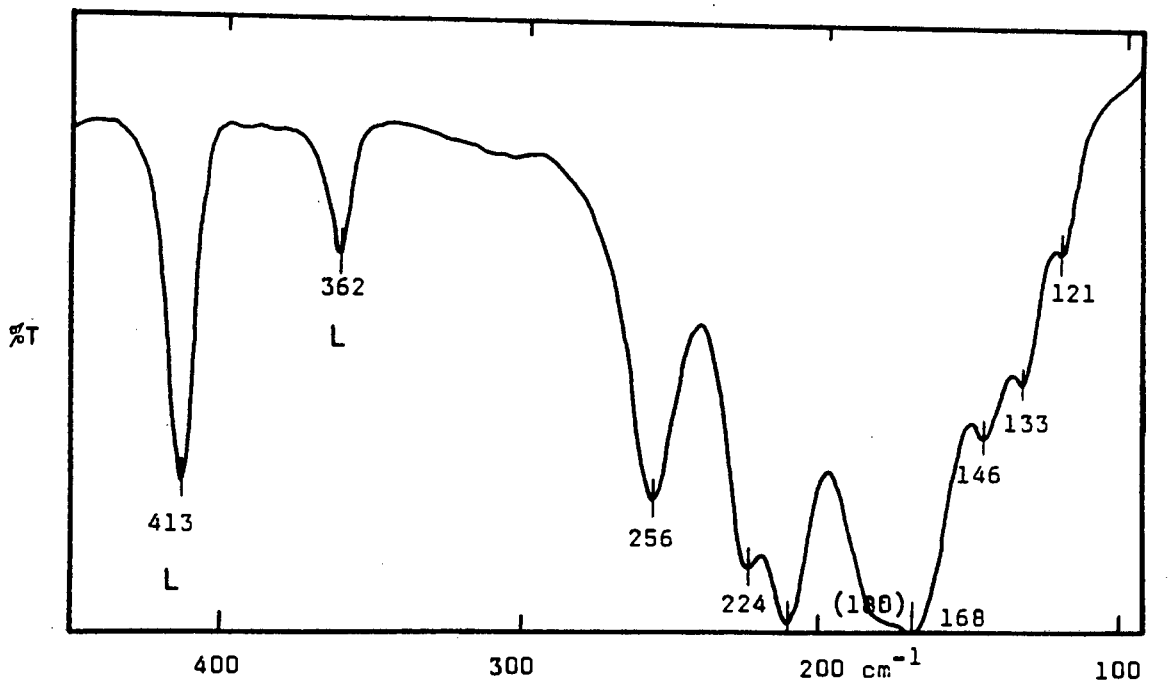

Fig. 2.31 : The far-infrared spectrum of $Co(3\text{-}NCpy)_2Cl_2$.

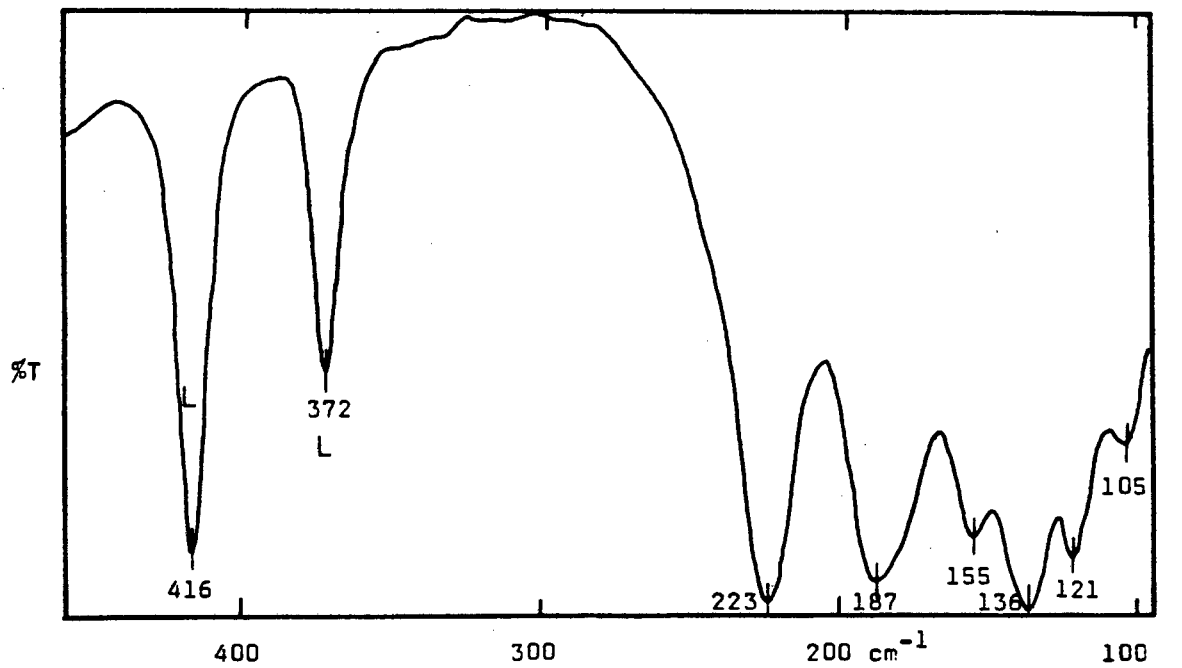

Fig. 2.32 : The far-infrared spectrum of $Co(3\text{-}NCpy)_2Br_2$.

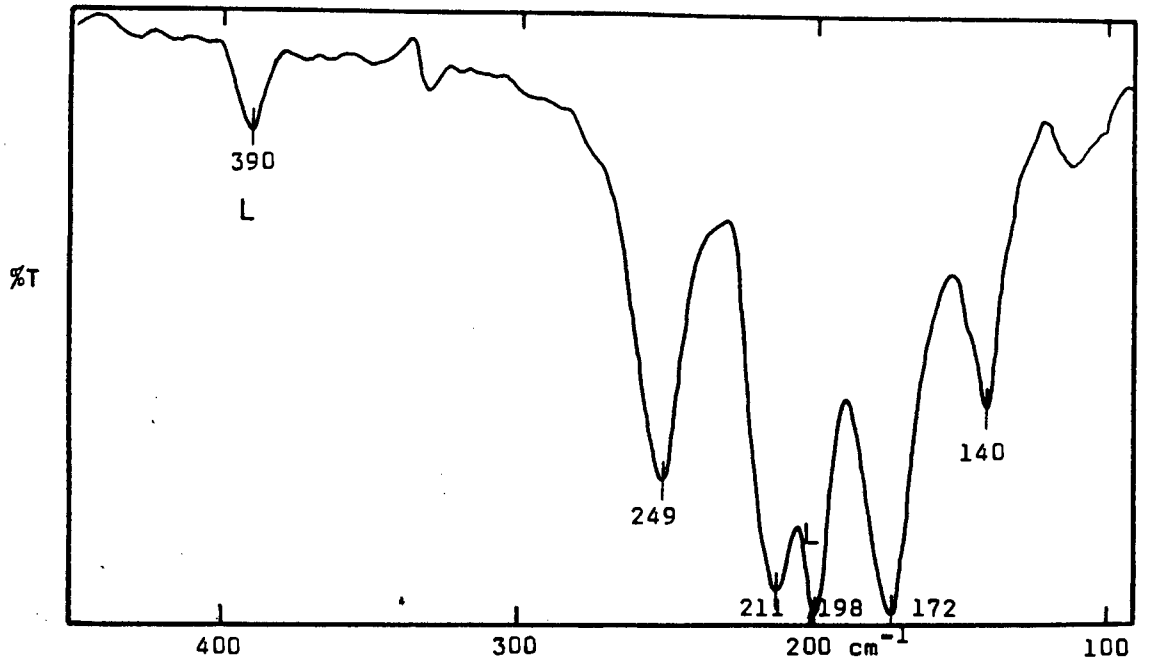

Fig. 2.33 : The far-infrared spectrum of $Co(4\text{-}NCpy)_2Cl_2$.

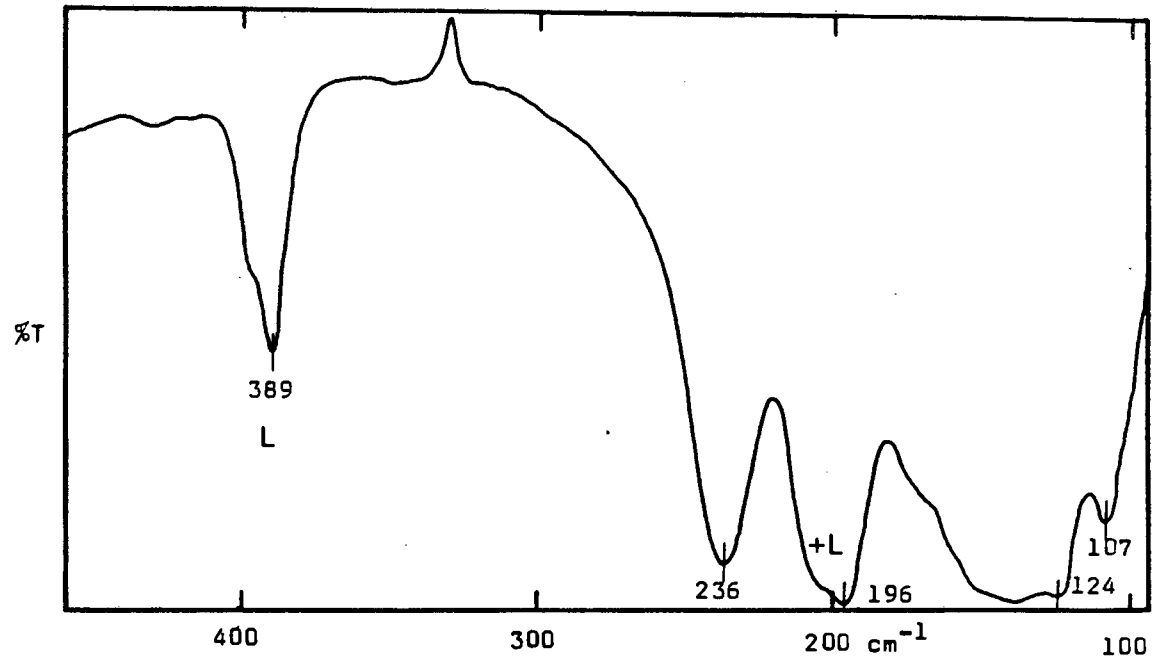

Fig. 2.34 : The far-infrared spectrum of $Co(4\text{-}NCpy)_2Br_2$.

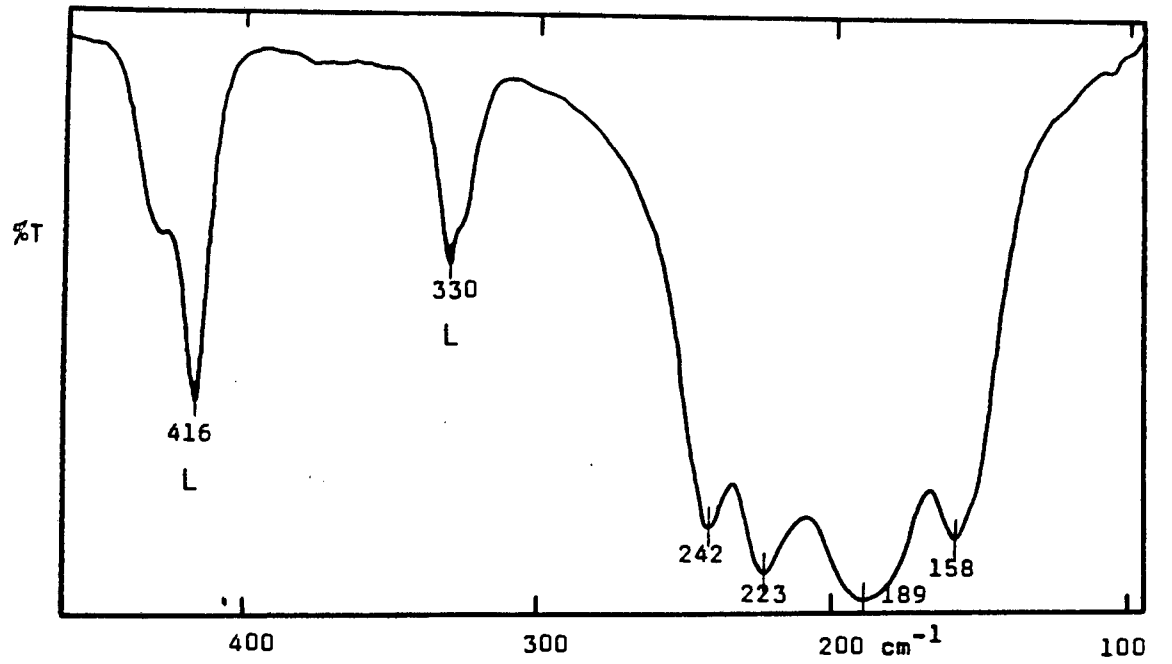

Fig. 2.35 : The far-infrared spectrum of $Co(3\text{-}Clpy)_2Cl_2$.

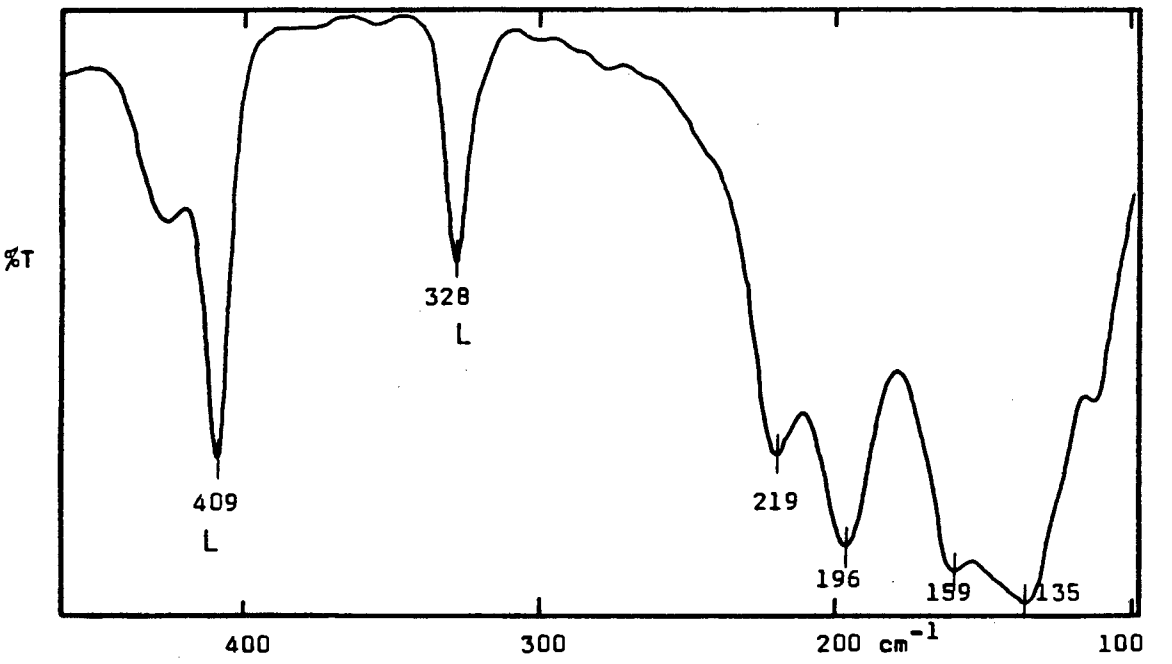

Fig. 2.36 : The far-infrared spectrum of $Co(3\text{-}Clpy)_2Br_2$.

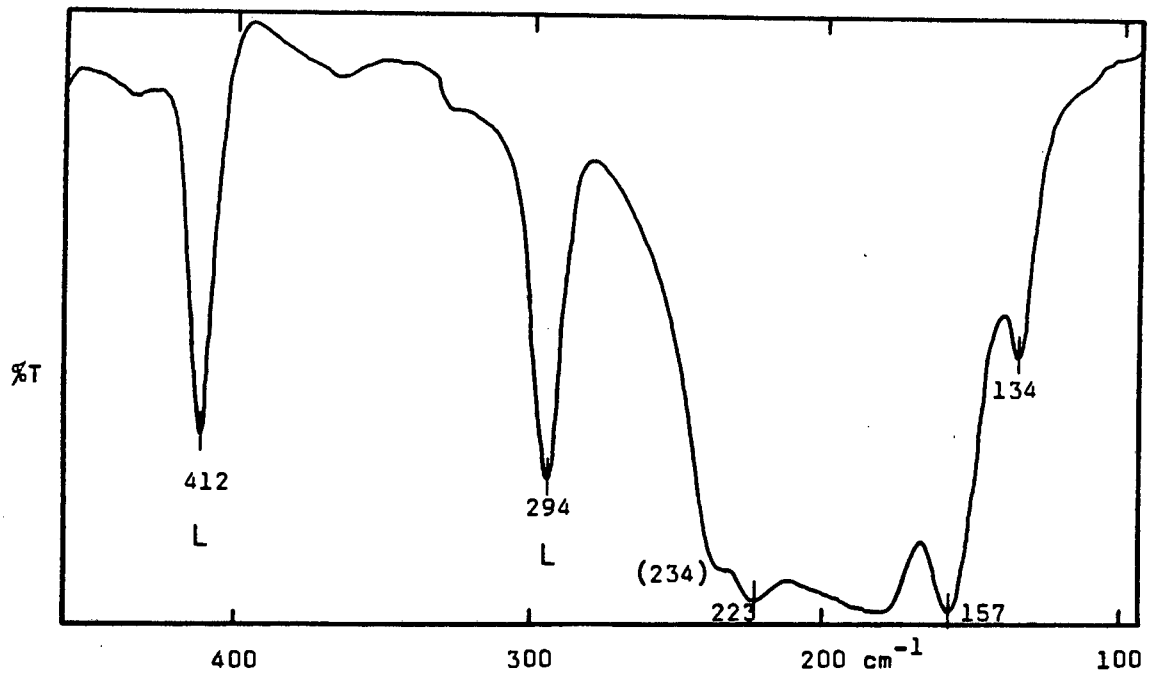

Fig. 2.37 : The far-infrared spectrum of $Co(3\text{-}Brpy)_2Cl_2$.

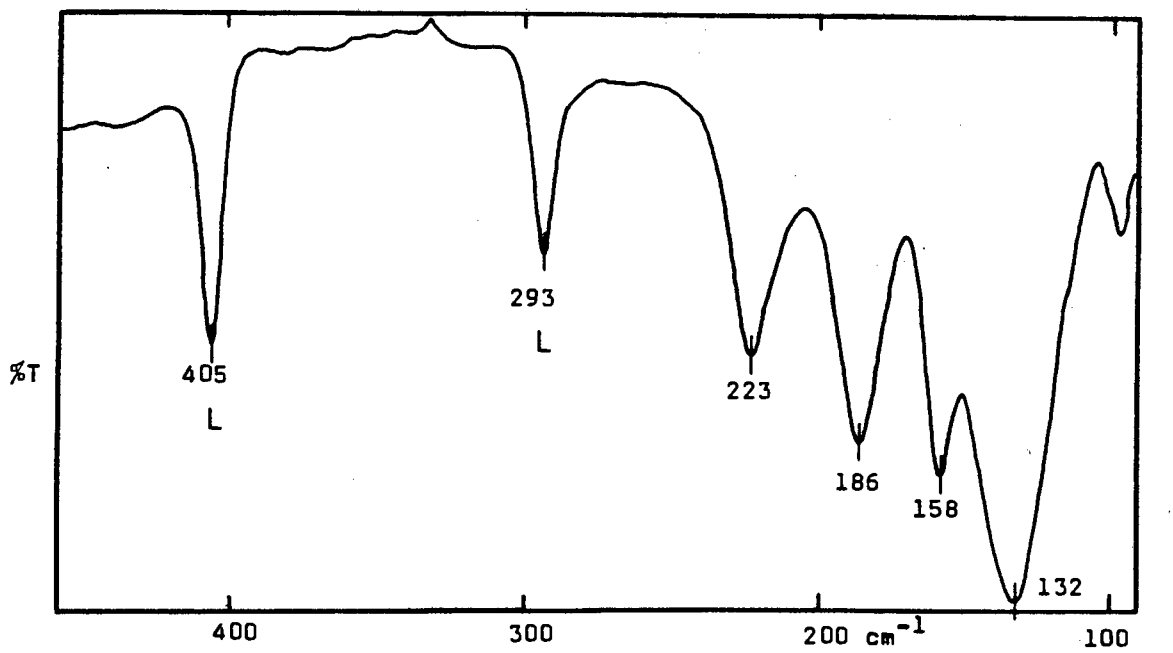

Fig. 2.38 : The far-infrared spectrum of $Co(3\text{-}Brpy)_2Br_2$.

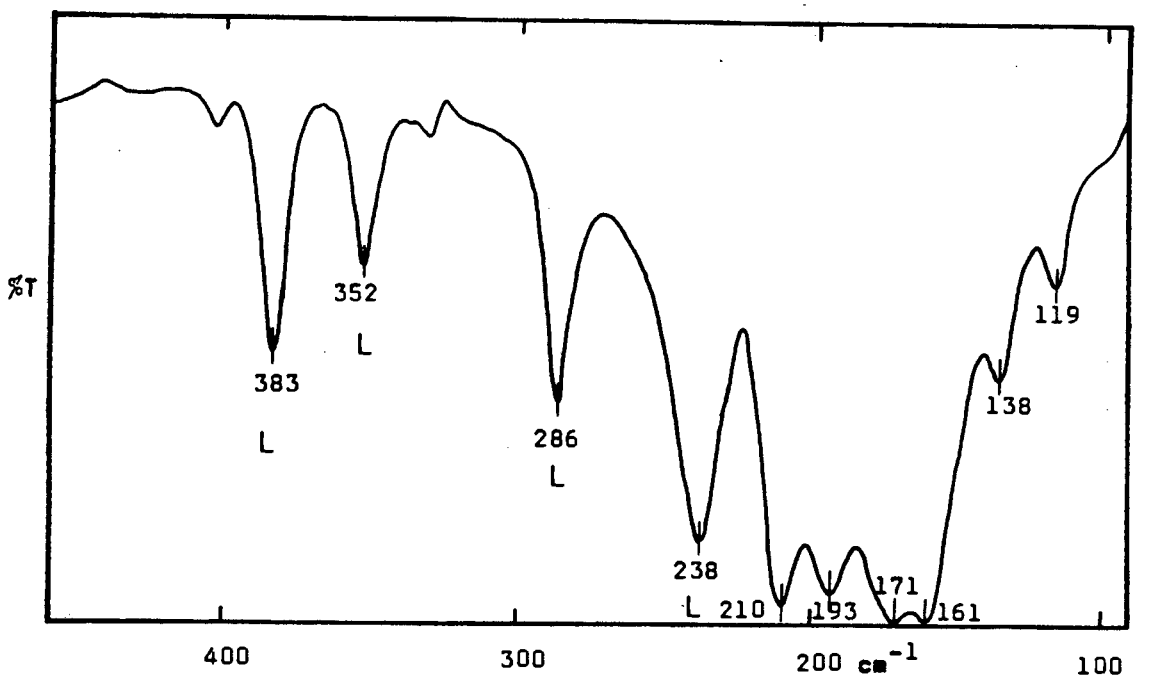

Fig. 2.39 : The far-infrared spectrum of $Co(4\text{-}C_6H_5py)_2Cl_2$.

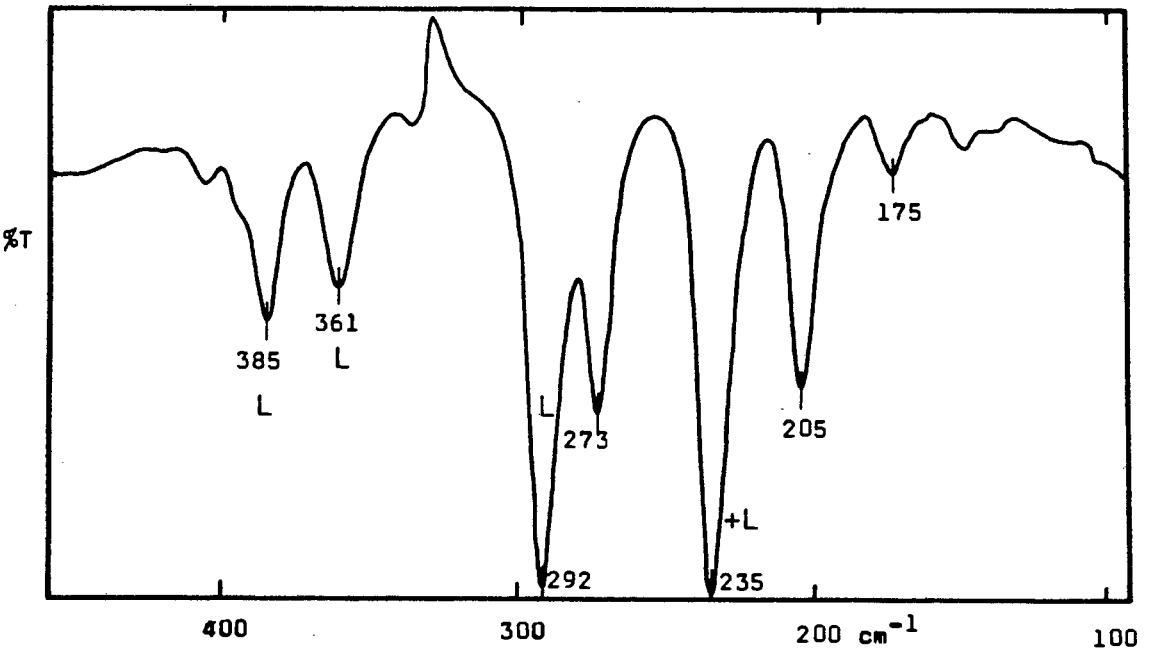

Fig. 2.40 : The far-infrared spectrum of $Co(4\text{-}C_6H_5py)_2Br_2$.

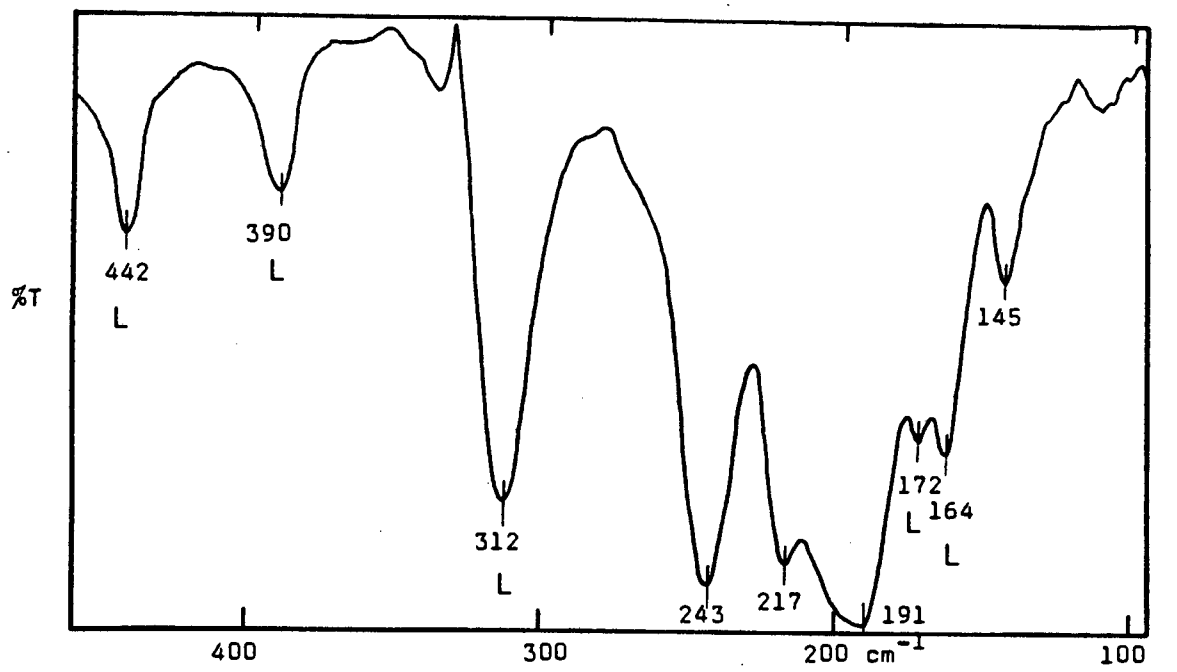

Fig. 2.41 : The far-infrared spectrum of $Co(3\text{-}HOOCpy)_2Cl_2$.

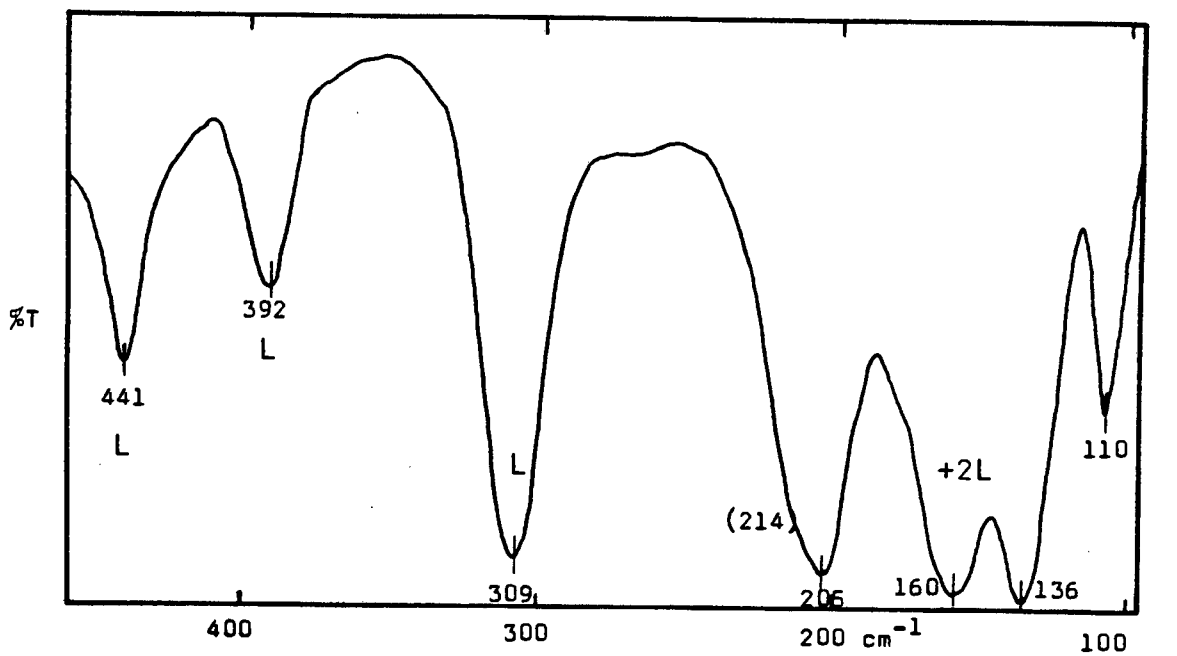

Fig. 2.42 : The far-infrared spectrum of $Co(3\text{-}HOOCpy)_2Br_2$.

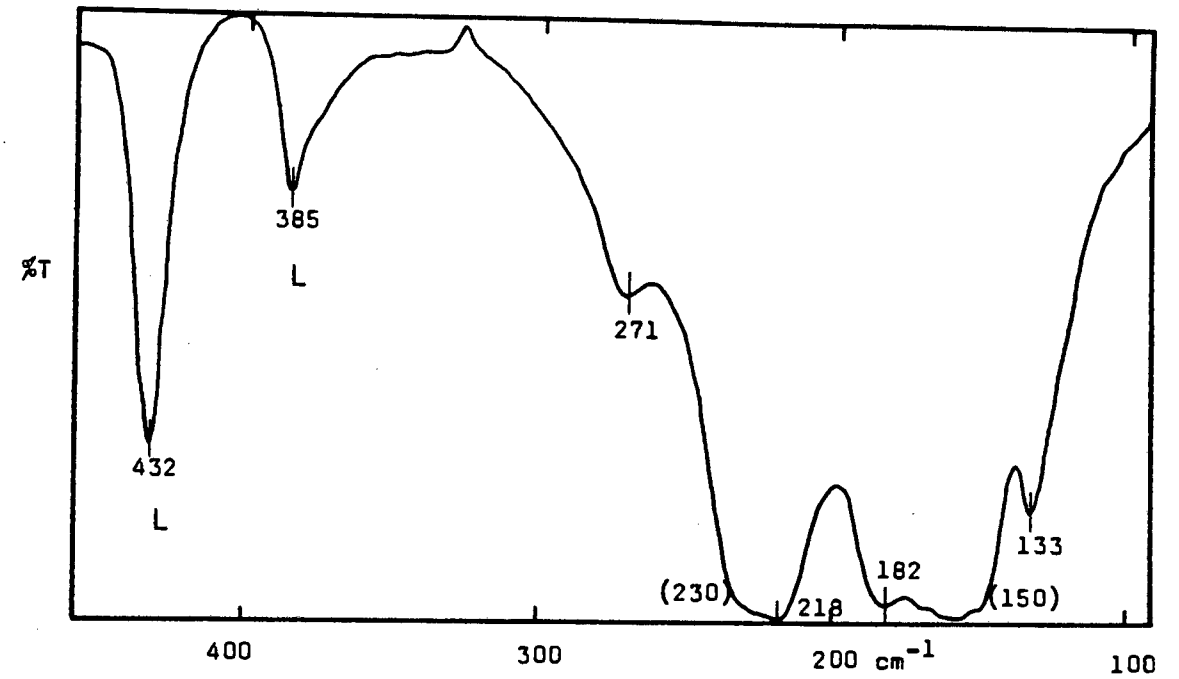

Fig. 2.43 : The far-infrared spectrum of $Co(3\text{-}CH_3COpy)_2Cl_2$.

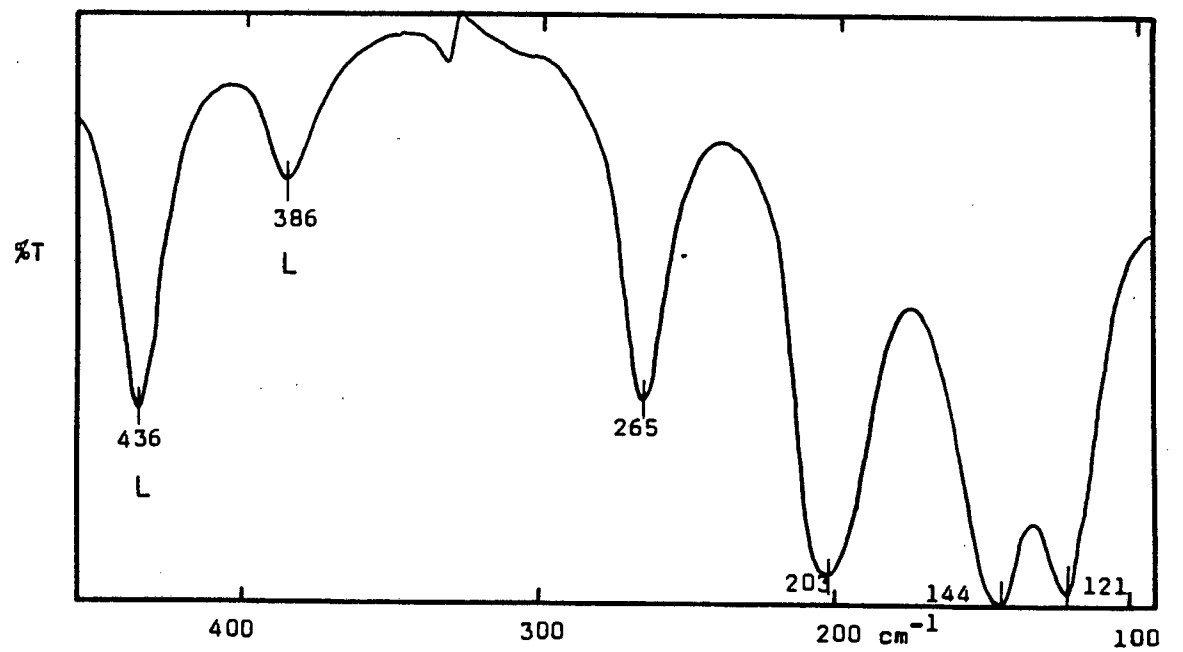

Fig. 2.44 : The far-infrared spectrum of $Co(3\text{-}CH_3COpy)_2Br_2$.

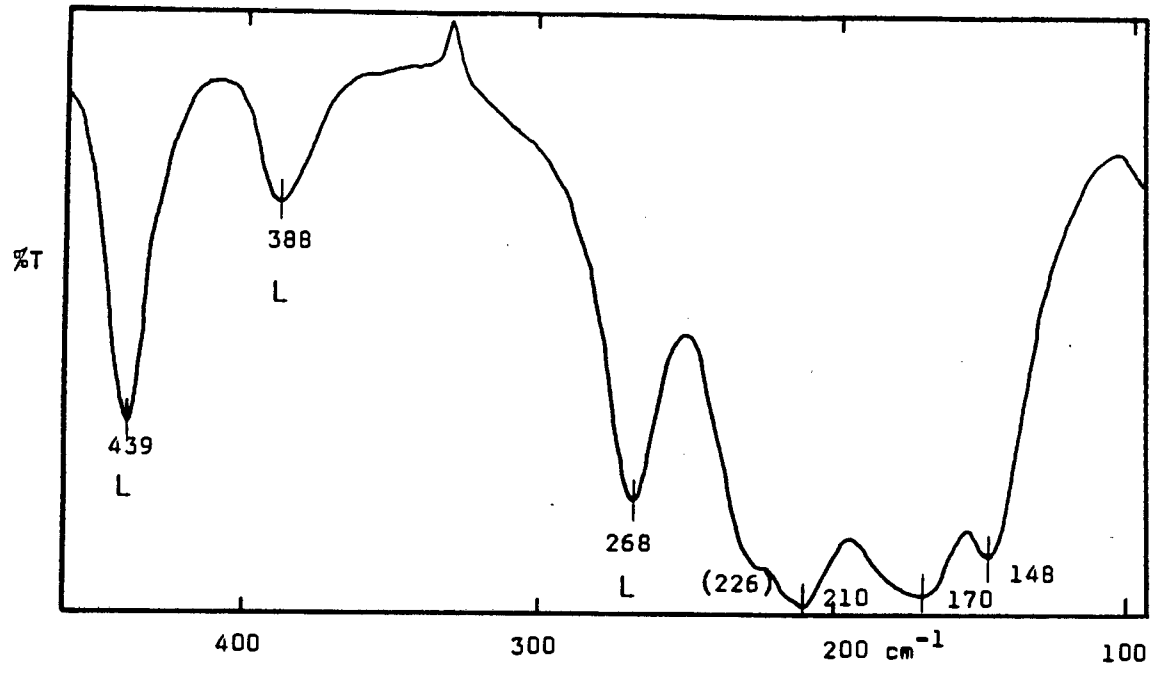

Fig. 2.45 : The far-infrared spectrum of $Co(4\text{-}CH_3COpy)_2Cl_2$.

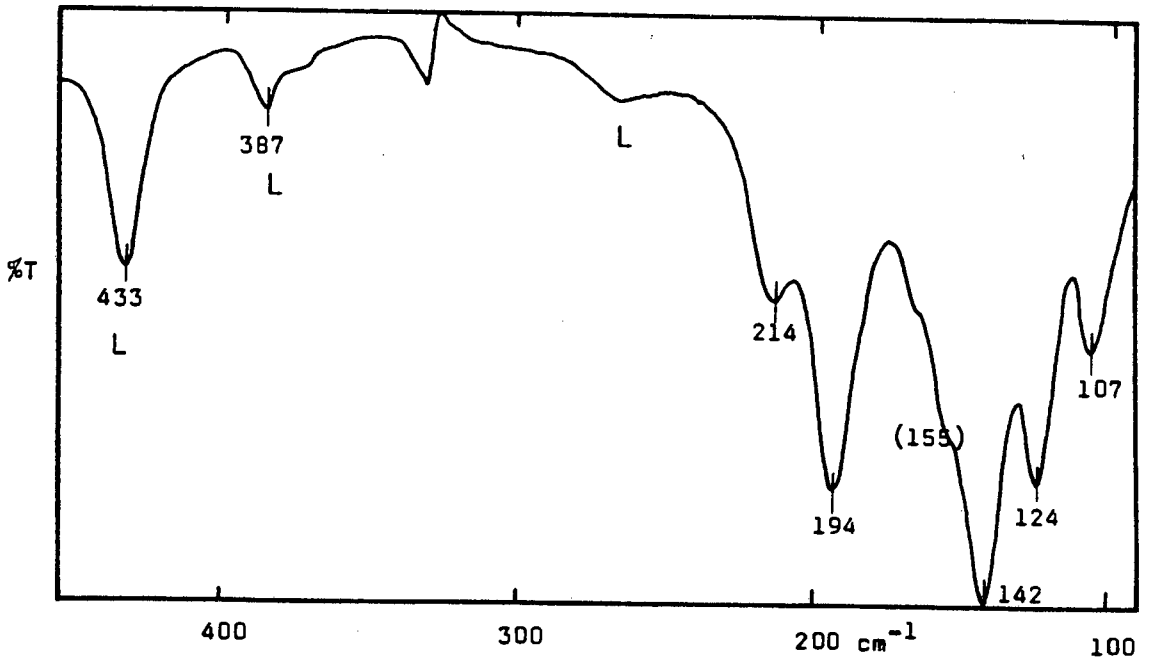

Fig. 2.46 : The far-infrared spectrum of $Co(4\text{-}CH_3COpy)_2Br_2$.

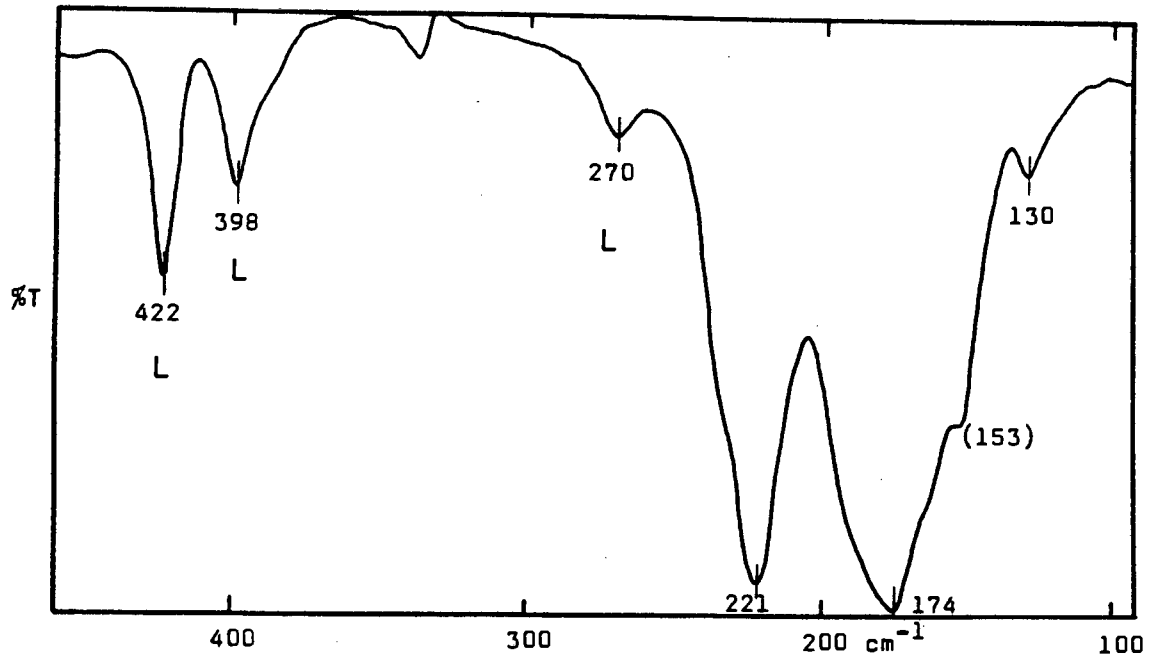

Fig. 2.47 : The far-infrared spectrum of $Co(3\text{-}H_2NCOpy)_2Cl_2$.

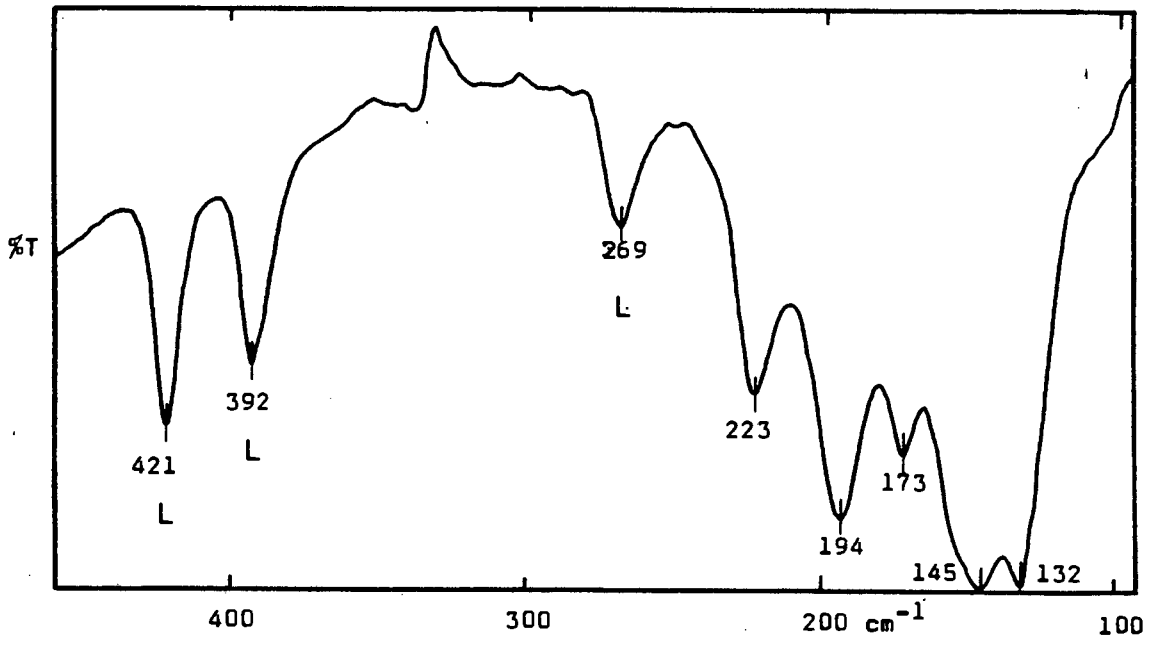

Fig. 2.48 : The far-infrared spectrum of $Co(3\text{-}H_2NCOpy)_2Br_2$.

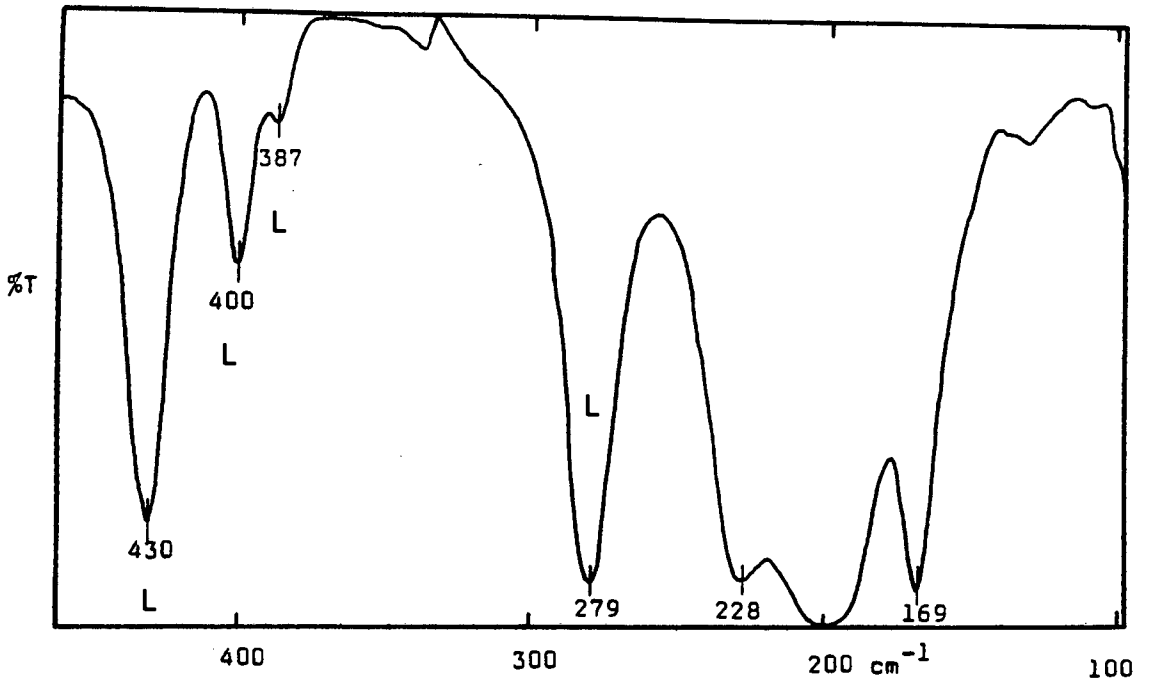

Fig. 2.49 : The far-infrared spectrum of $Co(4\text{-}H_2NCOpy)_2Cl_2$.

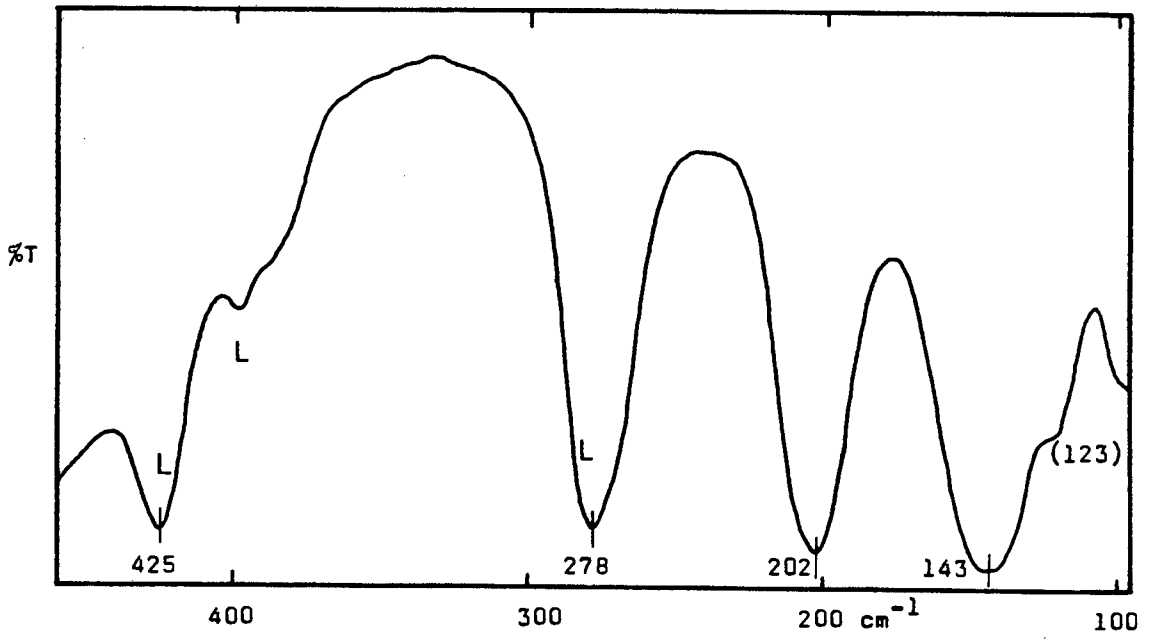

Fig. 2.50 : The far-infrared spectrum of $Co(4\text{-}H_2NCOpy)_2Br_2$.

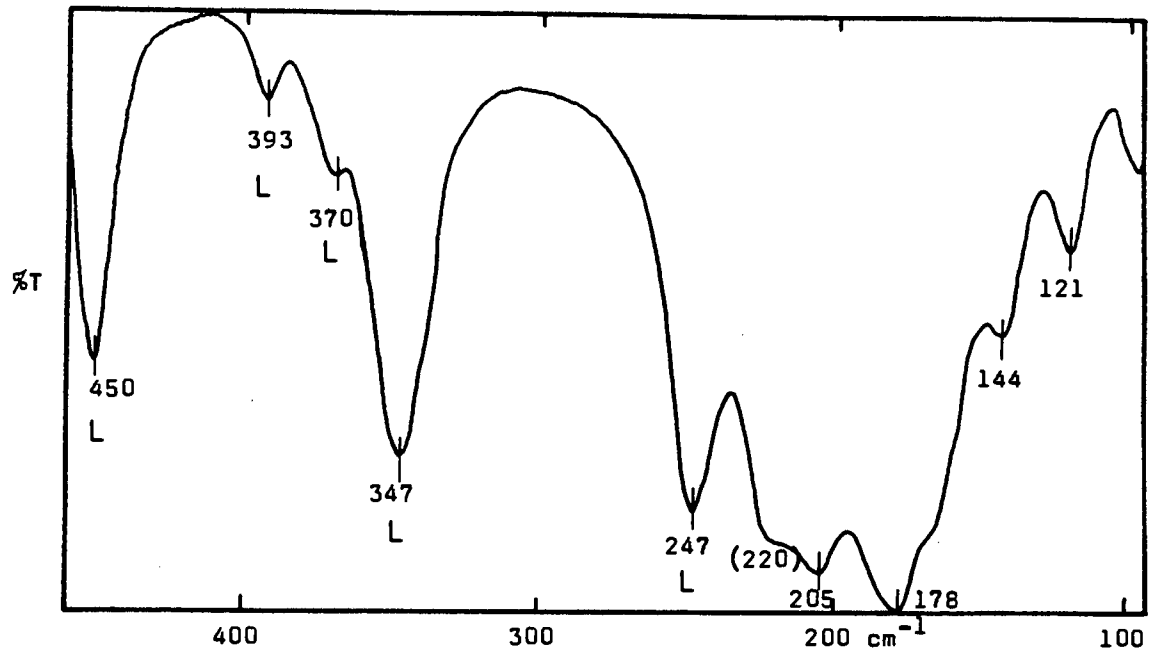

Fig. 2.51 : The far-infrared spectrum of $Co(3\text{-}CH_3OCOpy)_2Cl_2$.

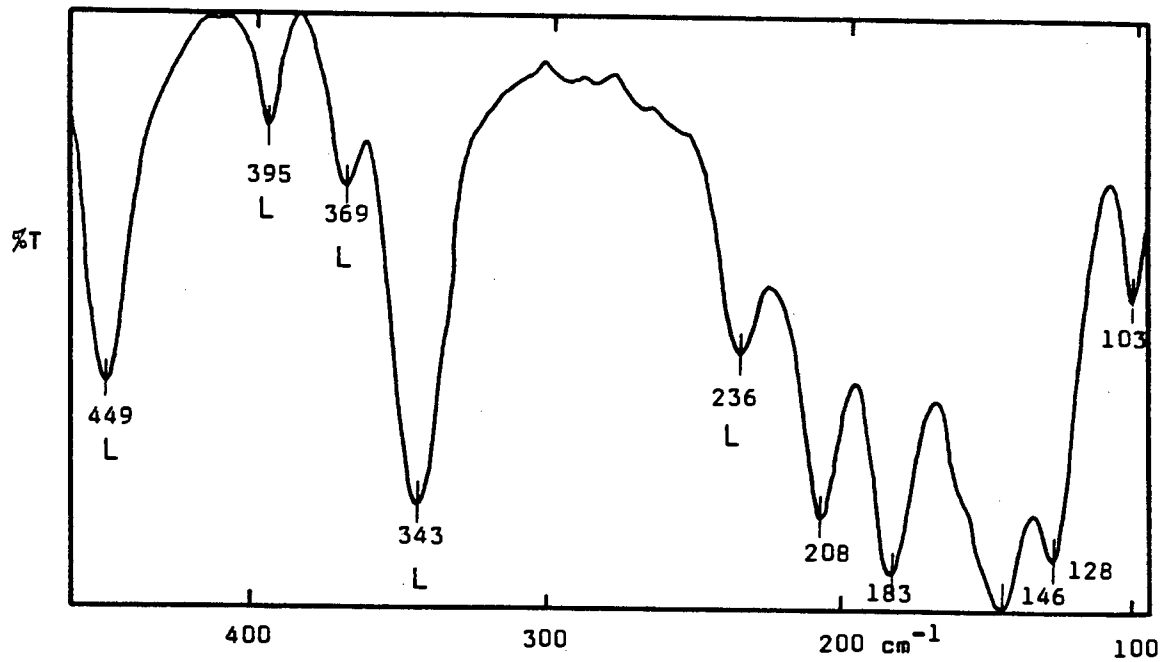

Fig. 2.52 : The far-infrared spectrum of $Co(3\text{-}CH_3OCOpy)_2Br_2$.

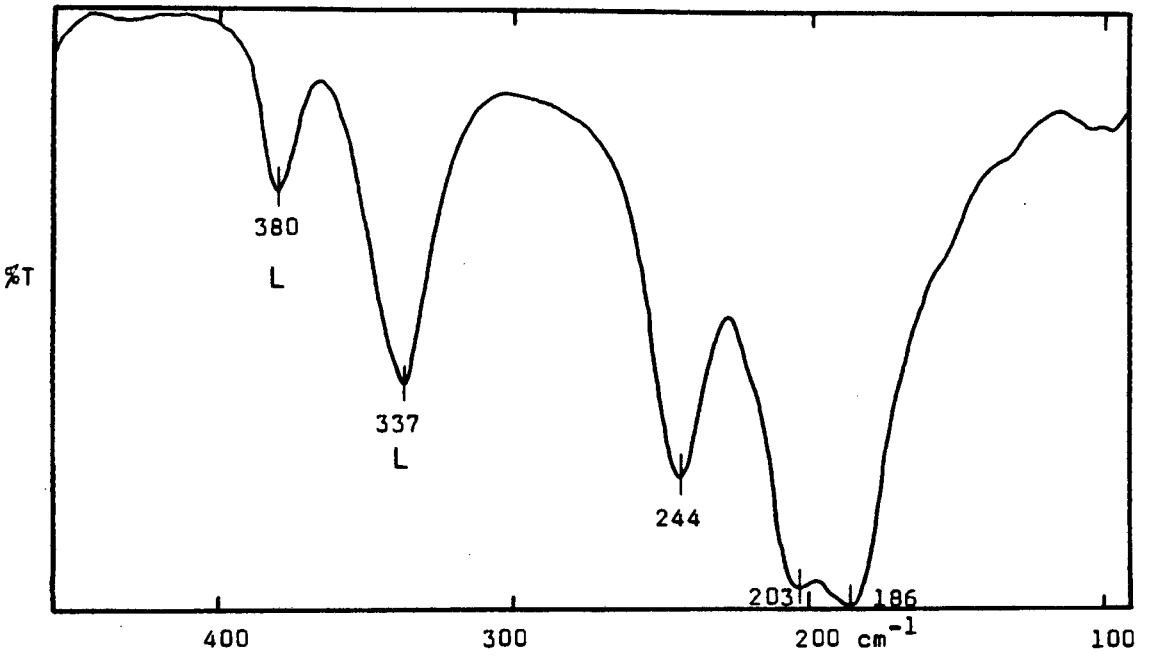

Fig. 2.53 : The far-infrared spectrum of $Co(4\text{-}CH_3OCOpy)_2Cl_2$.

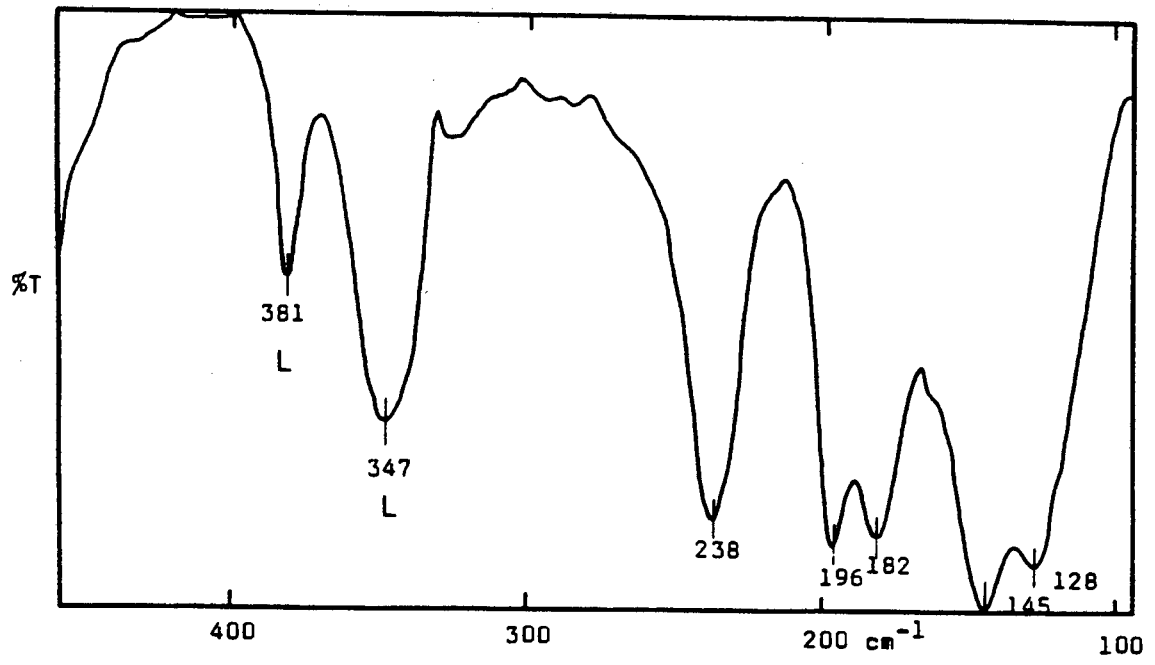

Fig. 2.54 : The far-infrared spectrum of $Co(4\text{-}CH_3OCOpy)_2Br_2$.

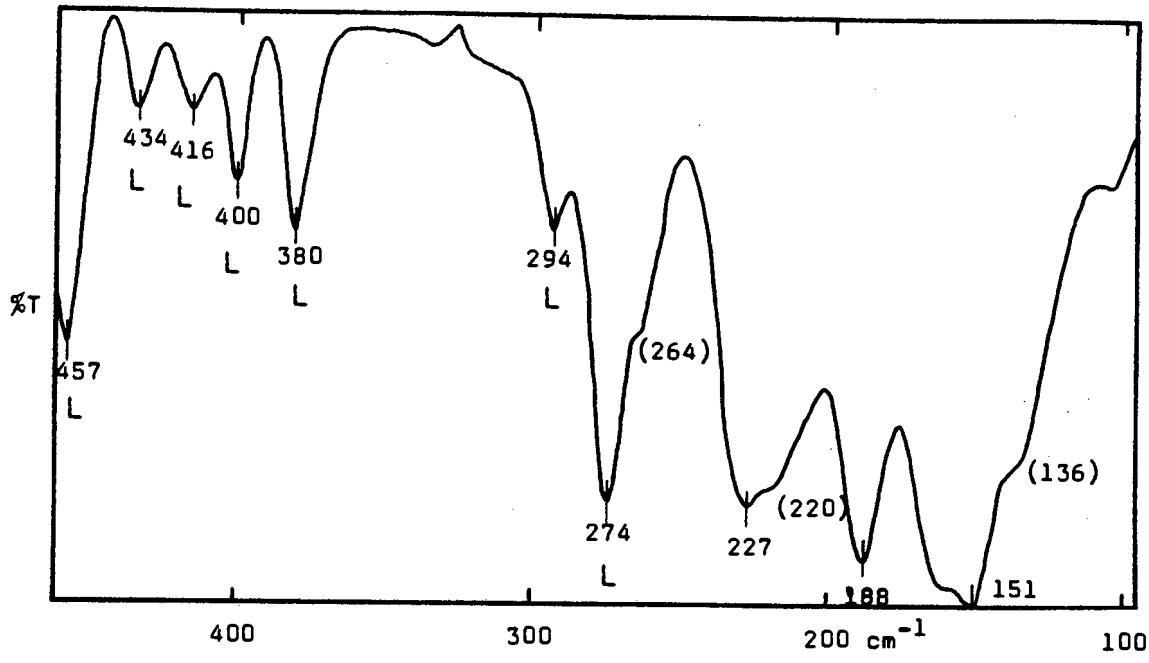

Fig. 2.55 : The far-infrared spectrum of $Co(3\text{-}C_6H_5COpy)_2Cl_2$.

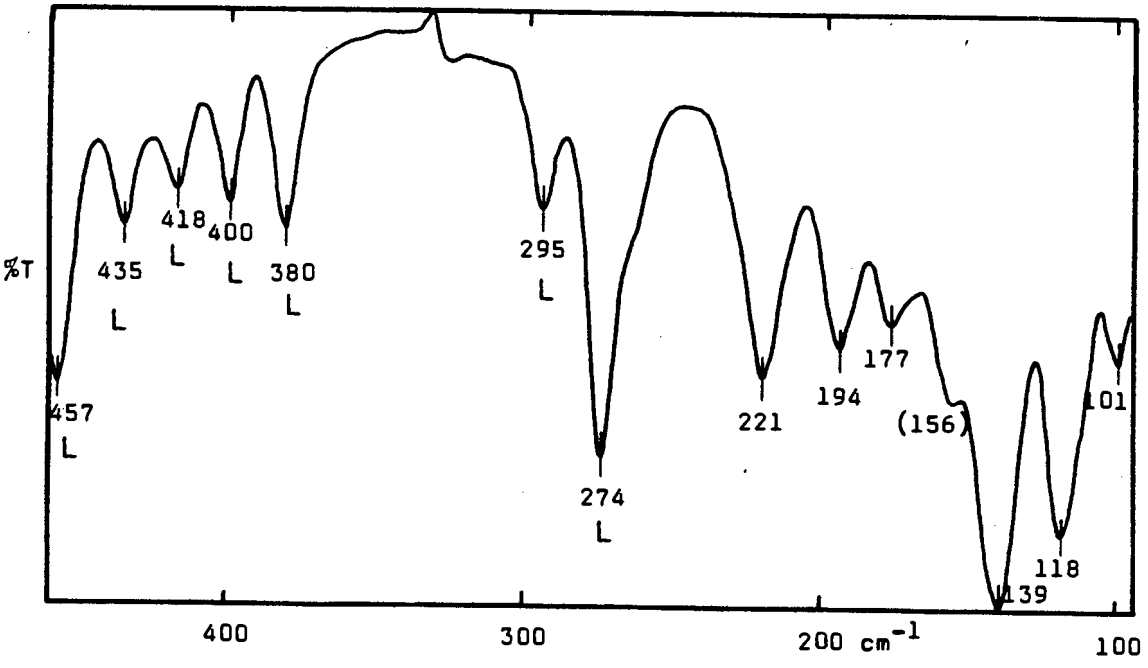

Fig. 2.56 : The far-infrared spectrum of $Co(3\text{-}C_6H_5COpy)_2Br_2$.

frequencies are in good agreement with reported data. It is interesting to note that the mass effects of the substituents markedly shift the M-N stretching frequencies. The νCo-N in the 4-*t*-butylpyridine complex occurs around 210 cm^{-1}, whereas this mode is assigned to the bands around 250 cm^{-1} in the unsubstituted complex. Hence, the rule of νM-N (tetrahedral) > νM-N (octahedral) which generally serves as a diagnostic probe for distinguishing different CN's around the metal, can only be straightforwardly applied if the mass effect of the substituent is taken into account. In our series of compounds, this substituent effect overrides the bonding capacity of the cobalt ion.

In 1970, GOLDSTEIN and UNSWORTH[83,84,85] published, for the first time, some Raman and ir spectra of octahedral polymeric halogen-bridged transition metal(II) complexes of pyridine. In contrast to previous reports of that time, the 'νM-X' are assigned to bands below 200 cm^{-1}, based on group theoretical predictions and low temperature measurements. The vibrations of the chain polymers, i.e. the in-plane deformations of $\{MX_2\}_n$, were treated satisfactorily in terms of line group symmetry (D_{2n}): two principal ν_bM-X of strong intensity were predicted and observed around 180 and 160 cm^{-1} for MCl_2, and around 150 and 140 cm^{-1} for MBr_2 chains. Only one ir-active νM-N mode is expected, but in many cases two (or three) are observed. The ir-forbidden ν_sM-N becomes activated if the pyridine orientations* (pyridine rings are inclined to the

---

* An example of the importance and consequence of the orientations of the pyridine rings can be found in dichlorobis(pyridine)copper(II)[74]. The steric repulsion between the α-hydrogen atoms of the pyridine nuclei and the chlorine atoms, causes the planes of the pyridine nuclei to be inclined to the Cl-Cu-Cl axis[86]. This becomes more pronounced when the α-positions are substituted with alkyl groups. Close approach of adjacent chlorine atoms is prevented so that the copper atom is surrounded by only four donor atoms. Consequently, no copper-halogen bridging is observed and the largest Cu-Cl distance becomes too great to give rise to a stretching mode.

$\{CoCl_2\}_n$ chain axis) are taken into account (C_2) or if a complete factor group analysis is carried out (C_{2h}^4). In order to confirm their assignments, the authors recorded the spectra of some pyridine-d_5 complexes. We have to point out that the application of isotopic labelling methods on the polymeric $[Co(R\text{-}py)_2X_2]$ complexes is far less practical. As can be seen from our spectra, the strong band overlap in the region 250-100 cm^{-1} makes the spectra very complicated and well-defined bandshifts are hard to observe. Furthermore, because of the relative low symmetry of the polymers and the fact that some internal vibrations, in particularly the bridged cobalt-halogen modes are at the same time lattice-like modes, strong coupling between various modes of vibration is generally expected. This will result in decreased sensitivity of the metal-ligand bands towards isotopic substitution.

Table 2.14 lists our assigned bands in the spectra of polymeric $[Co(R\text{-}py)_2X_2]$ complexes and other unassigned bands above 100 cm^{-1}.

The assignment of ν_bM-X is in agreement with the halogen-substitution criteria. The ν_bM-X shifts to lower frequencies when X is changed from Cl to Br. Those bands which are relatively insensitive to changes in X are attributed to νM-N. However, some degree of X-dependence of the νM-N does occur due to the above-mentioned coupling with the vibrations of the $\{CoX_2\}$ chains. None of the metal-ligand modes can be considered as a pure vibration. Thus, in this discussion, when we describe a band as assigned to a particular vibrational mode, we imply that the band originates predominantly from that mode and understand that other modes are likely to contribute also to the vibrational energy of that band. The empirical rule of νM-Br/νM-Cl = 0.74 in octahedral metal carbonyl halides $M(CO)_5X$ and $M(CO)_4X_2$ is not followed exactly. For the halogen-bridged octahedral polymers, the ratio ν_bM-Br/ν_bM-Cl falls in a wider range of 0.75 ± 0.05. The regions in which the ν_bM-Cl and ν_bM-Br occur are 190-155 cm^{-1} and 150-120 cm^{-1}, respectively.

TABLE 2.12

Cobalt-to-nitrogen and cobalt-to-halogen vibrational frequencies of tetrahedral complexes (cm^{-1}).

compound	νCo-N		νCo-X	
	ν_1	ν_2	ν_3	ν_4
$Co(py)_2Cl_2$	251	226	347	304
$Co(py)_2Br_2$	253 (sh)	175	277	244
$Co(py)_2I_2$	246[b]	159	246	238
$Co(3\text{-}CH_3py)_2Cl_2$	250 (sh)	242	343	306[a]
$Co(3\text{-}CH_3py)_2Br_2$	243[b] (vs br)	178	272	243
$Co(4\text{-}CH_3py)_2Cl_2$	248	236	352[a]	308
$Co(4\text{-}CH_3py)_2Br_2$	254 (sh)	249	276	235
$Co(4\text{-}H_2Npy)_2Cl_2$	269		310	296
$Co(4\text{-}HOpy)_2Cl_2$	241	232	306	290
$Co(3,4\text{-}diCH_3py)_2Cl_2$	231		347	307.5[a]
$Co(3,4\text{-}diCH_3py)_2Br_2$	232	168	270	244
$Co(3,5\text{-}diCH_3py)_2Cl_2$	230	212	344	305
$Co(3,5\text{-}diCH_3py)_2Br_2$	230 (sh)		275	236
$Co(4\text{-}C_2H_5py)_2Cl_2$	241		341	300
$Co(4\text{-}C_2H_5py)_2Br_2$	240 (sh)		270	232
$Co(4\text{-}(CH_3)_2Npy)_2Cl_2$	226 (br)		334	305
$Co(4\text{-}(CH_3)_2Npy)_2Br_2$	230		260	246
$Co(4\text{-}(CH_3)_3Cpy)_2Cl_2$	209		347	312.5
$Co(4\text{-}C_6H_5COpy)_2Cl_2$	210	169	348	307
$Co(4\text{-}C_6H_5COpy)_2Br_2$	209	162	281	234
$Co(4\text{-}C_6H_5COpy)_2I_2$	210[a]	155	261	229
$Co(4\text{-}C_6H_5py)_2Br_2$	235[b] (vs br)	175	273	235

[a] mean of doublet

[b] coincident with other bands

sh = shoulder, br = broad band

TABLE 2.13

Cobalt-ligand bending vibrational frequencies (cm^{-1}) of tetrahedral complexes.

compound	δN-Co-N ν_5		δN-Co-X ν_6		δX-Co-X ν_7	other bands
$Co(py)_2Cl_2$	168m		138s		98mbr	
$Co(py)_2Br_2$	150w		131m		72s	
$Co(py)_2I_2$	145m		125m	76sh	64s	
$Co(3\text{-}CH_3py)_2Cl_2$	155sh		136s		96s	
$Co(3\text{-}CH_3py)_2Br_2$	150vvw		124vw		69m	
$Co(4\text{-}CH_3py)_2Cl_2$	140vvwsh		125sh		105vs	198w
$Co(4\text{-}CH_3py)_2Br_2$			112vvw		83m	
$Co(4\text{-}H_2Npy)_2Cl_2$	164w		133vs		112s	247s L 199vw
$Co(4\text{-}HOpy)_2Cl_2$	152sh	144sh	134vvs		111s	
$Co(3,4\text{-}diCH_3py)_2Cl_2$	164vvw		127w		92m	
$Co(3,4\text{-}diCH_3py)_2Br_2$	144vw		113vw		69m	
$Co(3,5\text{-}diCH_3py)_2Cl_2$	149vw		136w		95m	191vw 168vvw
$Co(3,5\text{-}diCH_3py)_2Br_2$	139vw		127w		63m	200w 153w
$Co(4\text{-}C_2H_5py)_2Cl_2$			114sh		101s	
$Co(4\text{-}C_2H_5py)_2Br_2$			98w		70s	164vvw
$Co(4\text{-}(CH_3)_2Npy)_2Cl_2$					113sbr	
$Co(4\text{-}(CH_3)_2Npy)_2Br_2$					68s	
$Co(4\text{-}(CH_3)_3Cpy)_2Cl_2$					104s	
$Co(4\text{-}C_6H_5COpy)_2Cl_2$	169vw	140sh	110sbr		92s	
$Co(4\text{-}C_6H_5COpy)_2Br_2$	137w		123m		73s	
$Co(4\text{-}C_6H_5COpy)_2I_2$	130vwsh		117w		63w	85vwbr
$Co(4\text{-}C_6H_5py)_2Br_2$	150vvw				68s	

L = ligand band

TABLE 2.14 continued/

compound	νCo-N		ν_bCo-X			other bands		
$Co(3\text{-}HOOCpy)_2Cl_2$	243s	217m	191sbr	172m		164m	145w	
$Co(3\text{-}HOOCpy)_2Br_2$	214sh	205s	136s			160sbr	110m	
$Co(4\text{-}HOOCpy)_2Cl_2$	244s	204s	190sbr	166sbr				
$Co(3\text{-}CH_3OCOpy)_2Cl_2$	220sh	205s	178s	166sh		144wsh	121w	
$Co(3\text{-}CH_3OCOpy)_2Br_2$	208s		146sbr	128m		183s		
$Co(4\text{-}CH_3OCOpy)_2Cl_2$	203s		186sbr					
$Co(4\text{-}CH_3OCOpy)_2Br_2$	196m		145s	128s		182m		
$Co(4\text{-}C_6H_5py)_2Cl_2$	210s		171s	161s		193s	138w	119w
$Co(3\text{-}Brpy)_2Cl_2$	234sh	223s	180sbr	157s		134w		
$Co(3\text{-}Brpy)_2Br_2$	223m		132s			186m	158m	
$Co(3\text{-}C_6H_5COpy)_2Cl_2$	227m	220sh	188s	160sh		151s	136sh	
$Co(3\text{-}C_6H_5COpy)_2Br_2$	222m	194m	156sh?	139s	118s	177m	101m	

Finally, we may mention the formation of hydrated cobalt complexes of type $CoL_2X_2.2H_2O$ from $[CoL_2X_2]$ complexes (where L are methyl-substituted pyridines), when left standing in air. By taking up two molecules of water, Co(II) becomes octahedrally coordinated as indicated by the colour change from blue to violet. Extra infrared bands, not present in the spectra of the anhydrous complex of the same ligand, are observed and are characterized as follows:

bands (cm^{-1}) around	assignment
3400 strong broad	νOH_2
1600 overlapped with ligand bands	δOH_2
600 medium broad	ρOH_2
500 medium broad	ωOH_2

This is consistent with the reported data of GOODGAME and HAYWARD[87] on related hydrated complexes of cobalt halides.

2.5 EFFECTS OF MATRIX, TEMPERATURE AND PRESSURE ON THE INFRARED SPECTRA

(i) matrix effects

To examine the effect of a solid state matrix on the spectrum of $[Co(py)_2Cl_2]$ (oct), samples were run in the various alkali salt pellets, the spectra being depicted in Fig. 2.57 and Fig. 2.58A. Spectra in KCl and NaF discs are identical, i.e., the position and the relative intensity of all ligand bands are the same, as well as the spectra run as Nujol mulls (see Table 2.8). This rules out the idea that Nujol mulls could be considered as intermediate between the solid and liquid state. Comparing the spectra obtained as KBr and KI pellets, differences are readily noted. These matrices have a pronounced effect on the number 18b and 6a bands of the coordinated pyridine. The very weak side band of 18b occurring

at 1062 cm^{-1} as observed in the chloride matrix, becomes very strong while at the same time the 18b band decreases in intensity as one follows the matrix sequence KCl, KBr, KI. This intensity stealing manifests itself also for the new 643 cm^{-1} band in the bromide matrix at the price of the number 6a band. The lowest frequency ligand band at 432 cm^{-1} shows a right-side shoulder in KBr, which becomes clearly resolved in KI.

Halide substitution reactions which take place between the halides of the matrix and the halides constituting the compound are commonly observed. The solid state reactions of $M(LH_2)X_2$ type complexes with various alkali halides were studied by DESSEYN *et al.*[88]. The halide exchange readily occurs at room temperature when the metal-to-halide band type is strongly electrovalent. If more covalent character is present, as in CoL_2X_2 complexes, no halide substitution is noted in the KBr matrix. The band at about 280 cm^{-1} corresponding to the terminal Co-Br stretching mode, appears after heating the pellet to 100°C (see Fig. 2.61). A further point is the occurrence of bridging halide groups which have to be transformed first into terminal halides of the monomers by either applying heat or pressure, in order to exchange with the alkali halides. The reaction $[Co(py)_2Cl_2]$ with solid KI proceeds more rapidly and occurs even at room temperature. The Co-I stretching mode observed at about 240 cm^{-1} becomes more intense shortly after heating the KI disc for a few minutes at elevated temperatures.

(ii) temperature effect

The temperature has a marked effect on the pyridine vibrations. Although the peak positions are relatively insensitive to temperature, the intensities of some pyridine bands are decreased to a large extent. Some vibrations disappear with an increase in temperature. This effect

is shown in Figs. 2.58, 2.59 and 2.61. The $[Co(py)_2Cl_2]$ (oct) samples were treated for 24 hours at the recorded temperatures in the matrix concerned. In the NaF matrix at 100°C the intensities of the number 14 band at 1367 cm^{-1} and the number 3 band at 1241 cm^{-1} decrease, while the 8b band at 1578 cm^{-1} and the 10b band at 878 cm^{-1} become inactive. The latter bands involve mainly νring and γ(CH) vibrations. The relative motion of the atoms participating in the vibration, must alter in such a way that no nett change in dipole moment occurs during the vibration. In addition, splitting of the numbers 14, 11 and 4 bands is also observed in the spectra obtained in the KCl and KBr matrices (see Figs. 2.59 and 2.61). The 18b and 6a bands undergo the major frequency shifts. All ir spectra of $[Co(py)_2Cl_2]$ in KCl, KBr and KI pellets at higher temperatures, showed the 18b band occurring at 1069 cm^{-1} and the 6a band at 645 cm^{-1}, i.e., a downward shift of 15 cm^{-1} and an upward shift of about 10 cm^{-1}, respectively, relative to those obtained at ambient temperature. Comparing Fig.2.59 B with C, we clearly see that both spectra remain identical, so that we may conclude that any possible decomposition of the complex over the temperature-range examined is inhibited by the matrix. The shift of the 16b band from 432 cm^{-1} to 425 cm^{-1} together with the appearance of the terminal Co-Cl bands at 347 cm^{-1}, indicate a change in coordination number around the cobalt ion. This change of geometry is in agreement with the conversion of the polymeric octahedral form to the monomeric tetrahedral form and is well illustrated by Fig. 2.60. This phenomenon has also been noticed by POSTMUS *et al.*[89]. The authors reported the preparation of pure monomer by heating the polymeric form in a polyethylene matrix near this colour transition. We can state, as shown in Fig. 2.62, that this conversion is completed if the 16b band exhibits a single peak corresponding to one form, rather than a doublet.

By heating $[Co(py)_2Cl_2]$ to a temperature of 160°C before pressing in

a KCl matrix, decomposition occurs and a hydrated product is formed. The typical coordinated water bands can be distinguished from the crystal water bands which are present due to the hygroscopic nature of KCl. The hydrated complex has a strong broad band centred near 3300 cm^{-1} and a sharp band at 3550 cm^{-1} due to the O-H stretches. The H-O-H scissoring occurring near 1630 cm^{-1} is partly obscured by the 8a ligand vibrational mode. Extra bands are observed at 830 and 795 cm^{-1} which are assigned to the H_2O rocking and wagging modes.

The temperature behaviour of the metal-ligand vibrations is different. LEVER *et al.*[71] found evidence that the skeletal modes increase in frequency, sometimes by as much as 11 cm^{-1}, when the sample is cooled to liquid nitrogen temperature. WONG[77,78] used low temperature data as a guide to assign and to distinguish the $[Zn(py)_2Cl_2]$ skeletal vibrations from lattice vibrations. It should be noted however that care must be taken since the latter appear to be temperature sensitive too[90]. All our ir spectra were recorded at room temperature ($\sim 23^{\circ}C$), hence only one of the two νCo-N modes expected in tetrahedral CoL_2X_2 complexes, was frequently observed (see Table 2.12).

(iii) pressure effect

Pressure studies on ML_2X_2 type complexes, where L = pyridine and substituted pyridines and M = Co and Zn, have previously been reported by FERRARO *et al.*[91,92] and WONG[78]. The investigators have demonstrated that spectral measurements at high pressures serve to distinguish lattice modes from internal vibrational modes. The former show appreciable shifts towards high wavenumber (blue shifts) which are approximately linear with pressure, whereas the peak positions of the latter exhibit only minor shifts, if any. The pressure dependence of the frequencies ($d\nu/dp$) is

related by the mode Grüneisen parameter (γ_i) to the compressibility of the crystal (K) in the equation :

$$\gamma_i = \frac{1}{K} \frac{d\ln\nu_i}{dp} \qquad (1)$$

It is found that the Grüneisen parameters of the metal-to-ligand skeletal vibrations are less than unity, while those of the pure and partial lattice modes are larger than those of the skeletal modes.

An interesting observation is the exceptionally high sensitivity to pressure of the Zn-N stretching mode. WONG[78] estimated a shift of 1.86 cm^{-1} per kilobar pressure, which is greater than that of the lattice modes of most covalent, ionic or molecular crystals reported in the literature. He stated that this is probably caused by the delocalized nature of the Zn-N bonds.

In polymeric $[Co(py)_2Cl_2]$, one would expect that the bridged cobalt-halide stretching vibrations (ν_bCo-X) are pseudo-lattice-like in their behaviour to pressure, since the polymer involves long chains of cobalt-halide bridges. This has been verified and published by POSTMUS *et al.*[89]. By applying high-pressure techniques, the authors were able to assign the bridging Co-X stretching vibrations for the first time. The symmetric and asymmetric cobalt-to-ligand vibrations of the monomer may be distinguished by the fact that the intensity of the symmetric mode is more suppressed by increasing pressure than that of the asymmetric mode. This is explained by the change in molecular volume which occurs during the symmetric vibration, while, for the asymmetric, the volume remains essentially constant. Hence, a closer packing of molecules at high pressure will interfere more with the symmetric than with the asymmetric vibrations[92]. For the same reason, the bending vibrations are expected to be less sensitive to pressure than the corresponding stretching vibrations.

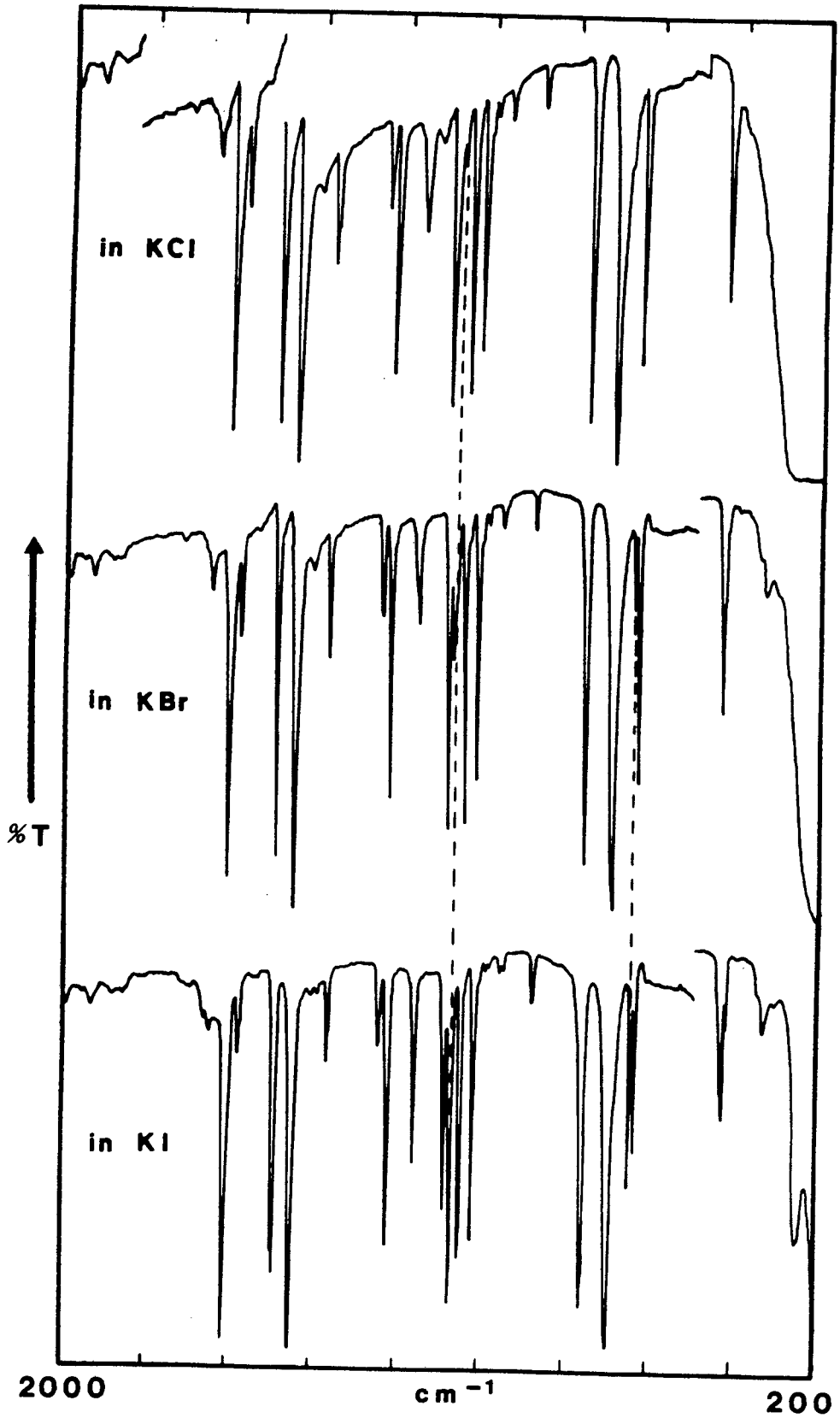

Fig. 2.57 : The ir spectra of $[Co(py)_2Cl_2]$ in different alkali-halide matrixes.

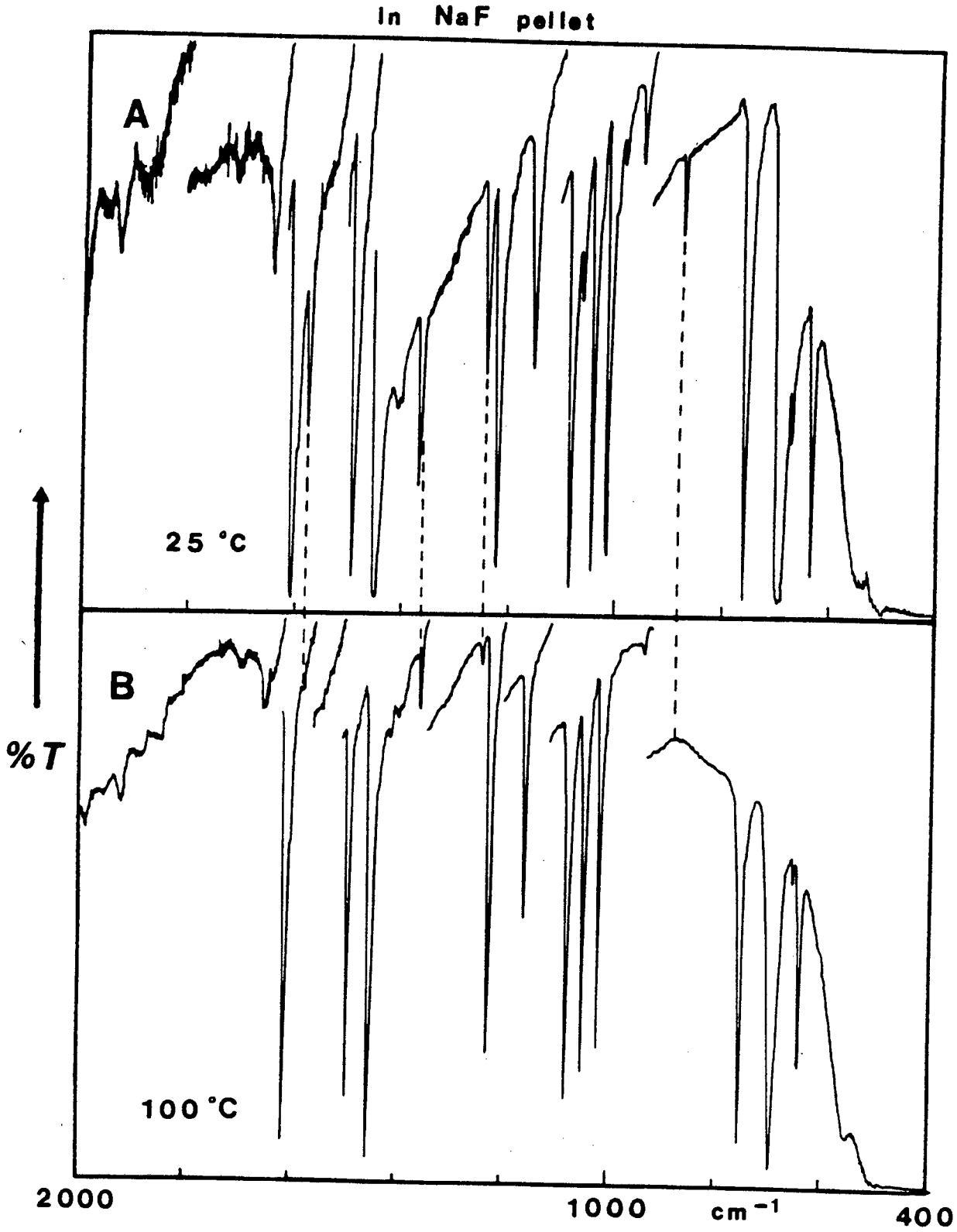

Fig. 2.58 : The effect of temperature on the spectra of $[Co(py)_2Cl_2]$ in a NaF pellet.

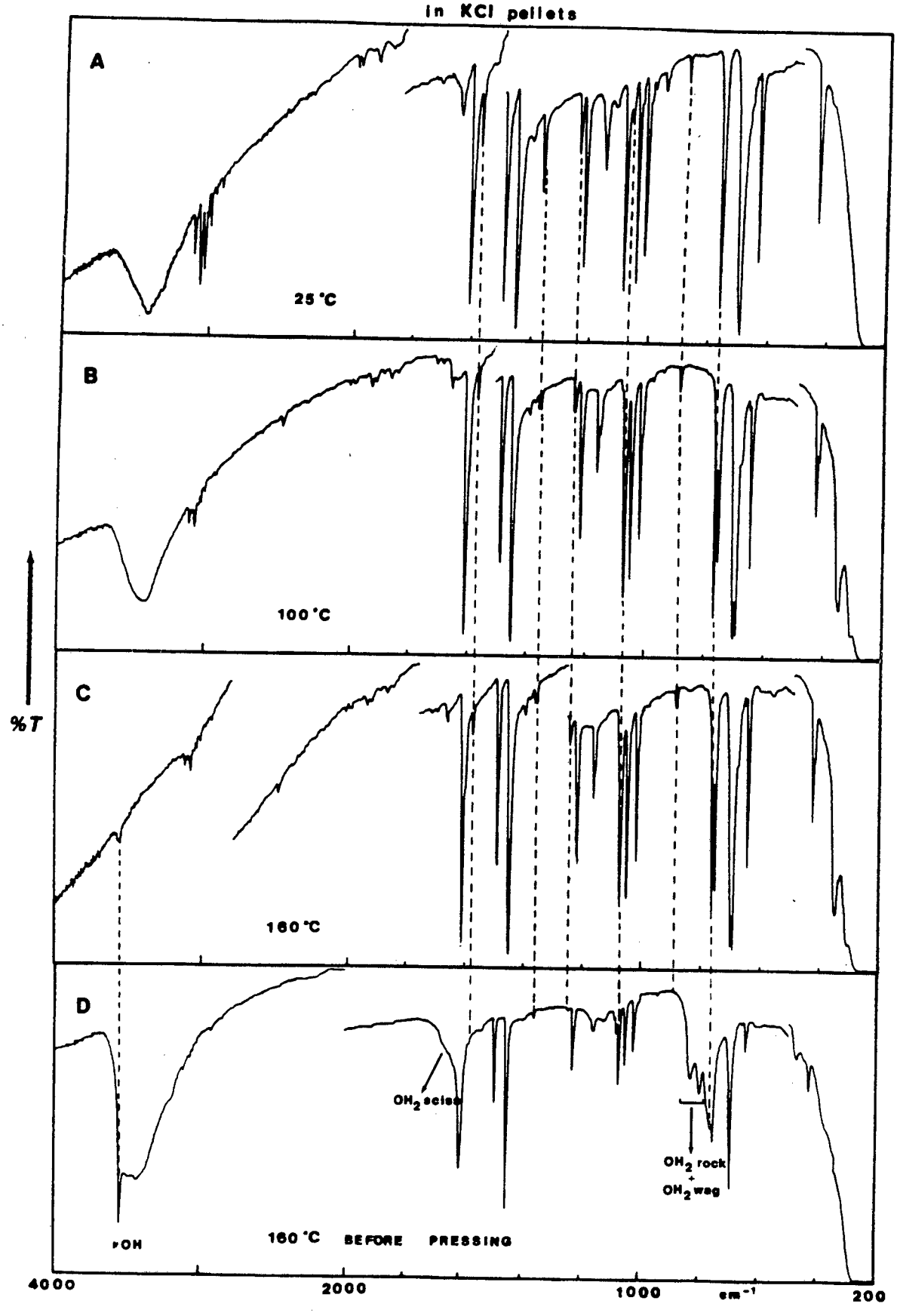

Fig. 2.59 : The ir spectra of $[Co(py)_2Cl_2]$ at different temperatures.

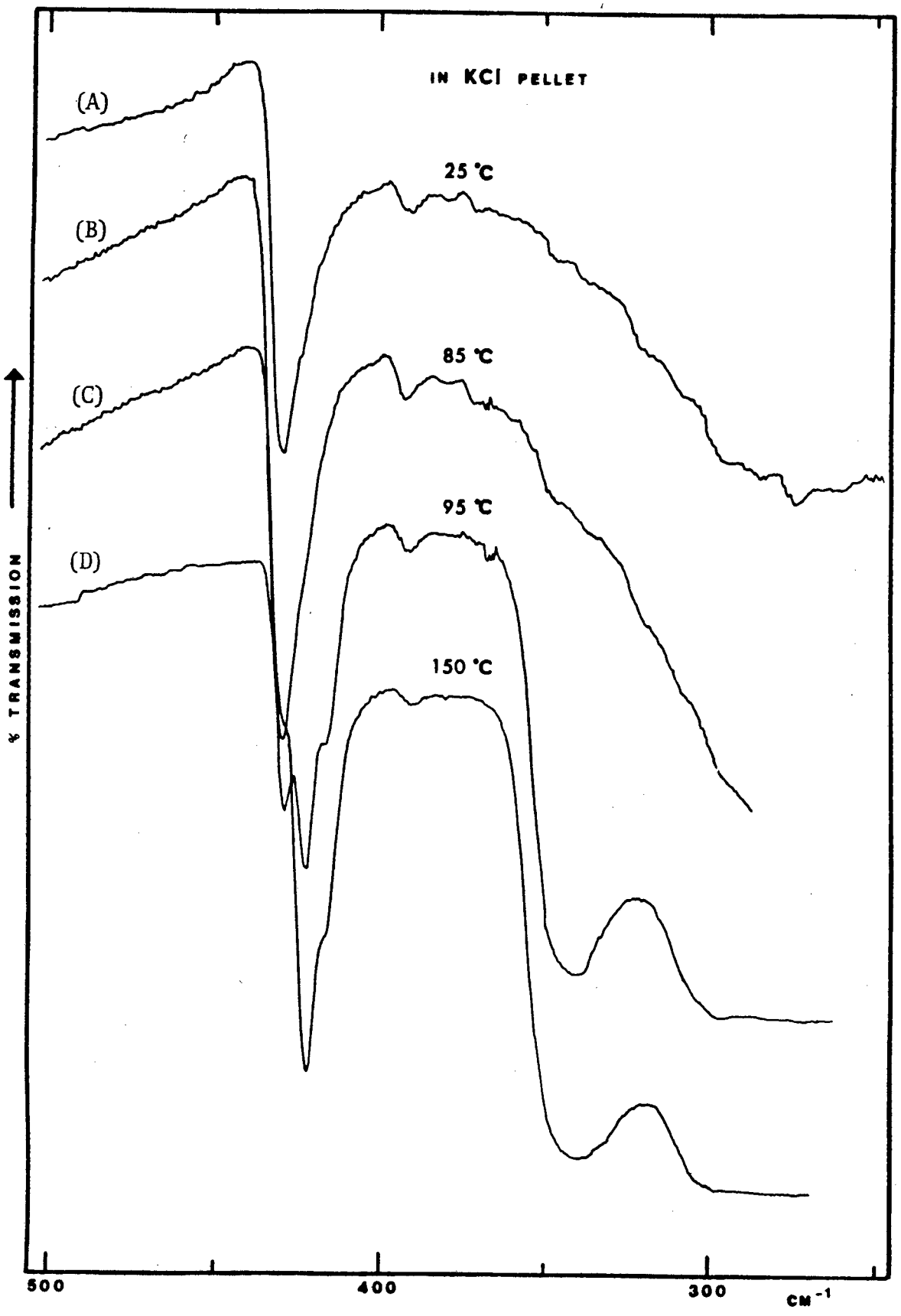

Fig. 2.60 : The effect of temperature on the spectrum of $[Co(py)_2Cl_2]$; the conversion of polymer to monomer.

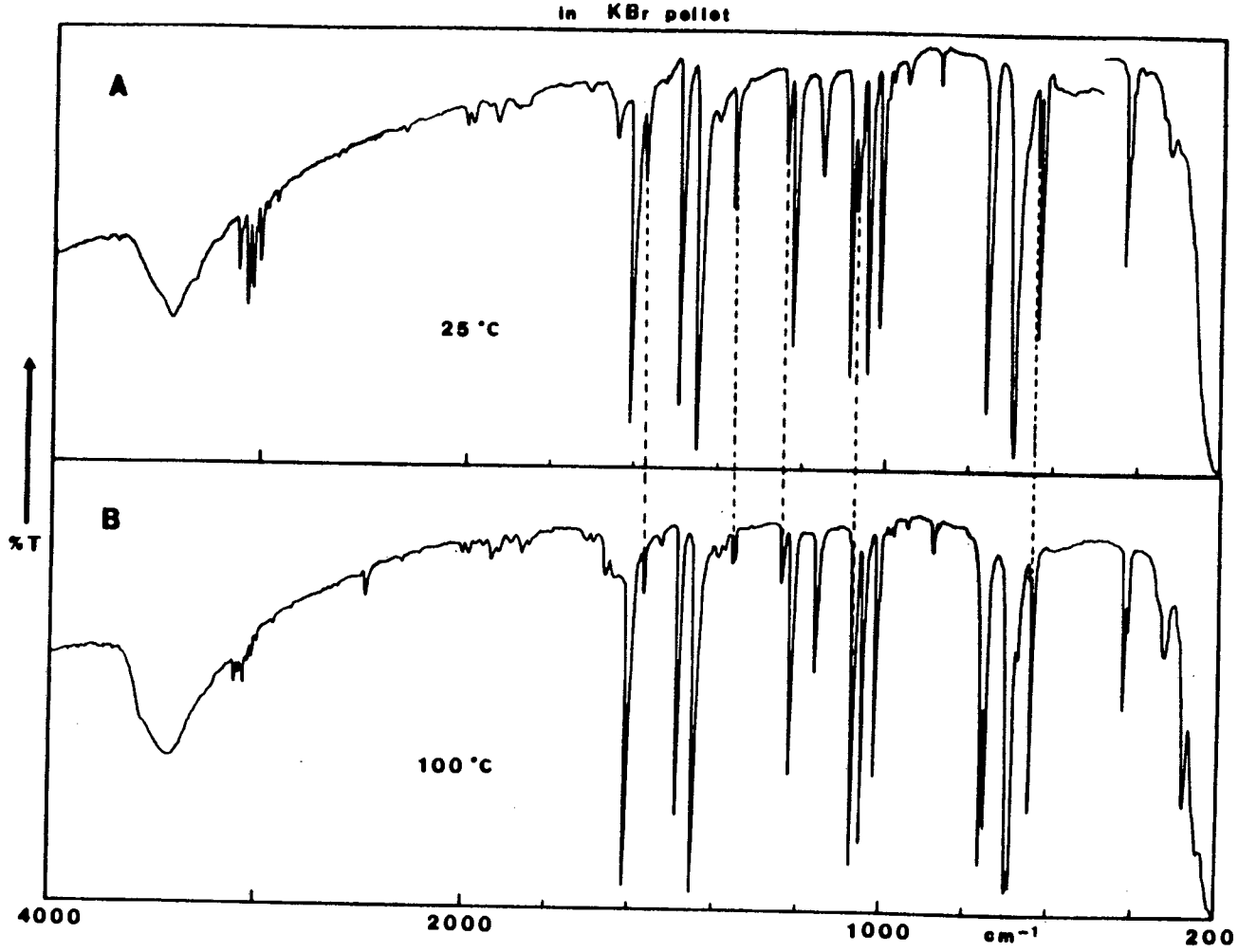

Fig. 2.61 : The effect of temperature on the spectrum of $[Co(py)_2Cl_2]$ in a KBr pellet.

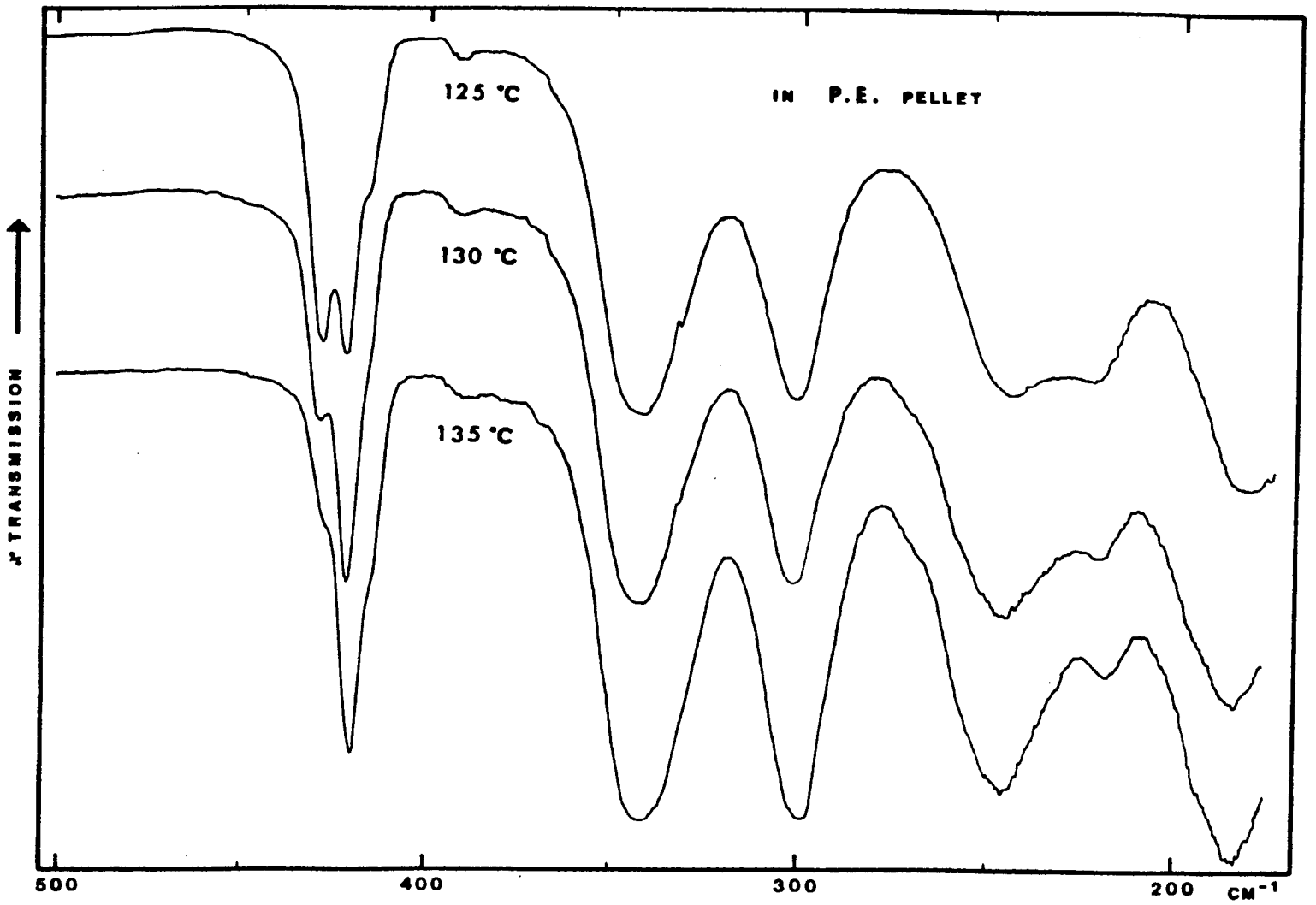

Fig. 2.62 : The far-infrared spectra of monomeric $[Co(py)_2Cl_2]$.

2.6 NATURE OF THE COORDINATION BOND

Quantitative relationships between the electronic effects of the substituents in organic compounds and their chemical reactivity have been widely studied and applied. The earliest and most familiar is the Hammett equation[93], in which the substituent constant, σ, is a measure of the electron withdrawing or electron releasing ability of the substituent, relative to hydrogen. While HAMMETT originally studied the ionization constants of substituted benzoic acids, similar structure-reactivity correlations have been tested by FISCHER *et al.*[94] for reactions of substituted pyridines. In the analysis of the Hammett equation for the dissociation constants of substituted pyridines, the author showed that their derived sigma values did not significantly differ from Hammett's original or from Taft's inductive constants for 4-(+M) substituents, whereas the 4-(-M) substituents appear to exhibit inductive effects only. These results were explained in terms of the effect of the nitrogen atom in withdrawing π-electrons from the 4-position. In this work, the Hammett constants, as reviewed by JAFFE[95], are used since they form the most extensive set available, but Fischer's values for the substituent constants, especially for groups with strong mesomeric effects, will be selected.

Empirical results have shown that simple relations exist between the variation of vibrational frequencies and the electronic effects of ring substituents. For example, the νO-H bands of phenols[96] and carboxylic acids[97] vary linearly with respect to the electron withdrawing tendencies of the substituents; a reverse trend is observed for the νN-H of anilines[98] and amines[99]. Other examples may be found in ref.100. It is well established that such relationships also generally exist for metal complexes. The νC=O and νM-O in various alkylamine, aniline and pyridine adducts of Ni(II) and Zn(II) acetylacetonates[101,102], the νM-L in metal(II) salicylaldimine[103],

anthranilate[104] and 8-hydroxyquinolate complexes[105] correlate well with the substituent constants.

Multiple bonds are very common in coordination compounds and are usually detected by a comparison of bond lengths if the geometry of the molecule is known. Alternatively, ir stretching frequencies or the related force constants and bond orders can be applied. Other frequently used methods are U.V. and visible spectroscopy and, depending on the magnetic properties and the complexity of the ions involved, e.s.r. spectroscopy and ab initio molecular orbital (MO) calculations.

The two distinctly different bonds are described in terms of symmetry planes or axes present in the molecule. The σ-bond has maximum electron density on the internuclear axis, while the π-bond is located in a single nodal plane containing the two nuclei, imposing restrictions on rotation of the two joined nuclei. π-Bonding in tetrahedral molecules is more difficult to define in view of the absence of suitable planes or axes. Evidence for the existence of π-bonds in tetrahedral oxy-ions, XO_4^{n-} (X = Si, P, S or Cl) in which the $3d_z^2$ and the $3d_{x^2-y^2}$ orbitals are involved, is demonstrated by CRUICKSHANK[106], based on structural arguments and approximate MO calculations. In order for multiple bond formation to occur, the orbitals involved must (1) have suitable symmetry, (2) have large overlaps, and (3) be of comparable energy.

As a consequence of excessive build-up of electron density on the metal by complex formation, charge can be transferred back to the ligand along π-bonds. This concept of back coordination or bonding is closely related to the electroneutrality principle. It was developed and exploited to explain the stability and reactivity of metal-olefin complexes in which the acceptors are classified as 'soft', e.g. Pt and Ag[107]. Although experimental evidence for back coordination is generally contentious since

alternative explanations are possible, the major arguments for its existence, as summarized in a review paper by PETTIT[108], are found in : (1) the trans effect, (2) nmr coupling constants, (3) ir stretching frequencies, and (4) thermodynamic properties. Note that these arguments are essentially based on the assumption that inductive effects are transmitted along σ-bonds and that their influence on π-back-bonds is not related linearly to their influence on σ-bonds.

It has been suggested that pyridine can behave as π-acceptor through the π^* antibonding orbitals of the aromatic system. This is supported by GILL's statement[59] that the electron density in the ring stays the same after donor-acceptor interaction with a transition metal. Double bonding between cobalt and pyridine was also proposed by NELSON *et al.*[10] and the extent of M-to-L π-bonding was dependent on the π-acceptor capacities of differently substituted pyridines in the following order :

py ≥ 4-alkylpy > 3-alkylpy ≥ 3,4-lut > 3,5-lut.

The relative importance of π-contribution which is controlled by the effect of the substituent, was determined by WONG and BREWER[109] in zinc and copper complexes with 4-substituted pyridines. On the basis of the lower first ionization potential, one can expect that the back-donating ability of cobalt ion will be higher than zinc ion and comparable to copper ion. Further, infrared spectroscopic evidence of back-bonding in pyridine complexes is provided by MILICEV[110]. The author based his conclusions on KROSS's observation[111] that the position of the umbrella bending band (number 11) is dependent on the electron density of the ring, and systematic shifts of that band towards lower frequency were observed in adducts where back-bonding is expected to occur.

To examine the relative bond strength of the Co-N bond in

$[Co(R\text{-}py)_2Cl_2]$ complexes, the νCo-N are plotted against the substituent constants. In order to observe variations of νCo-N caused by the electronic effect of the substituents only, and not originating from their mass effects, allowance was made for the mass effects by assuming that the pyridine ring is vibrating against the mass of the remainder of the molecule during the Co-N stretching vibration. By using the well-known relationship :

$$\frac{\nu_i}{\nu} = \sqrt{\frac{\mu}{\mu'}} \qquad (2)$$

where μ = reduced mass of pyridine and species $[Co(py)Cl_2]$;
μ' = reduced mass of substituted pyridine and species $[Co(R\text{-}py)Cl_2]$ and ν is the mean frequency (239 cm^{-1}) of the principal νCo-N bands in the pyridine complex (R=H), the shift in νCo-N arising from the mass effect of R can then be calculated as :

$$\Delta\nu_i = \nu - \nu_i \qquad (3)$$

The $\nu(Co\text{-}N)_{corr}$ defined by :

$$\nu(Co\text{-}N)_{corr} = \nu(Co\text{-}N) + \Delta\nu \qquad (4)$$

is the value of νCo-N corrected for the mass effect (see Table 2.15). These corrected values are used for the tetrahedral complexes in constructing Fig. 2.63. It is clearly that the application of equation (2) results in an overestimation of the mass effect; in the case of the octahedral complex structures, it would assume that the pyridine ring is vibrating against the infinite mass of the polymeric chain. Hence, no correction for the mass effect is made for the polymers.

The absence of a linear relationship between the νCo-N and the substituents may well indicate the complexity of the balance between σ and π-contribution. The substitution of both strongly electron releasing and electron withdrawing groups (such as $-NH_2$ and -CN, respectively) causes

a strengthening of the coordination bond as reflected by the higher νCo-N values. One may consider this discontinuity to result from the relative importance of the σ- and π-contribution. σ-Coordination bond strength is enhanced by electron releasing substituents which make the non-bonding electron pair at the pyridine nitrogen atom more available for donation. This migration of electron density of substituent to the ring is controlled by the relative energy levels of the highest occupied and the lowest vacant orbitals of ring and substituent[112] and can be understood by using a simple MO model[113]. At the same time, any π-backbonding from the metal is inhibited by the increased electron density on the ring. The reverse applies for complexes with electron withdrawing groups substituted on the pyridine, where electron density can be donated back from the metal to the delocalized system on the ring. We conclude that the predominant contribution of σ- or π-bonding to the total bond strength is entirely influenced by the substituents on the pyridine ring. This is also supported by WONG and BREWER[109], who suggested the following qualitative comparison :

	electron releasing subst.	electron withdrawing subst.
σ-bond	strong	weak
π-bond	not important	appreciable

Furthermore, by assuming that the pK_a values are a good measure of the ligand's donating abilities, we may predict a relative magnitude of σ-bonding in Co(II) complexes of substituted pyridines as follows :

$4H_2Npy > 4C_2H_5py > 4CH_3py > 3CH_3py > py > 3Clpy > 4NCpy$

with pK_a values of 9.10, 6.03, 5.98, 5.63, 5.22, 2.81 and 1.90, respectively[114,115]. Although some trend between the νCo-N and pK_a values can be seen, a significant relationship for all ligands with electron releasing substituents is not completely observed. Probably other factors, such as

steric hindrance, play an important role in the position of the metal-ligand modes. From Table 2.15, it is clearly observed that the stronger acids (e.g. 3Clpy, 3HOOCpy, or 3NCpy) give rise to higher νCo-N compared to pyridine, as a result of the induced cobalt to nitrogen back-bonding.

In analogy with MILICEV's paper, we use the displacement of the out-of-plane C-H bending mode (number 11) as a probe to detect any π-backbonding in some of our cobalt complexes. The frequency shifts are as follows:

for complexes where σ-coordination is predominant

$Co(R\text{-}py)_2Cl_2$	shifts (cm^{-1})
R = 3,4-di-CH_3	+18
4-CH_3	+19
4-C_2H_5	+19
4-$C(CH_3)_3$	+25

for complexes with π-bonding

R = 4-COOH	-20.5
3-$COCH_3$	-14
4-C_6H_5	-12
3-CH_3	- 3

TABLE 2.15

Frequencies of νCo-N observed and corrected for mass effects of R in $[Co(R\text{-}py)_2Cl_2]$: units are cm^{-1}.

R	σ	ν_i (eqn. 2)	Δν (eqn. 3)	νCo-N (obs.)	$\nu(Co\text{-}N)_{corr}$ (eqn.4)
tetrahedral complexes					
H	0	-	-	(239)	-
3-CH_3	-0.07	223.5	15.5	246	261.5
3,5-di-CH_3	-0.14	210	29	230	259
4-C_2H_5	-0.15	211	28	241	269
4-CH_3	-0.17	223.5	15.5	248	263.5
4-$C(CH_3)_3$	-0.20	192	47	209	256
3,4-di-CH_3	-0.24	210	29	231	260
4-OH	-0.36	222	17	(255)	272
4-$N(CH_3)_2$	-0.60	200	39	226	265
4-NH_2	-0.66	223	16	269	285
octahedral complexes					
4-C_6H_5	-0.03			193	
H	0			232	
3-$COCH_3$	0.12			218	
3-$CONH_2$	0.28			221	
4-$COOCH_3$	0.28			203	
3-$COOCH_3$	0.35			220	
3-COOH	0.36			243	
3-Cl	0.40			241	
4-$COCH_3$	0.52			226	
4-CN	0.55			249	
4-$CONH_2$	0.63			228	
3-CN	0.64			256	

values in brackets are means of the principal νCo-N

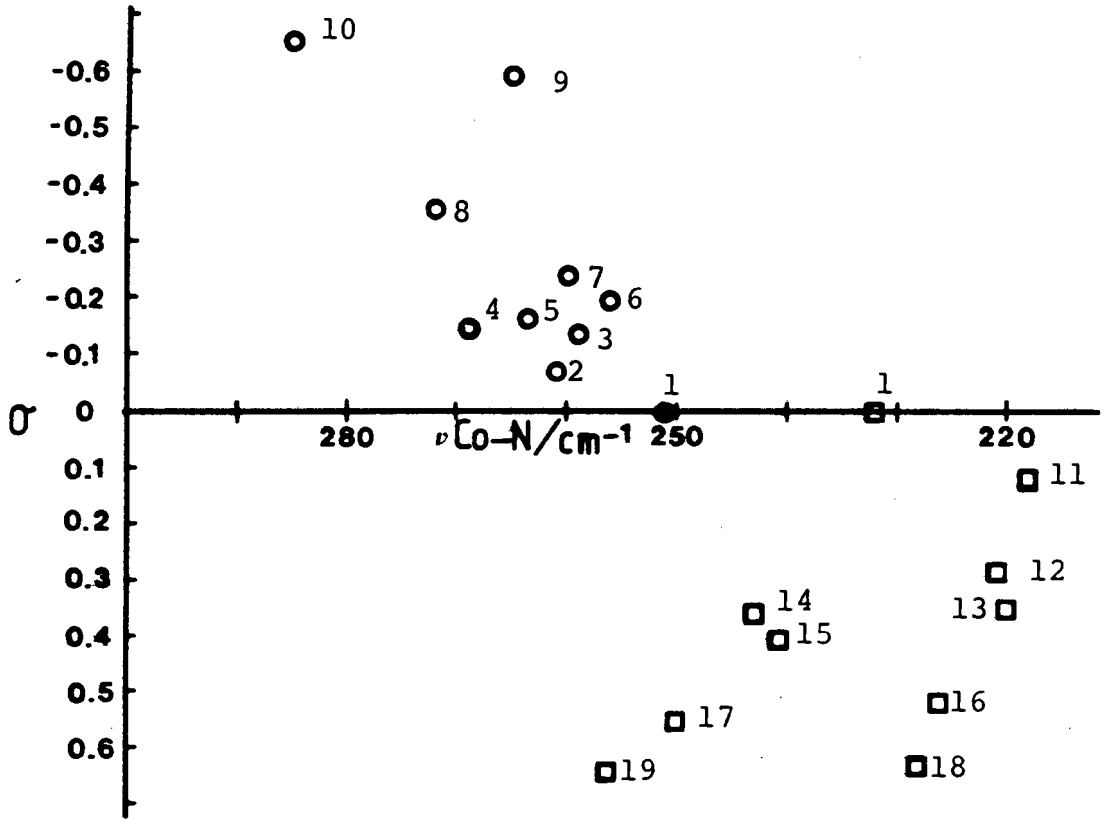

Fig. 2.63 : The variation of νCo-N with substituents constants of R.

● tetrahedral monomer, ◘ octahedral polymer

1=H ; 2=3-CH_3 ; 3=3,5-di-CH_3 ; 4=4-C_2H_5 ; 5=4-CH_3 ; 6=4-$C(CH_3)_3$; 7=3,4-di-CH_3 ; 8=4-OH ; 9=4-$N(CH_3)_2$; 10=4-NH_2 ; 11=3-$COCH_3$; 12=3-$CONH_2$; 13=3-$COOCH_3$; 14=3-COOH ; 15=3-Cl ; 16=4-$COCH_3$;17=4-CN ; 18=4-$CONH_2$; 19=3-CN

REFERENCES

1. GMELIN's Handbuch der Anorganischen Chemie, "Kobalt". No. 58A, Verlag Chemie, Weinheim, 1961.
2. J.W. MELLOR, "A Comprehensive Treatise on Inorganic and Theoretical Chemistry", Vol. 14, Longmans, London, 1935.
3. F. FISCHER, H. TROPSCH, *Brennst. - Chem.*, 7(1926)97.
4. Battele Memorial Institute, "Cobalt Monograph", Centre d'Information du Cobalt, Brussels, 1960.
5. F.A. COTTON, G. WILKINSON, "Advanced Inorganic Chemistry, a Comprehensive Text", John Wiley, New York, 1980(4th ed.)
6. T.J. SWIFT, *Inorg. Chem.*, 3(1964)526.
7. R.H. PRINCE, P. WYETH, *J. Inorg. Nucl. Chem.*, 43(1981)845.
8. L.J. ADMIRAAL, G. GAFNER, *Chem. Comm.*, (1968)1221.
9. M. LAING, E. HORSFIELD, *Chem. Comm.*, (1969)902.
10. H.C.A. KING, E. KOROS, S.M. NELSON, *J. Chem. Soc.*, (1963)5449.
11. H.H. JAFFE, M. ORCHIN, "Theory and Applications of Ultraviolet Spectroscopy", John Wiley, New York, 1962.
12. D.M. ADAMS, "Metal-Ligand and Related Vibrations: A Critical Survey of the Infrared and Raman Spectra of Metallic and Organometallic Compounds", Edward Arnold, London, 1967.
13. J.R. FERRARO, "Low-Frequency Vibrations of Inorganic and Coordination Compounds", Plenum Press, New York, 1971.
14. S. AKYÜZ, A.B. DEMPSTER, J.E.D. DAVIES, K.T. HOLMES, *J. Chem. Soc., Dalton trans*, (1976)1746.
15. GMELIN's Handbuch der Anorganischen Chemie, "Kobalt", No. 58B, Verlag Chemie, Weinheim, 1963.
16. N.S. GILL, R.S. NYHOLM, G.A. BARCLAY, T.I. CHRISTIE, P.J. PAULING, *J. Inorg. Nucl. Chem.*, 18(1961)88.

17. R.B. BENTLEY, M. GERLOCH, J. LEWIS, P.N. QUESTED, *J. Chem. Soc.*, A(1971)3751.

18. P.J. CLARKE, H.J. MILLEDGE, *Acta Cryst.*, B31(1975)1543; 1554.

19. D.P. GRADDON, E.C. WATTON, *Aust. J. Chem.*, 18(1965)507.

20. G. BEECH, *Thermochim. Acta*, 3(1972)297.

21. N.S. GILL, H.J. KINGDON, *Aust. J. Chem.*, 19(1966)2197.

22. J.de O. CABAL, H.C. KING, T.M. SHEPHERD, E. KOROS, S.M. NELSON, *J. Chem. Soc.*, A(1966)1348.

23. M. LAING, G. CARR, *Acta Cryst.*, B31(1975)2683.

24. R.M. MORRISON, R.C. THOMPSON, J. TROTTER, *Can. J. Chem.*, 57(1979)135.

25. M.M. KADOOKA, L.G. WARNER, K. SEFF, *Inorg. Chem.*, 15(1976)812.

26. J.R. ALLAN, C.L. JONES, L. SAWYER, *J. Inorg. Nucl. Chem.*, 43(1981)2707.

27. N.S. GILL, R.S. NYHOLM, P. PAULING, *Nature*, 182(1958)168.

28. R.S. NYHOLM, *Proc. Chem. Soc.*, (1961)273.

29. D.P. GRADDON, K.B. HENG, E.C. WATTON, *Aust. J. Chem.*, 21(1968)121.

30. J.E. HUHEEY, "Inorganic Chemistry, Principles of Structure and Reactivity", Harper and Row, New York, 1978(2nd ed.).

31. D. NICHOLLS, "Complexes and First-Row Transition Elements", Macmillan, London, 1974.

32. R.L. CARLIN, in "Transition Metal Chemistry" Vol.1, Chpt. 1, (R.L. CARLIN ed.) Edward Arnold, London, 1965.

33. C.J. BALLHAUSEN, C.K. JORGENSEN, *Acta Chem. Scand.*, 9(1955)397.

34. S. BUFFAGNI, T.M. DUNN, *Nature*, 188(1960)937.

35. D.C. HARRIS, M.D. BERTOLUCCI, "Symmetry and Spectroscopy", Oxford University Press, New York, 1978.

36. M. ORCHIN, H.H. JAFFE, "Symmetry, Orbitals and Spectra", Wiley-Interscience, New York, 1971.

37. W.L. DARBY, L.M. VALLARINO, *Inorg. Chim. Acta,* 48(1981)215.

38. D.A. THORNTON, *Coord. Chem. Rev.,* 55(1984)113.

39. S. PINCHAS, I. LAULICHT, "Infrared Spectra of Labelled Compounds", Academic Press, London, 1971.

40. K. NAKAMOTO, K. SHOBATAKE, B. HUTCHINSON, *Chem. Comm.,*(1969)1451.

41. K. NAKAMOTO, *Agnew. Chem., Int. Ed. Engl.,* 11(1972)666.

42. S. PINCHAS, J. SHAMIR, *J. Chem. Soc., Perkin II,* (1975)1098.

43. J.B. HODGSON, G.C. PERCY, *Spectrochim. Acta,* 32A(1976)1291.

44. G.C. PERCY, *Spectrochim. Acta,* 32A(1976)1287.

45. G.C. PERCY, H.S. STENTON, *J. Chem. Soc., Dalton trans.,* (1976)1466, 2429.

46. C.H. KLINE, J. TURKEVICH, *J. Chem. Phys.,* 12(1944)300.

47. E.B. WILSON, *Phys. Rev.,* 45(1934)706.

48. A. LANGSETH, R.C. LORD, *K. Dan. Vidensk. Selsk. Mat.-Fys. Medd.,* 16(1938).

49. L. CORRSIN, B.J. FAX, R.C. LORD, *J. Chem. Phys.,* 21(1953)1170.

50. J.K. WILMHURST, H.J. BERNSTEIN, *Can. J. Chem.,* 35(1957)1183.

51. D.A. LONG, F.S. MURFIN, E.L. THOMAS, *Trans. Faraday Soc.,* 59(1963)12.

52. H.D. STIDHAM, D.P. DILELLA, *J. Raman Spectrosc.,* 8(1979)180; 9(1980)90; 9(1980)247.

53. D.P. DILELLA, *J. Raman Spectrosc.,* 9(1980)239.

54. J.A. DRAEGER, *Spectrochim. Acta,* 39A(1983)809.

55. S. AKYÜZ, A.B. DEMPSTER, R.L. MOREHOUSE, S. SUZUKI,*J. Mol. Struct.,* 17(1973)105.

56. V.N. FILIMONOV, D.S. BYSTROV, *Opt. Spectrosc.,* 12(1962)31.

57. H. TAKAHASHI, K. MAMOLA, E.K. PLYLER, *J. Mol. Spectrosc.,* 21(1966)217.

58. D.L. CUMMINGS, J.L. WOOD, *J. Mol. Struct.,* 20(1974)1.

59. N.S. GILL, R.H. NUTTAL, D.E. SCAIFE, D.W.A. SHARP, *J. Inorg. Nucl. Chem.*, 18(1961)79.

60. R.J.H. CLARK, C.S. WILLIAMS, *Inorg. Chem.*, 4(1965)350.

61. A.T. HUTTON, D.A. THORNTON, *Spectrochim. Acta*, 34A(1978)645.

62. H.O. DESSEYN, B.J. VAN DER VEKEN, J.R. MOSS, B.J. SMITH, P.VERHOEVEN, D.A. THORNTON, *Spectrochim. Acta*, 40A(1984)467.

63. G.A. FOULDS, J.B. HODGSON, A.T. HUTTON, M.L. NIVEN, G.C. PERCY, P.E. RUTHERFORD, D.A. THORNTON, *Spectrosc. Lett.*, 12(1979)25.

64. G.A. FOULDS, D.A. THORNTON, *Spectrochim. Acta*, 37A(1981)917.

65. J.B. HODGSON, G.C. PERCY, D.A. THORNTON, *J. Mol. Struct.*, 66(1980)81.

66. S.J. ARCHER, T.P.E. AUF DER HEYDE, G.A. FOULDS, D.A. THORNTON, *Transition Met. Chem.*, 7(1982)59.

67. D.A. LONG, E.L. THOMAS, *Trans. Faraday Soc.*, 59(1963)783.

68. J.R. ALLAN, D.H. BROWN, R.H. NUTTAL, D.W.A. SHARP, *J. Inorg. Nucl. Chem.*, 27(1965)1305.

69. W.R. McWHINNIE, *J. Inorg. Nucl. Chem.*, 27(1965)2573.

70. C.W. FRANK, L.B. ROGERS, *Inorg. Chem.*, 5(1966)615.

71. A.B.P. LEVER, B.S. RAMASWAMY, *Can. J. Chem.*, 51(1973)1582.

72. M. KEETON, A.B.P. LEVER, B.S. RAMASWAMY, *Spectrochim. Acta*, 26A(1970)2173.

73. J. BURGESS, *Spectrochim. Acta*, 24A(1968)277.

74. M. GOLDSTEIN, E.F. MOONEY, A. ANDERSON, H.A. GEBBIE, *Spectrochim. Acta*, 21(1965)105.

75. C. POSTMUS, J.R. FERRARO, W. WOZNIAK, *Inorg. Chem.*, 6(1967)2030.

76. Y. SAITO, M. CORDES, K. NAKAMOTO, *Spectrochim. Acta*, 28A(1972)1459.

77. P.T.T. WONG, *Can. J. Chem.*, 52(1974)2005.

78. P.T.T. WONG, *J. Chem. Phys.*, 63(1975)5108.

79. A.T. HUTTON, D.A. THORNTON, *Spectrochim. Acta*, 34A(1978)645.

80. J.E. RUEDE, D.A. THORNTON, *J. Mol. Struct.*, 34(1976)75.

81. M.A. PORAI-KOSHITS, L.O. ATOVMYAN, G.N. TISHCHENKO, *Zh. Strukt. Khim.*, 1(1960)337.

82. I.B. BARANOVSKII, G.Ya. MAZO, *Russ. J. Inorg. Chem.*, 18(1973)981.

83. M. GOLDSTEIN, W.D. UNSWORTH, *Spectrochim. Acta*, 28A(1972)1107

84. M. GOLDSTEIN, W.D. UNSWORTH, *Inorg. Chim. Acta*, 4(1970)342.

85. M. GOLDSTEIN, W.D. UNSWORTH, *Inorg. Nucl. Chem. Letters*, 6(1970)25.

86. E.G. COX, E. SHARRATT, W. WARDLAW, K.C. WEBSTER, *J. Chem. Soc.*, (1936)129.

87. M. GOODGAME, P.J. HAYWARD, *J. Chem. Soc.*, A(1971)3406.

88. H. HOFMANS, H.O. DESSEYN, J. SHAMIR, R. DOMMISSE, *Inorg. Chim. Acta*, 54(1981)L227.

89. C. POSTMUS, J.R. FERRARO, A. QUATTROCHI, K. SHOBATAKE, K. NAKAMOTO, *Inorg. Chem.*, 8(1969)1851.

90. I. NAKAGAWA, *Coord. Chem. Rev.*, 4(1969)423.

91. J.R. FERRARO, S.S. MITRA, C. POSTMUS, *Inorg. Nucl. Chem. Lett.*, 2(1966)269.

92. C. POSTMUS, K. NAKAMOTO, J.R. FERRARO, *Inorg. Chem.*, 6(1967)2194.

93. L.P. HAMMET, "Physical Organic Chemistry", McGraw-Hill, New York, 1940.

94. A. FISCHER, W.J. GALLOWAY, J. VAUGHAN, *J. Chem. Soc.*, (1964)3591.

95. H.H. JAFFE, *Chem. Rev.*, 53(1953)191.

96. P.J. STONE, H.W. THOMPSON, *Spectrochim. Acta*, 10(1957)17.

97. M. St.C. FLETT, *Trans. Faraday Soc.*, 44(1948)767.

98. P.J. KRUEGER, H.W. THOMPSON, *Proc. Roy. Soc., London*, 243A(1957)143.

99. P.J. KRUEGER, D.W. SMITH, *Can. J. Chem.*, 45(1967)1605.

100. D. HADZI, in "Infrared Spectroscopy and Molecular Structure", Chapt. 7, (M. DAVIES ed.), Elsevier, Amsterdam, 1963.

101. J.M. HAIGH, N.P. SLABBERT, D.A. THORNTON, *J. Inorg. Nucl. Chem.*, 32(1970)3635.

102. J.M. HAIGH, N.P. SLABBERT, D.A. THORNTON, *J. Mol. Struct.*, 7(1971)199.

103. G.C. PERCY, D.A. THORNTON, *J. Inorg. Nucl. Chem.*, 34(1972)3357;3369; 35(1973)2319; 2719.

104. G.S. SHEPHARD, D.A. THORNTON, *J. Mol. Struct.*, 16(1973)321.

105. G.S. SHEPHARD, Ph.D., thesis, University of Cape Town, South Africa, 1973.

106. D.W.J. CRUICKSHANK, *J. Chem. Soc.*, (1961)5486.

107. R.G. PEARSON, *Science*, 151(1966)172.

108. L.D. PETTIT, *Q. Rev. Chem. Soc.*, 25(1971)1.

109. P.T.T. WONG, D.G. BREWER, *Can. J. Chem.*, 46(1968)131 ; 47(1969)4589.

110. S. MILICEV, *J. Mol. Struct.*, 25(1975)189.

111. R.D. ROSS, V.A. FASSEL, M. MARGOSHES, *J. Am. Chem. Soc.*, 87(1956)1332.

112. S. NAGAKURA, J. TANAKA, *J. Chem. Phys.*, 22(1954)236.

113. D.G. BREWER, P.T.T. WONG, *Can. J. Chem.*, 44(1966)1407.

114. H.C. BROWN, D.H. McDANIEL, O. HAFLIGER, in "Determination of Organic Structures by Physical Methods", Chapter 14, (E.A. BRAUDE and F.C. NACHOD eds.), Academic Press, New York, 1955.

115. S.F. MASON, *J. Chem. Soc.*, (1959)1247 ; 1253.

CHAPTER 3

NORMAL COORDINATE ANALYSIS - THEORY

3.1 THE VIBRATIONAL PROBLEM

3.1.1 Introduction

To solve the vibrational problem, we reduce the problem of a multi-body case to a single-body problem in much the same way as a diatomic molecule is treated mathematically like a single particle by introducing the mass-weighting factor, μ of reduced mass. In the Wilson GF matrix method[1,2] for the analysis of polyatomic molecules, the G matrix is the factor which does not only contain information about the constituent atomic masses but must necessarily hold structural information: bond lengths and angles. The Wilson method uses as the basic coordinates or basic vectors, five internal coordinates, namely (1) bond stretch, (2) valence angle bend, (3) out-of-plane wag, (4) torsion, and (5) linear bend which all are proven by DECIUS[3] to completely describe the normal coordinates. In one of the later chapters we wish to determine the 3N-6 normal modes with N the number of atoms, for a molecule of type ML_2X_2 where L and X are ligands in tetrahedral arrangement around the central metal M. In this case only the bond stretch (Δr) and the valence angle bend ($\Delta\phi$) are sufficient to describe the normal modes of vibration considering the ligands L and X to behave as single point masses.

The potential, V, and the kinetic, T, energy expressions in terms of the mass-geometry-weighted normal coordinates, Q, can be written according to WILSON *et al.*[1] as:

$$2V = \sum_{i=1}^{3N-6\ *} \lambda_i Q_i^2 \quad ; \quad 2T = \sum_{i=1}^{3N-6} \dot{Q}_i^2$$

---

* summation over 3N-5 coordinates for linear molecules

Rewritten in matrix notation which we adopt throughout this work, the energies have the following forms:

$$2V = Q^t.\Lambda.Q \quad ; \quad 2T = \dot{Q}^t.\dot{Q} \tag{1}$$

where Q is the column vector of the normal coordinates, $\dot{Q}$ is its time derivative with elements $\dot{Q}_i = \frac{d}{dt} Q_i$ and Λ is the diagonal matrix containing the eigenvalues (λ_i) corresponding to the fundamental vibrations or normal modes. Q^t and $\dot{Q}^t$ are the transpose matrices of Q and $\dot{Q}$, respectively. The matrix multiplication is specified by a dot between two matrices. Within the harmonic approximation, these expressions have no cross terms. The normal coordinates are defined to be mutually orthogonal, meaning physically that by excitation of one normal mode all others are not influenced.

Let us represent R as the matrix of internal coordinates. The energy expressions can then be expressed as:

$$2V = R^t.F.R \quad ; \quad 2T = \dot{R}^t.G^{-1}.\dot{R} \tag{2}$$

where G^{-1} and F are the inverse kinetic and the potential energy matrices, respectively. The advantage of the Wilson GF matrix method and hence its popularity, lies in the ease of interpretation of the elements of the F matrix: the force constants in terms of familiar stretches and bends. On the other hand the mathematics involved in the construction of the kinetic energy matrix is the most difficult task[2].

We define a transformation matrix, L, which relates the normal coordinates to the internal coordinates as:

$$R = L.Q \tag{3}$$

The potential and kinetic energy can be rewritten as:

$$2V = Q^t.L^t.F.L.Q \quad ; \quad 2T = \dot{Q}^t.L^t.G^{-1}.L.\dot{Q} \tag{4}$$

Comparison of equations (4) with equations (1) yields two important identities :

$$L^t.F.L = \Lambda \qquad (5)$$

$$L^t.G^{-1}.L = E \qquad \text{or} \qquad G = L.L^t \qquad (6)$$

where E is the unit matrix. Equation (5) indicates the relationship between the F matrix and the experimental set of vibrational frequencies utilized by some new methods for solving the inverse vibrational problem (e.g. the parameter methods and the eigenvector method of Becher and Mattes). The normalization requirements of the L matrix are determined by equation (6). Therefore we can write:

$$L^t.F.L = E.\Lambda = L^t.G^{-1}.L.\Lambda$$

Left-multiplying successively by $(L^t)^{-1}$ and G we obtain :

$$G.F.L = L.\Lambda \qquad (7)$$

This is the vibrational eigenvalue problem or the secular equation.

Because of the symmetry properties of the molecules studied, we can use symmetrized internal coordinates or symmetry coordinates, S, which are linear combinations of the internal coordinates. In practice the general 3N-6 dimensional problem reduces into smaller order problems, one for each irreducible representation of the applied point group. The new matrix, U, which transform the internal coordinates into the symmetry coordinates, given by :

$$S = U.R$$

follows the conditions of normality and orthogonality, summarized in :

$$\sum_k U_{ik} U_{jk} = \delta_{ij} \qquad (\delta = \text{Kronecker-delta})$$

where U_{ik} is a coefficient in the ith symmetry coordinate and the summation is carried out over all internal coordinates. The choice of a set of symmetry coordinates is not unique[4]; they can be obtained by the formula of NIELSEN and BERRYMAN[5]. For example, a coordinate, S_j^i, the jth symmetry coordinate corresponding to the ith irreducible representation, is generated by:

$$S_j^i = \sum_R \chi_i(R)\ R\ P^j, \qquad (8)$$

where $\chi_i(R)$ is the character for the vibrational species, i, covering the point group operation, R. P^j is the "generating coordinate" and the equation is summed over all operations of the group. P^j may be a single internal coordinate or some linear combination of internal coordinates but it is chosen so that the resulting S_j's belonging to the ith irreducible representation are mutually orthogonal.

The new expression for the G and F matrices in terms of the symmetry coordinates, G^{sym} and F^{sym}, are

$$G^{sym} = U.G.U^t \quad ; \quad F^{sym} = U.F.U^t \qquad (9)$$

and the secular equation can be stated as:

$$G^{sym}.F^{sym}.L^{sym} = L^{sym}.\Lambda$$

with L^{sym} being: $L^{sym} = U.L$

3.1.2 The Potential Energy Distribution

We want to know how well each symmetry coordinate depicts the normal coordinates. In other words what is the contribution of each S_i, to the total potential energy of a given normal coordinate Q_n. Using equation 4a and assuming the MORINO *et al.*[6] proposition, the potential energy distribution of one normal coordinate is given by :

$$2V(Q_n) = Q_n^2 \sum_{i,j} F_{ij} L_{in} L_{jn}$$

By neglecting all terms except the largest ones when i = j, only the diagonal elements in the F matrix are taken up. Since we are interested in their relative contribution (as a percentage), the potential energy distribution matrix, PED, is defined by the following expression :

$$PED_{ij} = \frac{F_{ii} L_{ij}^2}{\sum_i F_{ii} L_{ij}^2} \times 100 \qquad (10)$$

where PED_{ij} is an element of the PED matrix which gives the contribution of the ith symmetry coordinate to the jth normal coordinate. The denominator serves as a normalization factor. These are the values given in later tables under the column P.E.D. (%).

We read in ref.2 "Band assignments are possible if the appropriate element of the PED matrix make up most of the potential energy of the normal coordinate in question." Hence in this way we are able to "label" a normal coordinate as a particular kind of vibration.

3.1.3 The construction of the kinetic energy matrix

The Wilson's[1] formula to calculate the elements of the G matrix, g_{ij}, is defined as :

$$g_{ij} = \sum_{\alpha=1}^{N} \mu_\alpha \bar{s}_i \circ \bar{s}_j \qquad (11)$$

where the small circle represents the scalar product of the two $\bar{s}$ vectors and μ_α, the reciprocal of the mass of atom α. The summation runs over all atoms participating in the internal coordinates, i and j. The $\bar{s}$ vectors are defined in terms of unit vectors, $\bar{e}_{\alpha\beta}$, directed along the bonds, except for the linear bend. For the physical meaning of the vector $\bar{s}_{i\alpha}$ we

quote from "Molecular Vibrations"[1]: "Let all atoms except α be in their equilibrium positions. The direction of $\bar{s}_{i\alpha}$ is the direction in which a given displacement of atom α will produce the greatest increase of internal coordinate i."

Let us analyse in more detail the internal coordinates we are dealing with in this study.

1) The bond stretch ($\Delta r_{\alpha\beta}$); this coordinate can be visualized in Fig. 3.1.

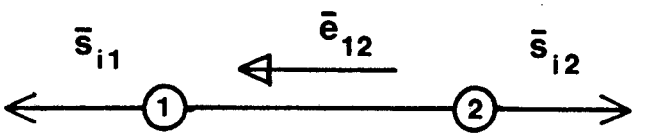

Fig. 3.1 : Definition of the unit vector and $\bar{s}$ vectors for the increase in interatomic distance between atoms 1 and 2.

The $\bar{s}$ vectors for atoms 1 and 2 are

$$\bar{s}_{i1} = + \bar{e}_{12} \quad ; \quad \bar{s}_{i2} = - \bar{e}_{12} \qquad (12)$$

2) The valence angle bend ($\Delta\phi_{\alpha\gamma\beta}$); from Fig. 3.2 which illustrates the definition of the unit vectors,

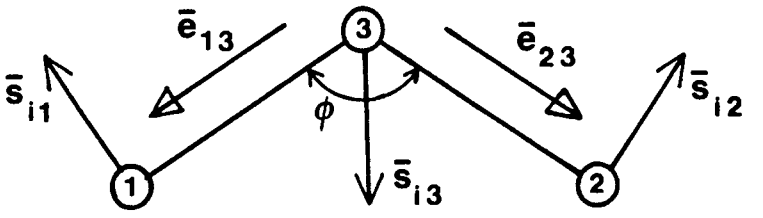

Fig. 3.2 : Construction of the $\bar{s}$ vectors for the increase in the valence angle ϕ formed by two bonds.

The following expressions of $\bar{s}_{i\alpha}$ are obtained:

$$\bar{s}_{i1} = \frac{\cos\phi\ \bar{e}_{13} - \bar{e}_{23}}{r_{13}\sin\phi} \quad ; \qquad (13)$$

$$\bar{s}_{i2} = \frac{\cos\phi\ \bar{e}_{23} - \bar{e}_{13}}{r_{23}\sin\phi} \quad ; \qquad (14)$$

$$\bar{s}_{i3} = -(\bar{s}_{i1} + \bar{s}_{i2}) \quad ; \qquad (15)$$

where r_{13} is the bond length between atoms 1 and 3 and ϕ the bond angle.

These and other formulae for the additional internal coordinates: the out-of-plane wag ($\Delta\gamma$) and the torsion ($\Delta\tau$) are given earlier by WILSON[7] and all are collected in "Molecular Vibrations"[1]. The derivation of the Wilson's $\bar{s}$ vectors has been subject to several methods[8,9,10]. Most noticeable is the consistent derivation of the complete set by McINTOSH *et al.*[11] which includes new expressions for the out-of-plane wag.

The construction of the G matrix using the method of WILSON and DECIUS is a tedious and time consuming task to perform algebraically. In his paper[12], DECIUS presented tables containing all possible combinations (G_{rr}, $G_{r\phi}$, $G_{\phi\phi}$, $G_{r\tau}$, $G_{\phi\tau}$, $G_{\tau\tau}$) for different bond angles (ϕ = 90°, 109°28' and 120°) to evaluate the g elements. WHITMER[13] has published an algorithm for the computation of these elements using the readily available internal coordinates as input. An alternative method which is easily modified for computing purposes, is proposed by OVEREND *et al.*[14]. Assuming NAKAMOTO's derivation[15] the G matrix can be written as:

$$G = B.M^{-1}.B^{t} \qquad (16)$$

where M^{-1} is a diagonal matrix whose elements are the reciprocals of the atomic masses. The B matrix containing the components of the $\bar{s}$ vectors (as compared with equation 11), is the transforming matrix defining

internal coordinates in terms of Cartenian coordinates:

$$R = B.X \qquad (17)$$

In analogy to equation 9a, the symmetrization of the G matrix is defined as :

$$G^{sym} = U.B.M^{-1}.B^{t}.U^{t} \qquad (18)$$

In the case of a linear bend ($\phi = 180^{o}$) the equations 13 to 15 cannot be used, and FERIGLE and MEISTER[16] have discussed appropriate formulae, while GANS[17] has proposed a new derivation using supplementary planes defined by other atoms in the molecule to describe the motion of the linear bending coordinate.

Expression 18 has been incorporated into our GMATRIX-programme, originally written by VAN DER VEKEN[18] in Fortran IV for use on the IBM 1130 computer. We have modified the programme to Fortran (ASCII) level 10R1 on the SPERRY-UNIVAC 1100 computer at this University. Input consists of (1) the geometrical parameters (i.e. atomic masses, bond lengths) for the molecule in which all atoms are identified by a code number, (2) the coordinates of the unit vectors in reference to an arbitrary atom, (3) coded instructions for calculating the B matrix of the different internal coordinates and (4) coded instructions defining the symmetry coordinates.

3.1.4 The Isotope Rules

Under the Börn-Oppenheimer approximation the molecular force field is a function of the electronic structure of the molecule only and is not influenced by the masses of the constituent nuclei. Therefore, changes in vibrational frequencies are expected if the kinetic coefficients in the G matrix are altered by isotopic substitution. The best known quantitative relation, involving the isotope effect is the TELLER-REDLICH product rule[19,20]. This rule can be proven on polynomial expansion in the n

eigenvalues, λ, of the determinant of the GF matrix from the secular equation (7):

$$\prod_k \lambda_k = |G.F| = |G|.|F| \tag{19}$$

If we apply this equation to an isotopically substituted molecule:

$$\prod_k \lambda_k^i = |G^i| \cdot |F| \tag{20}$$

where the superscript i refers to the considered isotopic species and then divide one equation by the other, we obtain the product rule:

$$\frac{\prod_k \lambda_k}{\prod_k \lambda_k^i} = \frac{|G|}{|G^i|} \tag{21}$$

which applies separately to the product of eigenvalues belonging to each irreducible representation.

In addition there exists certain sum rules stated as:

$$\sigma_\alpha = \sum_{i,j} G_{ij}F_{ij} = \sum_\alpha n_\alpha \sum_k \lambda_k = 0 \tag{22}$$

where the sum is over a suitable combination of isotopic forms (α) of the molecule and over the eigenvalues under a particular symmetry species. Higher order isotopic rules as intermediates between product and sum rules, are all far less practical[21]. These rules hold exactly only when correction is made for anharmonicities in the fundamental modes of vibration.

3.1.5 Solution to the vibrational problem

Suppose we know the values of the harmonic force constants and we want to calculate the vibrational frequencies and normal modes. For deriving the eigenvalues and eigenvectors of the non-symmetric GF matrix,

the method of MIYAZAWA[22] to proceed by a two-step diagonalization technique* involving symmetric matrices, is used. The well-known method for obtaining the eigenstructure of a symmetric matrix is the one invented by JACOBI[23] which we will apply here and in further computerized methods.

Let P and Π be the eigenvectors and eigenvalues of the symmetric inverse kinetic energy matrix :

$$G.P. = P.\Pi \qquad (23)$$

From the fact that P is orthonormal, we can form a matrix $D = P.\Pi^{\frac{1}{2}}$ such that $D.D^t = G$ hold, where the elements of the diagonal matrix, $\Pi^{\frac{1}{2}}$, are the square roots of the corresponding elements of Π. The second eigenvalue problem of the symmetric $D^t.F.D$ matrix results in the same eigenvalues as GF and an eigenvector matrix Y related to L of secular equation (7) by :

$$L = P.\Pi^{\frac{1}{2}}.Y \qquad (24)$$

Proof: by definition $D^t.F.D.Y = Y.Q$

multiplying by D $G.F.(D.Y) = (D.Y).Q$ (Q.E.D.)

For very large molecules it becomes necessary to solve its vibrational eigenvalue problem by means of a high speed computer. We have written a programme, named GFMATRIX in Fortran(ASCII) level 10R1 for use on the University's computer. A listing of the main body is presented in appendix I. MIYAZAWA's method is embedded in the subroutine NROOT.

3.2 MOLECULAR FORCE FIELD CALCULATIONS

3.2.1 Introduction

As shown in the previous paragraph, the molecular vibrations are

---

* also described in ref. 8, page 102

described within the harmonic approximation by the eigenvalue equation (7) or its alternative determinantal form :

$$|G.F - E.\Lambda| = 0 \qquad (25)$$

In practice, the G matrix elements are known from the equilibrium configuration and the eigenvalues, λ_i's are related to the observed vibrational frequencies by :

$$\lambda_i = 4\pi^2 c^2 \nu_i^2 \qquad (26)$$

where c is the velocity of light, and hence we have to determine the elements of the F matrix. In other words the inverse eigenvalue problem is to be solved. This implies the estimation of $\frac{1}{2}n(n+1)$ unknown force constants from n vibrational frequencies which is a mathematical impossibility. Additional information such as isotopic shifts, Coriolis coupling constants, centrifugal distortion constants, mean amplitudes of vibration, etc ...[24,25,26] are necessary for determining the exact force field. However, most of these data can only be measured in the gaseous state; thus, for most molecules, limited frequency data are available. Hence, approximation methods are needed which reduce the number of unknowns to an equal or lesser number of data; model force fields in which constraints are imposed on the force constants.

Several types of model force fields have been proposed, which include the central force field[27], the simple valence force field [27], the orbital valence force field[28] and the hybrid orbital force field[29,30]. For large molecules the modified or internal valence force field introduced by SCHACHTSCHNEIDER and SNYDER[31,32] for alkanes, the Urey-Bradley-Schimanouchi force field[14,33,34,35] which is still very popular in the literature, and the group coordinate force field[36,37] formerly named the local symmetry force field[26] are currently used. Practical examples have been reviewed previously[34,38,39].

Even in most of these models an analytical solution is not possible, so that further refining of the force constants is required by the least-squares method[14,40,26]. This method does not always lead to satisfactory results, some of the difficulties encountered being summarized by ALDOUS and MILLS[41] : slow convergence or even divergence, multiple solutions, singularity of the Jacobian matrix and non-linearity between the force constants and frequencies.

Over the last 20 years new approaches have been suggested for the calculation of force constants applying a generalised valence force field (GVFF). This field includes in its potential energy function all possible interactions between the basic coordinates. In such treatments there exists a multiplicity of solutions corresponding to the n! permutations of assigning the frequencies to motion coordinates[42,43]. In this connection, the parameter method of TOROK and PULAY[44,45,46] is a great contribution, providing further mathematical constraints to remove the indeterminacy of solutions to inverse vibrational problems.

Any real, symmetric and positive definite F matrix can be represented by :

$$F = P.\Pi^{-\frac{1}{2}}.X.\Lambda.X^{t}.\Pi^{-\frac{1}{2}}.P^{t} \qquad (27)$$

where the arbitrary real orthogonal matrix X (i.e. determinant +1) is expressed as a function of $\frac{1}{2}n(n-1)$ independent parameters: rotation angle, antisymmetric or exponential parameters in the n-dimensional problem. The normal coordinate transformation matrix, L, is purely kinematic defined in terms of G matrix characteristics as given in the diagonalization equation (23) ;

$$L = P.\Pi^{\frac{1}{2}}.X \qquad (28)$$

This method allows a search for maximum and minimum values of the force constants in which the experimental frequencies are reproduced, and

selection of the best solution is based on the criterion of keeping the sum of the squares of the distances between the set of normal coordinates and symmetry coordinates to a minimum ;

$$\sum_{i=1}^{n} |Q_i - S_i|^2 \quad = \quad \text{minimum} \qquad (29)$$

Various authors have formulated other such decision criteria, implicit or explicit, in the following methods which are differentiated by the choice of the matrix X : BILLES' method[47,48,49], the maximal F trace approach of FREEMAN[50], the concept of characteristic set of valence coordinates by HERRANZ and CASTANO[51,52], the progressive rigidity method[53 to 57] and the viral theorem approach of REDINGTON and ALJIBURY[58], etc. The force constants calculated by these kinematic models are shown by PANCHENKO *et al.*[59] to have limited transferability to isotopic molecules and they are not a good starting point for the least-squares procedure in which approximate force constants are refined to fit additional data such as isotopic frequencies and Coriolis coefficients.

Iterative methods, firstly introduced by FADINI[60] and developed into a computational method by SAWODNY[61] are based on a step by step introduction of the off-diagonal elements of the G matrix. FADINI proceeds from the Cayley-Hamilton theorem which states that each square matrix satisfies its characteristic equation, i.e. the secular equation (7) can be written as :

$$\sum_{i=0}^{n} c_i (G.F)^i \quad = \quad 0 \qquad (30)$$

where 0 is a square zero matrix of order n. This polynomial expression is used to obtain a system of n^2 algebraic equations in n^2 unknown elements F_{ij}. The coefficients, c_i, are related to the eigenvalues, λ_i, known from experiment. The initial approximation of the F matrix based on the idea

of characteristic vibrations, is given by the relation :

$$F_o = (G_d)^{-1}.\Lambda \qquad (31)$$

where the subscript o indicates the zeroth approximation and the G_d matrix contains only the diagonal elements. For the mth step the solution F_m has the form of an approximate solution F_{m-1} plus a small correction term ΔF_m :

$$F_m = F_{m-1} + \Delta F_m \qquad (32)$$

which is then used for linearization of equation (30).

Fadini's method has been the subject of much criticism : (1) AVERBUKH *et al.*[62] stated that the stepwise transition from G_d to G makes no sense and that the initial choice of F_o is not justified; (2) ALIX *et al.*[63] proved it mathematically incorrect; (3) WAIT *et al.*[64] showed from numerical results that the method does not predict isotopic shifts and minimizes the off-diagonal force constants. Finally, (4) because of the insufficient equations no unique solution can be obtained[65].

Another iterative method is the eigenvector method (EVM) suggested by BECHER and MATTES[66] which transfers the eigenvectors of an approximate solution calculated at the mth step to the exact solution of the secular equation. The transformation of F_o defined by expression (31), to F is achieved through repetitive application of equation (5). Unlike previous methods, this procedure does not contain any mathematical inconsistencies.

More flexibility is encountered in the CHACON and MAIZKE[67] development of the eigenvector method which considers possible dependencies of symmetry force constants belonging to different irreducible representations. Any number of force constants between n and $\frac{1}{2}n(n+1)$ can be determined.

An equivalent form of the method of BECHER and MATTES is found in

the matrix polynomial expansion method (MPEM) of ALIX[63,68,69]. This method is much simpler in computation and omits the practical difficulty of solving an eigenvalue problem for a non-symmetric matrix.

For most of these methods similar results and physically acceptable force fields are obtainable only if small kinetic coupling (mass coupling) exists between the symmetry coordinates. In their excellent review, ALIX *et al.*[70] have studied these and various approximation methods for calculation of force constants using a general valence force field in their mathematical approach in relation to their physical significance and their practical limitations. Finally, let us note here the potential application of stepwise coupling methods, especially the BECHER and MATTES method, in estimating mean amplitudes of vibrations directly from experimental frequencies in electron diffraction studies[71].

In the following paragraphs we will present a brief description of two iterative methods, namely, EVM and MPEM.

3.2.2 The Eigenvector Method

In the first approximation of the F matrix, BECHER and MATTES[66] assumed the situation for totally uncoupled vibrations. By neglecting all mass and force constant coupling determined by the off-diagonal elements in the kinetic and potential energy matrices respectively, each frequency is *a priori* attributed to one symmetry coordinate. Hence the eigenvector matrix, L, is reduced to the unit matrix, and the initial F_o matrix follows from the eigenvalue equation (7) as :

$$F_o = (G_d)^{-1}.\Lambda exp \qquad (33)$$

where Λexp is the diagonal eigenvalue matrix computed from the experimental frequencies through eq.(26). In further calculations, the off-diagonal elements of the G matrix are introduced stepwise. At the mth step the G matrix is given by :

$$G_m = f\left(\frac{m}{m_o}\right)(G - G_d) + G_d \qquad (34)$$

with m_o being the total number of steps used and the eigenvalues and eigenvectors are calculated as :

$$G_m.F_{m-1}.L_m = L_m.\Lambda calc \qquad (35)$$

Using the properties of the G and F matrices expressed in equations (5) and (6), the new force constants matrix is obtained as :

$$F_m = (L_m^{-1})^t.\Lambda exp.L_m^{-1} \qquad (36)$$

It is important that the order of the eigenvalues and eigenvectors calculated in each step by eq. (35) is the same as the order used in eq. (33) before one applies eq. (36). This is achieved by the criterion -- assuming the relation of the normal coordinates and symmetry coordinates stated by :

$$S = L^{sym}.Q \qquad (37)$$ --

each eigenvector corresponds to that symmetry coordinate which makes up most of its normal coordinate. This decision is settled according to the information obtained from the potential energy distribution also calculated at each step. Rearrangement of the eigenvectors is done by placing their most contributing symmetry coordinate onto a diagonal position in the L^{sym} matrix. At the end of the iteration process, the experimental frequencies are reproduced exactly.

The stepwise introduction of the off-diagonal G matrix elements can be accomplished by several ways of coupling[72] e.g. a linear coupling term as suggested by SAWODNY[61]. In their discussion of the convergence of the Becher and Mattes method, VAN DER VEKEN[73] concluded that the results became independent of the coupling method for large values of m_o. However, better convergence is observed using the square-root coupling function :

$$G_m = \left(\frac{m}{m_o}\right)^{\frac{1}{2}}(G - G_d) + G_d \qquad (38)$$

We have chosen the EVM not only for its elegant way of computation (the flow-diagram is presented in Fig. 3.3) but also for its applicability to problems of greater dimensions. Appendix II is a listing of our main programme BECMAT to calculate general valence force constants.

3.2.3 Criticism and Application Limits

AVERBUKH *et al.*[62] have strongly criticized the method of BECHER and MATTES as being mathematically incorrect. The fallacy of this method is connected with the basic formulation of the problem. The true potential energy matrix can uniquely be determined if not only the frequencies but also the modes of vibrations are known. There exists an infinite set of F matrices satisfying equation (36) which reproduce identically the experimental frequencies when substituted in the secular expression (7). Hence, this argument cannot serve as proof that the solution obtained is indeed the physically true solution. According to the authors the method must give useful vibrational results. The criteria are the invariance of the force constants for all the series of isotopic species of the molecule and the transferability to some homologous series of compounds.

To refute the first part of this criticism, we make mention of the papers by ALIX *et al.*[63,70] in which they analysed the theoretical and physical significance of the EVM and concluded that the method is mathematically without any contradiction. The closeness of the calculated force constants to the physically true solution, hence its reliability, has been previously demonstrated by VAN DER VEKEN[18,83].

In the following series of examples, we have calculated general valence force fields by the EVM. Transferability is tested by predicting

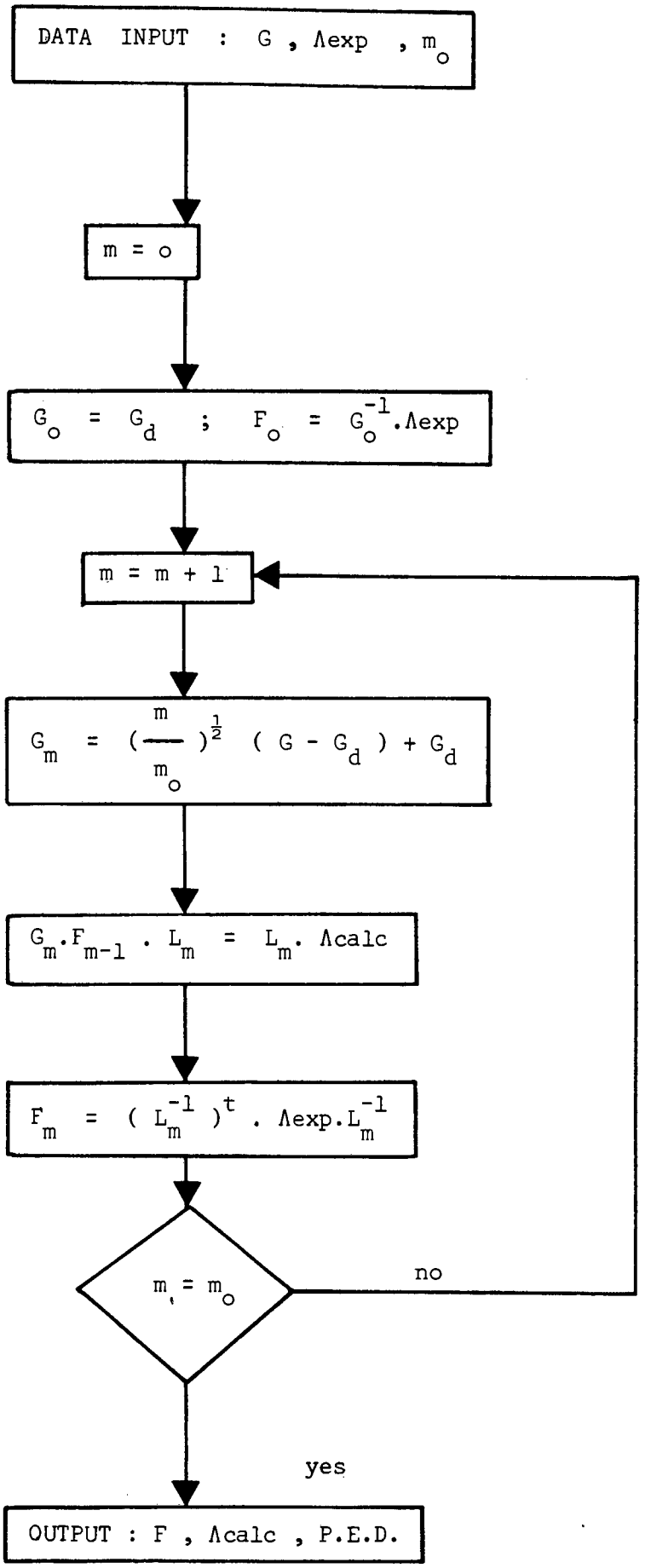

Fig. 3.3: The eigenvector method flowchart.

the observed frequencies of isotopically related compounds.

Normal coordinate treatment of the in-plane vibrations of *trans*-*N*-methylacetamide have been performed by MIYAZAWA *et al.*[74], by JAKES *et al.*[75] and REY-LAFON *et al.*[76]. The complex nature of the characteristic amide vibrations as suggested from the interactions between stretching and bending modes, makes the choice of this compound a particularly valuable criterion. The first workers assumed as intramolecular potential function an Urey-Bradley interaction type; they used force constants from diformylhydrazine and other molecules of similar structures to calculate the frequencies of CH_3-COND-CH_3. We have adopted the same experimental data and symmetry coordinates as in their paper[74]. In Table 3.1, are listed the observed frequencies (column 1), the calculated frequencies by the authors (column 2), and by us (column 4), together with the percentage deviations (columns 3 and 5), and their average values. From the average deviations it may be concluded that the results obtained by the BECHER and MATTES method are better than those reported by MIYAZAWA.

Availability of extensive experimental frequencies of eight isotopic species made it possible for JAKES[75] to refine the force constants. Later corrections for eliminations of redundancies by REY-LAFON *et al.*[76] leads to a complete valence force field model of *N*-methylacetamide (NMA). We have calculated the force field of CD_3-CONH-CD_3, and no converging results could be obtained assuming the same assignment of νCC and νN-CD_3 as the authors since contribution of the νCC is situated in bands between 1150 and 580 cm^{-1}.

TABLE 3.1

Observed and calculated frequencies of CH_3-COND-CH_3 using MIYAZAWA's data (ref.74).

obs.	calc.	calc-obs. %	calc.	calc-obs %
1642	1630	-0.73	1652	-0.61
1475	1421	-3.66	1450	-1.69
1121	1076	-4.01	1135	1.25
960	928	-3.33	998	3.96
870	953	9.54	872	0.23
627	601	-4.15	627	0.00
436	431	-1.15	431	-1.15
292	277	-5.14	273	-6.51
average deviation (%)		3.96		1.93

However, if we assign νCC to 821 and νN-CD_3 to 1098, as proposed by DESSEYN[77], the method now reproduces the frequencies and the relevant force constants. With this force field, the frequencies of NMA and its deuterated derivatives : CH_3-CONH-CD_3 and CD_3-CONH-CH_3 are recalculated and summarized in Table 3.2. The relative error in percentage derived from absolute values as:

$$\text{error (\%)} = \frac{|\bar{\nu} \text{ calc} - \bar{\nu} \text{ obs}|}{\bar{\nu} \text{ obs}} \times 100 \qquad (39)$$

are in the same order as the corresponding compounds in Table 3.2 for JAKES *et al.* 0.63 ; 1.97 ; 0.74 and for REY-LAFON *et al.* 0.87 ; 2.00 ; 1.10. It is evident that our approximate solution related to the information regarding only one molecule is surprisingly close to the refined solution. Consequently, the results can serve as an excellent starting point for the least-squares method to fit other spectral data, where available.

The following example shows the applicability of the method to isotopes other than deuterium in which more coupling can be expected. Treatment of the in-plane vibrations of trans nitrous acid as shown by VAN DER VEKEN[78] leads to a force field which allows the prediction of small isotopic shifts with convincing accuracy. The author reported the calculated frequencies for six isotopically substituted derivatives involving ^{15}N and ^{18}O isotopes.

From the above examples we may conclude that the BECHER and MATTES procedure yields a valence force field fulfilling the requirements stated by AVERBUKH *et al.*[62], and hence can be considered as practically useful.

Applicability of the EVM is limited by its formulation of the starting approach to the inverse vibrational problem. ALIX *et al.*[70]

TABLE 3.2

Calculated frequencies for various deuterated species of *N*-methylacetamide using the force field of CD_3-CONH-CD_3 together with the differences from the observed frequencies (in cm^{-1}).

	CD_3-CONH-CD_3		CH_3-CONH-CH_3		CH_3-CONH-CD_3		CD_3-CONH-CH_3	
assignment		$\Delta\bar{\nu}$		$\Delta\bar{\nu}$		$\Delta\bar{\nu}$		$\Delta\bar{\nu}$
amide I	1645	0	1645	15	1645	2	1645	2
amide II	1555	0	1559	10	1555	9	1559	8
amide III	1326	0	1332	32	1329	27	1329	3
νN-Me	1098	0	1143	18	1101	44	1140	20
νCC	821	0	840	43	840	50	821	21
amide IV	574	0	602	26	598	8	577	15
ρNCO	394	0	415	24	409	21	400	7
δN-Me	266	0	277	12	267	10	276	12
error (%)	.00		3.02		2.76		1.71	

stated that the force field reproducing the experimental frequencies, is the closest to the force field of the uncoupled initial solution. In other words, the method offers a solution for small off-diagonal elements in the potential energy matrix. VAN DER VEKEN[73] has demonstrated this graphically for the two-order problem of the f_2-vibrations of the phosphate ion. In the uncommon case of strong force constant coupling within one symmetry species the method leads to poor results[79]. It is however very powerful for molecules where strong kinematic coupling is expected. Generally speaking we can state that the better the basic coordinates describe the normal coordinates, the closer the solution is to the exact force field. Since in this case the off-diagonal force constants become smaller than the diagonal force constants, each of the coordinates has its corresponding frequency and the assignment of observed ir and Raman bands is for this reason straightforward.

Consequently, the results will be very sensitive to the choice of symmetry coordinates because these motion coordinates are as usual only approximations to the normal modes. The force constants and the potential energy distributions can be considered sufficiently reliable if they are virtually independent of such a choice. That the EVM also obeys this condition is thoroughly studied in a series of papers on normal coordinate analysis of malononitriles[80-83].

As an illustration, we have computed the force field of the $^{64}Zn(py)_2Cl_2$ complex utilizing the same assignments of the experimental frequencies as published by SAITO *et al.*[84]. Hereby three sets of symmetry coordinates are used which differ in the description of the bending motions around the central zinc ion of the a_1-symmetry species. The changes in the logical potential energy distribution results are given in Table 3.3. If, as in this example convergent values for the force

TABLE 3.3

Infrared frequencies, assignments and potential energy distributions of the tetrahedral $^{64}Zn(py)_2Cl_2$ complex for different sets of symmetry coordinates (a_1-vibrations only).

frequencies	assignment (basic coordinate)	P.E.D. (set I)*	P.E.D. (set II)	P.E.D. (set III)
296.5	νZnCl (S_1)	66 S_1 + 19 S_2 + 15 S_3	62 S_1 + 19 S_2 + 15 S_3	63 S_1 + 19 S_2 + 15 S_3
203.9	νZnN (S_2)	59 S_2 + 22 S_1 + 18 S_3	53 S_2 + 24 S_1 + 18 S_3	56 S_2 + 23 S_1 + 18 S_3
154.0	δNZnN (S_3)	59 S_3 + 20 S_2 + 20 S_4	59 S_3 + 30 S_2	72 S_3 + 26 S_2
109.9	δXZnX (S_4)	80 S_4 + 16 S_3	83 S_4 + 17 S_3	92 S_4

* only contributions greater than 10% are reported.

constants are obtained for all sets, selection of the best one is possible by comparison of calculated and observed shifts upon isotopic substitution, cf. Table 3.4.

TABLE 3.4

Observed and calculated isotopic shifts (in cm^{-1}) for $^{64}Zn(py)_2Cl_2$ and $^{64}Zn(py\text{-}d_5)_2Cl_2$ complexes on the a_1-vibrations.

Obs. (ref.[84])	Calc. (set I)	Calc. (set II)	Calc. (set III)
.2	.3	.4	.4
4.1	2.2	2.0	2.2
≈7(*)	2.4	4.0	4.2
.7	1.6	.7	.6

(*) shift difficult to determine because of poor bandshape.

3.2.4 The Matrix Polynomial Expansion Method

In their paper, ALIX and BERNARD[63] stated that $\frac{1}{2}n(n-1)$ additional conditions are sufficient to determine a unique solution of the secular equation (7). These conditions are given by the relation of commutation of the matrix products ($G_m.F^s_{m-1}$), ($G_m.F^s_m$) and ($G_m.\Delta F^s_m$) where ΔF^s_m is the matrix of correction, defined by equation (32) and superscript s indicates symmetric matrices. Using the Cayley-Hamilton theorem, it is possible to rewrite the secular equation (7) as :

$$\sum_{i=0}^{n} c_i \left(G_m F^s_{m-1} + G_m \Delta F^s_m \right)^i = 0 \qquad (40)$$

The expansion of this equation, applying Newton's binomial theorem, leads to :

$$\sum_{i=0}^{n} c_i \left(G_m F^s_{m-1} \right)^i + \sum_{i=1}^{n} i c_i \left(G_m F^s_{m-1} \right)^{i-1} \left(G_m \Delta F^s_m \right) + \ldots = 0 \qquad (41)$$

from which the solution, ΔF^s_m, is obtained in an iteration process ($1 < r < r_o$), based on the linearization of this polynomial expression. The asymmetric solution, ΔF^{as}_m, at each step r is given by :

$$\Delta F^{as}_{m,r} = \left[-\sum_{i=1}^{n} i c_i \left(G_m F^s_{m-1,r-1} \right)^{i-1} G_m \right]^{-1} \sum_{i=1}^{n} c_i \left(G_m F^s_{m-1,r-1} \right)^i \qquad (42)$$

The correction matrix is symmetrized as :

$$\Delta F_{m,r} = \tfrac{1}{2} \left(\Delta F^{as}_{m,r} + \left(\Delta F^{as}_{m,r} \right)^t \right) \qquad (43)$$

The general expression (41) is essentially the matrix polynomial expansion of the eigenvector method. For numerical results showing the equivalence to the EVM, see Sec. 4.1.2. The flow-diagram (Fig. 3.4) describes the double iteration procedure; the m-iteration introducing stepwise the G_{ij} elements and the r-iteration solving the polynomial expression (41). In Appendix III a copy of our main routine to calculate the force field from a set of vibrational frequencies by the (MPEM) method will be found.

The advantages of the MPEM over other methods can be summarized as : (1) correctness from the mathematical point of view and uniqueness of the correction matrix against the multiplicity of solutions as in Fadini's method, (2) calculation of only square n x n matrices against $n^2 \times n^2$ in the former methods, (3) it is unnecessary to compute eigenvalues and eigenvectors at each step, (4) suppression of the inconvenience of rearranging the columns of L_m according to the assignment

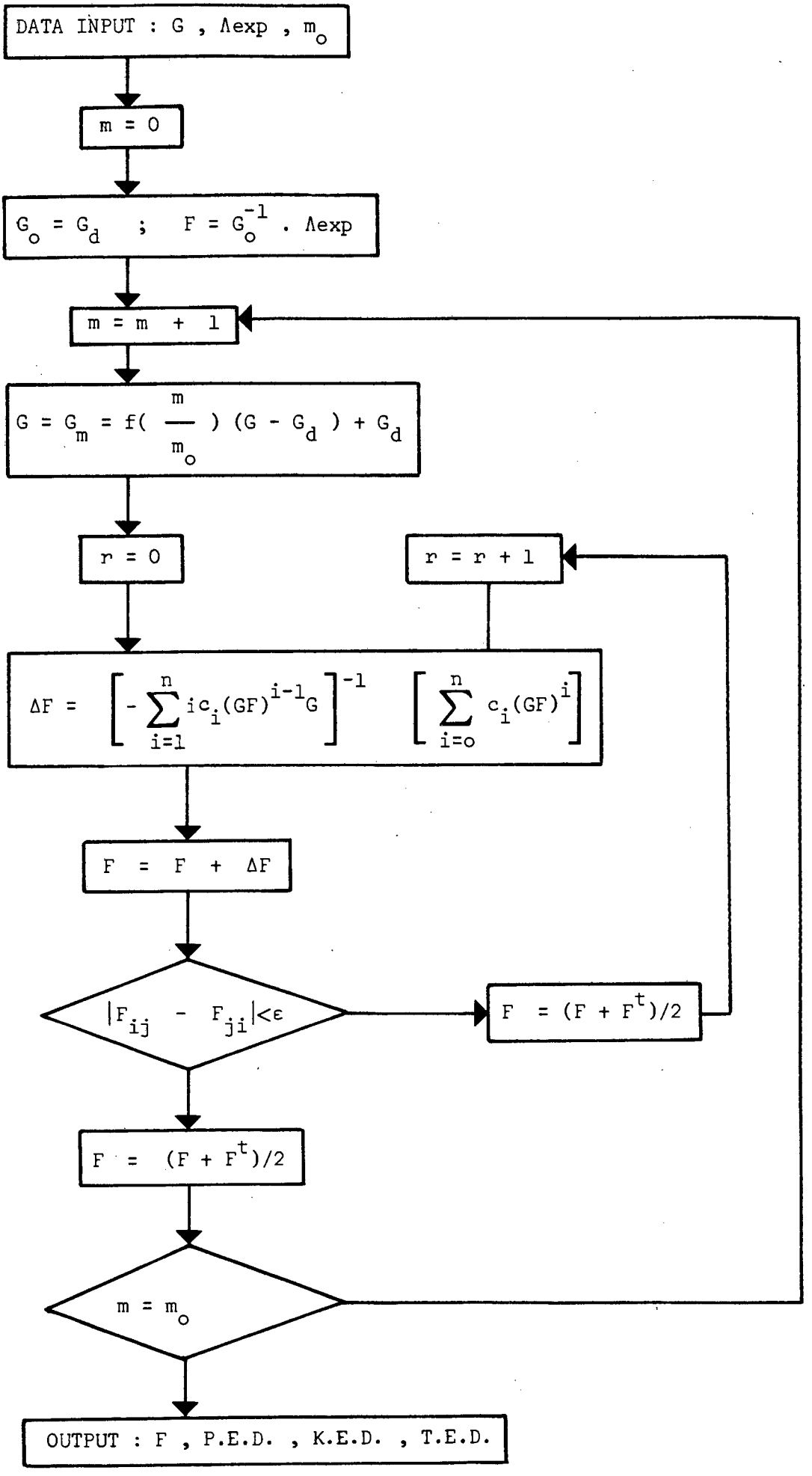

Fig. 3.4 : The matrix polynomial expansion method flowchart (from ref.63)

of the eigenvalues as encountered in the Becher-Mattes method and because the criterion of P.E.D. fails in cases with strong kinematic coupling[63,73], (5) the ability to produce a force constant matrix at all times.

In addition, kinetic (K.E.D.) and total energy distributions (T.E.D.) among the symmetry coordinates are calculated in which the former takes into account the contributions of the kinematic coupling constants (G_{ij}^{-1}). The T.E.D. is formulated by ALIX *et al.*[85] in terms of the contributions of all potential and kinematic constants (F_{ij} and G_{ij}^{-1}) and is expressed for a given normal mode, Q_k, as :

$$\begin{aligned} TED_{ij} &= \tfrac{1}{2}(F_{ij}\lambda_k^{-1} + G_{ij}^{-1}) L_{ik}L_{jk} \\ &= \tfrac{1}{2}(V(F_{ij}) + T(G_{ij}^{-1})) \end{aligned} \qquad (44)$$

Application of the T.E.D. method is therefore especially useful for characterising strongly coupled vibrational modes in molecules.

3.2.5 Necessary Procedures in Determining Force Constants

In this Section we shall work out the preliminary steps to be taken in setting up a general valence force field for ML_2X_2 tetrahedral molecules belonging to the point group C_{2v}. Similarly to the method of FERRARO *et al.*[86] we distinguish the following points.

1) Choice of a model and two types of internal coordinates. These coordinates as defined in Fig.3.5, are :

changes in bond lengths : Δr_1, Δr_2, Δt_1, Δt_2

changes in bond angles : $\Delta\alpha$, $\Delta\gamma_{13}$, $\Delta\gamma_{14}$, $\Delta\gamma_{23}$, $\Delta\gamma_{24}$, $\Delta\beta$

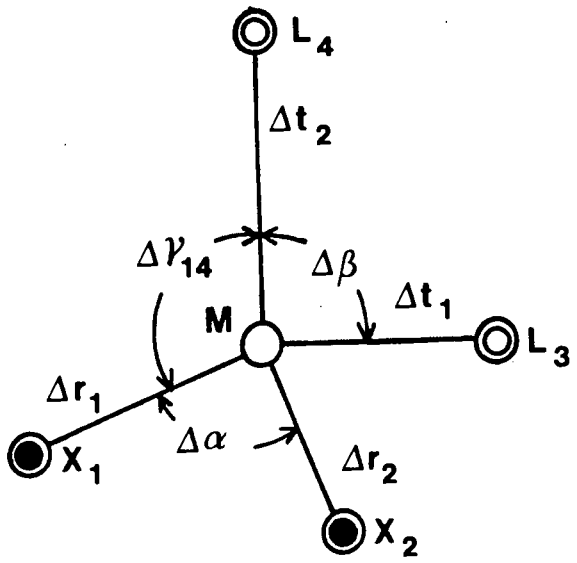

Fig. 3.5 : The molecular model and the internal coordinates of ML_2X_2 tetrahedral molecules.

Note that there are ten internal coordinates and only nine normal vibrational modes, hence there exists a redundancy.

2) Construction of the F matrix.

The complete potential energy expression using these internal coordinates is :

$$2V = f_r \sum_{i=1}^{2} (\Delta r_i)^2 + f_t \sum_{i=1}^{2} (\Delta t_i)^2 + 2f_{rr}(\Delta r_1)(\Delta r_2)$$

$$+ 2f_{tt}(\Delta t_1)(\Delta t_2) + 2f_{rt} \sum_{i,j=1}^{2} (\Delta r_i)(\Delta t_j) + f_\alpha (r_o \Delta\alpha)^2$$

$$+ f_\beta (t_o \Delta\beta)^2 + f_\gamma \sum_{i=1}^{4} (r_o \Delta\gamma_i)^2 + 2f_{\alpha\beta}(r_o\Delta\alpha)(t_o\Delta\beta)$$

$$+ 2f_{\alpha\gamma} \sum_{i=1}^{4} (r_o\Delta\alpha)(r_o\Delta\gamma_i) + 2f_{\beta\gamma} \sum_{i=1}^{4} (t_o\Delta\beta)(r_o\Delta\gamma_i)$$

$$+ 2f_{\gamma\gamma} \sum^{(2)} (r_o\Delta\gamma_{ij})(r_o\Delta\gamma_{kl}) + 2f_{\gamma\gamma_t} \sum^{(2)} (r_o\Delta\gamma_{ij})(r_o\Delta\gamma_{kj})$$

$$+ 2f_{\gamma\gamma_r} \sum^{(2)} (r_o\Delta\gamma_{ji})(r_o\Delta\gamma_{jk}) + 2f_{r\alpha} \sum_{i=1}^{2} (\Delta r_i)(r_o\Delta\alpha)$$

$$+ 2f_{t\alpha} \sum_{i=1}^{2} (\Delta t_i)(r_o\Delta\alpha) + 2f_{r\beta} \sum_{i=1}^{2} (\Delta r_i)(t_o\Delta\beta)$$

$$+ 2f_{t\beta} \sum_{i=1}^{2} (\Delta t_i)(t_o\Delta\beta) + 2f_{r\gamma} \sum^{(4)} (\Delta r_i)(r_o\Delta\gamma_{ij})$$

$$+ 2f_{t\gamma} \sum^{(4)} (\Delta r_i)(r_o\Delta\gamma_{ij}) + 2f'_{r\gamma} \sum^{(4)} (\Delta r_i)(r_o\Delta\gamma_{jk})$$

$$+ 2f'_{t\gamma} \sum^{(4)} (\Delta t_i)(r_o\Delta\gamma_{jk}) \qquad (45)$$

where (2) and (4) are the number of contributing terms for that particular interaction type. The angle deformation coordinates have been multiplied by a distance r_o or t_o which is one of the equilibrium bond lengths forming the angle, to allow for consistent energy units. The coefficients of this energy function are the unknown force constants which constitute the F matrix of order 10 (Table 3.5). The f_r, f_t, f_α, f_β and f_γ are the constants associated with the restoring forces acting along the bonds, r and t and the angles between two bonds, α, β and γ respectively. The off-diagonal elements; f_{rr}, f_{tt} and f_{rt} are the interactions between the two stretches; $f_{\gamma\gamma}$ and $f_{\alpha\beta}$ are the interaction of angle bends not sharing common bonds; $f_{\alpha\gamma}$ and $f_{\gamma\gamma_r}$ are the interaction of angle bends having the r bond as common side and $f_{\gamma\beta}$ and $f_{\gamma\gamma_t}$ having the t bond as common side. The interaction constants between stretches and angle distortions of which they are a side are listed : $f_{r\alpha}$, $f_{t\beta}$, $f_{r\gamma}$ and $f_{t\gamma}$ and of which they are not a side named : $f_{r\beta}$, $f_{t\alpha}$, $f'_{t\gamma}$ and $f'_{r\gamma}$.

TABLE 3.5

The F matrix in internal coordinates for ML_2X_2-type molecules (tetrahedral).

F	Δr_1	Δr_2	Δt_1	Δt_2	$\Delta\alpha$	$\Delta\gamma_{13}$	$\Delta\gamma_{14}$	$\Delta\gamma_{23}$	$\Delta\gamma_{24}$	$\Delta\beta$
Δr_1	f_r	f_{rr}	f_{rt}	f_{rt}	$f_{r\alpha}$	$f_{r\gamma}$	$f_{r\gamma}$	$f'_{r\gamma}$	$f'_{r\gamma}$	$f_{r\beta}$
Δr_2		f_r	f_{rt}	f_{rt}	$f_{r\alpha}$	$f'_{r\gamma}$	$f'_{r\gamma}$	$f_{r\gamma}$	$f_{r\gamma}$	$f_{r\beta}$
Δt_1			f_t	f_{tt}	$f_{t\alpha}$	$f_{t\gamma}$	$f'_{t\gamma}$	$f_{t\gamma}$	$f'_{t\gamma}$	$f_{t\beta}$
Δt_2				f_t	$f_{t\alpha}$	$f'_{t\gamma}$	$f_{t\gamma}$	$f'_{t\gamma}$	$f_{t\gamma}$	$f_{t\beta}$
$\Delta\alpha$					f_α	$f_{\alpha\gamma}$	$f_{\alpha\gamma}$	$f_{\alpha\gamma}$	$f_{\alpha\gamma}$	$f_{\alpha\beta}$
$\Delta\gamma_{13}$		$f_{ij} = f_{ji}$				f_γ	$f_{\gamma\gamma_r}$	$f_{\gamma\gamma_t}$	$f_{\gamma\gamma}$	$f_{\gamma\beta}$
$\Delta\gamma_{14}$							f_γ	$f_{\gamma\gamma}$	$f_{\gamma\gamma_t}$	$f_{\gamma\beta}$
$\Delta\gamma_{23}$								f_γ	$f_{\gamma\gamma_r}$	$f_{\gamma\beta}$
$\Delta\gamma_{24}$									f_γ	$f_{\gamma\beta}$
$\Delta\beta$										f_β

3) Choice of motion coordinates which adequately describe the normal coordinates. Based on several symmetry elements, we will use symmetry coordinates to simplify the solution of force field problems. An appropriate set for ML_2X_2 is as follows:

for the a_1-vibration :

$$S_1 = 2^{-\frac{1}{2}}(\Delta r_1 + \Delta r_2)$$

$$S_2 = 2^{-\frac{1}{2}}(\Delta t_1 + \Delta t_2)$$

$$S_3 = \Delta\beta$$

$$S_4 = \Delta\alpha$$

$$S_{10} = 6^{-\frac{1}{2}}(\Delta\alpha \quad \Delta\gamma_{13} + \Delta\gamma_{14} + \Delta\gamma_{23} + \Delta\gamma_{24} + \Delta\beta)$$

= redundant coordinate

for the a_1-vibration :

$$S_5 = 2^{-1}(\Delta\gamma_{13} - \Delta\gamma_{14} - \Delta\gamma_{23} + \Delta\gamma_{24})$$

for the b_1-vibration :

$$S_6 = 2^{-\frac{1}{2}}(\Delta r_1 - \Delta r_2)$$

$$S_7 = 2^{-1}(\Delta\gamma_{13} + \Delta\gamma_{14} - \Delta\gamma_{23} - \Delta\gamma_{24})$$

for the b_2-vibration :

$$S_8 = 2^{-\frac{1}{2}}(\Delta t_1 - \Delta t_2)$$

$$S_9 = 2^{-1}(\Delta\gamma_{13} - \Delta\gamma_{14} + \Delta\gamma_{23} - \Delta\gamma_{24})$$

The U matrix of the symmetry coordinates is written out in Table 3.6.

4) Transformation of the symmetry force constants.

Application of our computer programme will produce force constants in terms of symmetry coordinates. Internal force constants are obtained according to equation (9), their relationship is as follows :

symmetrized	GVFF
a) diagonal elements	
F_{11}	$f_r + f_{rr}$
F_{22}	$f_t + f_{tt}$
F_{33}	f_β
F_{44}	f_α
F_{55}	$4f_\gamma - 4f_{\gamma\gamma_r} - 4f_{\gamma\gamma_t} + 4f_{\gamma\gamma}$
F_{66}	$f_r - f_{rr}$
F_{77}	$4f_\gamma + 4f_{\gamma\gamma_r} - 4f_{\gamma\gamma_t} - 4f_{\gamma\gamma}$
F_{88}	$f_t - f_{tt}$
F_{99}	$4f_\gamma - 4f_{\gamma\gamma_r} + 4f_{\gamma\gamma_t} - 4f_{\gamma\gamma}$
b) off-diagonal elements	
F_{12}	$2f_{rt}$
F_{13}	$2^{\frac{1}{2}}f_{r\alpha}$
F_{14}	$2^{\frac{1}{2}}f_{r\beta}$
F_{23}	$2^{\frac{1}{2}}f_{t\alpha}$
F_{24}	$2^{\frac{1}{2}}f_{t\beta}$
F_{34}	$f\alpha\beta$
F_{67}	$2(2)^{\frac{1}{2}}(f_{r\gamma} - f'_{r\gamma})$
F_{89}	$2(2)^{\frac{1}{2}}(f_{t\gamma} - f'_{t\gamma})$

One can see that it is impossible to derive values for all interaction force constants. In some cases it can be of interest to know several particular constants by neglecting those terms having little effect on

TABLE 3.6

The U matrix for ML_2X_2-type molecules (tetrahedral).

U	Δr_1	Δr_2	Δt_1	Δt_2	$\Delta\alpha$	$\Delta\gamma_{13}$	$\Delta\gamma_{14}$	$\Delta\gamma_{23}$	$\Delta\gamma_{24}$	$\Delta\beta$
S_1	.70711	.70711	.00	.00	.00	.00	.00	.00	.00	.00
S_2	.00	.00	.70711	.70711	.00	.00	.00	.00	.00	.00
S_3	.00	.00	.00	.00	.00	.00	.00	.00	.00	1.00000
S_4	.00	.00	.00	.00	1.00000	.00	.00	.00	.00	.00
S_{10}	00	.00	.00	.00	.40825	.40825	.40825	.40825	.40825	.40825
S_5	.00	.00	.00	.00	.00	.50000	-.50000	-.50000	.50000	.00
S_6	.70711	-.70711	.00	.00	.00	.00	.00	.00	.00	.00
S_7	.00	.00	.00	.00	.00	.50000	.50000	-.50000	-.50000	.00
S_8	.00	.00	.70711	-.70711	.00	.00	.00	.00	.00	.00
S_9	.00	.00	.00	.00	.00	.50000	-.50000	.50000	-.50000	.00

the potential energy. For example, one can set the force constants representing a stretch-bend or bend-bend interaction equal to zero if the two internal coordinates do not share a common bond or if the corresponding frequencies are widely separated.

5) If we express the masses in atomic mass units and the bond lengths in Ångstrom, the corresponding units of the force constants will be :

mdyne / Å for the stretching F matrix elements

mdyne . Å for the bending F matrix elements

mdyne for the stretch-bend interaction elements.

The relation between eigenvalue and wavenumber in equation (26) becomes :

$$\lambda = \left[\frac{\bar{\nu}}{1303.16}\right]^2 \qquad (46)$$

The usage of non-standardized units for the force constants is still common practice in the literature, however conversion to SI units can simply be performed by : mdyne = 10^{-8} N and Å = 100 pm.

3.2.6 Error Calculation of Force Constants

For discussion of the force constants it is of great advantage to know their associated uncertainty values. Application of the general formula :

$$\Delta F_{ij} = \sum_k \frac{\delta F_{ij}}{\delta \bar{\nu}_k} \Delta \bar{\nu}_k \qquad (47)$$

to an F matrix of large dimension will clearly be too time consuming. Therefore, we will present estimations of the errors on a numerical basis, considering only the diagonal force constants as significant in the discussion since they are mainly determined from the experimental frequencies. The uncertainties in these vibrational frequencies are

in their turn affected by the profile of the corresponding band and by the accuracy of the instrument. The interaction force constants as described by the off-diagonal elements, are related to the information obtained from small isotopic shifts, Coriolis coupling and centrifugal distortion constants, with accuracies usually smaller than those of the frequencies. The percentage errors on the F matrix elements for the in-plane vibration modes of *N*-methylacetamide assuming REY-LAFON's spectral data and assignment[76] are given in Table 3.7, column X. The uncertainties in the frequencies are taken to be 2 cm^{-1}. The columns I to VIII are the errors of F_{ij} attributed from each frequency, in column IX are listed the sum of the absolute partial errors. From the errors in the symmetry force constants, the errors in the internal force constants are easily calculated by applying the rules of error theory.

A similar calculation can be performed by using the harmonic oscillator formula. In this approach each normal coordinate is determined by one frequency, therefore that frequency can be correlated to one diagonal force constant, leading to the relation :

$$\Delta F_{ii} = 2 F_{ii} \frac{\Delta \bar{\nu}_i}{\bar{\nu}} \qquad (48)$$

The percentage values, column XI, are usually smaller than those obtained by the numerical method.

TABLE 3.7

Numerical calculation of uncertainties in the symmetry force constants of *N*-methylacetamide.

	I	II	III	IV	V	VI	VII	VIII	IX	X	XI
a) diagonal F matrix elements											
F_{11}	.02433	-.00053	.00193	-.00090	-.00209	.00060	-.00069	-.00159	.03266	.47	.31
F_{22}	-.00206	.02593	.00294	-.00003	-.00088	-.00077	-.00105	-.00055	.03421	.33	.24
F_{33}	-.00096	-.00056	.02163	.00024	.00059	-.00043	-.00206	-.00010	.02657	.64	.45
F_{44}	-.00019	-.00002	-.00216	.02297	.00059	-.00052	-.00024	-.00009	.02678	.47	.36
F_{55}	.00004	-.00002	-.00086	-.00009	.01189	-.00046	.00027	-.00001	.01364	.84	.63
F_{66}	-.00008	.00	-.00004	-.00008	-.00006	.01036	-.00012	.00	.01074	1.01	.91
F_{77}	-.00002	.00	.00003	.00	-.00030	-.00007	.00913	.00	.00955	1.58	1.38
F_{88}	.00	.00	-.00014	-.00012	-.00009	.00	.00	.00200	.00235	.33	.25
b) off-diagonal F matrix elements											
F_{12}	.00394	-.00197	.00361	-.00020	-.00093	-.00063	-.00066	-.00093	.01287	2.20	
F_{13}	-.00339	-.00021	.00796	-.00013	-.00160	.00014	-.00091	.00053	.01487	3.38	
F_{23}	-.000178	-.00067	.00678	.00	-.00165	.00007	-.00094	.00031	.0122	2.77	

Columns I - VIII: The errors of F_{ij} caused by the errors on λ_1 - λ_8. Column IX: Sum of the absolute partial errors. Column X: Percentage uncertainties calculated from Column IX. Column XI: Percentage uncertainties calculated by the harmonic oscillator approach.

REFERENCES

1. E.B. WILSON, J.C. DECIUS, P.C. CROSS,
"Molecular Vibrations", McGraw-Hill, New York, 1955.

2. D.F. McINTOSH, K.H. MICHAELIAN,
Can. J. Spectrosc., 24(1979)1, 35, 65.

3. J.C. DECIUS,
J. Chem. Phys., 17(1949)1315.

4. N.B. COLTHUP, L.H. DALY, S.E. WIBERLY,
"Introduction to Infrared and Raman Spectroscopy",
Academic Press, New York, 1964.

5. J.R. NIELSEN, L.H. BERRYMAN,
J. Chem. Phys., 17(1949)659.

6. Y. MORINO, K. KUCHITSU,
J. Chem. Phys., 20(1952)1809.

7. E.B. WILSON,
J. Chem. Phys., 9(1941)76.

8. D. STEELE,
"Theory of Vibrational Spectroscopy",
W.B. Saunders, Philadelphia, 1971.

9. R.L. HILDEBRANDT,
J. Mol. Spectrosc., 44(1972)599.

10. I.H. WILLIAMS,
J. Mol. Spectrosc., 66(1977)288.

11. D.F. McINTOSH, K.H. MICHAELIAN, M.R. PETERSON,
Can. J. Chem., 56(1978)1289.

12. J.C. DECIUS,
J. Chem. Phys., 16(1948)1025.

13. J.C. WHITMER,
J. Mol. Struct., 27(1975)443.

14. J. OVEREND, J.R. SCHERER,
J. Chem. Phys., 32(1960)1289, 1296, 1720.

15. K. NAKAMOTO,
"Infrared Spectra of Inorganic and Coordination Compounds",
John Wiley, New York, 1963.

16. S.M. FERIGLE, A.G. MEISTER,
J. Chem. Phys., 19(1951)982.

17. P. GANS,
Spectrochim. Acta, 26A(1970)281.

18. B. VAN DER VEKEN,
Ph.D. Thesis, University of Antwerp, Belgium, 1972.

19. O. REDLICH,
Z. Physik. Chem., Leipzig, 28B(1935)371.

20. E. TELLER, quoted in W.R. ANGUS, C.R. BAILEY, J.B. HALE *et al.*
J. Chem. Soc., (1936)971.

21. J.C. DECIUS, E.B. WILSON,
J. Chem. Phys., 19(1951)1409.

22. T. MIYAZAWA,
J. Chem. Phys., 29(1958)246.

23. C.G.J. JACOBI,
J. reine angew. Math., 30(1846)51.

24. I.M. MILLS,
Spectrochim. Acta, 16(1960)35.

25. I.M. MILLS,
in "Infrared Spectroscopy and Molecular Structure", Chapt. 5,
(M. DAVIED ed.), Elsevier, Amsterdam, 1963.

26. T. SHIMANOUCHI,
in "Physical Chemistry, An Advanced Treatise", Vol 4, Chapt. 6,
(H. EYRING *et al.* eds.), Academic Press, New York, 1970.

27. G. HERZBERG,
"Molecular Spectra and Molecular Structure
II. Infrared and Raman Spectra of Polyatomic Molecules",
Van Nostrand, Princeton, 1945.

28. D.F. HEATH, J.W. LINNETT,
Trans. Faraday Soc., 44(1948)556, 561, 873, 878, 884.

29. I.M. MILLS,
Spectrochim. Acta, 19(1963)1585.

30. W.T. KING,
J. Chem. Phys., 36(1962)165.

31 J.H. SCHACHTSCHEIDER, R.G. SNYDER,
Spectrochim. Acta, 19(1963)117.

32. R.G. SNYDER, J.H. SCHACHTSCHEIDER,
Spectrochim. Acta, 21(1965)169.

33. H.C. UREY, C.A. BRADLEY,
Phys. Rev., 38(1931)1969.

34. T. SHIMANOUCHI,
J. Chem. Phys., 17(1949)245, 734, 848.

35. T. SHIMANOUCHI,
Pure Appl. Chem., 7(1963)131.

36. T. SHIMANOUCHI, H. MATSUURA, Y. OGAWA, I. HARADA,
J. Phys. Chem. Ref. Data, 7(1978)1323; 9(1980)1149.

37. H. MATSUURA, M. TASUMI,
in "Vibrational Spectra and Structure", Vol 12, Chapt. 2,
(J.R. DURIG ed.), Elsevier, Amsterdam, 1983.

38. J.L. DUNCAN,
in "Molecular Spectroscopy", Vol 3, Chapt 2, The Chemical Society,
London, 1975.

39. T. SHIMANOUCHI, I. NAKAGAWA,
Ann. Rev. Phys. Chem., 23(1972)217.

40. D.E. MANN, T. SHIMANOUCHI, J.H. MEAL, L. FANO,
J. Chem. Phys., 27(1957)43.

41. J. ALDOUS, I.M. MILLS,
Spectrochim. Acta, 18(1962)1073.

42. D.E. FREEMAN,
J. Chem. Phys., 49(1968)4250.

43. E.J. O'REILLY,
J. Chem. Phys., 48(1968)1086.

44. P. PULAY, F. TOROK,
Acta Chim. Acad. Sci. Hung., 44(1965)287; 47(1966)273.

45. P. PULAY,
Acta Chim. Acad. Sci. Hung., 52(1967)49; 57(1968)373.

46. F. TOROK, P. PULAY,
J. Mol. Struct., 3(1969)1.

47. F. BILLES,
Acta Chim. Acad. Sci. Hung., 47(1966)53.

48. S.J. CYVIN, L.A. KRISTIANSEN, F. BRUNVOLL,
Acta Chim. Acad. Sci. Hung., 51(1967)217.

49. D.F. FREEMAN,
J. Mol. Spectrosc., 22(1967)305.

50. D.F. FREEMAN,
J. Mol. Spectrosc., 27(1968)27.

51. J. HERRANZ, F. CASTANO,
Spectrochim. Acta, 22(1966)1965.

52. J. HERRANZ, F. CASTANO,
An. Real. Soc. Esp. Fis. Quim., Ser. A, 62(1966)199.

53. P. TORKINGTON,
J. Chem. Phys., 17(1949)357, 1026.

54. A. MULLER,

Z. Physik. Chem., Leipzig, 238(1968)116.

55. C.J. PEACOCK, A. MULLER,

J. Mol. Spectrosc., 26(1968)454.

56. A. MULLER, C.J. PEACOCK,

Mol. Phys., 14(1968)393.

57. C.J. PEACOCK, A. MULLER, U. HEIDBORN,

J. Mol. Spectrosc., 30(1969)338.

58. R.L. REDINGTON, A.L.K. ALJIBURY,

J. Mol. Spectrosc., 37(1971)494.

59. Y.N. PANCHENKO, R.A. MUNOZ, N.F. STEPANOV, G.S. KOPTEV,

J. Mol. Struct., 12(1972)289.

60. A. FADINI,

Z. Angew. Math. Mech., 44(1964)506; 45(1965)29.

61. W. SAWODNY, A. FADINI, K. BALLEIN,

Spectrochim. Acta, 21(1965)995.

62. B.S. AVERBUKH, L.S. MAYANTS, G.B. SHALTUPER,

J. Mol. Spectrosc., 30(1969)310.

63. A. ALIX, L. BERNARD,

J. Mol. Struct., 20(1974)51.

64. S.C. WAIT, R.A. RADER, T.J. DURNICK,

J. Mol. Spectrosc., 29(1969)494.

65. N.K. MOROZOVA, N.F. KOVALENKO, V.P. MOROZOV,

Opt. Spectrosc., 30(1971)121.

66. H.J. BECHER, R. MATTES,

Spectrochim. Acta, 23A(1967)2449.

67. O. CHACON, P. METZKE,

J. Mol. Struct., 9(1971)243.

68. A. ALIX, B. VAN DER VEKEN,

Bull. Soc. Chim. Belg., 84(1975)111.

69. A. ALIX, L. BERNARD,

C. R. Hebd. Seances Acad. Sci., Ser. B, 276(1973)933.

70. A. ALIX, H.H. EYSEL, B. JORDANOV, R. KEBABCIOGLU, N. MOHAN, A. MULLER,

J. Mol. Struct., 27(1975)1.

71. R.L. HILDERBRANDT,

J. Mol. Struct., 13(1972)33.

72. E. WENDLING, S. MAHMOUDI,

Bull. Soc. Chim. France, (1970)4248.

73. B. VAN DER VEKEN, H. DESSEYN, M. HERMAN,

Bull. Soc. Chim. Belg., 81(1972)555.

74. T. MIYAZAWA, T. SHIMANOUCHI, S.-I. MIZUSHIMA,

J. Chem. Phys., 29(1958)611.

75. J. JAKES, S. KRIMM,

Spectrochim. Acta, 27A(1971)19.

76. M. REY-LAFON, M.T. FOREL,

Spectrochim. Acta, 29A(1973)471.

77. H.O. DESSEYN,

Aggregaat Hoger Onderwijs, University of Antwerp, Belgium, 1975.

78. B. VAN DER VEKEN,

J. Mol. Struct., 15(1973)300.

79. A. FADINI,

Z. Physik. Chem., Leipzig, 243(1970)229.

80. H.O. DESSEYN, B.J. VAN DER VEKEN, M.A. HERMAN,

J. Mol. Struct., 13(1972)219.

81. H.O. DESSEYN, B.J. VAN DER VEKEN, L. VAN HAVERBEKE, M.A. HERMAN,

J. Mol. Struct., 13(1972)227.

82. B.J. VAN DER VEKEN, H.O. DESSEYN,

J. Mol. Struct., 23(1974)427.

83. L. VAN HAVERBEKE, H.O. DESSEYN, B.J. VAN DER VEKEN, M.A. HERMAN, *J. Mol. Struct.*, 25(1975)53.

84. Y. SAITO, M. CORDES, K. NAKAMOTO, *Spectrochim. Acta*, 28A(1972)1459.

85. A. ALIX, A. MULLER, *J. Mol. Struct.*, 24(1975)229.

86. J.R. FERRARO, J.S. ZIOMEK, "Introductory Group Theory and Its Application to Molecular Structure", Plenum Press, New York, 1975(2nd ed.).

CHAPTER 4

NORMAL COORDINATE ANALYSIS - EXAMPLES

4.1 ANALYSIS OF THE INFRARED ACTIVE FRAMEWORK VIBRATIONS OF *cis*-$[PtL_2Cl_2]$, WHERE L = pz AND an , AND OF *cis*-$[Pt(Him)_2(NO)_2)_2]$

4.1.1 Introduction

Previous work in this laboratory involves the assignment of metal-ligand modes based on the effects of halide substitution and ligand deuteration. Since a clearcut distinction between the deformation modes around the central metal is not possible on the basis of the deuteration studies[1], a normal coordinate treatment of the skeletal vibration will justify not only the assignment by the potential energy distribution calculations, but in addition, quantitative data on the degree of coupling between these modes is provided.

Point-mass model (PMM) approximations where the ligand, L is considered to behave as one dynamic unit, have been successfully applied to the framework vibrations of tetrammine complexes of platinum, copper and zinc as well as hexacoordinate transition metal amine complexes[2,3,4,5]. The validity of such approach is confirmed for the pyrazine and imidazole complexes but an unacceptable value for the internal valence force constant f(Pt-N) is obtained for the aniline complex. In the latter compound, the consequences of the PMM on the force constants is discussed and compared with data from *cis*-$[Pt(NH_3)_2Cl_2]$.

4.1.2 Point-Mass Model and General Considerations

The *cis*-PtL_2X_2 skeletons are treated as five-body systems with all ligands considered as single point masses, belonging to the point group C_{2v}. The validity of such a model has been studied in detail by numerous authors[2,3,4] and found applicable to the Pt-complexes especially when small

ligand-framework coupling is expected. Some of the investigators have demonstrated the usefulness of transferring force constants from the point-mass model to the whole complex. The differences between the calculated frequencies (PMM approximation minus final values for the whole complex) are found to be positive and relatively small. Compared to the normal coordinate analysis of the whole complex, the force constants for the framework vibrations (assuming PMM) fall within the error limits of the different pseudo-exact force fields[3,4], which confirms their reliability. In our ligand systems, apart from minor shifts and splittings, each ligand band of the free molecule is faithfully reproduced in the ir spectrum of its complex. Nearly all ligand bands appear above 400 cm^{-1}, except one imidazole band at 174 cm^{-1} and one aniline band at 230 cm^{-1}, and are therefore well separated from the metal-ligand vibrational modes, occurring in the region 400-100 cm^{-1}. CYVIN *et al.*[3] calculated the ligand frequency shifts on complexation for tetra-coordinated square-planar ammine complexes and concluded that the differences are caused by small kinematic coupling between ligand and metal. Hence, the force fields of the complexed ligands remain, to a first approximation, essentially the same as those of the free ligands.

A square-planar structure is assumed for the framework of our molecular model. The adopted model, the internal coordinates and the numbering of the atoms are shown in Fig. 4.1.

No X-ray structure determination on *cis*-$[Pt(pz)_2Cl_2]$ and *cis*-$[Pt(Him)_2(NO_2)_2]$ are reported, therefore bond lengths are selected by comparison with those of the structurally related *cis*- and *trans*-$[Pt(py)_2Cl_2]$ and *trans*-$[Pt(pm)_2Cl_2]$ complexes (Table 4.1). A bond distance shortening of 0.01 Å for Pt-Cl and a bond distance lengthening of 0.04 Å for Pt-N is allowed in the *cis*-configurations due to the

operating *trans*-effect. For the sake of convenience we have adopted identical structural parameters from the *cis*-$[Pt(NH_3)_2Cl_2]$ for the *cis*-$[Pt(an)_2Cl_2]$ compound. This is accounted for by the indifference of the stretching force constants on the bond length values since in the corresponding expressions of the G matrix elements no bond distances are included. Noteworthy features are the ratio dependences determined by the ratio of bond distances of :

$$\frac{G_\alpha}{G^*_\alpha} = \left[\frac{r^*}{r}\right]^2 \propto \frac{F^*_\alpha}{F_\alpha}$$ for the bending force constants and

$$\frac{G_{r\alpha}}{G^*_{r\alpha}} = \frac{r^*}{r} \propto \frac{F^*_{r\alpha}}{F_{r\alpha}}$$ for the interaction force constants

between stretches and angle bonds, where the superscript, *, refers to the altered bond distance. The effects of bond lengths on the stretching and bending symmetry force constants as calculated by the method of Becher and Mattes is illustrated below for the imidazole system :

bond length (Å)	2.03	2.18	2.38
F_{11} (ν_s Pt-X)	1.874	1.874	1.874
F_{44} (δX-Pt-X)	.741	.856	1.020

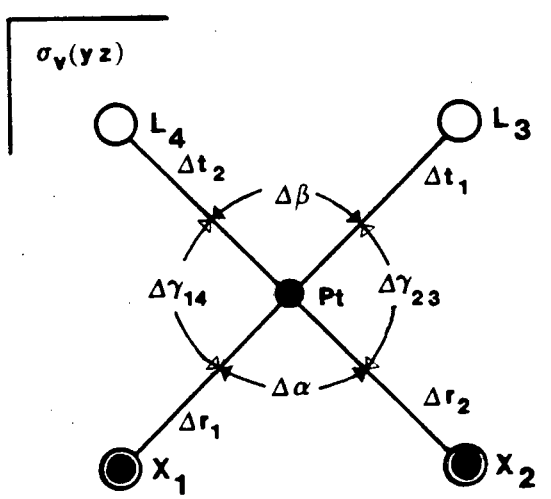

Fig. 4.1 : The model and the internal coordinates of *cis*-PtL_2X_2, symmetry C_{2v}.

TABLE 4.1

Bond lengths

complex	type	lit.-value	selected value
trans-$Pt(py)_2Cl_2$	Pt-N	1.98 (ref.6)	
	Pt-Cl	2.308	
cis-$Pt(py)_2Cl_2$	Pt-N	2.02 (ref.6)	
	Pt-Cl	2.296	
trans-$Pt(pm)_2Cl_2$	Pt-N	2.008 (ref.7)	
	Pt-Cl	2.296	
trans-$Pt(P(p\text{-}C_6H_4CH_3)_3)_2(NO_2)_2$	Pt-NO_2	2.03 (ref.8)	
cis-$Pt(NH_2)_2Cl_2$	Pt-N	2.01 (ref.9)	
	Pt-Cl	2.33	
cis-$Pt(an)_2Cl_2$	Pt-N		2.01
	Pt-Cl		2.33
cis-$Pt(pz)_2Cl_2$	Pt-N		2.05
	Pt-Cl		2.28
cis-$Pt(Him)_2(NO_2)_2$	Pt-N		2.05
	Pt-NO_2		2.03

All angles are chosen as 90 degrees.

The normal coordinate treatments are made for the infrared active in-plane vibrations only. The approach of the analysis is based on the assumption that the vibrational modes may be separated in stretches

$$\Gamma_{str} = 2\,a_1 + 2\,b_2$$

and bends

$$\Gamma_{bends} = 2\,a_1 + a_2 + b_1 + b_2 .$$

The set of symmetry coordinates together with the symbols referring to the localized vibrations which they describe, are given in Table 4.2 and were used to calculate the G matrices and to solve the inverse vibrational eigenvalue problem; i.e., the blocks of a_1 and b_2 are of order 4 and 3 respectively.

We mentioned in the previous chapter the equivalence of the Becher-Mattes method (EVM) and the polynomial expansion method of Alix (MPEM). This is demonstrated in the normal coordinate analysis of the framework vibrations of the pyrazine and imidazole complexes. Using the experimental frequencies of previous work[1,10], the in-plane force fields for each compound were computed by both methods. The results, the diagonal F matrix elements and the potential energy distributions (PED) are given in Tables 4.3 and 4.4. They show an excellent agreement well within the estimated deviations.

In the following Sections covering the platinum complexes, the results which include (1) the distribution of the potential energy within the normal modes, (2) the force constants in symmetry coordinates and (3) the calculated frequencies of the parent molecule and its isotopic analogues, are presented in tabular form. So far as the

TABLE 4.2

Symmetry coordinates for the infrared active in-plane vibrations of planar ML_2X_2 molecules belonging to the point group C_{2v}.

a_1-modes		description
S_1	$= 2^{-\frac{1}{2}} (\Delta r_1 + \Delta r_2)$	ν_s M-X
S_2	$= 2^{-\frac{1}{2}} (\Delta t_1 + \Delta t_2)$	ν_s M-L
S_3	$= \Delta\beta$	δL-M-L
S_4	$= \Delta\alpha$	δX-M-X
S_r	$= 2^{-1} (\Delta\alpha + \Delta\beta + \Delta\gamma_{14} + \Delta\gamma_{23})$	
b_2-modes		
S_5	$= 2^{-\frac{1}{2}} (\Delta r_1 - \Delta r_2)$	ν_{as} M-X
S_6	$= 2^{-\frac{1}{2}} (\Delta t_1 - \Delta t_2)$	ν_{as} M-L
S_7	$= 2^{-\frac{1}{2}} (\Delta\gamma_{14} - \Delta\gamma_{23})$	δL-M-X

TABLE 4.3

Equivalence of the EVM and the MPEM as applied to the skeletal vibrations of *cis*-$[Pt(pz)_2Cl_2]$.

	force constants			potential energy distribution							
	EVM	MPEM	error*		E V M				M P E M			
F_{11}	1.8864	1.8864	0.0223	S_1	85.98	7.09	6.12	.81	87.87	6.33	5.07	.74
F_{22}	1.7647	1.7644	0.0312	S_2	10.38	52.03	35.50	2.09	12.02	51.97	33.85	2.16
F_{33}	3.5160	3.5164	0.0693	S_3	.02	39.20	60.70	.08	.03	40.49	59.39	.09
F_{44}	.8061	.8061	0.0256	S_4	.08	1.22	1.87	96.83	.09	1.21	1.70	97.01
F_{55}	2.3062	2.3062	0.0362	S_5	80.43	13.32	6.26		79.91	14.35	5.73	
F_{66}	1.9390	1.9390	0.0227	S_6	12.39	83.59	4.02		11.60	84.93	3.47	
F_{77}	1.5887	1.5887	0.0376	S_7	7.88	.62	91.50		8.48	.72	90.80	

* estimated by the harmonic oscillator approach assuming an uncertainty of 2 cm^{-1} on the experimental frequencies.

TABLE 4.4

Equivalence of the EVM and the MPEM as applied to the skeletal vibrations of *cis*-$[Pt(Him)_2(NO_2)_2]$.

	force constants			potential energy distributions							
	EVM	MPEM	error	E V M				M P E M			
F_{11}	1.8742	1.8744	0.0244	S_1	66.48	11.26	20.71	1.56	69.02	10.04	19.47	1.47
F_{22}	1.5046	1.5045	0.0289	S_2	1.06	79.37	19.20	.38	1.20	78.44	19.96	.39
F_{33}	4.0334	4.0333	0.0653	S_3	27.37	10.80	61.17	.66	29.52	10.05	59.79	.64
F_{44}	.7413	.7413	0.0245	S_4	.23	1.54	.78	97.45	.26	1.46	.78	97.50
F_{55}	2.0421	2.0415	0.0259	S_5	84.89	10.94	4.17		86.16	10.24	3.60	
F_{66}	1.6190	1.6194	0.0285	S_6	11.76	83.15	5.09		12.77	82.56	4.67	
F_{77}	1.1806	1.1805	0.0313	S_7	.91	6.73	92.35		1.07	7.20	91.73	

contribution of the symmetry coordinates is concerned, only average values greater than 10% (rounded to the nearest 1%), are reported. The average force fields which predict isotopic shifts satisfactorily, were set up from the force fields of the isotopically labelled derivatives. The elements in the F matrix are rounded to the nearest 10^{-3} in accordance with their associated uncertainties.

Internal force constants are calculated from the symmetry force constants by means of equation (9) or its transformed form as :

$$F = U^{t}.F^{sym}.U$$

See Table 4.5 for force constant expressions. Since we considered a limited set of infrared active coordinates and because of the redundancy between the in-plane deformation modes, only the stretching and the stretch-stretch interaction force constants can be determined unambiguously. The final force constants are given in Table 4.17.

TABLE 4.5

F matrix elements and internal force constants for the framework of *cis*-$[PtL_2X_2]$ (point mass model).

a_1-species

$F_{11} = f_r + f_{rr}$ $\quad F_{12} = f_{rt} + f'_{rt}$ $\quad F_{13} = 2^{\frac{1}{2}} r f_{r\beta}$

$F_{22} = f_t + f_{tt}$ $\quad F_{14} = 2^{\frac{1}{2}} r f_{r\alpha}$ $\quad F_{23} = 2^{\frac{1}{2}} t f_{t\beta}$

$F_{33} = t^2 f_\beta$ $\quad F_{24} = 2^{\frac{1}{2}} t f_{t\alpha}$

$F_{44} = r^2 f_\alpha$ $\quad F_{34} = rt f_{\alpha\beta}$

b_2-species

$F_{55} = f_r - f_{rr}$ $\quad F_{56} = f_{rt} - f'_{rt}$

$F_{66} = f_t - f_{tt}$ $\quad F_{57} = r(f_{r\gamma} - f'_{r\gamma})$

$F_{77} = rt(f_\gamma - f_{\gamma\gamma})$ $\quad F_{67} = t(f'_{t\gamma} - f_{t\gamma})$

f_{rt} denotes the interaction between Δr and Δt on the same straight line, whereas f'_{rt} denotes those between Δr and Δt perpendicular to each other,

$f_{r\gamma}$ denotes the interaction between Δr and $\Delta\gamma$ having no common bonds, whereas $f'_{r\gamma}$ denotes those between Δr and $\Delta\gamma$ having a common bond (e.g., Δr_1 and $\Delta\gamma_{14}$ in Fig. 4.1), r and t are the equilibrium bond distances in Angstrom units.

4.1.3 *Cis*-$[Pt(pz)_2Cl_2]$

TABLE 4.6

Frequencies and potential energy distribution in normal vibrational modes of *cis*-$[Pt(pz)_2Cl_2]$.

symmetry and approx. description	frequency in cm^{-1}	P.E.D. in %
b_2 ν_{as} Pt-Cl	342	84 S_5 + 12 S_6
a_1 ν_s Pt-Cl	338	87 S_1
b_2 ν_{as} Pt-N	255	80 S_6 + 14 S_5
a_1 ν_s Pt-N	226	52 S_2 + 35 S_3 + 11 S_1
a_1 δ N-Pt-N	203	60 S_3 + 39 S_2
b_2 δ N-Pt-Cl	169	91 S_7
a_1 δ Cl-Pt-Cl	126	97 S_4

TABLE 4.7

Average values for the symmetry force constants of *cis*-$[Pt(pz)_2Cl_2]$.

a_1-species				
S_1	1.888	-.002	-.031	.007
S_2		1.765	.346	-.021
S_3			3.518	.005
S_4				.807
b_2-species				
S_5	1.942	-.053	.042	
S_6		2.246	.066	
S_7			1.608	

TABLE 4.8

Comparison of the observed frequencies with those calculated from the average force field of *cis*-$[Pt(pz)_2Cl_2]$ and *cis*-$[Pt(pz\text{-}d_4)_2Cl_2]$.

cis-$[Pt(pz)_2Cl_2]$		*cis*-$[Pt(pz\text{-}d_4)_2Cl_2]$	
obs.	calc.	obs.	calc.
342	342.1	342	341.8
338	338.1	338	337.9
255	251.9	245	248.1
226	225.5	222	222.6
203	203.4	199	198.6
169	169.9	169	168.1
126	126.1	126	125.9
error (%) : .33		error (%) : .35	

4.1.4 *Cis*-$[Pt(Him)_2(NO_2)_2]$

TABLE 4.9

Frequencies and the potential energy distribution in normal vibrational modes of *cis*-$[Pt(Him)_2(NO_2)_2]$.

symmetry and approx. description	frequency in cm^{-1}	P.E.D. in %
b_2 ν_{as} Pt-X*	315	85 S_5 + 11 S_6
a_1 ν_s Pt-X	307	67 S_1 + 20 S_3 + 11 S_2
a_1 δ N-Pt-N	247	60 S_3 + 28 S_1 + 10 S_2
b_2 ν_{as} Pt-N	227	83 S_6 + 12 S_5
a_1 ν_s Pt-N	208	79 S_2 + 19 S_3
b_2 δ X-Pt-N	151	92 S_7
a_1 δ X-Pt-X	121	97 S_4

* X = NO_2

TABLE 4.10

Average values for the symmetry force constants of *cis*-$[Pt(Him)_2(NO_2)_2]$.

a_1-species				
S_1	1.875	.084	-.173	.021
S_2		1.486	.110	.00
S_3			4.108	.016
S_4				.742
b_2-species				
S_5	2.044	-.049	.041	
S_6		1.599	.041	
S_7			1.193	

TABLE 4.11

Comparison of the observed frequencies with those calculated from the average force field of *cis*-$[Pt(Him)_2(NO_2)_2]$ and *cis*-$[Pt(Him\text{-}d_3)_2(NO_2)_2]$.

cis-$[Pt(Him)_2(NO_2)_2]$		*cis*-$[Pt(Him\text{-}d_3)_2(NO_2)_2]$	
obs.	calc.	obs.	calc.
315	315.1	315	314.9
307	307.4	307	306.6
247	248.5	247	245.5
227	225.6	221	222.4
208	207.2	202	202.8
151	151.7	151	150.3
121	121.1	121	120.9
error (%) : .33		error (%) : .33	

4.1.5 *Cis*-$[Pt(an)_2Cl_2]$

General valence force field calculations were performed using the experimental frequencies of THORNTON *et al.*[11] and assuming point masses for an of 93 and 17 a.m.u. respectively. With both obtained force fields the isotopic shifts of ^{15}N- and d_5-labelled aniline complexes were predicted. Since neither of the two point mass models reproduce satisfactorily the observed shifts, it is reasonable to consider aniline to behave as a point mass greater than ammine but smaller than its molecular mass. As shown in Table 4.12, with m_{an} = 93 the values are approximately 2X too small, whereas if m_{an} = 17 the shifts are 3X to 4X overestimated.

TABLE 4.12

Observed and calculated isotopic shifts of *cis*-$[Pt(an)_2Cl_2]$ (in cm^{-1}).

	obs.(ref.11)		calc.(m_{an}= 17)		calc.(m_{an}= 93)	
	^{15}N	d_5	^{15}N	d_5	^{15}N	d_5
ν_{as} Pt-an	4	11	7	24	1	3
ν_s Pt-an	2	10	7	30	1	4
δan-Pt-an	2	5	5	20	1	4
δan-Pt-Cl	0	3	3	11	0	1

TABLE 4.13

Frequencies and potential energy distribution in normal vibrational modes of *cis*-$[Pt(an)_2Cl_2]$.

symmetry and approx. description	frequency in cm^{-1}	P.E.D.* in %
b_2 ν_{as} Pt-N	374	63 S_6 + 34 S_5
b_2 ν_{as} Pt-Cl	331	67 S_5 + 33 S_6
a_1 ν_s Pt-Cl	329	55 S_1 + 38 S_2
a_1 ν_s Pt-N	293	56 S_2 + 42 S_1
a_1 δ N-Pt-N	177	91 S_3
b_2 δ N-Pt-Cl	147	97 S_7
a_1 δ Cl-Pt-Cl	109	97 S_4

* assuming a point mass of 93.1 a.m.u. for the nitrogen atoms.

TABLE 4.14

Average values for the symmetry force constants of *cis*-$[Pt(an)_2Cl_2]$.

a_1-species				
S_1	1.776	.290	-.089	.014
S_2		3.445	.084	-.010
S_3			2.760	-.007
S_4				.633
b_2-species				
S_5	2.163	-.423	.028	
S_6		4.827	.073	
S_7			1.226	

TABLE 4.15

Comparison of the observed frequencies with those calculated from the average force field of *cis*-[Pt(an)$_2$Cl$_2$], *cis*-[Pt(an-^{15}N)$_2$Cl$_2$] and *cis*-[Pt(an-d_5)$_2$Cl$_2$].

cis-[Pt(an)$_2$Cl$_2$]		*cis*-[Pt(an-^{15}N)$_2$Cl$_2$]		*cis*-[Pt(an-d_5)$_2$Cl$_2$]	
obs.	calc.	obs.	calc.	obs.	calc.
374	370.4	370	369.7	363	367.1
331	332.2	331	331.6	331	329.2
329	329.6	329	329.3	329	328.1
293	290.4	291	289.7	283	286.9
177	176.2	175	175.5	172	172.3
147	146.5	147	146.3	144	145.2
109	109.1	109	109.0	109	108.9
error (%) : .47		error (%) : .22		error (%) : .63	

4.1.6 Discussion

Point-mass modelling has been successfully applied to pz and Him complexes, the validity being confirmed by the calculation of the PED's, see Tables 4.6 and 4.9, respectively. The physically reasonable model can be comprehended as the coordination site is part of a rigid ring system and since, as stated above, the skeletal vibrations are only slightly coupled with the ligand vibrations. Furthermore, in cases where isotopic substitution (H/D and $^{14}N/^{15}N$) does not change the symmetry, the application of the product rule, as pointed out in Sec. 3.1.4, is relatively simple. The calculated and observed product

ratios of some studied complexes are given in Table 4.16. Any discrepancies are attributed to the fact that the fundamental frequencies are influenced by cubic and quartic terms in the potential energy[23]. The close agreement between the ratio-values indicates the relative unimportance of anharmonicity corrections. Hence, the assumption of considering the skeletal modes as strictly harmonic in the theoretical analysis, becomes more justified.

The significantly lower value for the Pt-N force constant in the Him complex as compared to the pz complex (Table 4.17), is in agreement with the polarization theory of the trans-effect. This theory involves essentially a ground-state weakening and polarization of the bond to the ligand trans to the superior directing group[12]. The approximate order of increasing trans-influence* is : Him $\approx$ pz < Cl^- < NO_2^-. In a more extensive series of *cis*-$[Pt(Him)_2X_2]$, where X = Cl, Br, I and NO_2 and, of which the ir data are published in ref.10, the Pt-Him stretching

TABLE 4.16

Product Ratios

class / complex	a_1 calc.	a_1 obs.	b_2 calc.	b_2 obs.
cis-$[Pt(pz)_2Cl_2]$	.961	.963	.976	.961
cis-$[Pt(Him)_2(NO_2)_2]$	.964	.971	.976	.974
cis-$[Pt(NH_3)_2Cl_2]$	.858	.862	.878	.931

* APPLETON *et al.*[13] made a careful distinction between the two terms "trans-effect" and "trans-influence". The "trans-effect"is a kinetic phenomenon, depending upon activation energies and stabilities of transition states while the thermodynamic concept of "trans-influence" was defined in 1966 by PIDCOCK *et al.*[14] referring to bond-weakening in equilibrium states of complexes.

TABLE 4.17

Internal valence force constants of *cis*- PtL_2X_2 skeletons (in mydne/Å).

	cis-[$Pt(pz)_2Cl_2$]	*cis*-[$Pt(Him)_2(NO_2)_2$]	*cis*-[$Pt(an)_2Cl_2$]
f(Pt-X)	1.915 (.045)[+]	1.960 (.050)	1.970 (.048)
f(Pt-L)	2.006 (.067)	1.543 (.057)	(4.1 (.1))[*]
f(Pt-X/Pt-X)	.027 (.001)	.085 (.003)	.194 (.008)
f(Pt-L/Pt-L)	.241 (.010)	.057 (.002)	.691 (.028)
f(Pt-X/Pt-L)	.028 (.001)	.018 (.001)	.067 (.003)
f'(Pt-X/Pt-L)	.026 (.001)	.067 (.003)	.357 (.014)

[+] The values within parentheses are the uncertainties derived from the average force fields applying the harmonic oscillator approach for the stretching force constants and assuming a relative error of 4% on the stretch-stretch interaction force constants.

[*] The Pt-L stretching force constant in *cis*-[$Pt(an)_2Cl_2$] must be regarded as very approximate, since, in the calculation, L is considered as a single point mass (see Discussion 4.1.6). The f' force constant indicates the interaction between bonds perpendicular to each other.

frequency of the trans-isomers are appreciably higher than the average of the two νPt-Him frequencies observed in the *cis*-isomers. The differences (*trans*-freq. minus *cis*-freq.) are rationalized in terms of the trans-directing power which increases in the order Cl < Br < I < NO_2 as summarized below :

group	Cl	Br	I	NO_2
trans-νPt-Him	287	313	301	280
cis-<νPt-Him>	284.5	284.5	272.5	217.5
differences	2.5	28.5	28.5	62.5

An analogous distinction for the pz series is not clearly possible since one of the components of νPt-pz coincides with, or is close to, δpz-Pt-pz[1]. In these cases, coupling between these modes is expected. The PED calculations indeed show strong coupling between S_2 (ν_sPt-L) and S_3 (δL-Pt-L), see Table 4.6. Consequently, it is noted that the F_{23} matrix element is the highest of all other interaction elements constituting the in-plane force field of the pz complexes. The steric interaction of the neighbouring coordinated pyrazines is reflected by the Pt-pz stretching interaction constant which is about 12% of the Pt-pz stretching force constant.

In contrast with SABATINI's conclusion[15], it is not so evident that the Urey-Bradley force field is a poor approximation for these types of molecules since interactions between opposite bonds (amongst other interactions) do not appear in the Urey-Bradley potential function. These interactions, as shown by our general valence force constant calculations, are less than 5% of the stretching values. Thus, they are unimportant and may be neglected.

For the evaluation of the PMM approach for *cis*-$[Pt(an)_2Cl_2]$, we have studied the effect of a variable aniline mass on the most relevant stretching force constants. Therefore, we have changed the mass of L, stepwise until it is smaller than the effective mass of the ligand ammine. In the plots of force constants versus mass, Figs. 4.2 and 4.3, an expected decrease of f(Pt-N) (curve A) is observed since $F = \Lambda.G^{-1}$ and where G is a function of the reciprocal masses of the atoms. The virtual indepencence of f(Pt-Cl) on aniline mass is a demonstration of the pure character of the νPt-Cl modes, and indeed, these bands are completely unaffected by ^{15}N- and d_5-labelling studies[11]. If the νPt-N frequencies are also altered, being finally the experimental frequencies of *cis*-$[Pt(NH_3)Cl_2]$ (curve E) taken from NAKAMOTO *et al.*[18], an increased dependence of f(Pt-N) on the mass becomes more noticeable. The changes of νPt-N are in the following sequence :

curve	A	B	C	D	E	
	374	409	444	479	517	
(an)						(NH_3)
	293	346	399	452	508	

This transition is carried out in steps to allow for test of convergence of the stepwise coupling method (EVM) applied. Since we have assumed identical geometry for the aniline and ammine complexes, direct information on the Pt-to-ligand force constants can be obtained from the graphs, i.e., Figs. 4.2 and 4.3.

TABLE 4.18

Force constants* (in mdyne $Å^{-1}$) of *cis*-$[Pt(NH_3)_2Cl_2]$.

	Nakamoto (ref. 18)	Hiraishi (ref. 19)	from graph
f(Pt-N)	2.39	2.35	2.38 ± 0.03
f(Pt-Cl)	1.82	1.81	1.92

* the values are the results of a general valence force field approach using the cited authors' experimental frequencies.

These graphical values are compared with calculated values from literature data in Table 4.18. By contrast , if we assume similar bond properties, e.g., bond energy and force constant, of the Pt-to-nitrogen bond in both complexes, we can extrapolate a more realistic point mass for the aniline ligand, i.e. about 44 a.m.u.

For the sake of completeness, we have given in Table 4.19 some force constants which have been calculated by both general valence force field (GVFF) and Urey-Bradley force field (UBFF) methods. Comparison of these force constants reported in the literature reveals large discrepancies. Some of the reasons for this fact have been pointed out by SCHMIDT and MULLER[22] as : (1) UB force constants determined on the basis of ir and Raman data only are not considered to be very reliable and, (2) sometimes force constants obtained by least-squares procedures produce the measured frequencies but are not physically meaningful. It should be noted that the internal GV force constants cannot be directly compared with the UB force constants, since the latter constants are generally expected to have lower values.

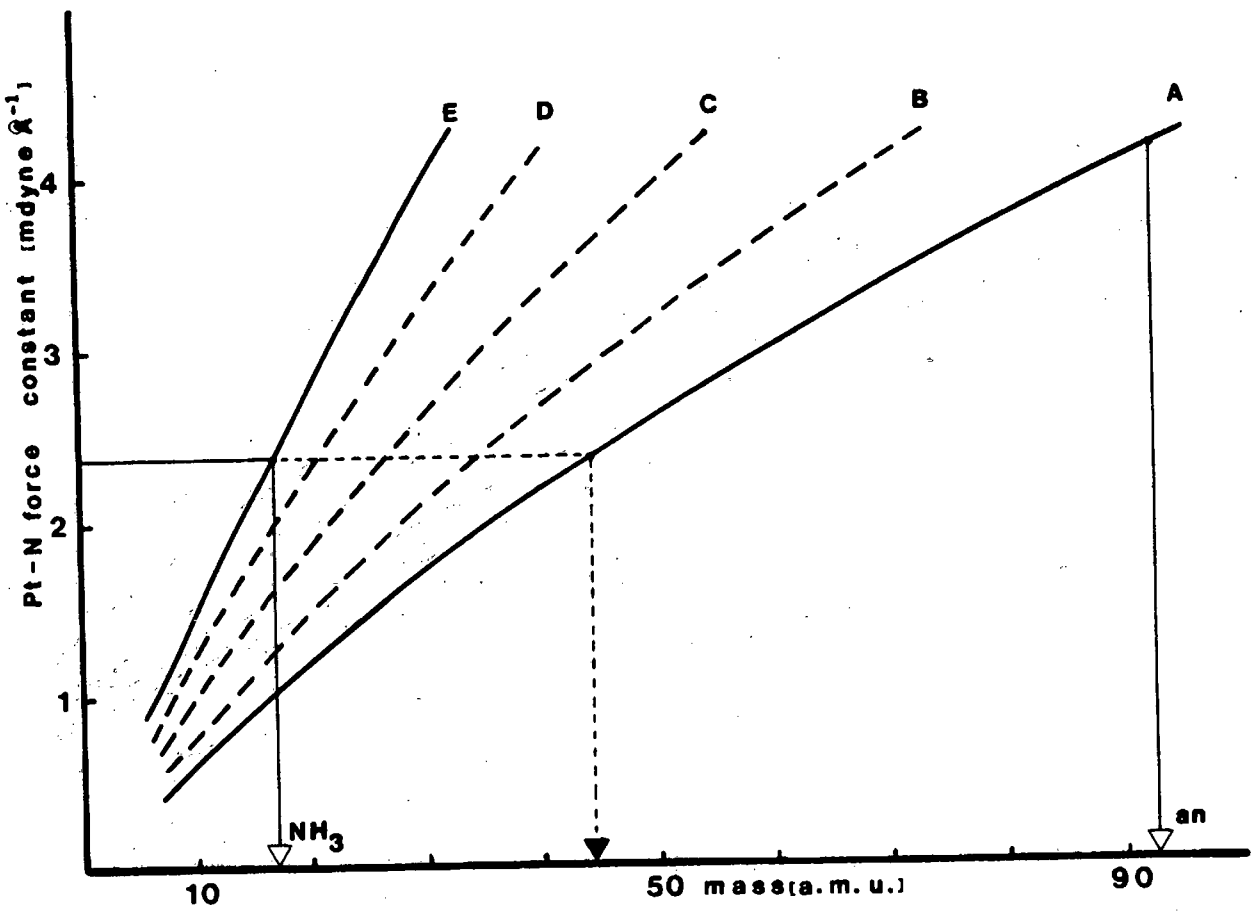

Fig. 4.2 : The effect of variable point mass of L on the Pt-N stretching force constant. See text for explanation.

TABLE 4.19

Stretching force constants of some square-planar tetra-coordinated Pt(II)-complexes (in mdyne/Å).

type	force field	value	complex	reference
Pt-N	UBFF	1.92	$[Pt(NH_3)_4]Cl_2$	16
		2.1	"	17
		2.8	"	5
		2.09	*trans*-$[Pt(NH_3)_2Cl_2]$	18
		1.92	"	19
		2.08	*cis*-$[Pt(NH_3)_2Cl_2]$	
	GVFF	2.44	$[Pt(NH_3)_4]Cl_2$	20
		2.54	"	21
Pt-Cl	UBFF	1.64	K_2PtCl_4	15
		1.82	*trans*-$[Pt(NH_3)_2Cl_2]$	18
		1.817	"	19
		1.797	*cis*-$[Pt(NH_3)_2Cl_2]$	
	GVFF	1.84	K_2PtCl_4	20
		1.78	"	15

4.2 NORMAL COORDINATE TREATMENT OF TETRAHEDRAL CoL_2X_2 TYPE COMPLEXES WHERE L = VARIOUSLY SUBSTITUTED PYRIDINES AND X = HALIDES

4.2.1 Introduction

Calculations of the vibrational frequencies of the tetrahedral complexes formed between cobalt halides and pyridine have been carried out by BEREZIN and GANIN[24]. In the proposed computational technique, the authors made use of the method of successive approximations in which they assumed the force field for the $CoCl_4^{2-}$ ion as an initial approximation to the force field for the CoN_2Cl_2 fragment. The force field for the complex as a whole was made up out of the force field for the CoN_2X_2 fragment and the force field for the pyridine rings which had been calculated previously[25]. Subsequent refinement of the initial force field yielded good agreement between the calculated and experimental frequencies for the stretching modes of the $Co(py)_2X_2$ complexes. BARVINOK and PANIN[26] also calculated the force constant matrix for the tetrahedral isomer of $[Co(py)_2Cl_2]$ from their low-frequency ir data using the Urey-Bradley model field.

The main purpose of this section is to check by means of theoretical vibrational analysis our proposed assignments of the skeletal vibrational frequencies given in Tables 2.12 and 2.13 of Section 2.4.3 (ii) and, to present general valence (GV) force constants for the cobalt-to-ligand bonds in tetrahedral complexes of the type CoL_2X_2. Some discrepancies in our force constants with literature values may be accounted for firstly, by the fact that previously reported assignments contradict one another in some respects. Secondly, the closeness of the calculated force constants to the physical true solution, and hence the accuracy to which force constants can be estimated, is strongly restricted by the applied computational method.

4.2.2 General Remarks

The model for the CoN_2X_2 skeleton is depicted in Fig. 3.5. The internal and vibrational coordinates are described in our previous theoretical Section 3.2.5. The geometrical parameters used were : Co-N, 2.03 Å ; Co-Cl, 2.24 Å ; Co-Br, 2.40 Å and Co-I, 2.58 Å. The bond lengths are taken, as averages, from crystallographically determined distances in the complexes : $Co(4\text{-vinylpy})_2Cl_2$[27], $Co(\gamma\text{-pic})_2Cl_2$[28] and $Co(2\text{-methoxypy})_2Cl_2$[29] and are in agreement with analogous distances of tetrahedrally coordinated cobalt in related structures[30-34]. The six angles around the cobalt atom were assumed to be tetrahedral. It is interesting to note that the distances become closer to the sum of the covalent radii of the constituent atoms in the sequence : Co-I, Co-Br, Co-Cl and Co-N. This suggests that the Co-N bond is essentially covalent.

Normal coordinate analyses were carried out by assuming that the pyridine ligand is a single atom having the total mass of $R\text{-}C_6H_4N$, where R = H or various substituents. The point mass model approach has been applied to metal-pyridine complexes and the validity of such an approximation has been confirmed by various investigators. In a study of the molecular force field of pyridine, SUZUKI and ORVILLE-THOMAS[35] stated that the force field of pyridine remains practically unchanged in going from the free molecule to its complexed form. They further showed that kinetic coupling between the low-frequency vibrations of the pyridine molecule and the metal is mainly responsible for the upward shifts of ligand bands on coordination (see also Section 2.4.3 (i)). Further, BEREZIN and GANIN[24] proved the consistency of their results when the force field for the complex was estimated to be the sum of the force fields of the skeleton CoN_2X_2 and the pyridine ligand. Lastly, we mention the successful normal coordinate

analyses of the skeletal vibrations of the $Zn(py)_2X_2$ type compounds which are isostructural with the cobalt analogues[36], as performed by NAKAMOTO *et al.*[37]. These authors reported band assignments based on the effects of metal isotope, ligand deuteration and halogen substitution and confirmed their results by normal coordinate analysis assuming a point mass for pyridine.

4.2.3 Results and Discussion

The results of a normal coordinate treatment of the skeletal vibrations of $Co(py)_2X_2$ type complexes are given in Tables 4.20 and 4.21. Our band assignments were all confirmed by the calculations of the potential energy distribution for each normal vibrational mode. As indicated by the P.E.D. values, the Co-X and Co-N stretching modes become strongly coupled in the bromo and iodo complexes. This is also found by NAKAMOTO *et al.*[37] for the related zinc complexes. The force constants for the tetrahedral $[Co(py)_2X_2]$ complexes are given in Table 4.21, in which they are compared with reported values from the literature. Table 4.22 shows the values calculated from our proposed assignments for the substituted pyridine complexes of cobalt chloride. Again, the results are in good agreement with those reported for related ammine complexes[38].

TABLE 4.20

Frequencies (cm^{-1}), assignments and potential energy distributions of tetrahedral $[Co(py)_2X_2]$ complexes, where X = halides.

freq.	assignment	potential energy distribution (%)
A) $Co(py)_2Cl_2$		
347	ν_{as}Co-Cl	90 ν_{as}Co-Cl
304	ν_{s}Co-Cl	67 ν_{s}Co-Cl + 27 ν_{s}Co-N
250	ν_{as}Co-N	73 ν_{as}Co-N + 27 δN-Co-Cl
226	ν_{s}Co-N	73 ν_{s}Co-N + 24 ν_{s}Co-Cl
168	δN-Co-N	98 δN-Co-N
138	δN-Co-Cl	90 δN-Co-Cl
98	δCl-Co-Cl	94 δCl-Co-Cl
B) $Co(py)_2Br_2$		
277	ν_{as}Co-Br	76 ν_{as}Co-Br + 24 δN-Co-Br
254	ν_{as}Co-N	72 ν_{as}Co-N + 28 δN-Co-Br
245	ν_{s}Co-Br	62 ν_{s}Co-Br + 30 ν_{s}Co-N
175	ν_{s}Co-N	60 ν_{s}Co-N + 28 ν_{s}Co-Br
150	δN-Co-N	85 δN-Co-N + 13 ν_{s}Co-N
131	δN-Co-Br	87 δN-Co-Br
72	δBr-Co-Br	95 δBr-Co-Br
C) $Co(py)_2I_2$		
246	ν_{as}Co-I	68 ν_{as}Co-I + 32 δN-Co-I
246	ν_{as}Co-N	71 ν_{as}Co-N + 29 δN-Co-I
238	ν_{s}Co-I	66 ν_{s}Co-I + 24 ν_{s}Co-N
159	ν_{s}Co-N	93 ν_{s}Co-N
145	δN-Co-N	87 δN-Co-N
125	δN-Co-I	85 δN-Co-I
64	δI-Co-I	73 δI-Co-I + 23 ν_{s}Co-N

TABLE 4.21

Force constants (in mdyne/Å) for tetrahedral $[Co(py)_2X_2]$ complexes, where X = halides.

compound	bond type	force constants		
		this work	ref. 24	ref. 26
$Co(py)_2Cl_2$	Co-N	1.29 ± 0.03[a]	1.20	1.42
	Co-X	1.30 ± 0.03	1.32	1.67
$Co(py)_2Br_2$	Co-N	1.06 ± 0.03	1.27	
	Co-X	1.33 ± 0.03	0.98	
$Co(py)_2I_2$	Co-N	1.05 ± 0.04	1.32	
	Co-X	1.47 ± 0.03	0.87	

[a] errors are calculated by the harmonic oscillator formula (equation 48, Chapter 3) and assuming an uncertainty of 2 cm^{-1} on the experimental frequencies

TABLE 4.22

Stretching force constants (in mdyne/Å) for tetrahedral $[Co(R\text{-}py)_2Cl_2]$ complexes.

R	f(Co-N)	f(Co-Cl)
3-CH_3	1.54 ± 0.06	1.31 ± 0.04
4-CH_3	1.48 ± 0.05	1.31 ± 0.04
4-NH_2	2.21 ± 0.07	1.15 ± 0.03
4-OH	1.44 ± 0.05	1.10 ± 0.03
3,4-di-CH_3	1.48 ± 0.05	1.33 ± 0.04
3,5-di-CH_3	1.32 ± 0.04	1.30 ± 0.04
4-C_2H_5	1.60 ± 0.06	1.29 ± 0.04
4-$N(CH_3)_2$	1.52 ± 0.06	1.26 ± 0.04
4-$C(CH_3)_3$	1.33 ± 0.04	1.36 ± 0.04
4-COC_6H_5	1.17 ± 0.03	1.33 ± 0.04

REFERENCES

1. G.A. FOULDS, D.A. THORNTON, *Spectrochim. Acta*, 37A(1981)917.
2. A.J. ALIX, M. MANFAIT, B.N. CYVIN, S.J. CYVIN, B.J. VAN DER VEKEN, T. THEOPHANIDES, *J. Chim. Phys. Phys.-Chim. Biol.*, 76(1979)475.
3. B.N. CYVIN, S.J. CYVIN, K.H. SCHMIDT, W. WIEGLER, A. MULLER *J. Mol. Struct.*, 30(1976)315.
4. B.N. CYVIN, S.J. CYVIN, K.H. SCHMIDT, A. MULLER, J. BRUNVOLL, *J. Mol. Struct.*, 32(1976)269.
5. S.-I. MIZUSHIMA, I. NAKAGAWA, M.J. SCHMELZ, C. CURRAN, J.V. QUAGLIANO, *Spectrochim. Acta*, 13(1958)31.
6. P. COLAMARINO, P.L. ORIOLI, *J. Chem. Soc., Dalton*, (1975)1656.
7. F.D. ROCHON, P.C. KONG, R. MELANSON, *Can. J. Chem.*, 59(1981)195.
8. J.A. KADUK, J.A. IBERS, *Inorg. Chem.*, 16(1977)3278.
9. G.H.W. MILBURN, M.R. TRUTER, *J. Chem. Soc.*, A(1966)1610.
10. S.J. ARCHER, T.P.E. AUF DER HEYDE, G.A. FOULDS, D.A. THORNTON, *Transition Met. Chem.*, 7(1982)59.
11. T.P.E. AUF DER HEYDE, G.A. FOULDS, D.A. THORNTON, G.M. WATKINS, *J. Mol. Struct.*, 77(1981)19.
12. F.A. COTTON, G. WILKINSON, "Advanced Inorganic Chemistry", Interscience Publishers, New York, 1972(3rd ed.).
13. T.G. APPLETON, H.C. CLARK, L.E. MANZER, *Coord. Chem. Rev.*, 10(1973)335.
14. A. PIDCOCK, R.E. RICHARDS, L.M. VENANZI, *J. Chem Soc.*, A(1966)1707.
15. A. SABATINI, L. SACCONI, V. SCHETTINO, *Inorg. Chem.*, 3(1964)1775.
16. T. SHIMANOUCHI, I. NAKAGAWA, *Inorg. Chem.*, 3(1964)1805.
17. H. POULET, P. DELORME, J.P. MATHIEU, *Spectrochim. Acta*, 20(1964)1855.

18. K. NAKAMOTO, P.J. McCARTHY, J. FUJITA, R.A. CONDRATE, G.T. BEHNKE, *Inorg. Chem.*, 4(1965)36.

19. J. HIRAISHI, I. NAKAGAWA, T. SHIMANOUCHI, *Spectrochim. Acta*, 24A(1968)819.

20. A. FADINI, A. MULLER, *Mol. Phys.*, 12(1967)145.

21. K.H. SCHMIDT, A. MULLER, *Inorg. Chem.*, 14(1975)2183.

22. K.H. SCHMIDT, A. MULLER, *Coord. Chem. Rev.*, 19(1976)41.

23. E.B. WILSON, J.C. DECIUS, P.C. CROSS, "Molecular Vibrations", McGraw-Hill, New York, 1955.

24. V.I. BEREZIN, V.V. GANIN, *Koord. Khim.*, 2(1976)1243.

25. V.I. BEREZIN, V.V. GANIN, *Koord. Khim.*, 2(1976)550.

26. M.S. BARVINOK, A.V. PANIN, *Russ. J. Inorg. Chem.*, 23(1978)1348.

27. L.J. ADMIRAAL, G. GAFNER, *Chem. Comm.*, (1968)1221.

28. M. LAING, G. CARR, *Acta Cryst.*, 31B(1975)2683.

29. J.R. ALLAN, C.L. JONES, L. SAWYER, *J. Inorg. Nucl. Chem.*, 43(1981)2707.

30. C.K. PROUT, P. MURRAY-RUST, *J. Chem. Soc.*, A(1969)1520.

31. R.M. MORRISON, R.C. THOMPSON, J. TROTTER, *Can. J. Chem.*, 57(1979)135.

32. M.M. KADOOKA, L.G. WARNER, K. SEFF, *Inorg. Chem.*, 15(1976)812.

33. A. MANGIA, M. NARDELLI, C. PELIZZI, G. PELIZZI, *J. Chem. Soc., Dalton Trans.*, (1972)996.

34. R.J. SUNDBERG, I. YILMAZ, D.C. MENTE, *Inorg. Chem.*, 16(1977)1470.

35. S. SUZUKI, W.J. ORVILLE-THOMAS, *J. Mol. Struct.*, 37(1977)321.

36. M.A. PORAI-KOSHITS, L.O. ATOVMYAN, G.N. TISHCHENKO, *Zh. Strukt. Khim.*, 1(1960)337.

37. Y. SAITO, M. CORDES, K. NAKAMOTO, *Spectrochim. Acta*, 28A(1972)1459.

38. J.R. FERRARO, "Low-Frequency Vibrations of Inorganic and Coordination Compounds", Plenum Press, New York, 1971.

CHAPTER 5

THE THERMAL ANALYSIS OF $[CoL_2X_2]$ COMPLEXES, WHERE X = Cl AND Br AND L = VARIOUSLY SUBSTITUTED PYRIDINES

5.1 INTRODUCTION

Although man recognized the effect of heat on materials since times predating recorded history, e.g. the extraction of copper from its ores was known in prehistoric times and the production of tin and iron by smelting was in progress before 3500 B.C., we had to wait until the end of the 19th century for major advances in thermoanalytical techniques. These contributions were the development of accurate temperature-measuring devices such as the thermocouple which is still used in commercial apparatus, by Le Chatelier in the 1880's and Roberts-Austin's idea (1899) of measuring the temperature difference between the sample and a thermally inert material, hence establishing the differential method. Early applications of thermal analysis were largely in the field of metallurgy and mineralogy; its development was continuous from the beginning of this century in the USSR especially, under Kurnakov and his pupil Berg (ref.1, Chapter 1). In the last forty years the field of interest shifted towards other regions of chemistry, e.g. widely used analytical applications of finding suitable weighing forms for various elements. A wide range of inorganic compounds have been investigated to determine their thermal stability, mechanism of decomposition and structure. Some of the reaction types employed are :

(1) dehydration

(2) decomposition reactions not involving the atmosphere

(3) oxidative degradation studies

In the field of organic chemistry, in addition to the studies outlined above, kinetics of decomposition and thermal degradation of polymers have received most attention (ref.1, Chapter 5).

Only recently, with the advent of modern differential analyzers, fast

and reliable quantitative measurements of transition energies became possible.

Early thermal studies of bis(pyridine)cobalt chloride and other related compounds have been published by OCONE *et al.*[2]. Thermochemical results of some limited series of substituted pyridine complexes of cobalt(II) halides have been reported by the following investigators : ALLAN *et al.*[3,4], BEECH *et al.*[5,6,7] and MORTIMER *et al.*[8]. Attempts to gain information on the stereochemistry of the cobalt ion in the decomposition products have been undertaken by ALLAN *et al.*[3] An idealised scheme of decomposition was proposed as :

$$CoL_2X_2(tet) \longrightarrow CoLX_2(oct) \longrightarrow CoL_{2/3}X_2(oct) \longrightarrow CoX_2(oct)$$

We quote from reference 3: "The violet form of bis(pyridine)cobalt(II) chloride has a chain structure with chlorine atoms bridging between two cobalt atoms and the structures of stoichiometry $CoLX_2$ and $CoL_{2/3}X_2$ may be built up by removing pyridines from such a chain to give double and triple chains in which each chlorine is acting as a bridge between three metals. If the chains are converted to infinite planes this gives the structures of anhydrous cobalt(II) chloride and bromide". Further, it is stated that these complex transformations appear to occur in the liquid phase.

BEECH[5] and MORTIMER[8], whose published results are significantly different from ours, have used quantitative differential thermal analysis to determine the heats of decomposition reactions of CoL_2X_2 where L = py, 3Cl-py, 3Br-py and X = Cl and Br among others. Difficulties associated with the reproducibility of the applied technique and factors inherent in the graphical data (see e.g. curve-shape in Section 5.2) form the major limitations to the accuracy obtainable in quantitative studies.

With the above in mind and mainly because no previous study of the thermal behaviour of an extensive series of cobalt pyridine complexes had ever been reported, we have carried our this work.

5.2 BASIC PRINCIPLES

The following abbreviations are employed in the text : TG - thermogravimetry, DTG - derivative thermogravimetry, DSC - differential thermal analysis. We can define TG as a dynamic method by which the weight of a substance in a controlled environment, is recorded as a function of temperature. DTG refers to the first derivative of the TG curve, showing a greater sensitivity. From reference 1, we quote : "DSC covers the technique of recording the energy necessary to establish zero temperature difference between a substance and a reference material against either time or temperature as the two specimens are subjected to identical temperature regimes ..,". The calorimetric technique, DTA is closely related to the latter method as it records the difference in temperature between the two specimens in an environment heated or cooled at a controlled rate.

Simplified TG and their DTG curves are shown in Figs. 5.1 and 5.2, of which the latter is for a compound A undergoing a decomposition reaction through a characterisable intermediate B. The temperature-range over which the transition occurs is determined by the initial and final temperatures, T_i and T_f, respectively. The maximum on the DTG curve represents the temperature, T_m. Because of the dependence of these temperatures on the quantity and particle size of the samples, it is difficult to express their significance. In order to have comparable decomposition temperatures, we define a new temperature, T, at the point of tangency of a line drawn at 45° to the baseline at the inflection

denoting the commencement of decomposition. In this manner, T will become less dependent on the curve-shape. The thermograms are plotted with percentage weight loss on the ordinate, hence loss of constituent ligand molecules to form new complexes and their decomposition mechanism can be observed. The appearance of two plateaux on the TG curve, in Fig. 5.2, characterise some thermal stability of compound A below temperature d and the formation of the thermally stable reaction product C above temperature e, while point b refers to the unstable transition compound B.

DSC and DTA curves for a substance undergoing a single endothermic reaction are shown in Figs. 5.3 and 5.4, respectively. The DSC peak temperature, T_p, does not necessarily correspond to the peak temperature on the DTA curve since differences in thermocouple-sample arrangement are applied for both cells. The extrapolated temperatures, T_o and T_1, which are the intersections of the lines extrapolated through the straightline portions of the DSC curve and the baseline as shown in Fig. 5.3, will differ only slightly from the temperatures, T_i and T_f, of their related TG curve if the sample mass is small. From the thermal curves of heat flow versus temperature which defines the amount of energy involved in a transition, quantitative calorimetry is possible. The enthalpies (ΔH values) are calculated from the equation :

$$\Delta H \ (J/g) = \frac{A}{m} \ (60BE\Delta qs)$$

where A = peak area, in cm^2; m = sample mass, in g; B = time base setting, in min/cm; E = cell calibration coefficient at the temperature of the experiment (dimensionless) and Δqs = Y-axis range, in J/s cm. From the DSC results which are plotted as Δq versus time using the T-axis as a time base, the area of the transition peak determined by the baseline as in Fig. 5.3, is measured with a planimeter. The

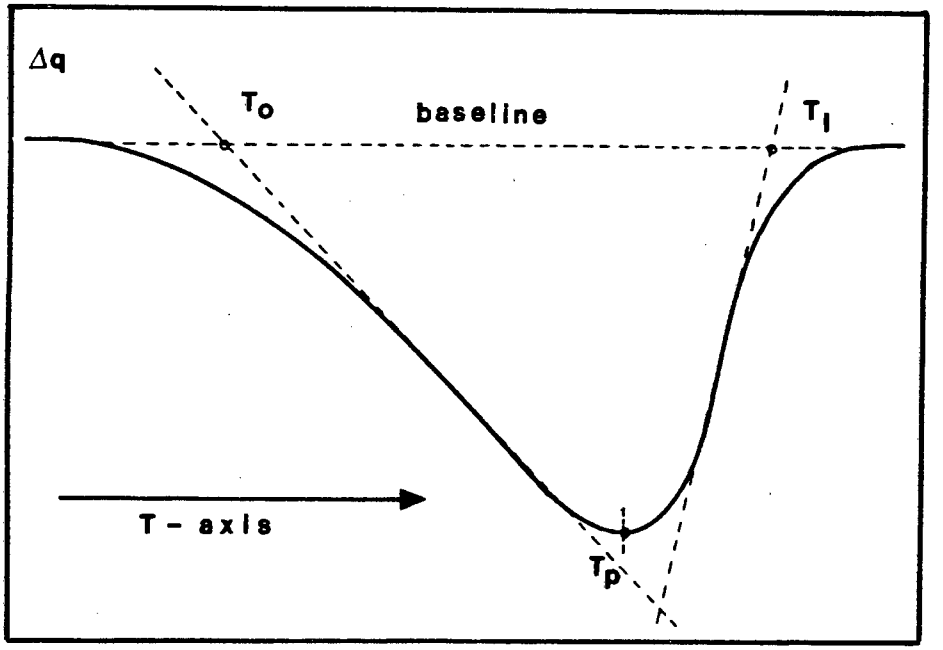

Fig. 5.3 : A thermal DSC curve showing heat flow versus time of temperature. See text for the symbols.

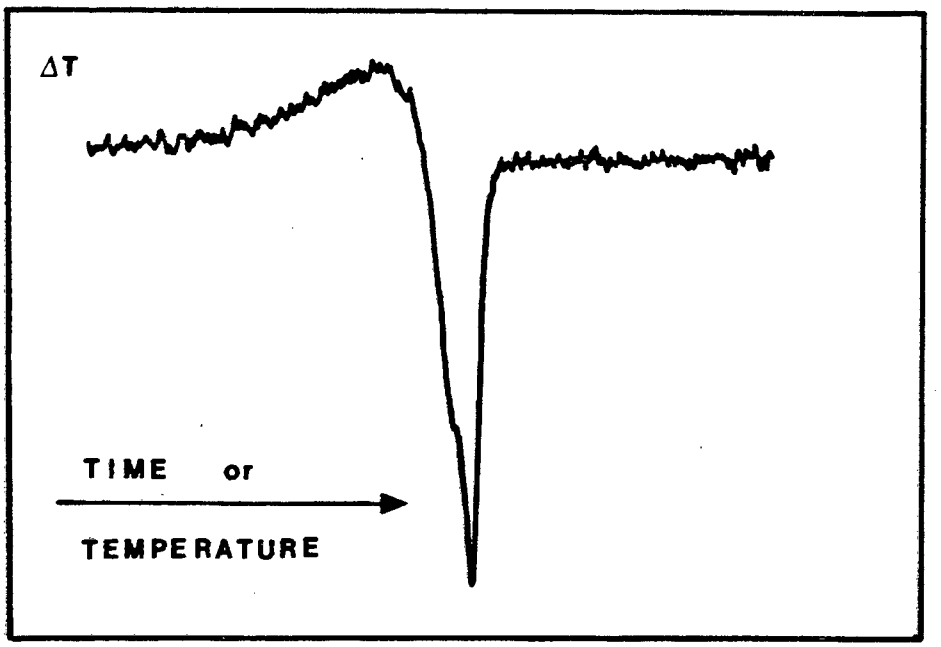

Fig. 5.4 : A typical endothermic DTA peak.

calibration coefficient varies with applied atmosphere and pressure but can be determined using materials of known heats of fusion. For this purpose, an indium sample which has a ΔH of 28.38 J/g at its melting point of 156.6°C is used. The coefficient remains essentially unchanged and hence the quantity (60BEΔqs) will be constant when operating under a given set of instrument settings.

Note that some portions of the DTA peak may overshoot the baseline before finally returning to it, e.g. in Fig. 5.30 yielding an apparently exothermic peak immediately after a sharp endothermic one. This is caused by the thermal diffusivity behaviour of the constructional material used for the specimen holder.

Other factors which can influence the temperature of decomposition or in general the shape of the thermal curves, are the thermal conductivity, the specific heat and the bulk density of the samples. Their contributions are minimal and we consider them equivalent for all compounds. For the DSC results it is assumed that large differences in packing forces are absent so that the heats of decomposition contain direct information on the metal-to-ligand bond strengths.

Owing to the non-existence of most cobalt complexes in the gas phase and thus lack of data for the appropriate heats of reactions (heats of sublimation), it is not possible to relate, ideally, the measured enthalpies to the gas-phase reactions. We must strongly emphasise that all measurements are only comparable under one rigidly controlled set of experimental conditions. Sample characteristics and programme rates being important parameters, the dependence of DSC data on these parameters were given by WATSON *et al.*[9] and VAN DOOREN and MULLER[10]. In order to obtain precise enthalpy change determinations, it is advisable, according to SIRACUSA and CUCINOTTA[11], to do an additional calibration of the measured

peak areas against a suitable range of sample weights. Recently, the influence of sample weight and heating rate upon the shape of the TG curves and thus, the decomposition temperature were shown by ZSAKI *et al.*[12]. The authors stated that some physically meaningful conclusions on the strength of the metal-ligand bond can be made from thermal curves if (1) they are recorded in well standardized working conditions and (2) closely related decomposition reactions are studied.

5.3 THERMOGRAVIMETRY

Thermograms of thirty-nine substituted pyridine complexes of cobalt(II) halides are shown in Figs. 5.5 to 5.24 and their relevant data are reported in Table 5.1. All decompositions were carried out under an atmosphere of dry nitrogen at a flow rate of 20 ml/min and at ambient pressure. A heating rate of 5 or 10°C/min was chosen depending on the sample mass of approximate 5 or 10 mg, respectively. No thermal curves could be obtained for $Co(3\text{-}CH_3COpy)_2Br_2$ and $Co(4\text{-}CH_3COpy)_2Br_2$ as a result of their spattering behaviour even by the slowest heating rate.

The complexes decompose to the appropriate cobalt halides directly or by way of intermediates in the following general scheme :

$$ML_2X_2\ (s) \longrightarrow MLX_2\ (s) + L\ (g) \quad (1)$$

$$ML_2X_2\ (s) \longrightarrow ML_{5/3}X_2\ (s) + 1/3\ L\ (g) \quad (1a)$$

$$ML_{5/3}X_2\ (s) \longrightarrow MLX_2\ (s) + 2/3\ L\ (g) \quad (1bc)$$

$$MLX_2\ (s) \longrightarrow MX_2\ (s) + L\ (g) \quad (2)$$

$$MLX_2\ (s) \longrightarrow ML_{2/3}X_2\ (s) + 1/3\ L\ (g) \quad (2a)$$

$$ML_{2/3}X_2\ (s) \longrightarrow ML_{1/3}X_2\ (s) + 1/3\ L\ (g) \quad (2b)$$

$$ML_{1/3}X_2\ (s) \longrightarrow MX_2\ (s) + 1/3\ L\ (g) \quad (2c)$$

$$ML_2X_2\ (s) \longrightarrow MX_2\ (s) + 2\ L\ (g) \quad (3)$$

where in the nomenclature 1 and 2 indicate the loss of the first and second pyridine-ligand (L), respectively and a, b, and c indicate the partial decomposition of the ligand. If reactions 2a and 2b occur simultaneously, the resulting reaction will be 2ab. Decomposition of the cobalt halides is referred to as 4.

TABLE 5.1

A) Decomposition according to the general scheme

complex	reaction	stable product	temperature-range T_i (°C)	T_m	T_f	weight loss (%) obs.	calc.
$Co(3\text{-}Clpy)_2Cl_2$	(1)	yes	149	169	174	32.0	31.8
	(2)	yes	221	243	249	32.0	31.8
$Co(3\text{-}Clpy)_2Br_2$	(1)	yes	156	176	183	26.0	25.5
	(2)	yes	208	235	240	26.0	25.5
$Co(3\text{-}Brpy)_2Cl_2$	(1)	yes	164	185	192	35.5	35.4
	(2)	yes	225	247	257	34.5	35.4
$Co(3\text{-}Brpy)_2Br_2$	(1)	yes	163	183	190	29.5	29.5
	(2)	yes	218	241	250	29.5	29.5
$Co(4\text{-}NCpy)_2Cl_2$	(1)	yes	171	188	195	30.0	30.8
	(2ab)	yes	247	265	272	22.5	20.5
	(2c)	yes	314	331	340	9.5	10.3
$Co(4\text{-}NCpy)_2Br_2$	(1)	yes	156	181	186	22.3	24.4
	(2ab)	no	238	262	269	17.6	16.3
	(2c)	yes	295	310	321	7.0	8.1
$Co(py)_2Cl_2$	(1a)	no	109	124	-*	27.5	27.5
	(1bc)	yes	-	143	148		
	(2a)	yes	191	205	210	9.0	9.2
	(2bc)	yes	243	263	270	17.0	18.3

* impossible to determine because of absence of plateau

TABLE 5.1 continued/

complex	reaction	stable product	temperature-range T_i(°C)	T_m	T_f	weight loss (%) obs.	calc.
$Co(py)_2Br_2$	(1a)	no	170	196	-*	21.0	21.0
	(1bc)	no	-	201	202		
	(2a)	no	204	218	221	6.8	7.0
	(2bc)	yes	230	249	254	13.5	14.0
$Co(3\text{-}CH_3py)_2Cl_2$	(1)	no	140	166	171	29.0	29.5
	(2a)	yes	174	184	187	10.0	9.8
	$(-CH_3)^a$	no	217	228	237	≈5	4.7
	(2bc)	yes	236	262	269	20.0	19.6
$Co(4\text{-}CH_3py)_2Cl_2$	(1)	yes	139	162	166	29.3	29.5
	(2a)	yes	197	213	218	9.5	9.8
	(2b)	no	247	265	-*	19.8	19.6
	(2c)	yes	-	277	281		
$Co(3\text{-}HOOCpy)_2Cl_2$*	(1)+(2a)	yes	229	241	245	42.8	43.6
	(2bc)	no[b]	365	375	379	24.4	21.8
$Co(3\text{-}HOOCpy)_2Br_2$	(1)+(2a)	no	243	275	291	36.0	35.3
	(2bc)	no[b]	373	403	413	22.0	17.7
$Co(3,4di\text{-}CH_3py)_2Cl_2$	(1)+(2a)	yes	200	232	239	42.0	41.5
	(2bc)	yes	289	301	305	20.3	20.8
$Co(4\text{-}C_2H_5py)_2Cl_2$	(1)+(2ab)	no	225	263	-	50.0	51.9
	(2c)	yes	-	283	289	10.5	10.4
$Co(4\text{-}C_6H_5COpy)_2Cl_2$	(1)+(2a)	no	234	258	-	49.0	49.2
	(2bc)	yes	-	310	314	23.8	24.6

* impossible to determine because of absence of plateau

[a] an intermediate step is observed corresponding to a weight loss of the methyl-group

[b] the cobalt halides start to decompose above 380°C

TABLE 5.1 continued/

complex	reaction	stable product	temperature-range T_i (°C)	T_m	T_f	weight loss (%) obs.	calc.
$Co(4\text{-}C_6H_5py)_2Cl_2$	(1)+(2a)	no	241	269	276	≈47	47.0
	(2b)	no	298	310	-*	≈23	23.5
	(2c)	yes	-	346	353		
$Co(3\text{-}CH_3COpy)_2Cl_2$	(1)+(2a)	no	199	225	233	41.0	43.4
	(2b)	no	264	289	-*	21.5	21.7
	(2c)	yes	-	331	338		
$Co(4\text{-}CH_3COpy)_2Cl_2$	(1)	no	219	245	249	32.0	32.6
	(2a)	no	276	340	346	10.0	10.9
	(2bc)+(4)	no	438	516	-		
$Co(3\text{-}CH_3OCOpy)_2Cl_2$	(1)	yes	162	182	187	33.5	33.9
	(2ab)	yes	248	265	270	24.0	22.6
$Co(3\text{-}CH_3OCOpy)_2Br_2$	(1)	no	161	181	188	27.3	27.8
	(2a)	yes	219	230	233	11.6	9.2
$Co(4\text{-}CH_3OCOpy)_2Cl_2$	(1)+(2a)	no	174	195	200	45.3	45.2
	(-Ac)	yes	235	248	256	≈16	14.6
$Co(4\text{-}CH_3OCOpy)_2Br_2$	(1a)	no	172	185	-*	25.5	27.8
	(1bc)	yes	-	194	206		
$Co(3\text{-}H_2NCOpy)_2Cl_2$	(1)+(2a)	no	267	291	296	43.5	43.5
	(2bc)	no	320	346	b.r.		
$Co(3\text{-}H_2NCOpy)_2Br_2$	(1)+(2ab)	no	257	278	303		44.0
$Co(4\text{-}H_2NCOpy)_2Cl_2$	(1)	no	278	304	-*	54.0	54.0
	(2ab)	no	-	326	336		
$Co(4\text{-}H_2NCOpy)_2Br_2$	(1)	no	266	281	-*	42.0	44.0
	(2a)	no	-	290	-*		
	(2b)	no	-	310	318		

b.r. : beyond the range studied ; Ac : acetate group

* : recorded at a heating rate of 1°C/min

TABLE 5.1 continued/

B) Decomposition with no characterisable intermediates and formation of stable cobalt halides.

complex	reaction	temperature-range			weight loss (%)	
		T	T_m	T_f(°C)	obs.	calc.
$Co(4\text{-}C_6H_5COpy)_2Br_2$	(3)	233	269	301	63.5	62.6
			295+			
$Co(3\text{-}C_6H_5COpy)_2Cl_2$	(3)	182	228+	277	75.0	73.8
			272			
$Co(3\text{-}C_6H_5COpy)_2Br_2$	(3)	231	291+	322	61.5	62.6
			320			
$Co(3\text{-}CH_3py)_2Br_2$	(3)	217	289	293	45.0	46.0
$Co(4\text{-}CH_3py)_2Br_2$	(3)	218	293	296	46.0	46.0
$Co(3,4di\text{-}CH_3py)_2Br_2$	(3)	230	304	313	49.0	49.5
$Co(4\text{-}C_2H_5py)_2Br_2$	(3)	215	290	295	49.5	49.5
$Co(4\text{-}C_6H_5py)_2Br_2$	(3)	246	311	336	56.5	58.7

C) Decomposition with no characterisable intermediates and decomposition of the cobalt halides (Temp. > 300°C)

complex	reaction	temperature-range (°C)			
		T	T_i	T_m	T_f
$Co(4\text{-}HOpy)_2Cl_2$	(3)	265	280	363+	488
	(4)	-	-	473	-
$Co(4\text{-}H_2Npy)_2Cl_2$	(3)	253	279	334	413
	(4)	-	-	385	-

TABLE 5.1 continued/

complex	reaction	temperature-range (°C)			
		T	T_i	T_m	T_f
$Co(4\text{-}(CH_3)_2Npy)_2Cl_2$	(3)	253	267	286	420
	(4)	-	-	403	-
$Co(4\text{-}(CH_3)_2Npy)_2Br_2$	(3)	268	277	293	420
	(4)	-	-	398	-

D) Irregular thermal behaviour and decomposition

complex	stable product	temperature-range (°C)			weight loss (%)	
		T_i	T_m	T_f	obs.	calc.
$Co(4\text{-}(CH_3)_3Cpy)_2Cl_2$	no	229	273	278	52.5	52.5
	no	302	319	325	13.0	15.0
$Co(3\text{-}CH_3COpy)_2Br_2$	see text					
$Co(4\text{-}CH_3COpy)_2Br_2$	see text					

+ a second maximum on the DTG curve is observed

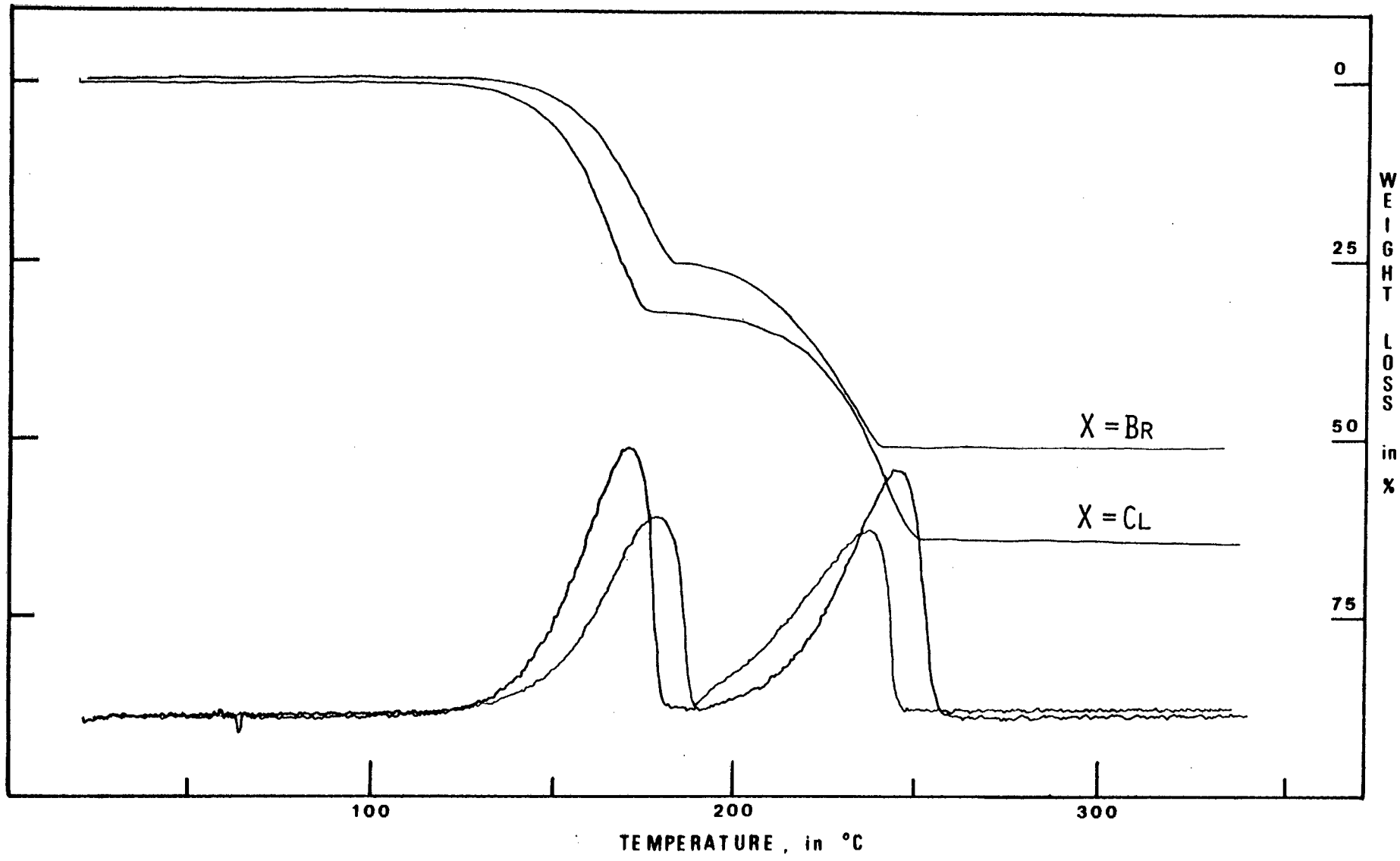

Fig. 5.5 : TG and DTG of $Co(3\text{-}Clpy)_2X_2$.

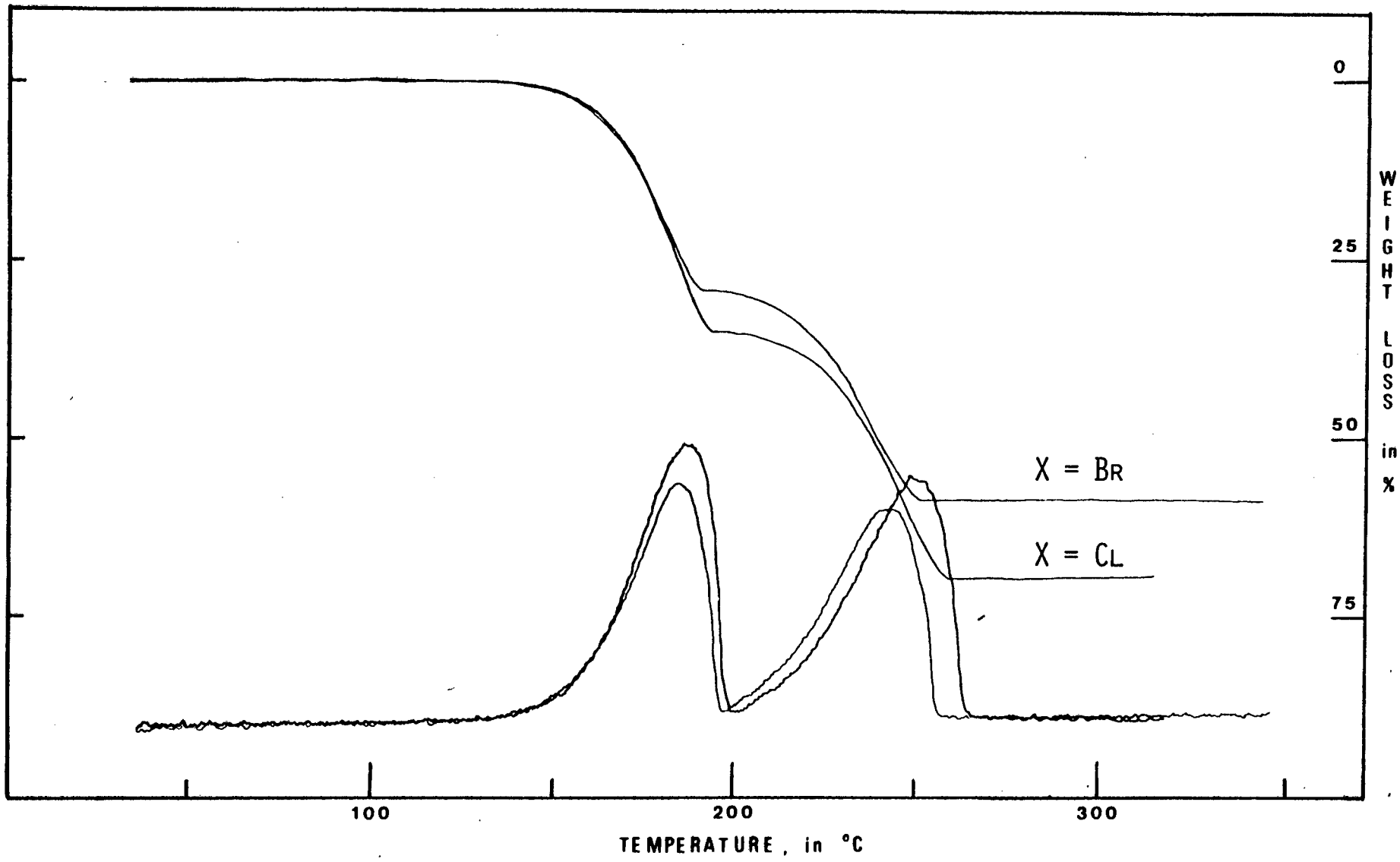

Fig. 5.6 : TG and DTG of $Co(3\text{-}Brpy)_2X_2$.

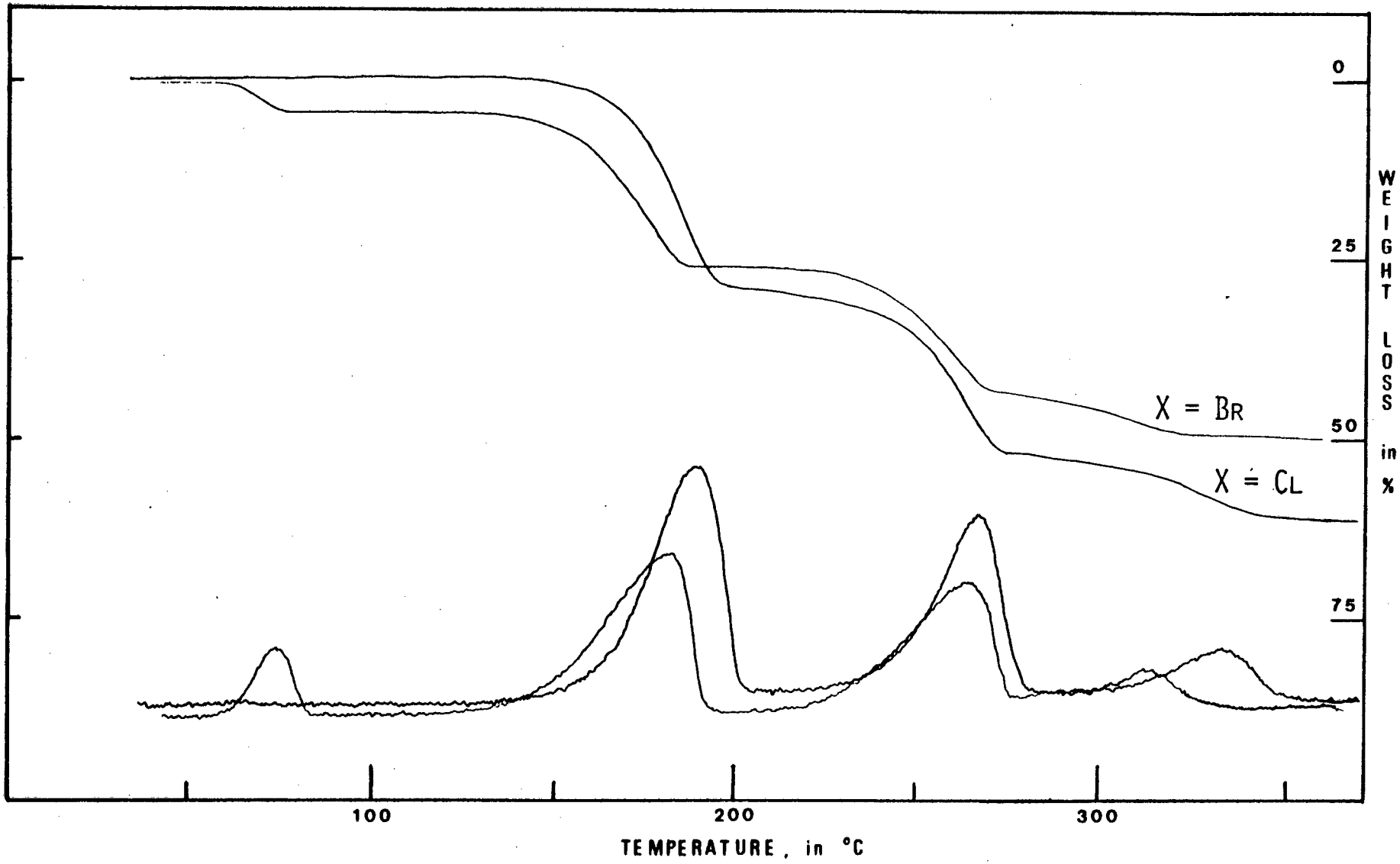

Fig. 5.7 : TG and DTG of $Co(4\text{-}NCpy)_2X_2$.

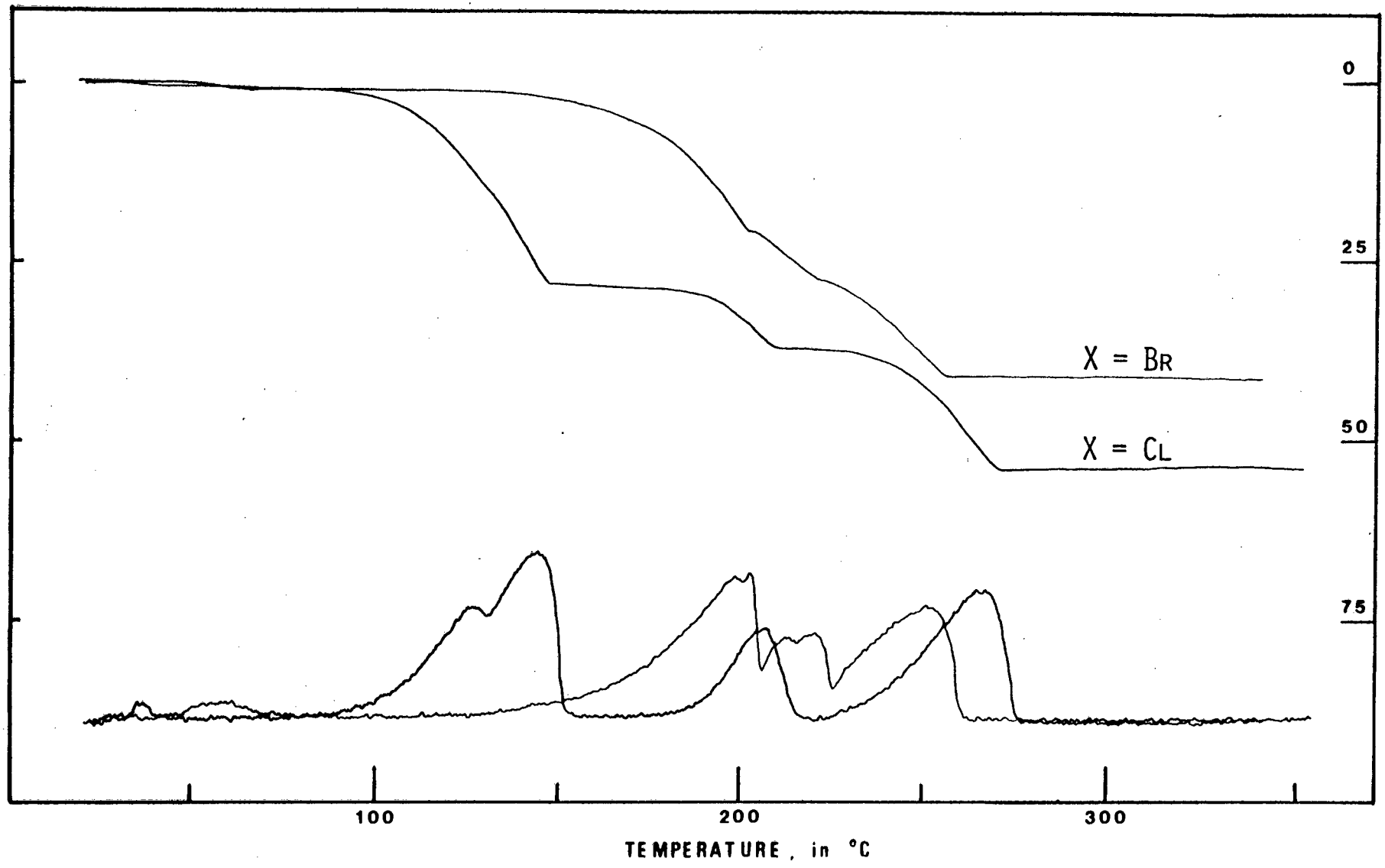

Fig. 5.8 : TG and DTG of $Co(py)_2X_2$.

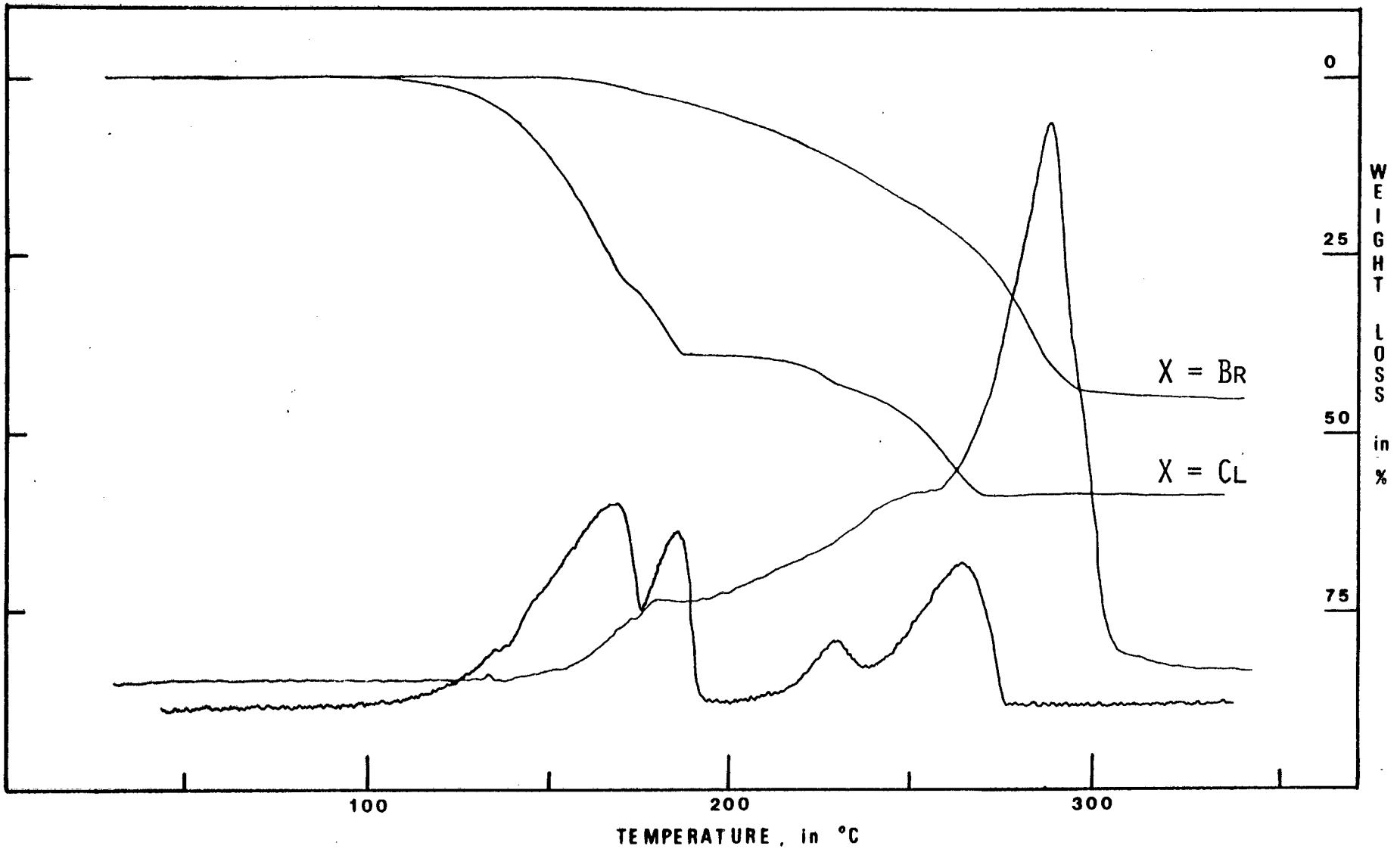

Fig. 5.9 : TG and DTG of $Co(3\text{-}CH_3py)_2X_2$.

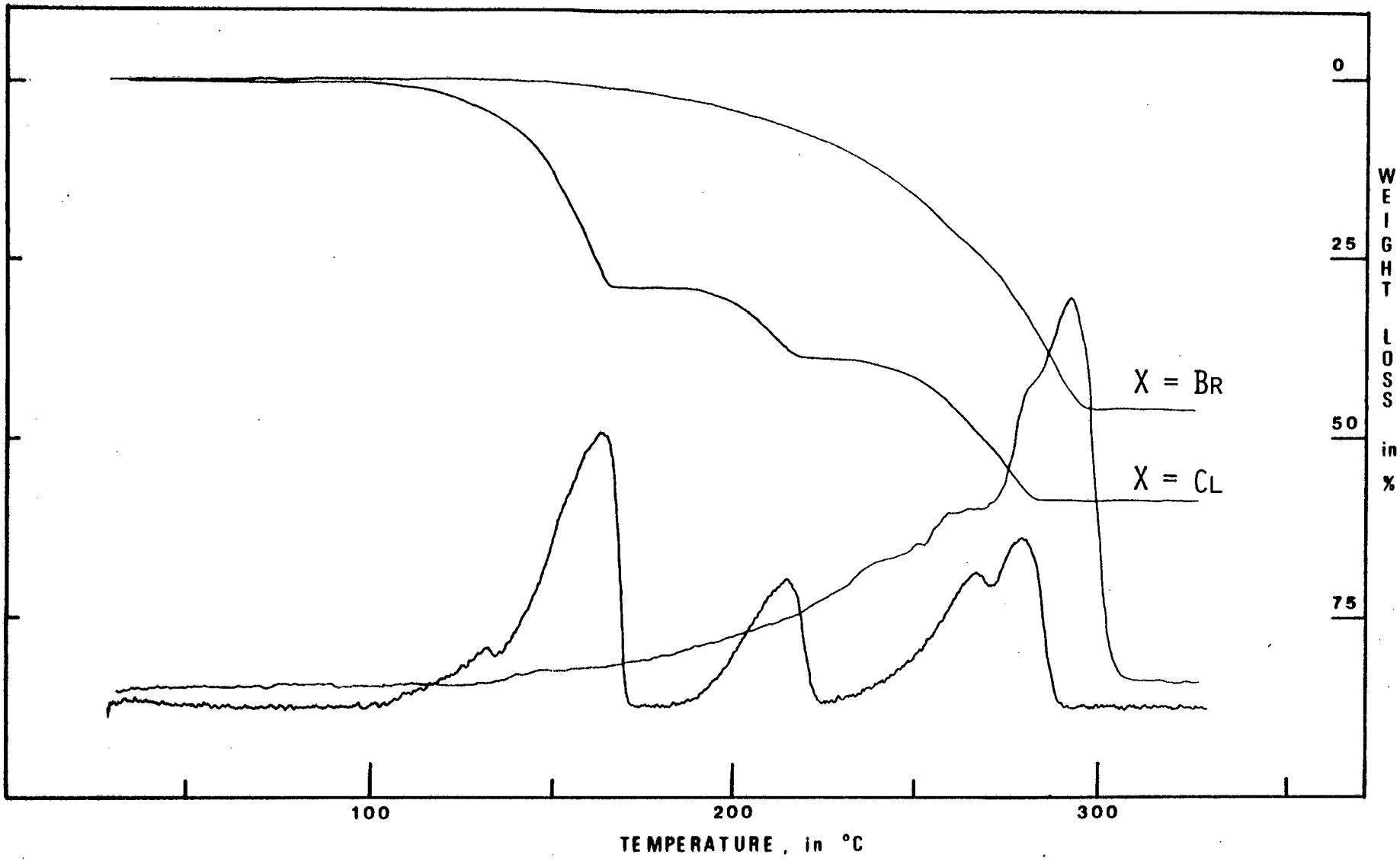

Fig. 5.10 : TG and DTG of $Co(4\text{-}CH_3py)_2X_2$.

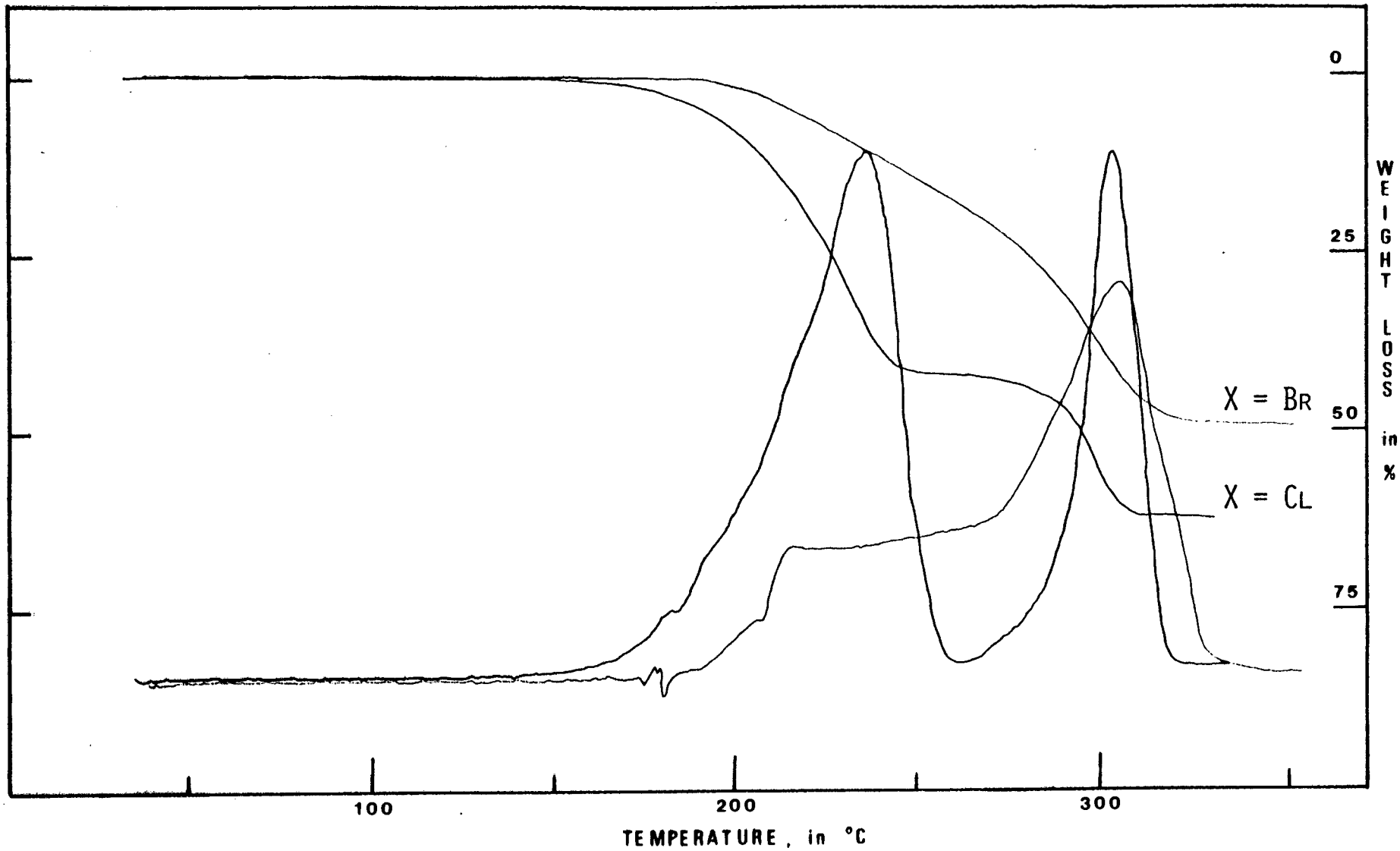

Fig. 5.11 : TG and DTG of $Co(3,4\text{-di-}CH_3py)_2X_2$.

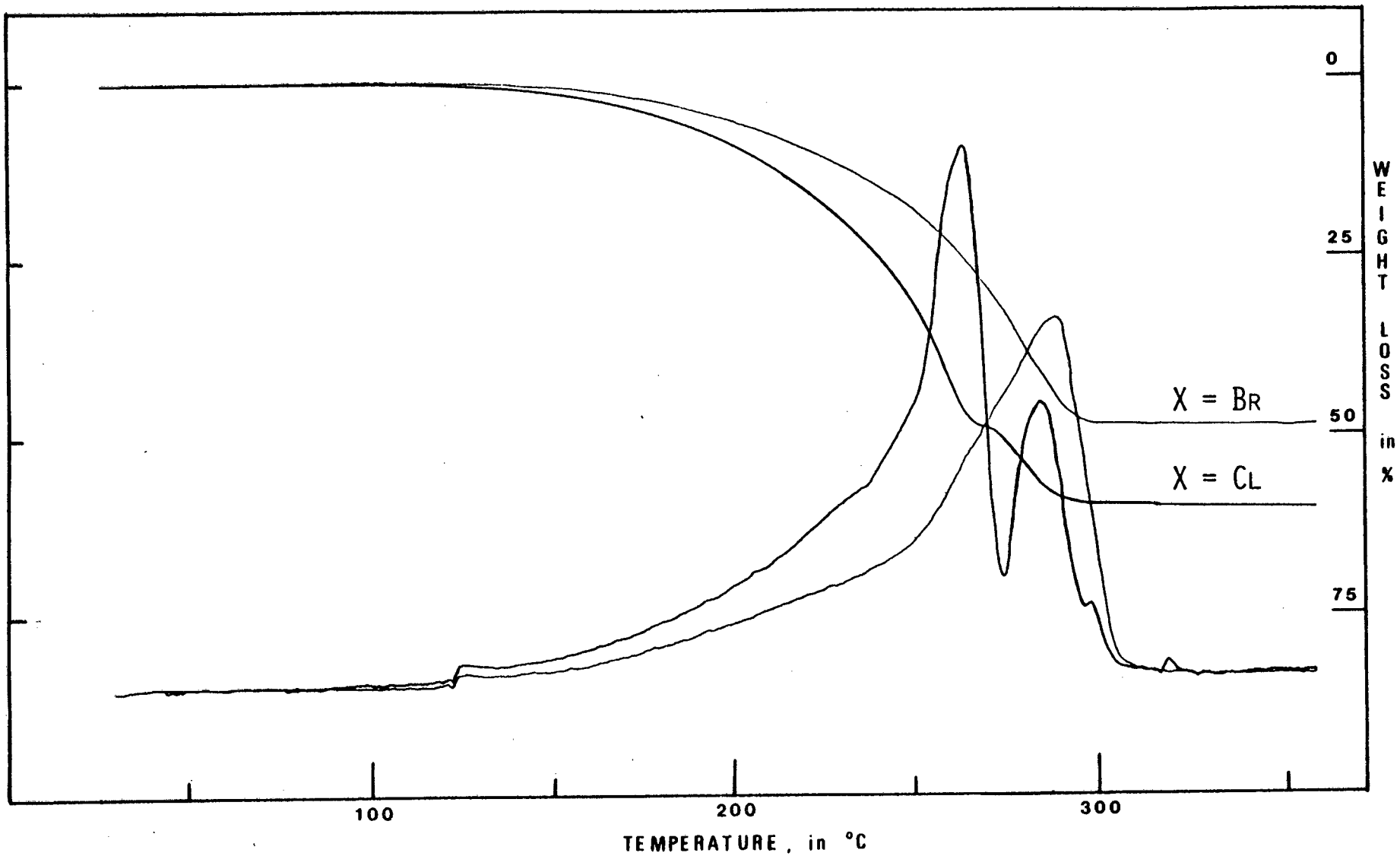

Fig. 5.12 : TG and DTG of $Co(4\text{-}C_2H_5py)_2X_2$.

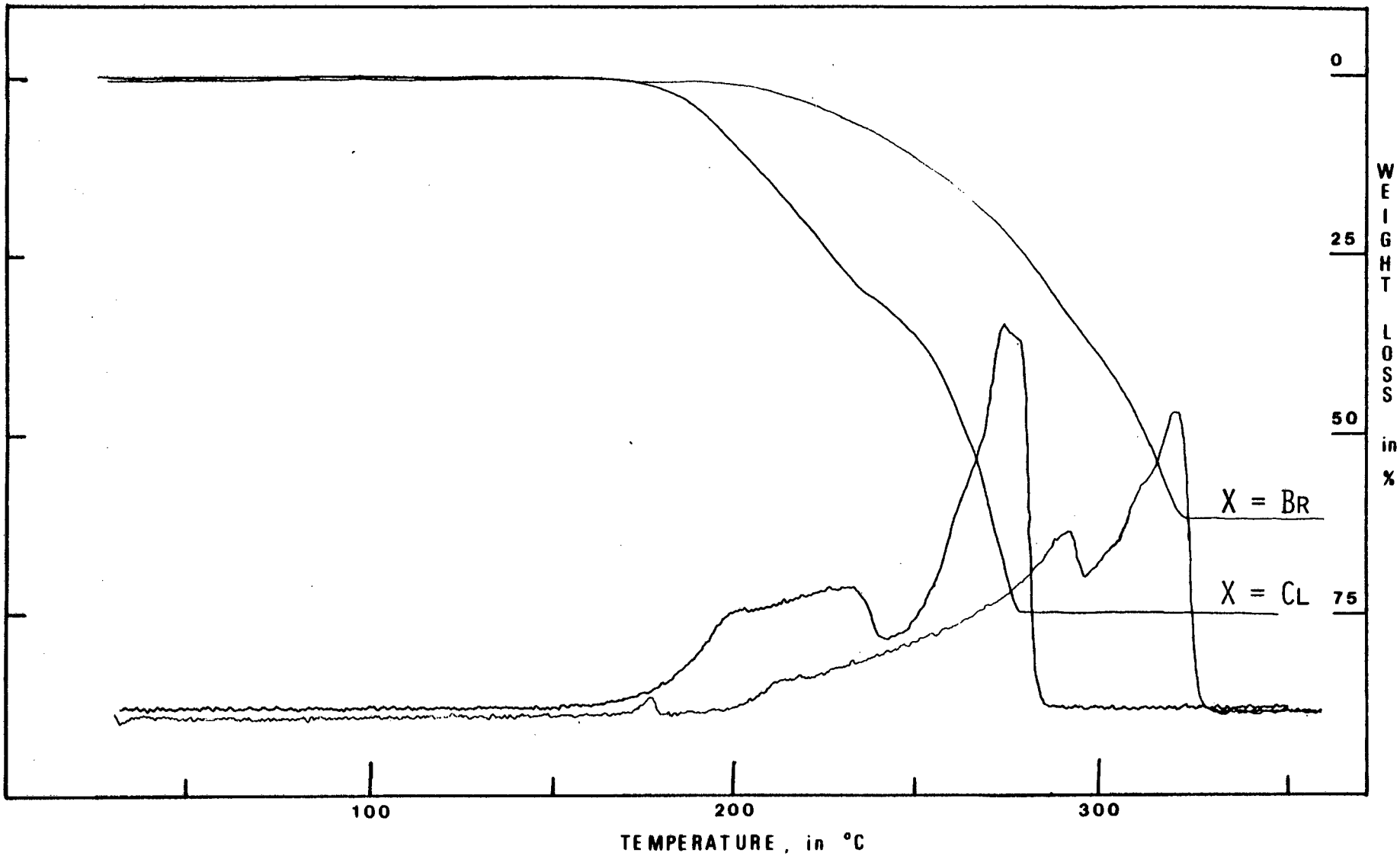

Fig. 5.13 : TG and DTG of $Co(3\text{-}C_6H_5COpy)_2X_2$.

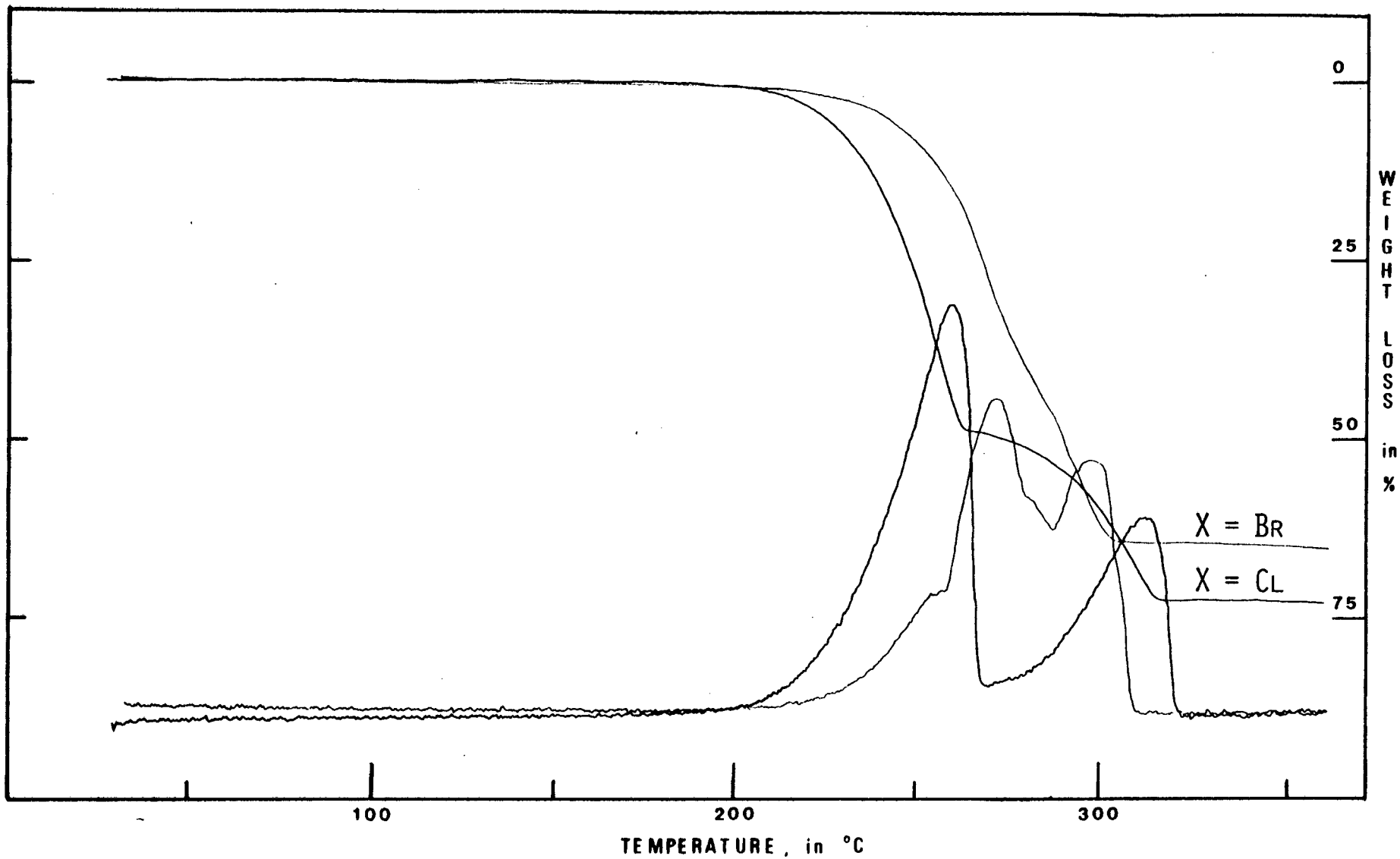

Fig. 5.14 : TG and DTG of $Co(4\text{-}C_6H_5COpy)_2X_2$.

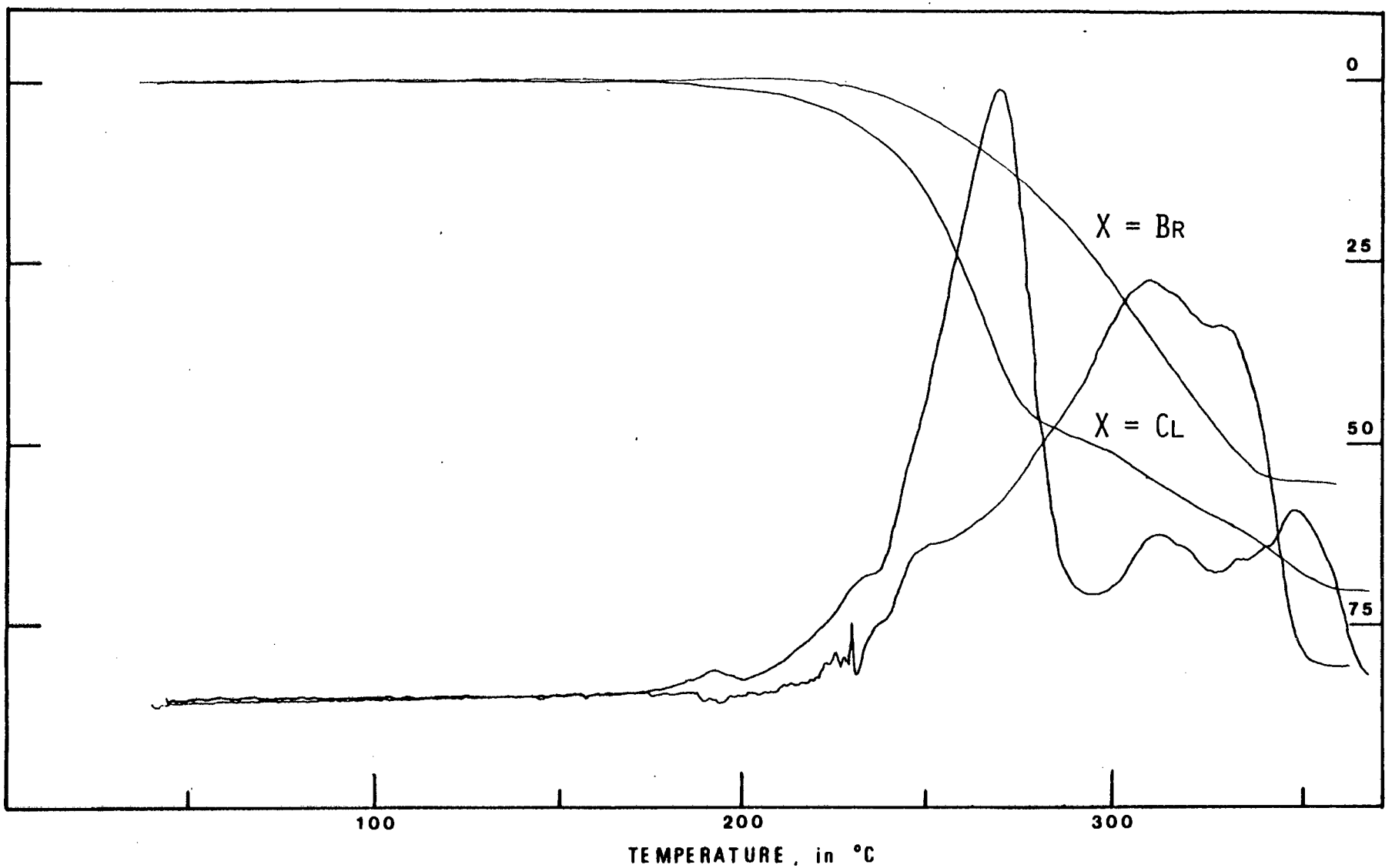

Fig. 5.15 : TG and DTG of $Co(4\text{-}C_6H_5py)_2X_2$.

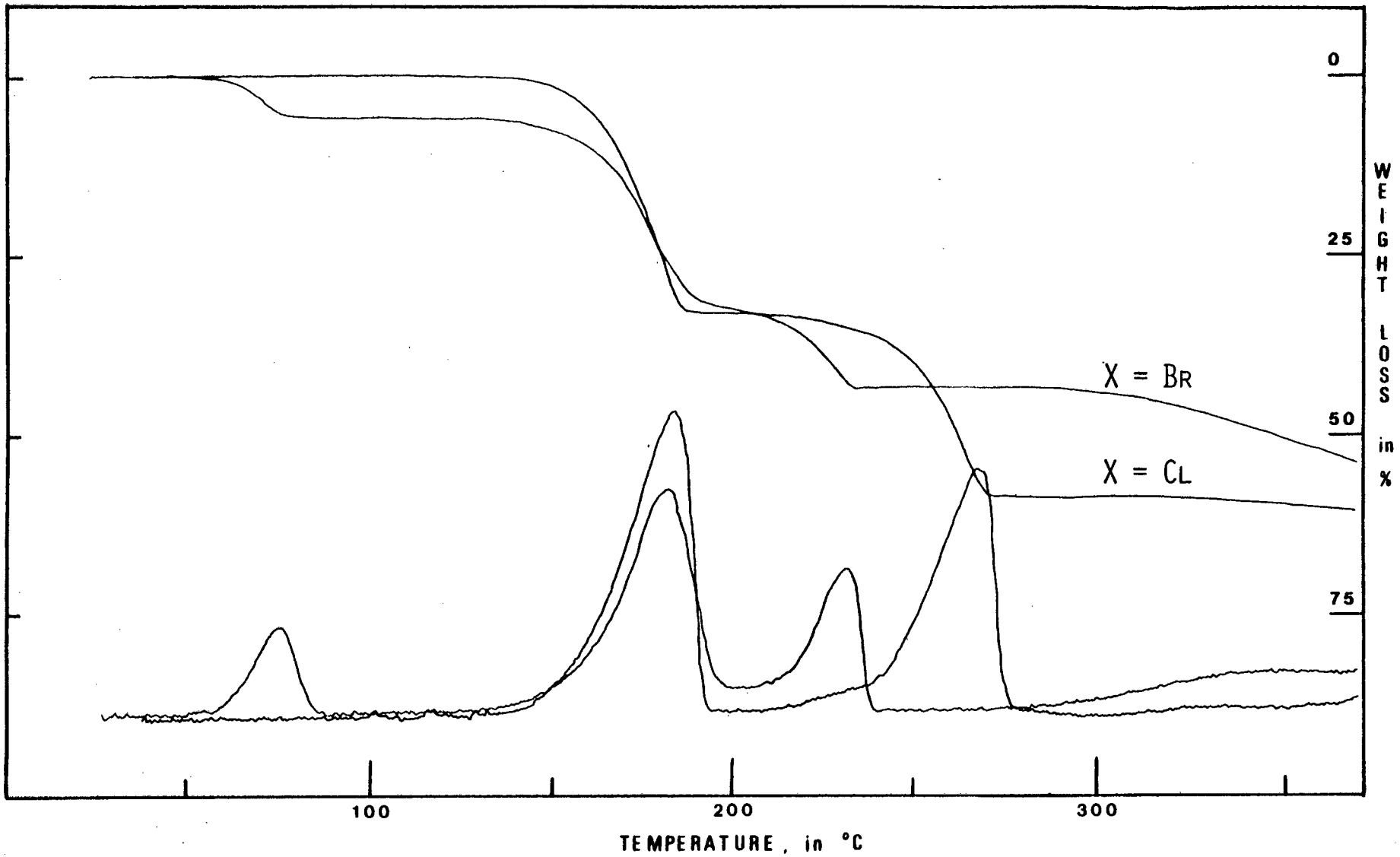

Fig. 5.16 : TG and DTG of $Co(3\text{-}CH_3OCOpy)_2X_2$.

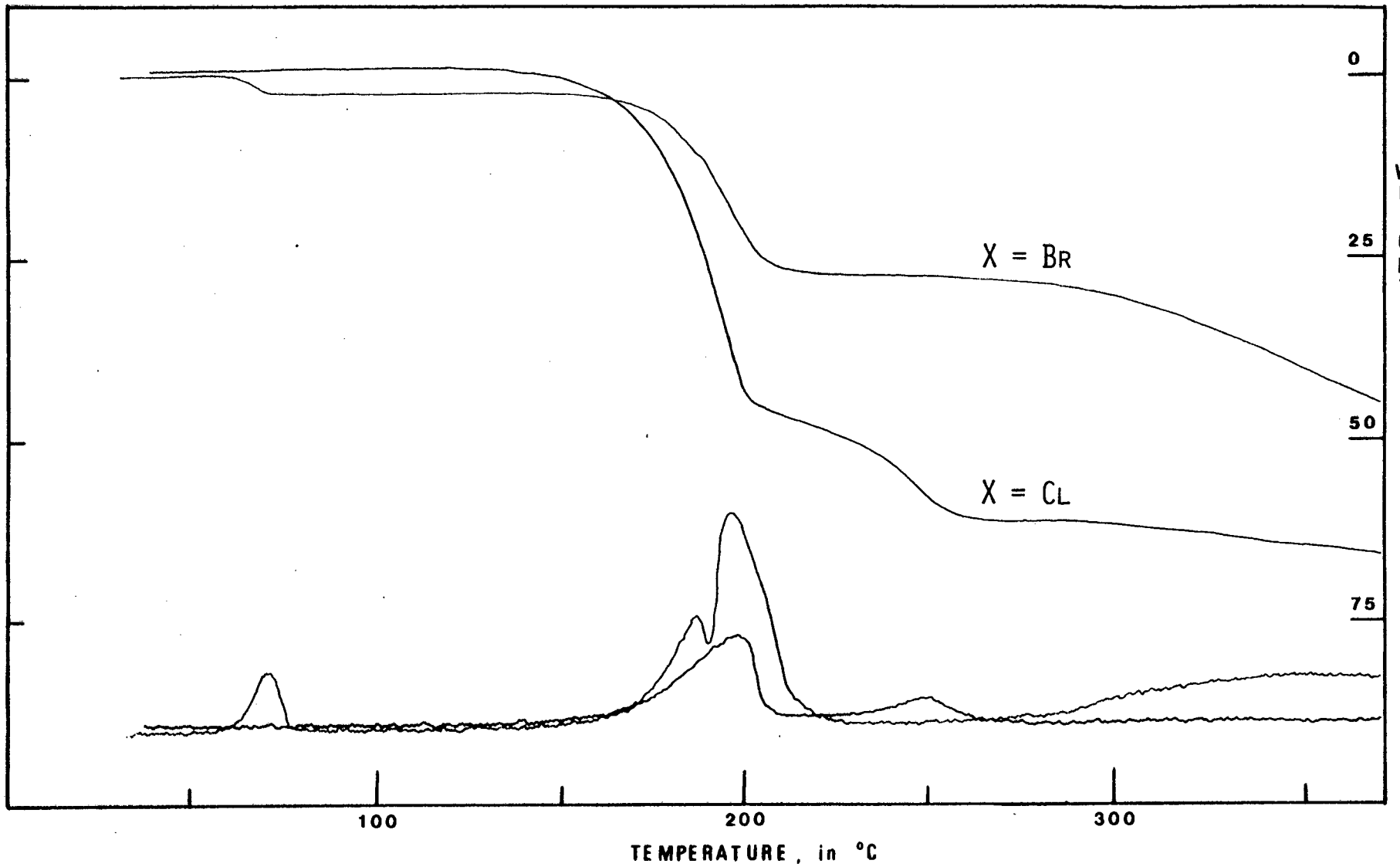

Fig. 5.17 : TG and DTG of $Co(4\text{-}CH_3OCOpy)_2X_2$.

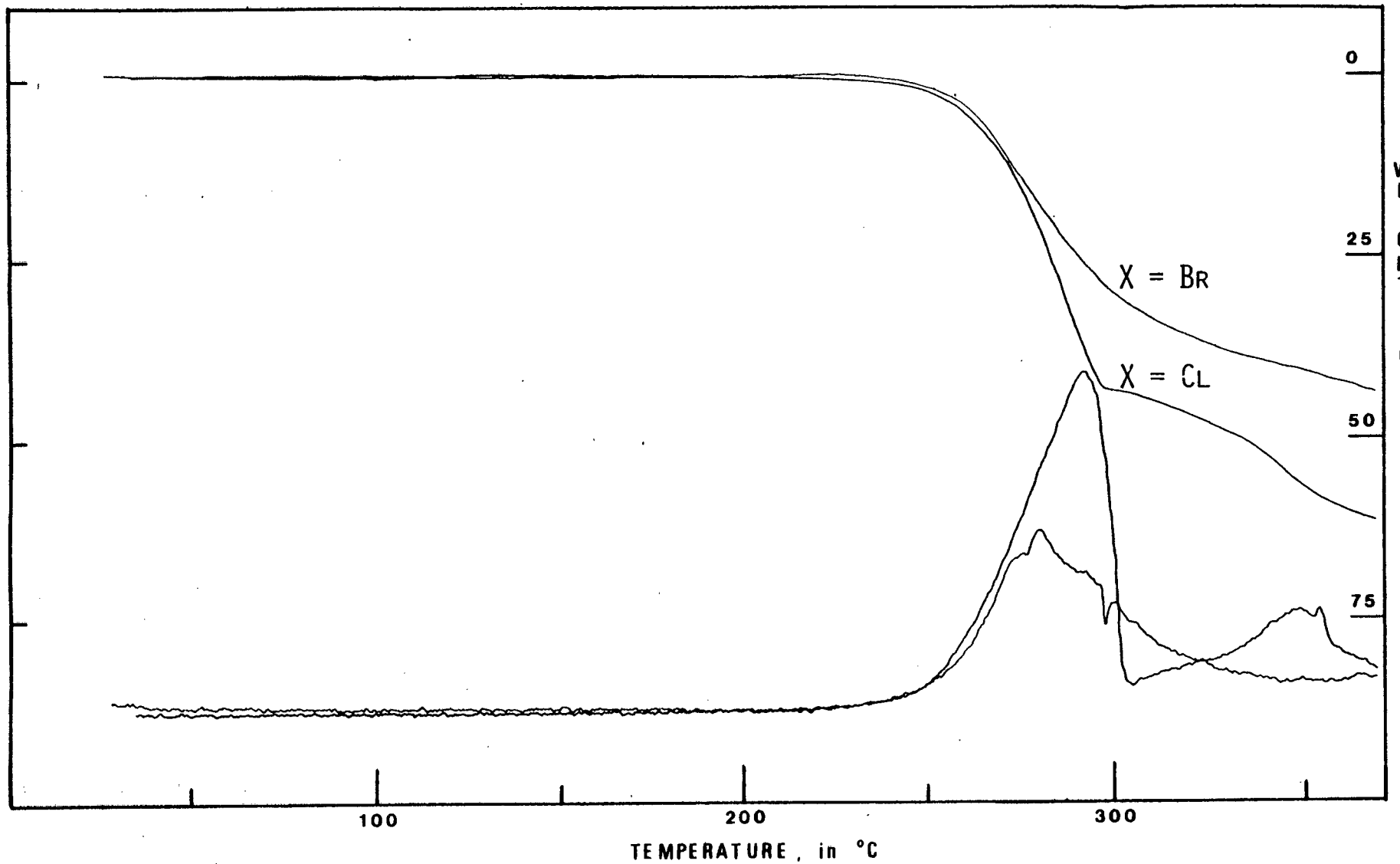

Fig. 5.18 : TG and DTG of $Co(3\text{-}H_2NCOpy)_2X_2$.

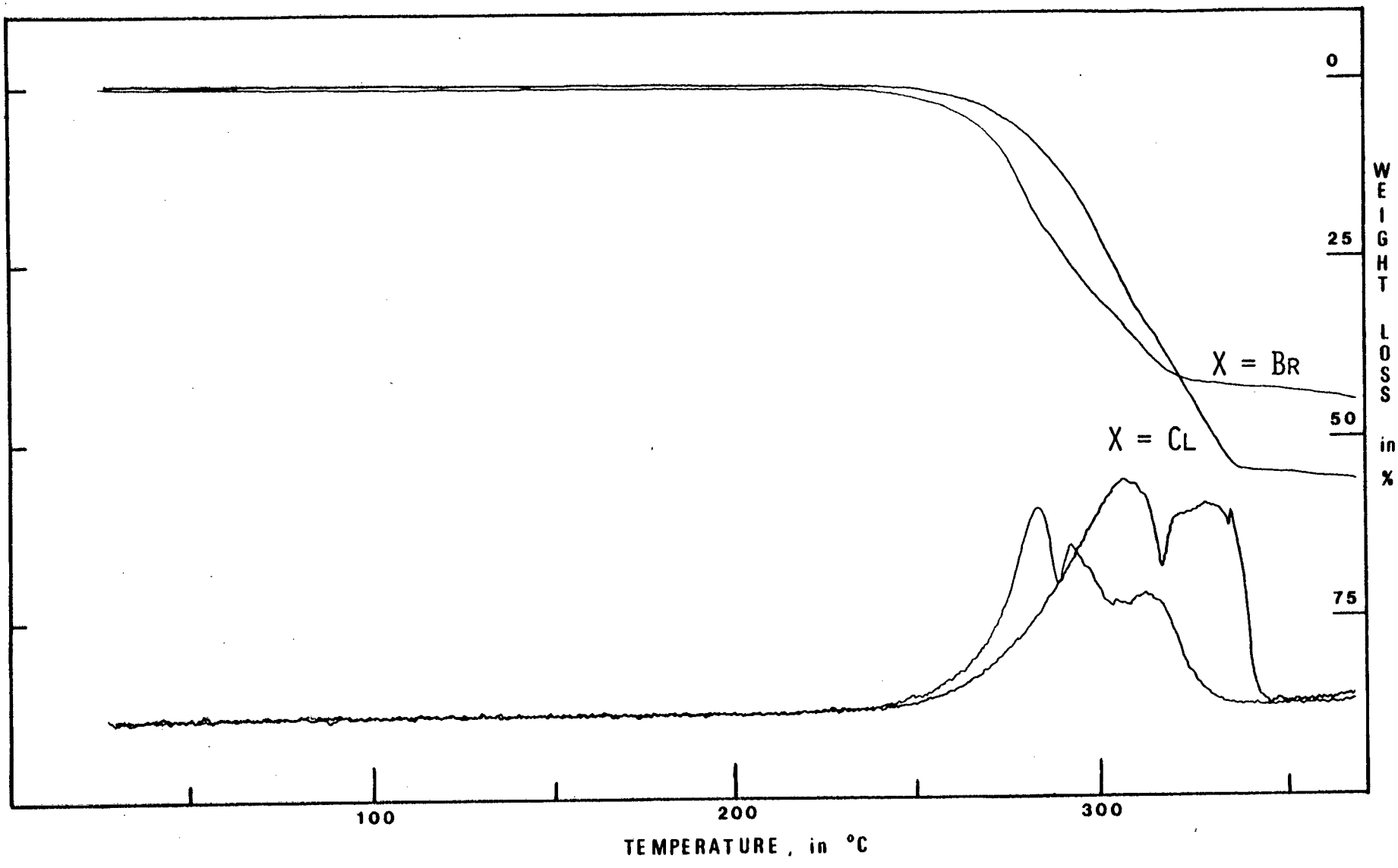

Fig. 5.19 : TG and DTG of $Co(4\text{-}H_2NCOpy)_2X_2$.

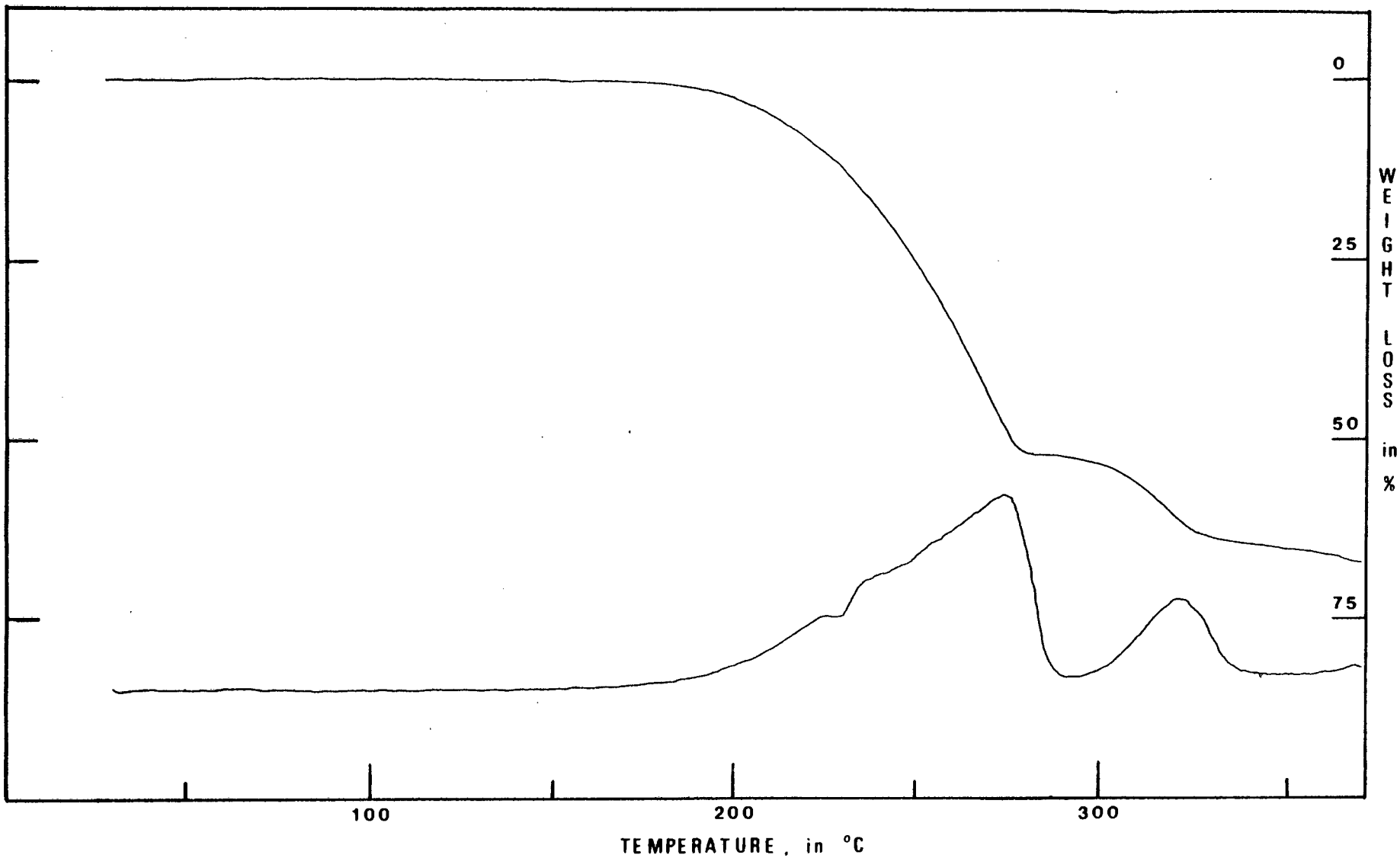

Fig. 5.20 : TG and DTG of $Co(4\text{-}(CH_3)_3Cpy)_2Cl_2$.

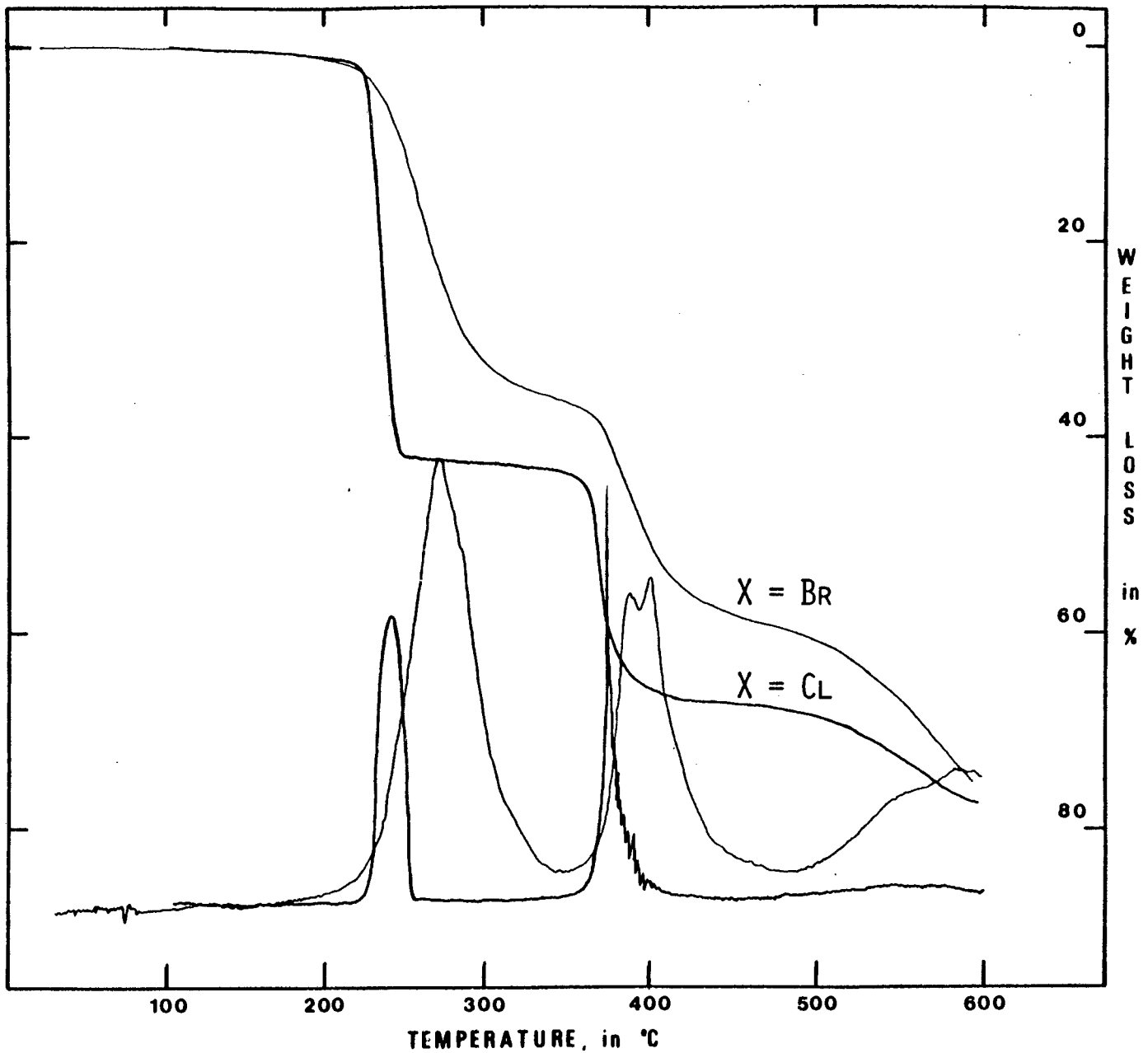

Fig. 5.21 : TG and DTG of

$Co(3\text{-}HOOCpy)_2X_2$.

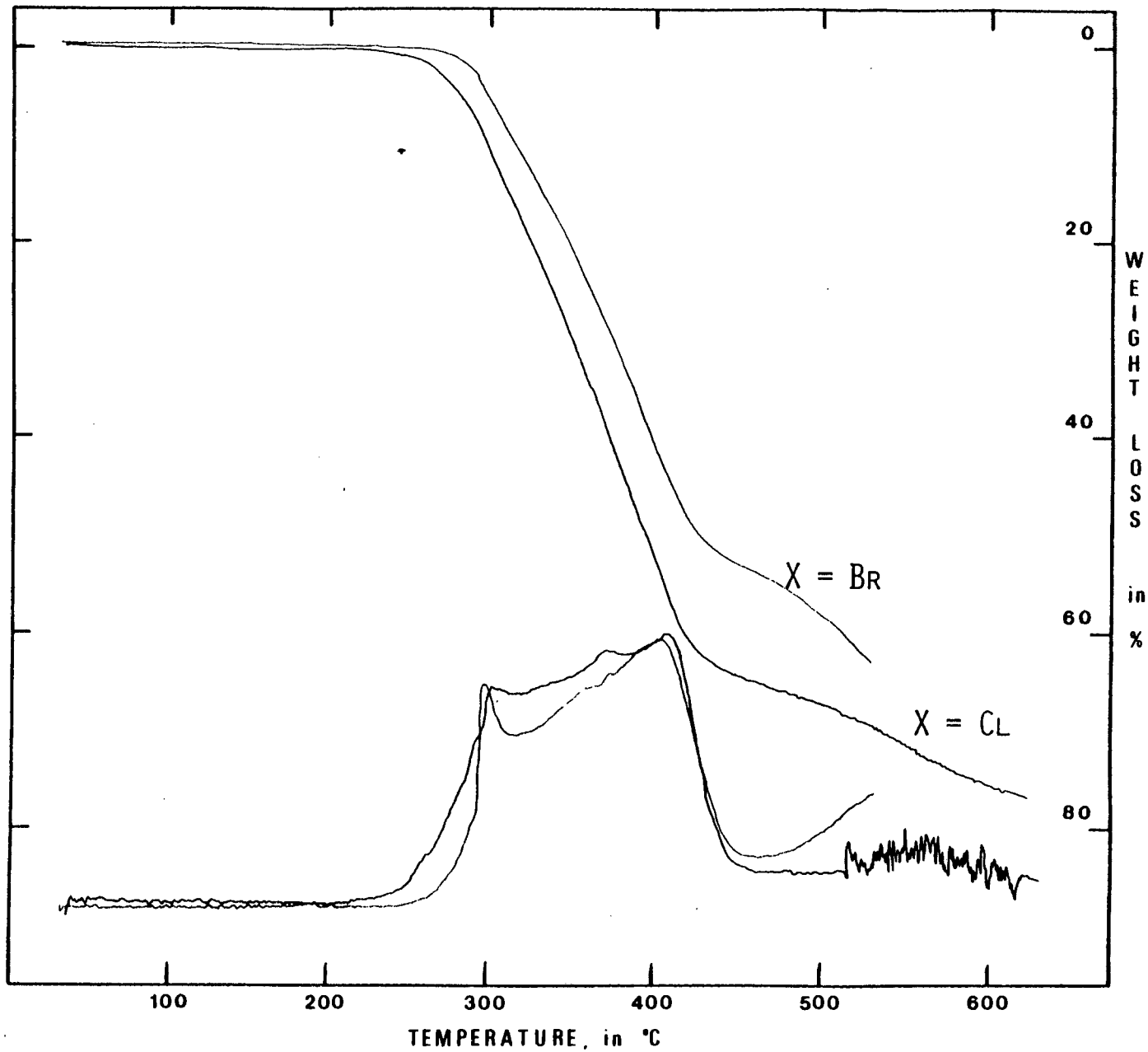

Fig. 5.22 : TG and DTG of

$Co(4\text{-}(CH_3)_2Npy)_2X_2$.

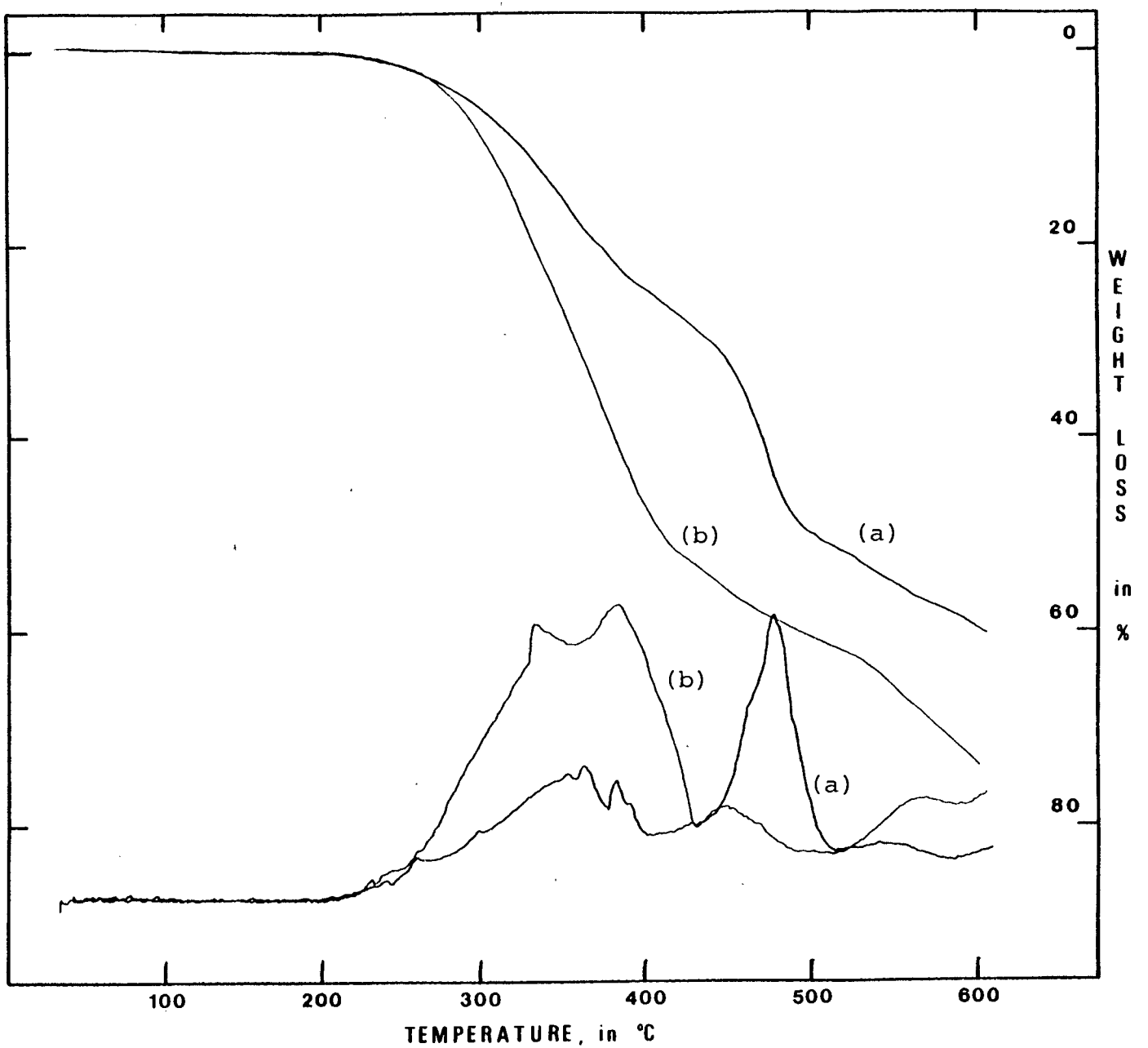

Fig. 5.23 : TG and DTG of

(a), $Co(4\text{-}HOpy)_2Cl_2$ and

(b), $Co(4\text{-}H_2Npy)_2Cl_2$.

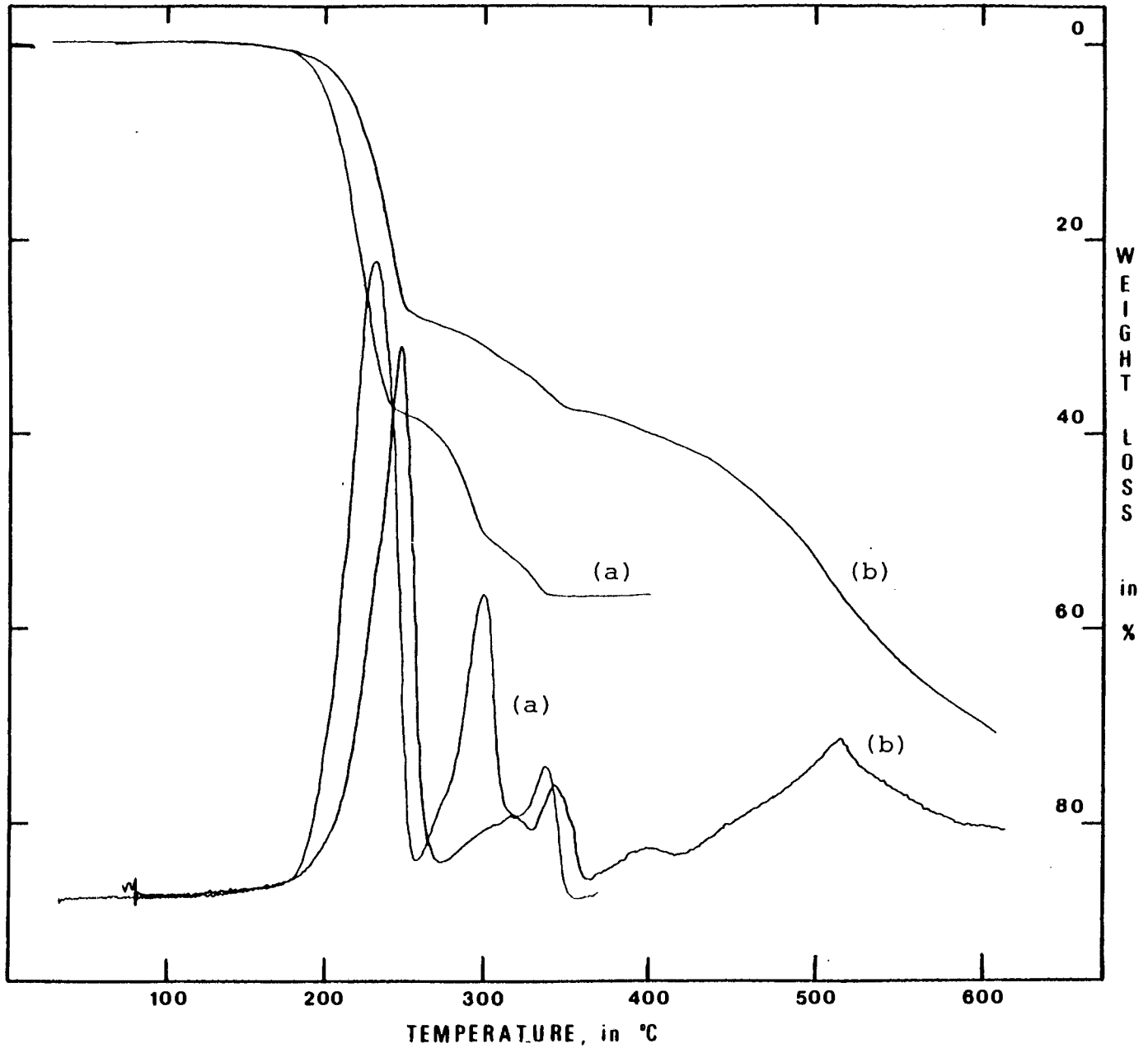

Fig. 5.24 : TG and DTG of

(a), $Co(3\text{-}CH_3COpy)_2Cl_2$ and

(b), $Co(4\text{-}CH_3COpy)_2Cl_2$.

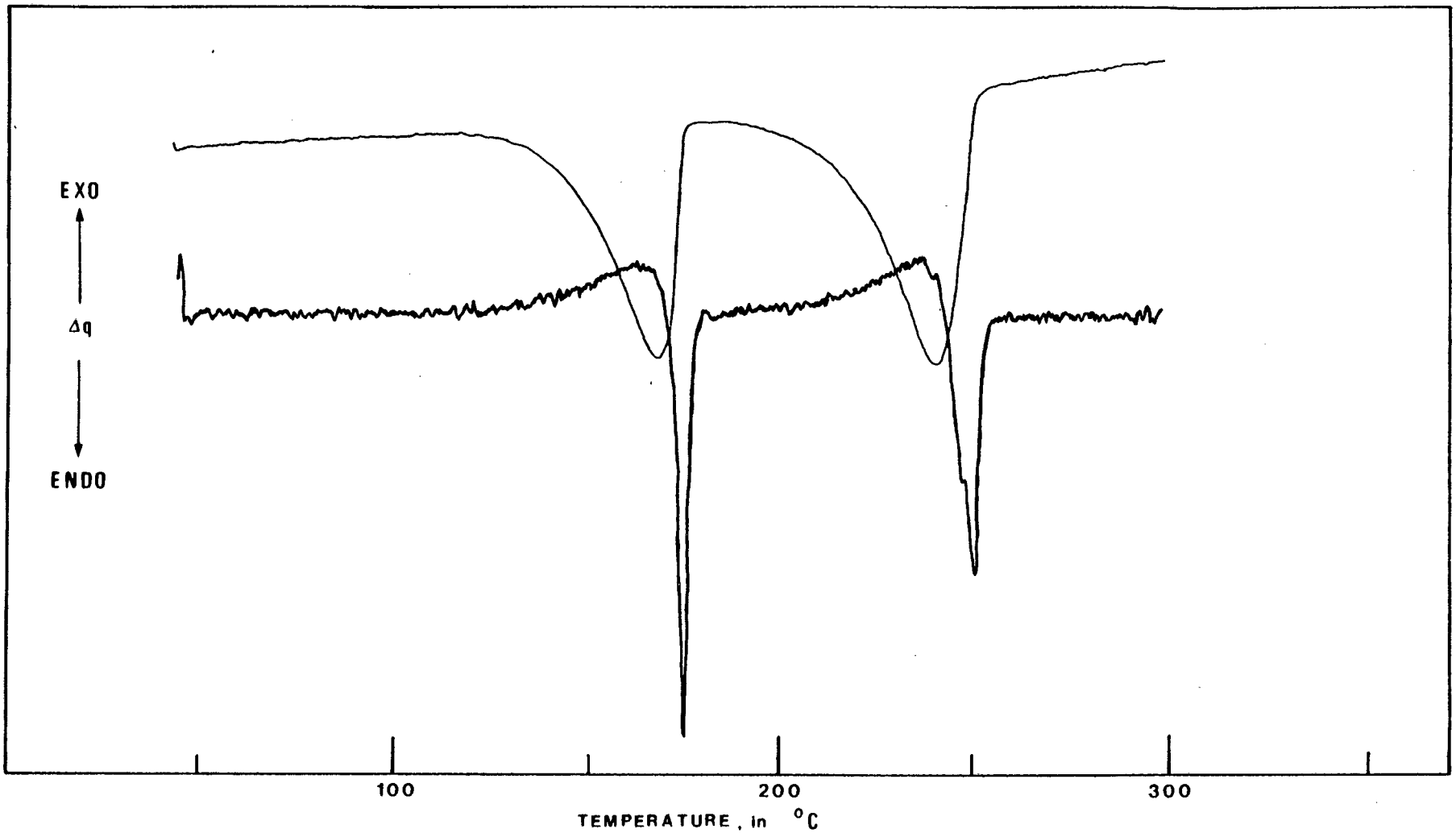

Fig. 5.25 : DSC and DTA (thicker curve) of $Co(3\text{-}Clpy)_2Cl_2$.

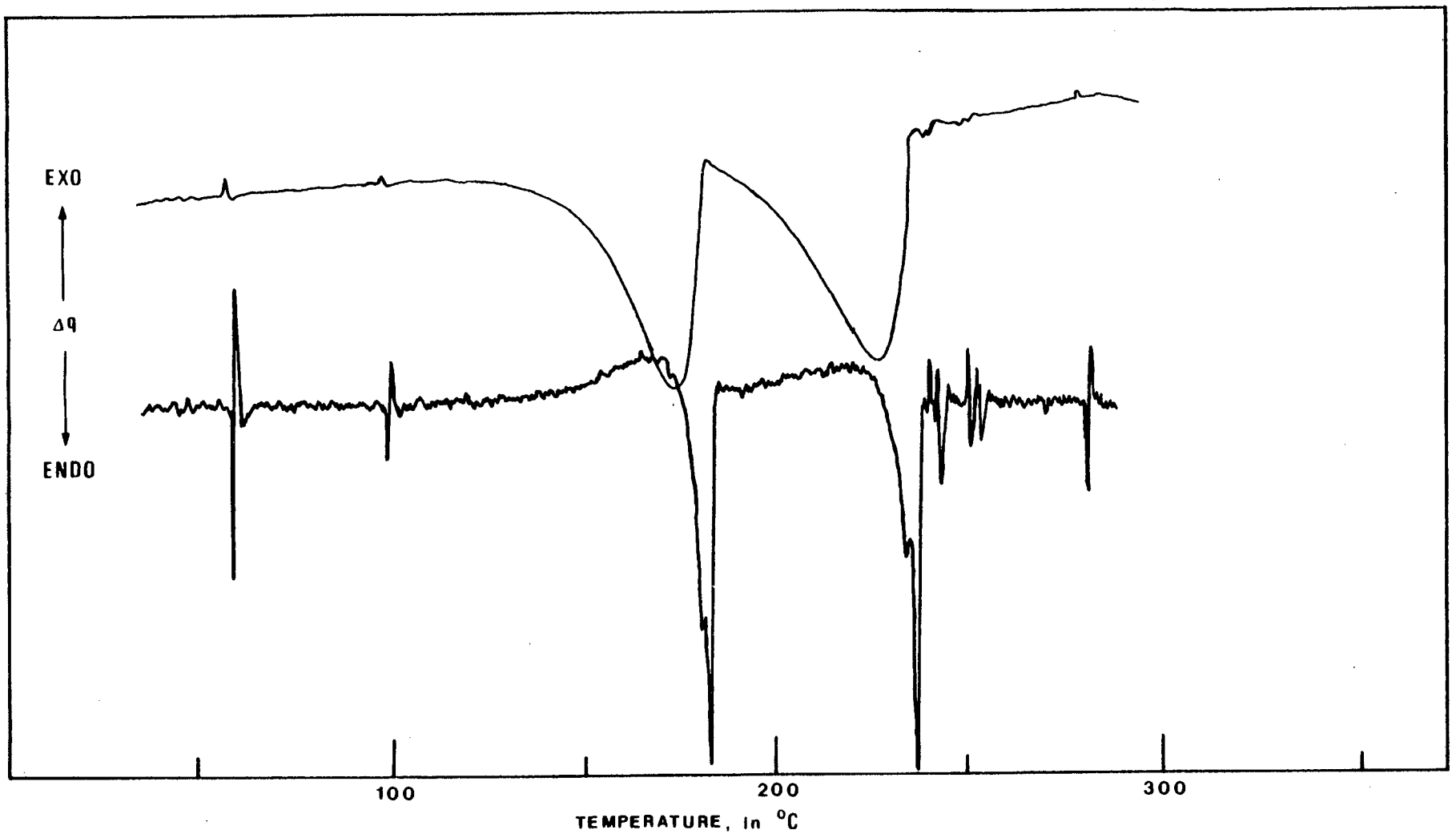

Fig. 5.26 : DSC and DTA (thicker curve) of $Co(3\text{-}Clpy)_2Br_2$.

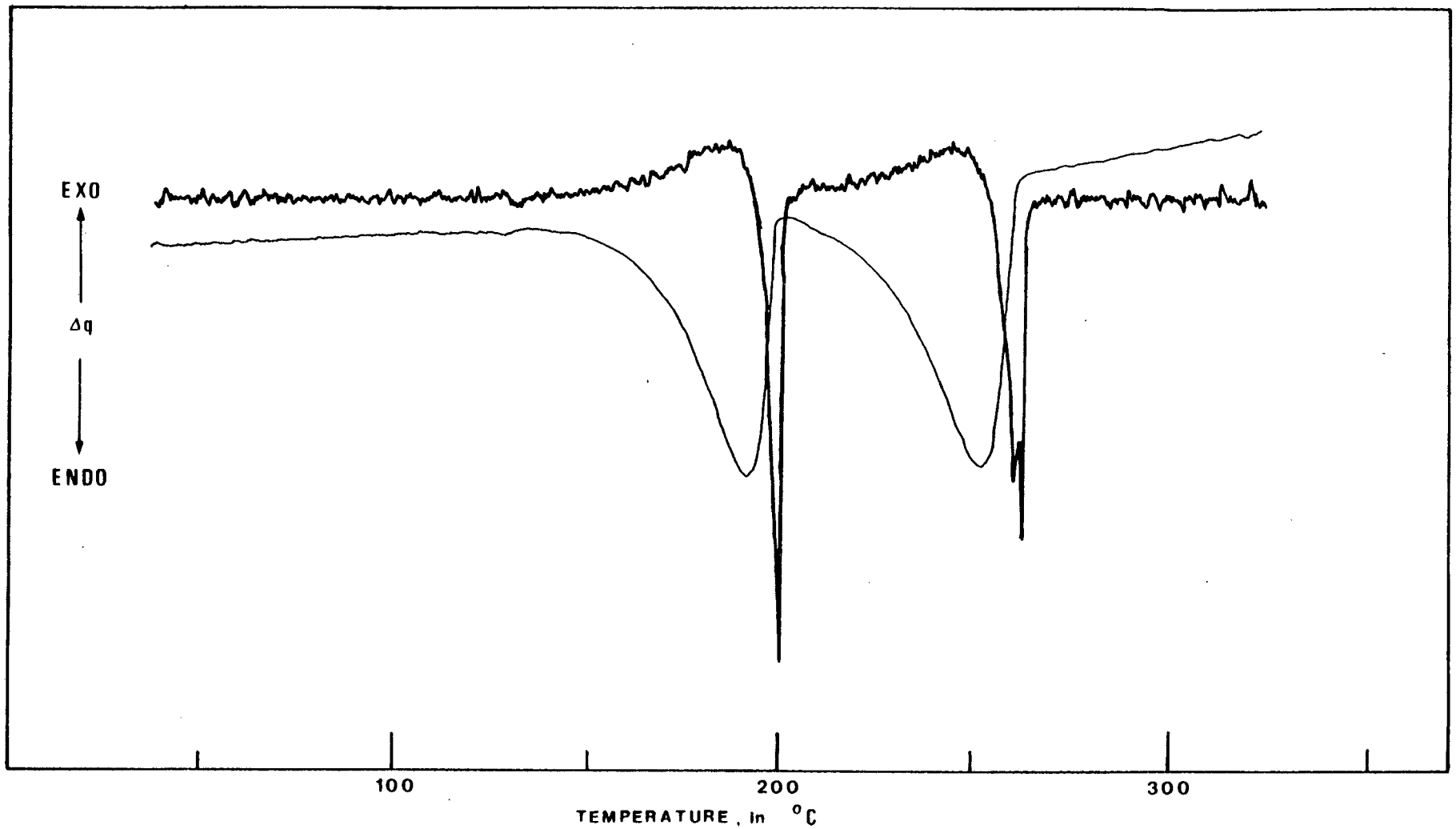

Fig. 5.27 : DSC and DTA (thicker curve) of $Co(3\text{-}Brpy)_2Cl_2$.

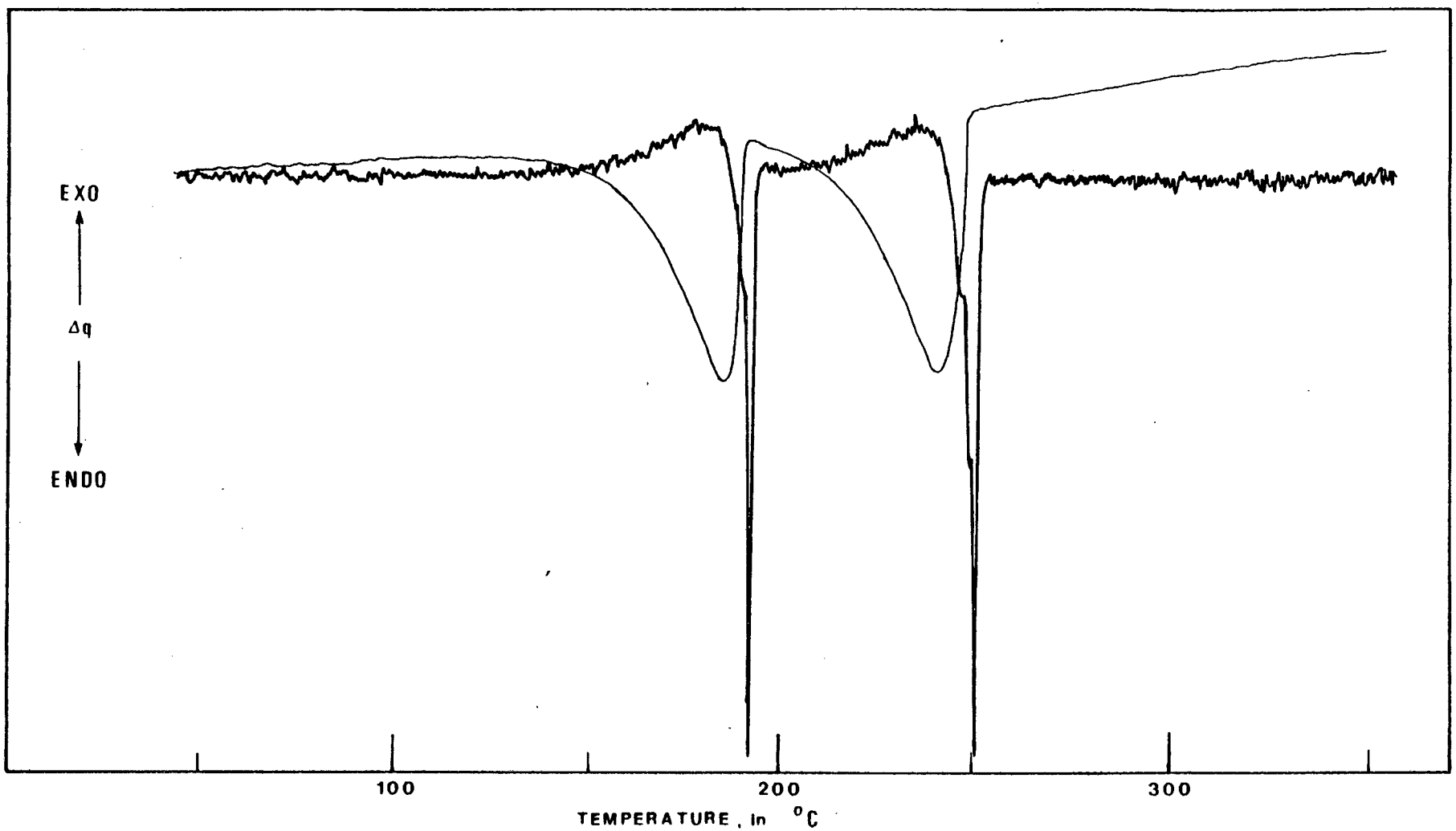

Fig. 5.28 : DSC and DTA (thicker curve) of $Co(3\text{-}Brpy)_2Br_2$.

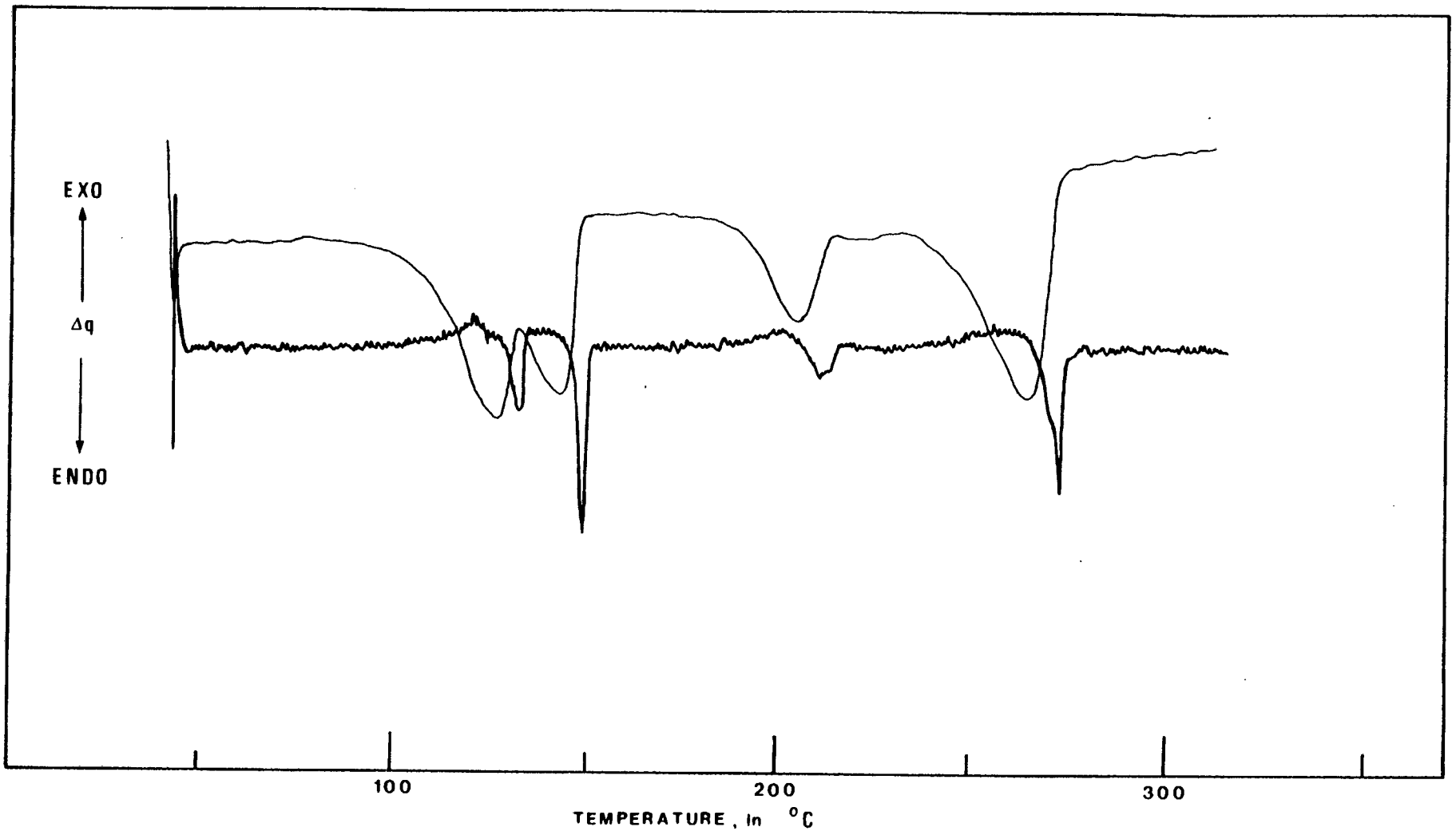

Fig. 5.29 : DSC and DTA (thicker curve) of $Co(py)_2Cl_2$.

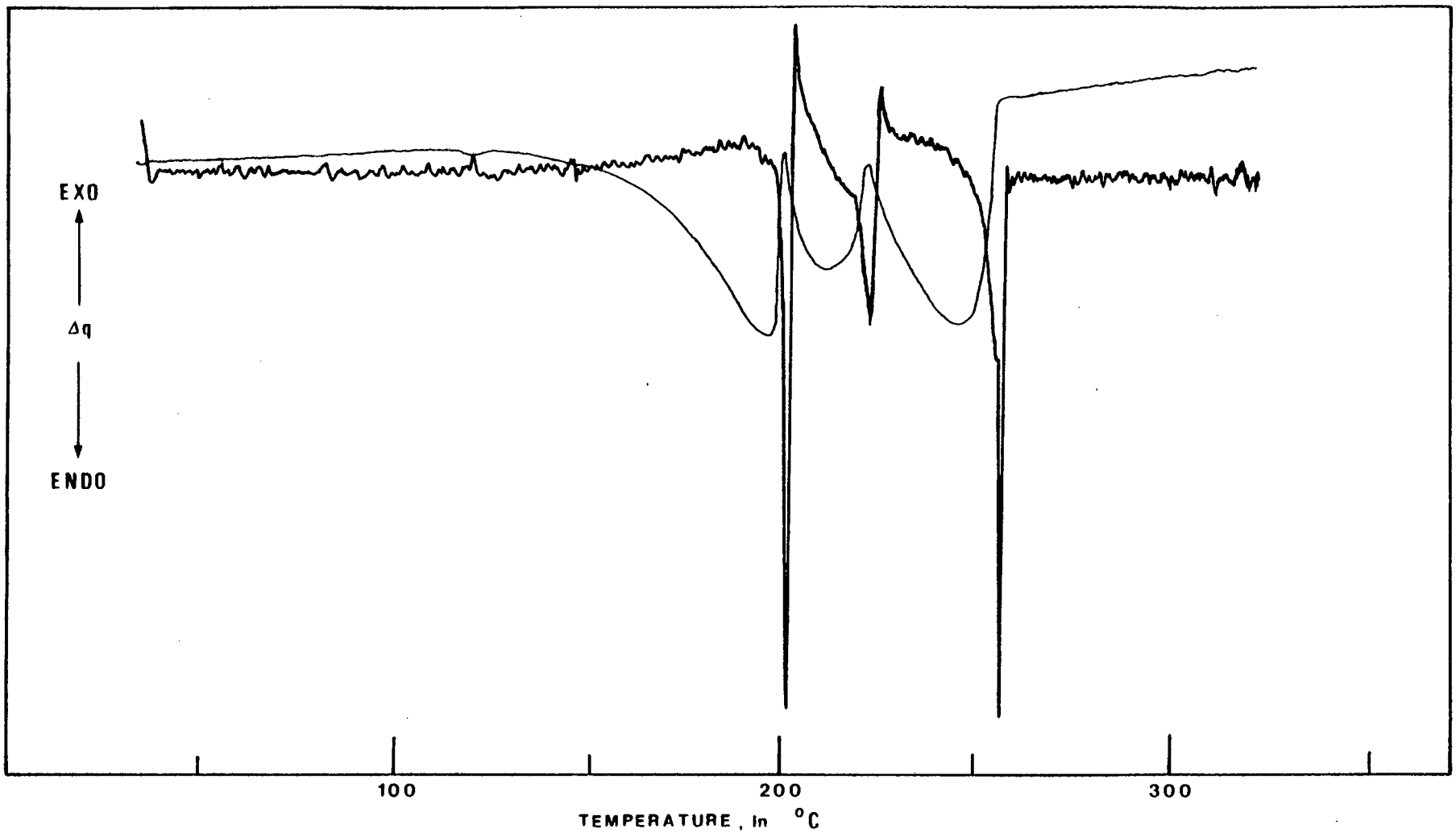

Fig. 5.30 : DSC and DTA (thicker curve) of $Co(py)_2Br_2$.

5.4 DIFFERENTIAL SCANNING CALORIMETRY

Calorimetric measurements were made at a programming rate of $5^{o}C$/min ensuring that the sample and reference platforms equilibrate and the heating rate stabilizes. The DSC cell was continuously purged with dry nitrogen at 20 ml/min and constant 5 mg of samples are placed in open aluminium pans. The enthalpies of the stepwise decomposition reactions of some complexes are reported in Table 5.2. The total enthalpy value, ΔH_t, corresponds to the overall decomposition reaction (3). The uncertainties which are mainly determined by the measurements of areas, are expressed as standard deviations of the mean. The DSC together with the DTA curves are represented in Figs. 5.25 to 5.30.

TABLE 5.2

DSC data for some substituted pyridine complexes of cobalt(II) halides.

complex	reaction	ΔH ($kJmol^{-1}$)
$Co(3\text{-}Clpy)_2Cl_2$	(1)	77.5 ± 0.1
	(2)	98.9 ± 0.2
	total	176.4 ± 0.2
$Co(3\text{-}Clpy)_2Br_2$	(1)	86.7 ± 0.3
	(2)	100.6 ± 0.4
	total	187.3 ± 0.5
$Co(3\text{-}Brpy)_2Cl_2$	(1)	86.8 ± 0.4
	(2)	110.3 ± 0.1
	total	197.1 ± 0.6

TABLE 5.2 continued/

complex	reaction	ΔH ($kJmol^{-1}$)
$Co(3\text{-}Brpy)_2Br_2$	(1)	89.0 ± 0.3
	(2)	108.3 ± 0.1
	total	197.3 ± 0.3
$Co(py)_2Cl_2$	(1)	74.4 ± 0.2
	(2)	100.5 ± 0.2
	total	174.9 ± 0.3
$Co(py)_2Br_2$	total	182.9 ± 0.4

5.5 DISCUSSION

The transition between the two forms : the violet and the blue forms, of $[Co(py)_2Cl_2]$ has been studied previously by differential thermal analysis. The transition which represents the octahedral-to-tetrahedral configurational change, corresponds to the endothermic peak observed by WENDLANDT[13] at 112°C. The enthalpy of this transition was found to be 13.4 ± 0.4 kJ mol^{-1}. However, this value can only be considered accurately if calorimetric measurements were done on sealed sample tubes since as our thermogram, Fig. 5.8, shows that decomposition of $[Co(py)_2Cl_2]$ starts at 110°C.

The infrared and far-infrared spectra of the various decomposition products of $[Co(py)_2Cl_2]$ are shown in Fig. 5.31 and Fig. 5.32, respectively. The spectra together with the magnetic data for the compounds given in Table 5.3, agree with the suggestion by ALLAN *et al.*[3] of an octahedral arrangement of ligands around the cobalt atom.

TABLE 5.3

compound	magnetic moment[14]	geometry
A $[Co(py)_2Cl_2]$	5.08	octahedral
C $[Co(py)Cl_2]$	5.46	octahedral
D $[Co(py)_{2/3}Cl_2]$	5.39	octahedral

The double chain structure of $CoLX_2$ type complexes is given in Fig. 5.33. Similarly, a triple chain structure can be built up by further removing pyridines which result in a polymer of stoichiometry $CoL_{2/3}X_2$. The spectrum (Fig. 5.32) of the unstable intermediate $[Co(py)_{5/3}Cl_2]$ (B), shows terminal Co-Cl bands which indicate the presence of some tetrahedral monomers. This corresponds to the above-mentioned configurational change in the solid state. It is interesting to note that by successive loss of pyridine ligands, the remaining Co-N bond becomes stronger, as reflected by the shift of νCo-N towards higher frequency. This is accompanied with no change in coordination number.

5.5.1 Thermogravimetric Results

For convenience sake, we have classified the various complexes together with their stereochemistry around the cobalt atom into groups depending on their decomposition temperature, T, as listed in Table 5.4.

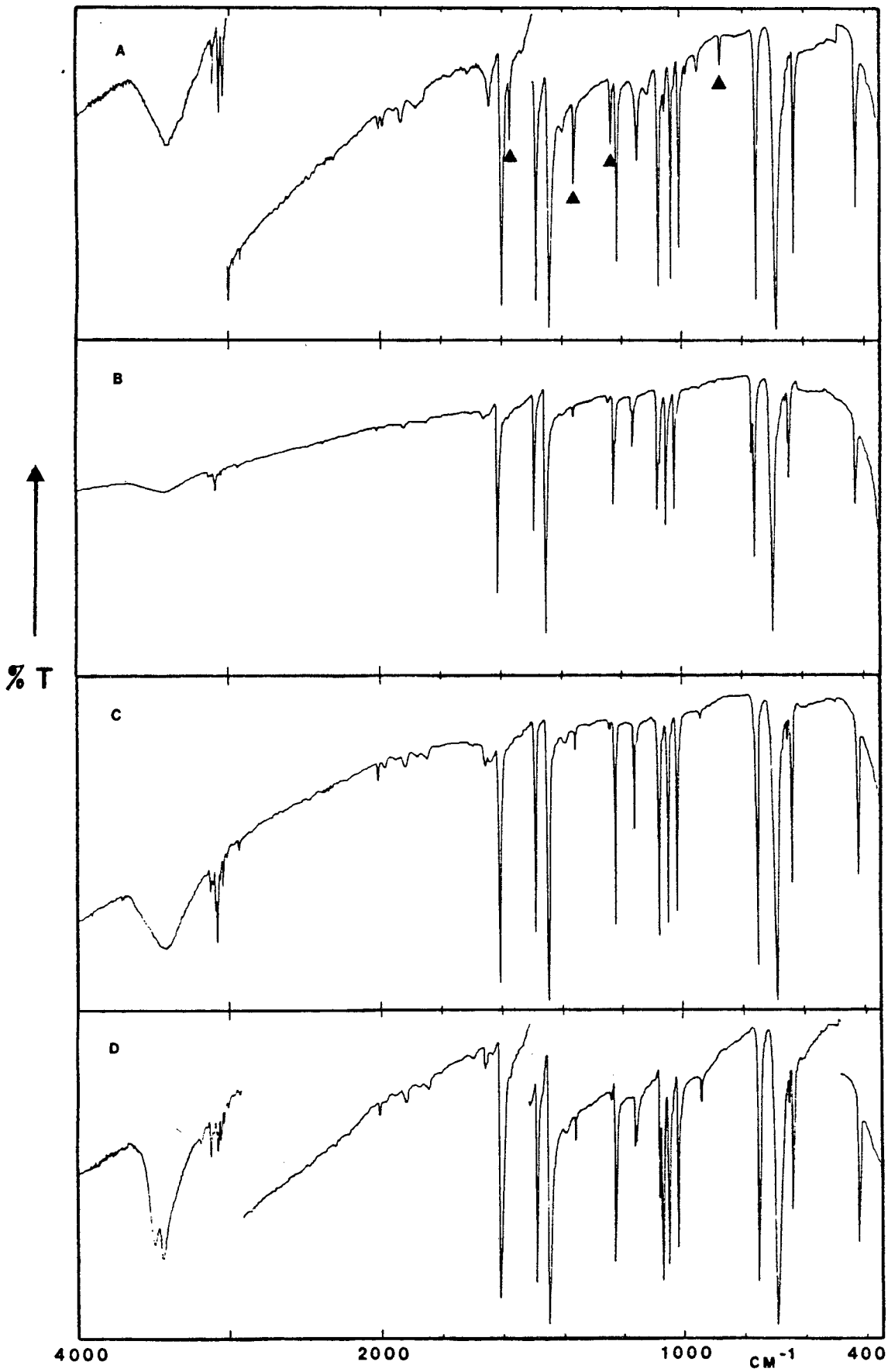

Fig. 5.31 : The infrared spectra of the decomposition products of $[Co(py)_2Cl_2]$ in N_2 atmosphere; (A) $Co(py)_2Cl_2$, (B) $Co(py)_{5/3}Cl_2$, (C) $Co(py)_1Cl_2$, (D) $Co(py)_{2/3}Cl_2$.
▲ indicates disappearing bands.

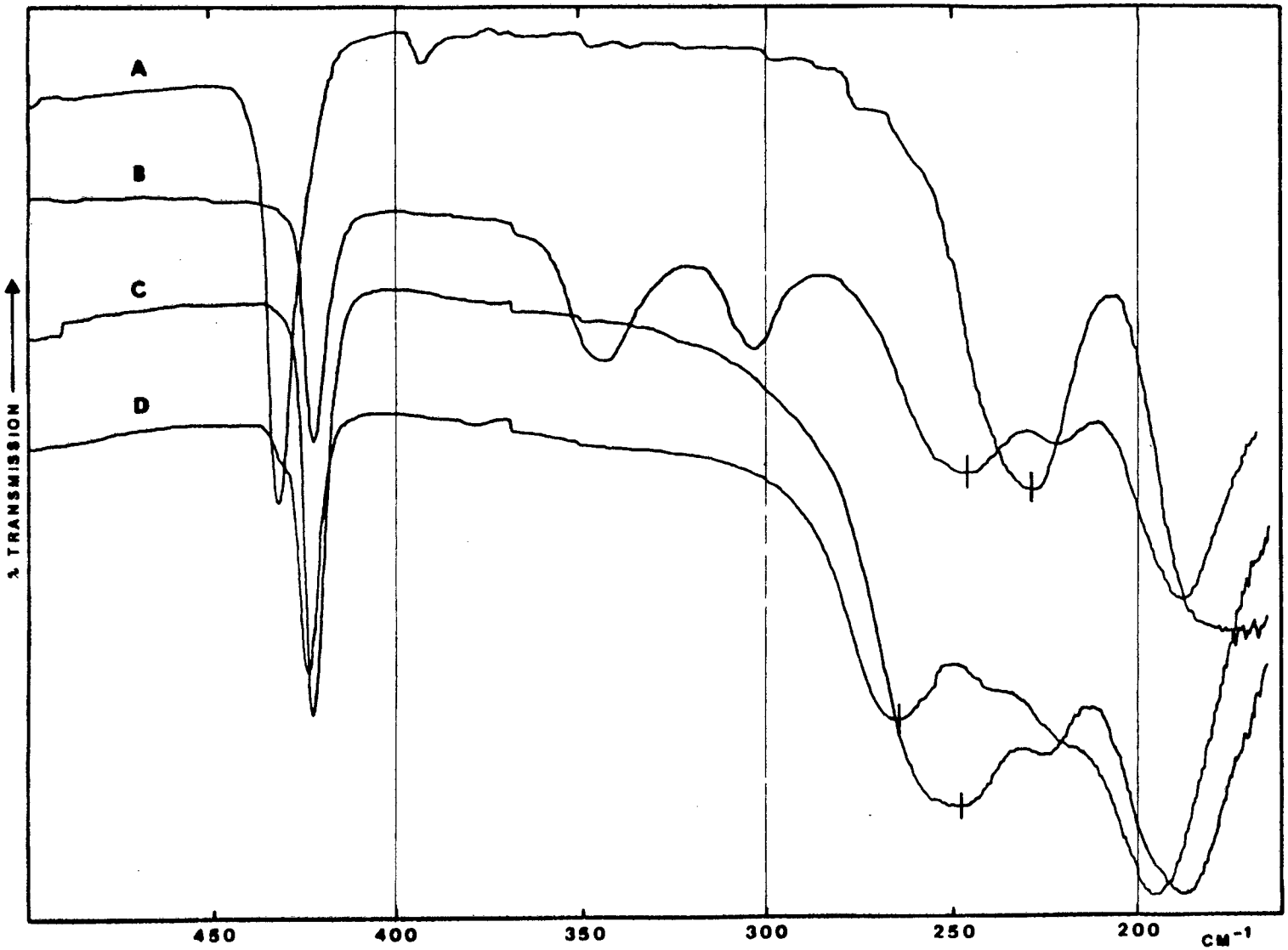

Fig. 5.32 : The far-infrared spectra of the decomposition products of $[Co(py)_2Cl_2]$ in N_2 atmosphere; (A) $Co(py)_2Cl_2$, (B) $Co(py)_{5/3}Cl_2$, (C) $Co(py)_1Cl_2$, (D) $Co(py)_{2/3}Cl_2$. The shift towards higher frequency of the νCo-N is clearly observed.

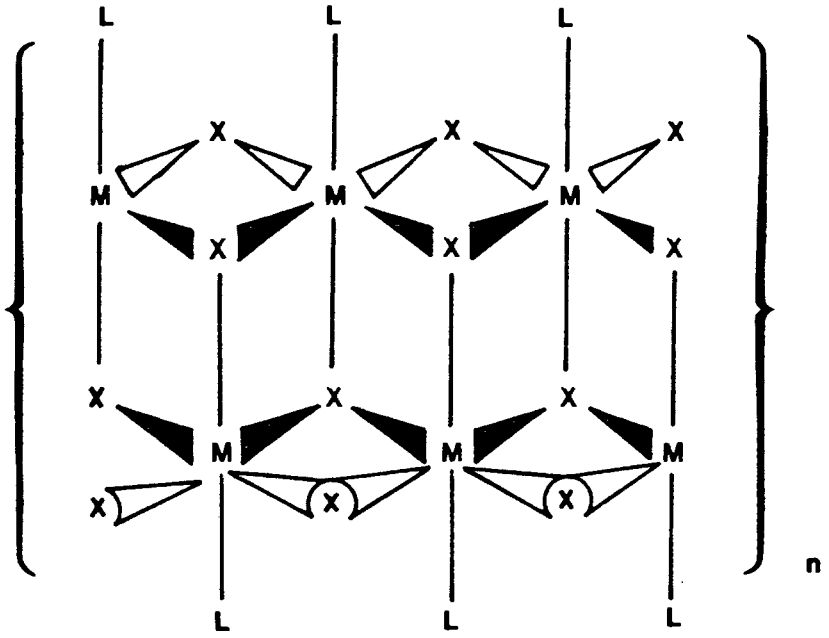

Fig. 5.33 : The chain-structure of the decomposition products of the MLX_2 type.

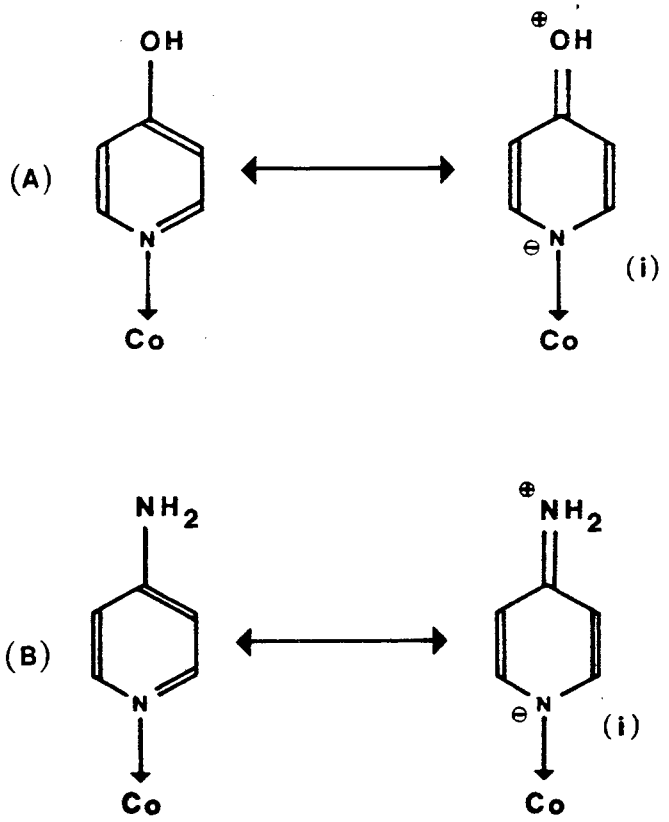

Fig. 5.34 : Resonance forms of $Co(4\text{-}HOpy)_2Cl_2$, (A) and $Co(4\text{-}H_2Npy)_2Cl_2$, (B).

TABLE 5.4

group	compound	(geometry)
(A) with T > 250°C		
	$Co(4\text{-}H_2Npy)_2Cl_2$, $Co(4\text{-}HOpy)_2Cl_2$, $Co(4\text{-}(CH_3)_2Npy)_2X_2$	(tet)
	$Co(3\text{-}H_2NCOpy)_2X_2$, $Co(4\text{-}H_2NCOpy)_2X_2$	(oct)
(B) 200 < T < 250°C		
	$Co(4\text{-}C_2H_5py)_2Br_2$, $Co(3\text{-}CH_3py)_2Br_2$, $Co(4\text{-}CH_3py)_2Br_2$	(tet)
	$Co(3,4\text{-di-}CH_3py)_2Br_2$, $Co(4\text{-}C_6H_5COpy)_2X_2$,	"
	$Co(4\text{-}(CH_3)_3Cpy)_2Cl_2$, $Co(4\text{-}C_6H_5py)_2Br_2$	"
	$Co(4\text{-}CH_3COpy)_2Cl_2$, $Co(4\text{-}C_6H_5py)_2Cl_2$, $Co(3\text{-}HOOCpy)_2X_2$,	(oct)
	$Co(3\text{-}C_6H_5COpy)_2Br_2$	"
(C) 175 < T < 200°C		
	$Co(3,4\text{-di-}CH_3py)_2Cl_2$	(tet)
	$Co(3\text{-}C_6H_5COpy)_2Cl_2$, $Co(3\text{-}CH_3COpy)_2Cl_2$	(oct)
(D) T < 175°C		
	$Co(py)_2Br_2$, $Co(3\text{-}CH_3py)_2Cl_2$, $Co(4\text{-}CH_3py)_2Cl_2$	(tet)
	$Co(py)_2Cl_2$, $Co(3\text{-}Clpy)_2X_2$, $Co(3\text{-}Brpy)_2X_2$, $Co(4\text{-}NCpy)_2X_2$,	(oct)
	$Co(3\text{-}CH_3OCO(py)_2X_2$, $Co(4\text{-}CH_3OCOpy)_2X_2$	"

where X = Cl and Br

It is apparent from the thermograms or Table 5.4 that the decomposition of the chloro-complexes starts at a lower temperature than the corresponding bromo-analogues. Only two exceptions to this empirical rule are observed in $[Co(4\text{-}H_2NCOpy)_2Cl_2]$ and $[Co(4\text{-}NCpy)_2Cl_2]$. A possible explanation for the greater thermal stability of the CoL_2Br_2 complexes lies in the more readily polarizable bromine atom which allows total Co-N bond strengthening

by encouraging any back-bonding from the cobalt to the nitrogen in pyridine. This is supported by our calorimetric measurements. We may note that this greater total bond strength for the bromo-complexes becomes more pronounced in systems where π-bonding effects are expected to contribute, as for instance in zinc complexes. WONG[15] performed an analysis of the force constants of $[Zn(py)_2Cl_2]$ and $[Zn(py)_2Br_2]$ where he showed indeed that the Zn-N bond in the bromo-complex is stronger than in the chloro-complex.

The temperatures of the group (A) compounds, together with the anomalies in the infrared low-frequency region could indicate an important contribution of the resonance form (i) shown in Fig. 5.34 which describe more adequately the bonding and electron distribution in e.g. $[Co(4\text{-}HOpy)_2Cl_2]$ and $[Co(4\text{-}H_2Npy)_2Cl_2]$ complexes. The increased electron density on the ring nitrogens will be inductively transmitted through the Co-N σ-bond. Although the increase of Co-N stretching frequencies are only clearly observed for the 4HO- and $4H_2N$- substituents with equivalent masses, the accompanied shifts towards lower wavenumber of the Co-Cl stretching modes are continuously manifested in the group (see Table 5.5). Decomposition occurs without forming of thermally stable products and at temperatures above 370°C where we calculated a loss in weight corresponding to the two pyridine-ligands, further decomposition of the cobalt halides is observed. Intermediate products of $[Co(3\text{-}H_2NCOpy)_2X_2]$ and $[Co(4\text{-}H_2NCOpy)_2X_2]$ complexes are observed as follows :

complex	intermediate
$Co(3\text{-}H_2NCOpy)_2Cl_2$	$CoL_{2/3}X_2$
$Co(3\text{-}H_2NCOpy)_2Br_2$	$CoL_{1/3}X_2$
$Co(4\text{-}H_2NCOpy)_2Cl_2$	$CoLX_2$, $CoL_{1/3}X_2$
$Co(4\text{-}H_2NCOpy)_2Br_2$	$CoLX_2$, $CoL_{2/3}X_2$, $CoL_{1/3}X_2$

TABLE 5.5

Metal-ligand stretching frequencies and decomposition temperatures of some group (A) complexes.

complex	νCo-X	νCo-N	T(°C)
$Co(4\text{-}HOpy)_2Cl_2$	306,290	241	265
$Co(4\text{-}H_2Npy)_2Cl_2$	310,296	269	253
$Co(4\text{-}(CH_3)_2Npy)_2Cl_2$	334,305	226	253
$Co(4\text{-}(CH_3)_2Npy)_2Br_2$	260,246	230	268
$Co(py)_2Cl_2$	346,304	251	-[a]
$Co(py)_2Br_2$	277,244	253	166

[a] tetrahedral monomer not recorded.

The cyanopyridine complexes, belonging to group (D), decompose via the $CoLX_2$ and $CoL_{1/3}X_2$ intermediates to their appropriate cobalt halides. The decomposition of these intermediates occurs at relatively high temperatures when compared to other complexes of the same group. We have to consider the possibility that cyanopyridines may contribute through the nitrile or the ring nitrogen atoms and both may be involved in coordination to produce thermally stable polymers. One would indeed expect partial ligand fragmentation exceeding the loss of the pyridine ligand for such cross-linked structures. Polymerization of cobalt complexes by coordination of the nitrile groups have been reported by FARHA and IWAMOTO[16]. Similarly stable polymers are found in 1,2- and 1,3-diazines and 1,3,5-triazine cobalt complexes as described by BEECH[7].

Of special interest is the fact that decomposition temperatures do seem to be influenced by the stereochemistry, they are reportedly

higher for smaller coordination number. Examples are found in Table 5.6, together with some relevant spectroscopic data.

TABLE 5.6

compound	T(^{o}C)	νCo-N(cm^{-1})	CN	λ_{max}(nm)
$Co(py)_2Cl_2$	104	233	6	525
$Co(py)_2Br_2$	166	253	4	620
$Co(4\text{-}C_6H_5py)_2Cl_2$	223	210	6	
$Co(4\text{-}C_6H_5py)_2Br_2$	248	235	4	

5.5.2 Calorimetric Results

Fig. 5.35 presents a plot of the enthalpy values of the compounds examined as a function of their decomposition temperature, T. As stated, the plot shows that the decomposition temperature may be correlated with the total metal-ligand bond strength. Stronger Co-N bonds are observed in the following ligand sequence : py < 3-Clpy << 3-Brpy. In the same way that the basicities of ligands, as determined by their pK_a values, are related to the strength of the Co-N σ-bond, the acidities can be used as a measure by which we might expect Co-N π-bonding to occur. In these complexes, π-bonding is an important consideration as it will markedly influence the Co-N bond strengths. The sequence is in accordance with the Hammett sigma values of the substituents. In a comparable study of the Co-N bond dissociation energies of various cobalt complexes, McNAUGHTON and MORTIMER[8] concluded that the relatively high value (D = 157.7 ± 5.5 kJ mol^{-1}) for $[Co(3\text{-}Clpy)_2Br_2]$ may indicate a large contribution of π-bonding. One may also argue that the νCo-N for the 3-bromopyridine complexes (which occurs around 223 cm^{-1}) would be expected at much lower frequency due to the mass effect if π-bonding is absent. Further evidence of the importance of π-bonding in determining the overall thermal stability may be found

in the work of BOWMAN and ROGERS[17]. The authors stated that by increasing the ligand base strength, thus forming predominantly stronger M-N σ-bonds, the thermal stability of the complexes decreased.

Decomposition of the 3-chloro- and 3-bromopyridine complexes occurs via a stable intermediate, $CoLX_2$. This is supported by the work of MORTIMER and McNAUGHTON[8]. Some large differences from the authors' reported enthalpy values should be noted. Their values are, on average, 51 kJ mol^{-1} smaller and no significant difference was observed between the values of the 3-chloro- and 3-bromopyridine complexes. In contrast, our value for the 3-bromopyridine complex is approximately 15 kJ mol^{-1} higher than those for the 3-chloropyridine complex, in sympathy with the substituent effect.

The heats of decomposition of all isomers of mono-cyanopyridine complexes were measured previously by DSC[7]. Some of the reported thermochemical data are summarized as follows :

compound	ΔH_{tot} (kJ mol^{-1})
$Co(4\text{-}NCpy)_2Cl_2$	150 ± 2
$Co(4\text{-}NCpy)_2Br_2$	161.7 ± 0.7
$Co(3\text{-}NCpy)_2Cl_2$	147 ± 2
$Co(3\text{-}NCpy)_2Br_2$	157 ± 1

The steric hindrance of the cyano groups are responsible for the low heats of decomposition compared to the halogenopyridine complexes, as suggested by BEECH *et al.*[7].

Comparison of the heats of decomposition of the chloro- and bromo-complexes, reveals a dependence of ΔH_{tot} on the nature of the halogen. The reason for this has been suggested by BEECH *et al.*[18]. There is a greater charge transfer in the bromo-complex which reduces the capacity

of cobalt to serve as an acceptor in forming L-to-M σ-bonds. However, it increases the M-to-L π-bonding when the ligand has suitable orbitals and thus determines, to a large extent, the total Co-N bond strength.

If we compare the heats of reaction within the decomposition scheme, we see that each of the heats of reaction (2) is greater than those of reaction (1). This may be discussed from two points of view. Firstly, the metal-pyridine bond may be strengthened because of the decreased steric crowding of the pyridine ligands and secondly, the bonding capacity of the metal ion is distributed over fewer bonds. The importance of steric effects of ligands has been pointed out first by GRADDON *et al.*[19]. BEECH and KAUFFMAN[20], also referred to steric as well as π-bonding effects to explain the greater metal-pyridine bond strength in isothiocyanate complexes as compared to analogous chlorides and bromides.

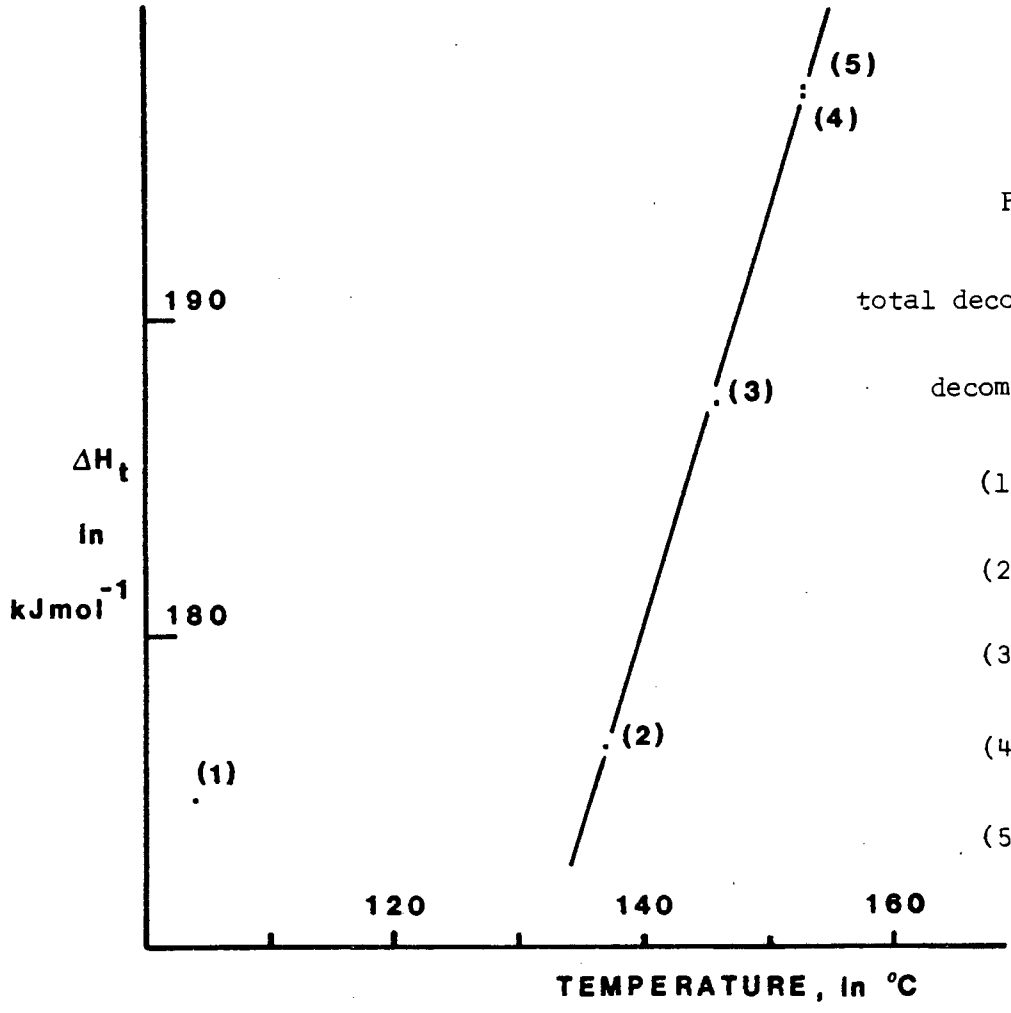

Fig. 5.35 : The heats of total decomposition reaction versus decomposition temperature of

(1) $Co(py)_2Cl_2$,

(2) $Co(3\text{-}Clpy)_2Cl_2$,

(3) $Co(3\text{-}Clpy)_2Br_2$,

(4) $Co(3\text{-}Brpy)_2Cl_2$,

(5) $Co(3\text{-}Brpy)_2Br_2$.

REFERENCES

1. R.C. MACKENZIE ed., "Differential Thermal Analysis"., Volume 1 Academic Press, London, 1970.
2. L.R. OCONE, J.R. SOULEN, B.P. BLOCK, *J. Inorg. Nucl. Chem.*, 15(1960)76.
3. J.R. ALLAN, D.H. BROWN, R.H. NUTTALL, D.W.A. SHARP, *J. Inorg. Nucl. Chem.*, 26(1964)1895.
4. J.R. ALLAN, G.M. BALLIE, *J. Thermal Anal.*, 14(1978)291.
5. G. BEECH, C.T. MORTIMER, E.G. TYLER, *J. Chem. Soc.*, A(1967)925.
6. G. BEECH, S.J. ASHCROFT, C.T. MORTIMER, *J. Chem. Soc.*, A(1967)929.
7. G. BEECH, *Thermochim. Acta*, 3(1972)297.
8. C.T. MORTIMER, J.L. McNAUGHTON, *Thermochim. Acta*, 10(1974)125.
9. E.S. WATSON, M.J. O'NEILL, J. JUSTIN, N. BRENNER, *Anal. Chem.*, 36(1964)1233.
10. A.A. VAN DOOREN, B.W. MULLER, *Thermochim. Acta*, 54(1982)115.
11. G. SIRACUSA, V. CUCINOTTA, *Thermochim. Acta*, 23(1978)185.
12. J. ZSAKO, C.S. VARHELYI, B. CSEGEDI, J. ZSAKO Jr., *Thermochim. Acta*, 45(1981)11.
13. W.W.WENDLANDT, *Chemist-Analyst*, 53(1964)71.
14. G. LIPTAY, *Thermochim. Acta*, 15(1976)159.
15. P.T.T. WONG, *Can. J. Chem.*, 52(1974)2005.
16. F. FARHA, R.T. IWAMOTO, *Inorg. Chem.*, 4(1965)844.
17. P.B. BOWMAN, L.B. ROGERS, *J. Inorg. Nucl. Chem.*, 28(1966)2215.
18. G. BEECH, C.T. MORTIMER, E.G. TYLER, *J. Chem. Soc.*, A(1969)512.
19. D.P. GRADDON, R. SCHULZ, E.C. WATTON, D.G. WEEDEN, *Nature*, 198(1963)1299.
20. G. BEECH, G.B. KAUFFMAN, *Thermochim. Acta*, 1(1970)93.

APPENDICES

COMPUTER PROGRAMMES

Appendix I

```
C*****************************************************************
C*****************************************************************
C*******                                                 *******
C******* G F - MATRIX,  EIGENVALUES AND EIGENVECTORS *******
C*******                                                 *******
C*****************************************************************
C*****************************************************************
C    purpose: calculation of vibrational frequencies
C             and transformation matrix, L,  if
C             the inverse kinetic, G, and the potential, F,
C             energy matrices are given
C
C    INPUT
C    -----
C       N     ORDER OF THE G AND F MATRICES (SYMMETRIC)  [I3]
C       G-MATRIX   (READ IN BY MATIN-ROUTINE)
C       F-MATRIX   (            "            )
C    OUTPUT
C    ------
C       MATRIX 1    G-MATRIX      (PRINTED BY MXOUT-ROUTINE)
C       MATRIX 2    F-MATRIX      (            "            )
C       MATRIX 3    GF-MATRIX     (            "            )
C       FREQUENCIES   (IN CM-1)
C       MATRIX 5    EIGENVECTORS                      ( " )
C                   NORMALIZED TO  L * L-transpose = E
C       MATRIX 6    NORMALIZED EIGENVECTORS           ( " )
C                   SO THAT  G = L * L-transpose  HOLDS
C
C$$$$$$$$$$$$$$$$$$$$$$$$$$$$$$$$$$$$$$$$$$$$$$$$$$$$$$$$$$$$$$$$
C     PROGRAMMED BY PAUL VERHOEVEN, INORGANIC CHEMISTRY DEPT.
C     UNIVERSITY OF CAPE TOWN (SPERRY-UNIVAC 1100 COMPUTER)
C*****************************************************************
C
      DIMENSION G(900), F(900), GF(900), LA(30), LB(30)
      DIMENSION EVEC(900), EIGV(900), GI(900), FA(900)
      DIMENSION EVAL(30), FREQ(30)

    5 FORMAT(20I3)
   15 FORMAT(1H , 5X, 6F10.2, /, 6X, 6F10.2, /, 6X, 6F10.1)
   25 FORMAT(1H , 15X, 24HVIBRATIONAL  FREQUENCIES, /,
     & 16X, 24(1H=) )
   35 FORMAT(1H1, 15X, 9HGF-MATRIX, /, 16X, 9(1H=))
   45 FORMAT(1H , ' DETERMINANT IS ZERO ', /////)
   55 FORMAT(1H1, 15X, 12HEIGENVECTORS, /, 16X, 12(1H=) )
   65 FORMAT(1H1, 15X, 31HEIGENVECTORS NORMALIZED BY L'FL, /,
     & 16X, 31(1H=) )

*****    MR AND MW THE LOGICAL UNIT NUMBERS    **************
*****    FOR READ AND WRITE STATEMENTS         **************
*****    READING OF THE INPUTDATA              **************
*****************************************************************
      MR = 5
      MW = 6
      READ (MR, 5) N
      ISIZE = N * N
      CALL MATIN  (ICODE, G, ISIZE, N, N, IS, IER)
      CALL MATIN  (ICODE, F, ISIZE, N, N, IS, IER)
```

Appendix I continued/

```
*****    ECHO OF INPUT MATRICES                    **************
*************************************************************
      CALL MXOUT  (1, G, N, N, 0, 40, 120, 1)
      CALL MXOUT  (2, F, N, N, 0, 40, 120, 1)

*****    CALCULATES THE PRODUCT MATRIX GF          **************
*************************************************************
      DO 10 I = 1, ISIZE
        GI(I) = G(I)
        FA(I) = F(I)
   10 CONTINUE
      DO 20 I = 1, N
      DO 20 K = 1, N
        KI = N * (I-1) + K
        GF(KI) = 0.
      DO 20 J = 1, N
        JI = N * (I-1) + J
        KJ = N * (J-1) + K
        GF(KI) = GF(KI) + G(KJ) * F(JI)
   20 CONTINUE

*****    COMPUTES THE DETERMINANT D                **************
*****    AND THE INVERSE OF G-MATRIX               **************
*************************************************************
      CALL MINV  (GI, N, D, LA, LB)
      IF ( D .LE. 0 ) THEN
          WRITE (MW, 45)
          STOP
      ELSE

*****    COMPUTES THE EIGENVALUES AND              **************
*****    THE EIGENVECTORS OF THE REAL              **************
*****    NONSYMMETRIC MATRIX G-INVERSE * F         **************
*************************************************************

          NN = N
          CALL NROOT  (NN, F, GI, EVAL, EVEC, 900, 30)
      ENDIF

*****    NORMALIZATION OF THE EIGENVECTORS         **************
*****    BY L-TRANSPOSED * F * L                   **************
*************************************************************
      DO 40 I = 1, N
        SUM = 0.
        DO 30 K = 1, N
        DO 30 J = 1, N
          KI = N * (I-1) + K
          JI = N * (I-1) + J
          KJ = N * (J-1) + K
          SUM = SUM + EVEC(KI) * EVEC(JI) * FA(KJ)
   30   CONTINUE
      DO 40 J = 1, N
        JI = N * (I-1) + J
        EIGV(JI) = EVEC(JI) * SQRT( EVAL(I) / SUM )
   40 CONTINUE
```

Appendix I continued/

```
*****    PRINTING OF OUTPUT-DATA                    **************
*****************************************************************
      WRITE (MW, 35)
      CALL MXOUT  (3, GF, N, N, 0, 40, 120, 2)
      WRITE (MW, 25)
      DO 50 I = 1, N
        FREQ(I) = 1303.16 * SQRT( EVAL(I) )
   50 CONTINUE
      WRITE (MW, 15) (FREQ(I), I = 1, N)
      WRITE (MW, 55)
      CALL MXOUT  (5, EVEC, N, N, 0, 40, 120, 1)
      WRITE (MW, 65)
      CALL MXOUT  (6, EIGV, N, N, 0, 40, 120, 1)
      STOP      'stop'
      DEBUG SUBCHK
      END
```

Appendix II

```
C*****************************************************************
C*****************************************************************
C****                                                         ****
C***    M E T H O D  of  B E C H E R  and  M A T T E S        ***
C****                                                         ****
C*****************************************************************
C*****************************************************************
C     PURPOSE     CALCULATIONS OF FORCE CONSTANTS
C     =======     -------------------------------
C             INPUT
C             =====
C     TITLE                                [20A4]
C     N    ORDER OF G AND F MATRICES       [I3]
C     MO   NUMBER ITERATION STEPS          [I3]
C     MATRIX G   (MATIN)
C     FREQ FREQUENCIES VECTOR   (IN CM-1)    [7F10.0]
C             OUTPUT
C             ======
C     MATRIX 1 G
C     FREQUENCIES   (IN CM-1)
C     MATRIX 2 FORCE CONSTANTS
C     MATRIX 3 NORMALIZED EIGENVECTORS
C     MATRIX 4 POTENTIAL ENERGY DISTRIBUTION
C$$$$$$$$$$$$$$$$$$$$$$$$$$$$$$$$$$$$$$$$$$$$$$$$$$$$$$$$$$$$$$$$
C     WRITTEN BY DR. B. VAN DER VEKEN, LABO ANORGANISCHE CHEMIE
C     UNIVERSITY OF ANTWERP (RUCA), BELGIUM (IBM 1130)
C     MODIFIED BY PAUL VERHOEVEN, INORGANIC CHEMISTRY DEPT, UCT
C     FOR THE SPERRY-UNIVAC 1100 COMPUTER
C     LITERATURE  BECHER, MATTES
C     SPECTROCHIM. ACTA, 23A(1967)2449
C*****************************************************************

      DIMENSION G(1296), GI(1296), F(1296), FA(1296)
      DIMENSION EVEC(1296), LA(36), LB(36)
      DIMENSION FREQ(36), EVAL(36), PED(36), TITLE(20)

 2000 FORMAT(I3)
 2005 FORMAT(20A4)
 2010 FORMAT(7F10.0)
 2015 FORMAT(1H1, 10X, 18H   FORCE CONSTANTS, 5X, 20A4, /,
     & 14X, 15(1H=), /)
 2020 FORMAT(7(3X, F8.2))
 2025 FORMAT(5X, 15HNUMBER OF STEPS, 5X, I2, /)
 2030 FORMAT(15X, 8HMATRIX G, /, 15X, 8(1H=))
 2035 FORMAT(////, 15X, 17HINPUT FREQUENCIES, /,
     & 15X, 17(1H=), /)
 2040 FORMAT(1H1, 15X, 15HFORCE CONSTANTS, /, 16X, 15(1H=))
 2045 FORMAT(1H1, 15X, 12HUNIT VECTORS, /, 16X, 12(1H"))
 2050 FORMAT(1H1, 15X, 29HPOTENTIAL ENERGY DISTRIBUTION, /,
     & 16X, 29(1H=), / , /)
 2055 FORMAT(1H , 'FREQUENCY', 36(4X, I2, 2X), /)
 2060 FORMAT(/, 1H , F8.2, 2X, 36(2X, F6.2))
 2065 FORMAT(1H , ' DETERMINANT IS ZERO ', /////)
```

Appendix II continued/

```
*******  READING AND PRINTING OF INPUTDATA                *******
************************************************************
      READ ( * , 2005) TITLE
      READ ( * , 2000) N
      READ ( * , 2000) MO
      ISIZE = N * N
      CALL MATIN  (ICODE, G, ISIZE, N, N, IS, IER)
      READ ( * , 2010) (FREQ(I), I = 1, N)
      WRITE ( * , 2015) TITLE
      WRITE ( * , 2025) MO
      WRITE ( * , 2030)
      CALL MXOUT  (1, G, N, N, 0, 40, 120, 1)
      WRITE ( * , 2035)
      WRITE ( * , 2020) (FREQ(I), I = 1, N)

*******  TRANSFORMING FREQUENCIES INTO EIGENVALUES    *******
************************************************************
      DO 10 I = 1, N
        FREQ(I) = (FREQ(I) * FREQ(I)) / (1303.16 ** 2.)
   10 CONTINUE

*******  INITIALIZE THE STARTING  Fo-MATRIX OF        *******
*******  THE UNCOUPLED VIBRATIONS                     *******
************************************************************
      DO 20 I = 1, ISIZE
        F(I) = 0.
   20 CONTINUE
      DO 30 I = 1, N
        II = N * (I-1)  +  I
        F(II) = FREQ(I) / G(II)
   30 CONTINUE

*******  START OF ITERATION CYCLE                     *******
************************************************************
      M = 0
   40 M = M + 1
      DO 50 I = 1, ISIZE
        FA(I) = F(I)
   50 CONTINUE


*******  STEPWISE INTRODUCTION OF THE NONDIAGONAL     *******
*******  G-MATRIX ELEMENTS                            *******
************************************************************
      DO 60 I = 1, N
      DO 60 J = 1, N
        IJ = N * (J-1)  +  I
        IF (  I-J  .EQ.  0  )  THEN
            GI(IJ) = G(IJ)
            GO TO 60
        ELSE
*******     SQUARE-ROOT COUPLING FUNCTION        *************
            gi(ij) = sqrt(float(m) / float(mo)) * g(ij)
************************************************************
        ENDIF
   60 CONTINUE
```

Appendix II continued/

```
*******  COMPUTES THE EIGENVALUES AND EIGENVECTORS     *******
*******  OF THE NONSYMMETRIC  G-inverse * F  MATRIX    *******
**************************************************************
      CALL MINV  (GI, N, D, LA, LB)
      IF ( D .LE. 0 ) THEN
          WRITE ( * , 2065)
          STOP
      ELSE
          NN = N
          CALL NROOT  (NN, F, GI, EVAL, EVEC, 1296, 36)
      ENDIF

*******  NORMALIZATION OF THE EIGENVECTORS             *******
*******  ACCORDING TO  L-transposed * F * L            *******
**************************************************************
      DO 75 I = 1, N
        SUM = 0.
        DO 70 K = 1, N
        DO 70 J = 1, N
          KI = N * (I-1)  +  K
          JI = N * (I-1)  +  J
          KJ = N * (J-1)  +  K
          SUM = SUM + EVEC(KI) * EVEC(JI) * FA(KJ)
   70   CONTINUE
        DO 75 J = 1, N
          JI = N * (I-1)  +  J
          EVEC(JI) = EVEC(JI) * SQRT(EVAL(I) / SUM)
   75 CONTINUE

*******  CALCULATION OF THE POTENTIAL ENERGY           *******
*******  DISTRIBUTION  (PED)                           *******
**************************************************************
      DO 86 J = 1, N
        DO 80 I = 1, N
          IJ = N * (J-1)  +  I
          II = N * (I-1)  +  I
          GI(IJ) = EVEC(IJ) * EVEC(IJ) * FA(II)
   80   CONTINUE
        SUM = 0.
        DO 83 I = 1, N
          IJ = N * (J-1)  +  I
          SUM = SUM + GI(IJ)
   83   CONTINUE
        DO 86 I = 1, N
          IJ = N * (J-1)  +  I
          GI(IJ) = GI(IJ) * 100./SUM
   86 CONTINUE

*******  ORDERING OF THE COORDINATES AND FREQUENCIES   *******
*******  ACCORDING TO PED                              *******
**************************************************************
      DO 99 I = 1, N
        J = 1
        K = J
   90   K = K + 1
        IK = N * (I-1)  +  K
        IJ = N * (I-1)  +  J
```

Appendix II continued/

```
      IF (  GI(IJ)-GI(IK)  .LT.  0  )  THEN
          IF ( K-N .LT. 0 ) THEN
              J = K
              GO TO 90
          ELSE
              DO 93 L = 1, N
                LK = N * (K-1)  +  L
                LI = N * (I-1)  +  L
                FA(LK) = EVEC(LI)
 93           CONTINUE
          ENDIF
          GO TO 99
      ELSE
          IF ( K-N .LT. 0 ) THEN
              GO TO 90
          ELSE
              DO 96 L = 1, N
                LJ = N * (J-1)  +  L
                LI = N * (I-1)  +  L
                FA(LJ) = EVEC(LI)
 96           CONTINUE
          ENDIF
      ENDIF
 99 CONTINUE

*******  CALCULATION OF THE F-MATRIX                          *******
*******  F  =  (L-inverse)-transp * FREQ * (L-inverse)  *****
**************************************************************
      CALL MINV  (FA, N, D, LA, LB)
      DO 100 I = 1, N
      DO 100 J = 1, N
        IJ = N * (J-1)  +  I
        F(IJ) = 0.
      DO 100 K = 1, N
        KI = N * (I-1)  +  K
        KJ = N * (J-1)  +  K
        F(IJ) = F(IJ)  +  FA(KI) * FA(KJ) * FREQ(K)
  100 CONTINUE

*******  DECISION OF ITERATION CYCLE                          *******
**************************************************************
      IF (  MO-M  .GT.  0  )  THEN
          GO TO 40
      ELSE

*******  FINAL COMPUTATION OF THE EIGENVALUES AND     *******
*******  THE EIGENVECTORS OF   G-inverse * F          *******
**************************************************************
          DO 110 I = 1, ISIZE
            FA(I) = F(I)
  110     CONTINUE
          CALL MINV  (G, N, D, LA, LB)
          NN = N
          CALL NROOT  (NN, F, G, EVAL, EVEC, 1296, 36)
      ENDIF
```

Appendix II continued/

```
*******  FINAL NORMALIZATION OF THE EIGENVECTORS       *******
*******  ACCORDING TO   L-transposed * F * L           *******
*****************************************************************
      DO 125 I = 1, N
        SUM = 0.
        DO 120 K = 1, N
        DO 120 J = 1, N
          KI = N * (I-1)  +  K
          JI = N * (I-1)  +  J
          KJ = N * (J-1)  +  K
          SUM = SUM + EVEC(KI) * EVEC(JI) * FA(KJ)
  120   CONTINUE
      DO 125 J = 1, N
        JI = N * (I-1)  +  J
        EVEC(JI) = EVEC(JI) * SQRT(EVAL(I) / SUM)
  125 CONTINUE


*******  FINAL CALCULATION OF THE POTENTIAL ENERGY     *******
*******  DISTRIBUTION                                  *******
*****************************************************************
      DO 136 J = 1, N
        DO 130 I = 1, N
          IJ = N * (J-1)  +  I
          II = N * (I-1)  +  I
          GI(IJ) = EVEC(IJ) * EVEC(IJ) * FA(II)
  130   CONTINUE
        SUM = 0.
        DO 133 I = 1, N
          IJ = N * (J-1)  +  I
          SUM = SUM + GI(IJ)
  133   CONTINUE
      DO 136 I = 1, N
        IJ = N * (J-1)  +  I
        GI(IJ) = GI(IJ) * 100./SUM
  136 CONTINUE

*******  PRINTING OF OUTPUT                            *******
*****************************************************************
      WRITE ( * , 2040)
      CALL MXOUT  (2, FA, N, N, 0, 40, 120, 1)
      WRITE ( * , 2045)
      CALL MXOUT  (3, EVEC, N, N, 0, 40, 120, 1)
      WRITE ( * , 2050)
      WRITE ( * , 2055) (I, I = 1, N)
      DO 140 I = 1, N
        EVAL(I) = 1303.16 * SQRT( EVAL(I) )
  140 CONTINUE
      DO 155 J = 1, N
        DO 150 I = 1, N
          IJ = N * (J-1)  +  I
          PED(I) = GI(IJ)
  150   CONTINUE
        WRITE ( * , 2060) EVAL(J), (PED(I), I = 1, N)
  155 CONTINUE
      STOP    'NORMAL TERMINATION'
      DEBUG SUBCHK
      END
```

```
C*************************************************************
C*************************************************************
C********   M A T R I X      P O L Y N O M I A L   ********
C********                                          ********
C********   E X P A N S I O N        M E T H O D   ********
C*************************************************************
C*************************************************************
C
C  purpose: calculation of a force field from
C           experimental frequencies
C
C  INPUT
C  -----
C     TITLE (maximum 80 characters long)
C     DIMENSION OF G-MATRIX (I3)
C     NUMBER OF ITERATION STEPS (I3)
C     MATRIX G (read in by matinsubroutine)
C     EXPERIMENTAL FREQUENCIES (7F10.0)
C
C  OUTPUT
C  ------
C     TITLE
C     MATRIX G
C     EXPERIMENTAL FREQUENCIES
C     MATRIX F
C     MATRIX EIGENVECTORS
C     POTENTIAL ENERGY DISTRIBUTION WITH IN
C     THE FIRST COLUMN THE CALCULATED FREQUENCIES
C     KINETIC ENERGY DISTRIBUTION
C     TOTAL VIBRATIONAL ENERGY DISTRIBUTION
C$$$$$$$$$$$$$$$$$$$$$$$$$$$$$$$$$$$$$$$$$$$$$$$$$$$$$$$$$$$$
C     WRITTEN BY DR. B. VAN DER VEKEN, LABO ANORGANISCHE
C     CHEMIE, UNIVERSITY OF ANTWERP (RUCA), BELGIUM
C     MODIFIED FOR THE UNIVAC 1100 BY
C     PAUL VERHOEVEN
C     INORGANIC CHEMISTRY DEPT.
C     UNIVERSITY OF CAPE TOWN
C     LITERATURE  1)  ALIX A.,  BERNARD L.
C                     J. MOL. STRUC., vol.20, 1974, pp.51-60
C                 2)  ALIX A.,  VAN DER VEKEN B.
C                     BULL. SOC. CHIM. BELG., vol.84
C                     nr.3, 1975, pp.111-123
C*************************************************************
      DIMENSION G(225), GA(225), F(225), GF(225), A(225),
     &B(225), P1(225), EVAL(15), IT(15), TITLE(20),
     &P2(225), CNU(16), FREQ(15), L(15), M(15), ICO(15)
      DATA IT/15*'S'/
 2000 FORMAT(7F10.0)
 2005 FORMAT(20I3)
 2010 FORMAT(20A4)
 2015 FORMAT(/, 1H , 13(F7.2, 2X))
 2020 FORMAT(1H1, 'MATRIX POLYNOMIAL EXPANSION METHOD', /,
     & 1H , 34('='), //)
 2025 FORMAT(1H , 'PRODUCT', 5X, 20A4, /, 1H , 7('='))
```

Appendix III continued/

```
 2030 FORMAT(/, 1H , 'NUMBER OF STEPS', 1X, I3, /,
     & 1H , 15('='), /)
 2035 FORMAT(1H , 'MATRIX G', /, 1H , 8('='))
 2040 FORMAT(/, 1H , 'EXPERIMENTAL FREQUENCIES', /,
     & 1H , 24('='))
 2045 FORMAT(1H1, 'MATRIX F', /, 1H , 8('='))
 2050 FORMAT(1H1, 'UNIT VECTORS', /, 1H , 12('='))
 2055 FORMAT(1H1, 'POTENTIAL ENERGY DISTRIBUTION', /,
     & 1H , 29('='), /)
 2060 FORMAT(1H , 'FREQUENCY', 15(3X, A1, I2, 1X), /)
 2065 FORMAT(/, 1H , F8.2, 1X, 15(1X, F6.2))
 2070 FORMAT(1H1, 'KINETIC ENERGY DISTRIBUTION', /,
     & 1H , 27('='), /)
 2075 FORMAT(1H1, 'TOTAL ENERGY DISTRIBUTION', /,
     & 1H , 25('='), /)
 3000 FORMAT(1H , 'M', I3)
 4000 FORMAT(1H , 'R', I3)

*****  MR AND MW ARE THE LOGICAL UNIT NUMBERS       ********
*****  FOR THE READ AND WRITE STATEMENTS            ********
*************************************************************
      MR=5
      MW=6

*****  READING AND PRINTING OF INPUTDATA            ********
*************************************************************
      READ(MR, 2010)TITLE
      READ(MR, 2005)N
      READ(MR, 2005)M0
      ISIZE = N * N
      CALL MATIN(ICODE, GA, ISIZE, N, N, IS, IER)
      READ(MR, 2000)(FREQ(I), I = 1, N)
      WRITE(MW, 2020)
      WRITE(MW, 2025)TITLE
      WRITE(MW, 2030)M0
      WRITE(MW, 2035)
      CALL MXOUT(1, GA, N, N, 0, 40, 120, 1)
      WRITE(MW, 2040)
      WRITE(MW, 2015)(FREQ(I), I = 1, N)

*****  TRANSFORMATION OF FREQUENCIES INTO EIGENVALUES  ****
*************************************************************
      DO 10 I = 1, N
        FREQ(I) = FREQ(I) ** 2 / (1303.16 ** 2)
   10 CONTINUE
```

Appendix III continued/

```
*****  CALCULATION OF THE POLYNOMIAL COEFFICIENTS  ********
*************************************************************
      CNU(N  +  1) = 1.
      DO 20 IP = 1, N
        SUM = 0.
        IFIN = 0
        DO 11 I = 1, IP
          ICO(I) = I
   11 CONTINUE
   12 PROD = 1.
        DO 13 I = 1, IP
          IPI = ICO(I)
          PROD = PROD*FREQ(IPI)
   13 CONTINUE
        SUM = SUM  +  PROD
        ITE = N + 1
        DO 14 I = 1, IP
          ITE = ITE-1
          J = IP-I  +  1
          ICO(J) = ICO(J)  +  1
          IF (ICO(J)-ITE) 15, 15, 14
   14 CONTINUE
        IFIN = 1
        GO TO 18
   15 IF (I-1) 18, 18, 16
   16 J = J + 1
        DO 17 I = J, IP
          ICO(I) = ICO(I-1)  +  1
   17 CONTINUE
   18 IF (IFIN-1) 12, 19, 12
   19 K = N-IP + 1
        CNU(K) = SUM * ((-1.) ** IP)
   20 CONTINUE

*****  CALCULATE THE STARTING F MATRIX              ********
*************************************************************
      DO 25 I = 1, ISIZE
        F(I) = 0.
   25 CONTINUE
      DO 30 I = 1, N
        II = N * (I-1)  +  I
        F(II) = FREQ(I) / GA(II)
   30 CONTINUE

*****  INITIALIZE THE M ITERATION                   ********
*************************************************************
      DO 1000 M1 = 1, M0
      WRITE(MW,  3000) M1

*****  STEPWISE INTRODUCTION OF THE NONDIAGONAL     ********
*****  G ELEMENTS                                   ********
*************************************************************
      DO 40 I = 1,  ISIZE
        G(I) = (FLOAT(M1) / FLOAT(M0)) * GA(I)
   40 CONTINUE
```

Appendix III continued/

```
      DO 50 I = 1, N
        II = N * (I-1)  +  I
        G(II) = GA(II)
   50 CONTINUE

*****  COMPUTES THE POLYNOMIAL EXPANSION MATRIX     ********
*****  AND INITIALIZE THE R ITERATION               ********
*****************************************************************
      IRQ = 0
  100 DO 51 I = 1, N
      DO 51 J = 1, N
        IJ = N * (J-1)  +  I
        GF(IJ) = 0.
      DO 51 K = 1, N
        IK = N * (K-1)  +  I
        KJ = N * (J-1)  +  K
        GF(IJ) = GF(IJ)  +  G(IK) * F(KJ)
   51 CONTINUE
      WRITE(MW,  4000) IRQ
      IRQ = IRQ  +  1
      DO 55 I = 1, ISIZE
        A(I) = 0.
        P1(I) = 0.
        P2(I) = 0.
   55 CONTINUE
      DO 60 I = 1, N
        II = N * (I-1)  +  I
        A(II) = 1.
   60 CONTINUE
      CNUI = CNU(1)
      DO 65 I = 1, ISIZE
        P2(I) = P2(I)  +  CNUI*A(I)
   65 CONTINUE
      DO 85 I = 1, N
        CNUI = CNU(I  +  1)
        DO 70 J = 1, ISIZE
          P1(J) = P1(J)  +  CNUI*FLOAT(I) * A(J)
   70 CONTINUE
        DO 71 J = 1, N
        DO 71 K = 1, N
          JK = N * (K-1)  +  J
          B(JK) = 0.
        DO 71 LL = 1, N
          JL = N * (LL-1)  +  J
          LK = N * (K-1)  +  LL
          B(JK) = B(JK)  +  A(JL) * GF(LK)
   71 CONTINUE
        DO 75 J = 1, ISIZE
          A(J) = B(J)
   75 CONTINUE
        DO 80 J = 1, ISIZE
          P2(J) = P2(J)  +  CNUI*A(J)
   80 CONTINUE
   85 CONTINUE
```

Appendix III continued/

```
*****  CALCULATION OF CORRECTION F MATRIX          *********
*****************************************************************
      DO 86 I = 1, N
      DO 86 J = 1, N
        IJ = N * (J-1)  +  I
        A(IJ) = 0.
      DO 86 K = 1, N
        IK = N * (K-1)  +  I
        KJ = N * (J-1)  +  K
        A(IJ) = A(IJ)  +  P1(IK) * G(KJ)
   86 CONTINUE
      CALL MINV(A, N, D, L, M)
      DO 87 I = 1, N
      DO 87 J = 1, N
        IJ = N * (J-1)  +  I
        B(IJ) = 0.
      DO 87 K = 1, N
        IK = N * (K-1)  +  I
        KJ = N * (J-1)  +  K
        B(IJ) = B(IJ)  +  A(IK) * P2(KJ)
   87 CONTINUE
      DO 90 I = 1, ISIZE
        F(I) = F(I)-B(I)
   90 CONTINUE
      IJK = 0

*****  EVALUATION OF SYMMETRY                        *********
*****************************************************************
      EPS = .001
      DO 95 I = 1, N
      DO 95 J = I, N
        IJ = N * (J-1)  +  I
        JI = N * (I-1)  +  J
        IF (ABS(F(IJ)-F(JI))-EPS) 93, 93, 94
   93 IJK = 0.
        GO TO 95
   94 IJK = 1
        GO TO 96
   95 CONTINUE

*****  SYMMETRIZATION OF THE F MATRIX              *********
*****************************************************************
   96 DO 97 I = 1, N
        K = I  +  1
      DO 97 J = K, N
        IJ = N * (J-1)  +  I
        JI = N * (I-1)  +  J
        F(IJ) = (F(IJ)  +  F(JI)) / 2.
        F(JI) = F(IJ)
   97 CONTINUE
      IF (IJK) 100, 1000, 100
 1000 CONTINUE
```

Appendix III continued/

```
*****  COMPUTES THE EIGENVALUES AND EIGENVECTORS  *********
*****  OF THE REAL NONSYMMETRIC MATRIX OF TYPE    *********
*****  G-INVERSE * F                              *********
**************************************************************
      DO 110 I = 1, ISIZE
        B(I) = F(I)
  110 CONTINUE
      CALL MINV(G, N, D, L, M)
      DO 111 I = 1, ISIZE
        GA(I) = G(I)
  111 CONTINUE
      CALL NROOT(N, B, G, EVAL, A)

*****  NORMALIZATION OF THE EIGENVECTORS          *********
*****  BY  L-TRANSPOSED * F * L                   *********
**************************************************************
      DO 130 I = 1, N
        SUM = 0.
        DO 120 K = 1, N
        DO 120 J = 1, N
          II = N * (I-1)
          KI = II  +  K
          JI = II  +  J
          KJ = N * (J-1)  +  K
          SUM = SUM  +  A(KI) * A(JI) * F(KJ)
  120 CONTINUE
      DO 130 J = 1, N
        JI = N * (I-1)  +  J
        A(JI) = A(JI) * SQRT(EVAL(I) / SUM)
  130 CONTINUE

*****  CALCULATION OF THE VIBRATIONAL             *********
*****  POTENTIAL ENERGY DISTRIBUTION              *********
**************************************************************
      DO 160 I = 1, N
      DO 160 K = 1, N
        IK = N * (K-1)  +  I
        B(IK) = 0.
        DO 140 J = 1, N
          JK = N * (K-1)  +  J
          IJ = N * (J-1)  +  I
          B(IK) = B(IK)  +  A(IK) * A(JK) * F(IJ)
  140 CONTINUE
        B(IK) = B(IK) / EVAL(K)
  160 CONTINUE
```

Appendix III continued/

```
*****  CALCULATION OF THE VIBRATIONAL                  *********
*****  KINETIC ENERGY DISTRIBUTION                     *********
*****************************************************************
      DO 165 I = 1, N
      DO 165 K = 1, N
        IK = N * (K-1)  +  I
        G(IK) = .0
      DO 165 J = 1, N
        JK = N * (K-1)  +  J
        IJ = N * (J-1)  +  I
        G(IK) = G(IK)  +  A(IK) * A(JK) * GA(IJ)
  165 CONTINUE

*****  CALCULATION OF THE TOTAL VIBRATIONAL            *********
*****  ENERGY DISTRIBUTION                             *********
*****************************************************************
      DO 166 I = 1, ISIZE
        GF(I) = B(I)  +  G(I)
  166 CONTINUE

*****  TRANSFORMATION OF EIGENVALUES INTO FREQUENCIES  ****
*****************************************************************
      DO 170 I = 1, N
        EVAL(I) = 1303.16 * SQRT(EVAL(I))
  170 CONTINUE

*****  PRINTING OF THE RESULTS                         *********
*****************************************************************
      WRITE(MW, 2045)
      CALL MXOUT(2, F, N, N, 0, 40, 120, 1)
      WRITE(MW, 2050)
      CALL MXOUT(3, A, N, N, 0, 40, 120, 1)
      WRITE(MW, 2055)
      WRITE(MW, 2060)(IT(I), I, I = 1, N)
      DO 190 I = 1, N
        DO 180 J = 1, N
          IJ = N * (I-1)  +  J
          FREQ(J) = B(IJ) * 100.
  180 CONTINUE
        WRITE(MW, 2065)EVAL(I), (FREQ(J), J=1, N)
  190 CONTINUE
      WRITE(MW, 2070)
      CALL MXOUT(4, G, N, N, 0, 40, 120, 1)
      WRITE(MW, 2075)
      CALL MXOUT(5, GF, N, N, 0, 40, 120, 1)
      STOP     'NORMAL PROGRAM TERMINATION'
      END
```